

Noise Modeling and Characterization of Nonlinear RF/Microwave Components

Richard Paul Hoft

*Submitted in accordance with the requirements for the degree of
Doctor of Philosophy*

The University of Leeds
School of Electronic and Electrical Engineering
Leeds, United Kingdom

April 2018

Declaration

The candidate confirms that the work submitted is his own and that appropriate credit has been given where reference has been made to the work of others. This copy has been supplied on the understanding that it is copyright material and that no quotation from the thesis may be published without proper acknowledgment.

Acknowledgments

There are many people who have contributed their support on my behalf during this endeavor. First, and most notable is the patience, encouragement, and love of my wife Ernestine. Without her backing, this research would not have been possible. Secondly, thanks go to Professor Ian Hunter from the University of Leeds for permitting me to work full-time during this activity. His guidance and support have been essential throughout the process of this venture. Thanks to my colleagues at Keysight Technologies, Inc. for valuable suggestions and technical insight and to the management and executives who backed this research financially and through provision of essential resources. A deep sense of gratitude goes to my parents for their enduring encouragement and support. Finally, I wish to recognize Louise Redmonds for her contribution to this work through her administrative expertise.

Abstract

A generalized scattered noise behavioral model for time-invariant nonlinear microwave circuits is presented. The formalism uses noise waves and large-signal scattering functions known as X-parameters to extract a multi-port network's noise correlation matrix. Further processing yields figures-of-merit including effective input noise temperature and noise factor. Within the small-input signal space, it will be shown that the above expressions reduce to a familiar form describing noise wave influence governed by the network's S-parameter functions. Using the generalized form, two examples given in context to embedded nonlinear one-port and two-port configurations are offered with each presented to matched termination networking. Both cases use a passive source and load in the analysis. Numerical versus simulated experimental results will be compared. Results in the two-port case yield its noise factor. Lastly, pursuant to this study, experimental work involving software simulation and hardware measurement activities will be proposed.

Contents

Declaration	i
Acknowledgments	ii
Abstract	iii
Contents	iv
List of Figures	vii
List of Abbreviations.....	ix
List of Symbols	xi
1 Introduction	1
1.1 Chronological History of Noise Concepts, Modeling, and Measurement.....	3
1.2 Organization of the Thesis.....	8
2 Signal and Noise-Wave Concepts	11
2.1 Signal Waves and Scattering Parameters.....	11
2.2 Traveling Noise-Waves	19
2.3 Noise-Wave Characteristics.....	22
2.3.1 Correlation.....	23
2.3.2 Auto-Correlation and Power Spectral Density	25
2.3.3 Cross-Correlation and Power Spectral Density	28
2.3.4 Noise Bandwidth	29
2.4 Network Analysis of Two Noisy Passive One-Ports	32

2.4.1 Noise-Wave Formalism	32
2.4.2 Exchangeable Noise-Power	34
2.4.3 Constraints on Validity of Analysis	36
3 Linear Network Noise Behavioral Modeling.....	41
3.1 Passive Components.....	42
3.1.1 Network Representation using S-parameters and Noise-Waves.....	42
3.1.1.1 One-Port Network.....	42
3.1.1.2 Multi-Port Network.....	44
3.1.2 Passive Component Network Analysis	48
3.1.3 Noise Temperature.....	55
3.2 Active Components	58
3.2.1 Network Representation using S-parameters and Noise-Waves.....	58
3.2.1.1 Two-Port Network.....	59
3.2.1.2 Multi-Port Network.....	64
3.2.2 Figures-of-Merit.....	65
3.2.2.1 Noise Factor	65
3.2.2.2 Effective Input Noise Temperature.....	69
3.2.2.3 Noise Parameters.....	70
4 Characterization and De-embedding a Linear Network's Noise Matrix.....	78
4.1 Two-Port Device Noise Measurement Model.....	79
4.2 Noise-Power Measurement	81
4.3 Linear Network Noise Extraction from its Cascaded Network.....	83
4.3.1 Noise Receiver Calibration	86
4.3.2 Noise Matrix Characterization of a Linear Two-Port Device.....	97
5 Nonlinear Network Noise Behavioral Modeling.....	108
5.1 Linear and Nonlinear (Time-Invariant) Network Behavioral Modeling.....	109
5.1.1 Linear Network Behavioral Modeling using S-parameters	109
5.1.2 Nonlinear (and Linear) Network Behavioral Modeling using X-parameters.....	115
5.2 Nonlinear Network Noise Modeling Using X-parameters.....	123
5.2.1 General Theory	123

5.2.1.1 Noise Correlation Matrix.....	124
5.2.1.2 Noise Factor	132
5.2.2 Noise Analysis of a Nonlinear One-Port Network	134
5.2.3 Noise Analysis of a Nonlinear Two-Port Network	140
5.2.4 Hardware Measurement Thought Experiment	150
5.2.4.1 Nonlinear One-Port Network.....	151
5.2.4.1.1 Calibration Algorithm	158
5.2.4.1.2 Measurement Algorithm	164
5.2.4.2 Nonlinear Two-Port Network.....	165
5.2.4.2.1 Calibration Algorithm	172
5.2.4.2.2 Measurement Algorithm	178
6 Conclusions and Recommendations	180
6.1 Conclusions.....	180
6.2 Recommendations for Further Work	181
Appendices	182
Appendix A.....	182
Appendix B.....	183
Appendix C.....	184
Appendix D	186
Appendix E.....	187
Appendix F	189
Publications.....	190
References	191

List of Figures

2.1 Circuit Representation of a Uniform Transmission Line	13
2.2 Transmission Line Connected to Z_1 with Traveling Waves $V^+(x)$ and $V^-(x)$	15
2.3 Transmission Line Connected to Z_1 with Traveling Waves a and b	18
2.4 Thermal Noise Voltage versus Time	19
2.5 One-Port Signal and Noise Model.....	20
2.6 Transmission Line Connected to Z_1 and Traveling Waves a , b , and \hat{b}_{gl}	22
2.7 Graphical Description of a Bandpass Filters Noise Bandwidth	31
2.8 Two Passive One-Ports Connected by a Lossless Transmission Line	32
2.9 Input-Noise Power Spectral Density $\hat{\phi}(f)$ Across Δf_n	37
3.1 Noisy One-Port Connected to a Lossless Transmission Line	42
3.2 Noisy Multiport Connected to Lossless Z_0 Transmission Lines	44
3.3 Noisy Multiport Network-S Embedded in a Termination Network-L	48
3.4 Embedded Passive One-Port Network-S. System is at Uniform Temperature T.....	52
3.5 Embedded Passive Two-Port Network-S. System is at Uniform Temperature T.....	53
3.6 Embedded Passive N-port Network-S. System at Temperature Equilibrium T	55
3.7 Passive System at Temperature Equilibrium	56
3.8 Active Two-Port Network-S Connected to Passive Termination Network-L	59
3.9 Two-Port Network Connected to Input and Output Terminations.....	66
3.10 3D Representation of Noise Factor versus Source Impedance.....	71
3.11 Scattered Noise-Wave Model of an Active Noisy Two-Port Amplifier.....	72
4.1 Two-Port Network Noise-Wave Model Connected To Passive Z_S And Noise Receiver	79
4.2 Noise Receiver Calibration – Noise Source Connected To Noise Receiver	87
4.3 Schematic Representation of the Receiver.....	94
4.4 Schematic Representation of the DUT Embedded in a Cascaded Network	104
5.1 Modern Vector Network Analyzer Block Diagram (4-Port PNA-X).....	113
5.2 The Keysight PNA-X Architecture with NVNA Application to Extract X-parameters.....	122
5.3a: Two connected noisy multi-ports, the nonlinear (n-port, m-harmonic) device and its linear termination network.....	125

5.3b Two connected noisy n-ports. Noise wave equations in matrix form can readily be devised by inspection	126
5.4 Simulation of a Noisy Nonlinear One-Port Match Embedded with its Source-Termination Network	135
5.5 Simulation of a Noisy Nonlinear Two-Port Match Embedded with its Source-Termination Network	142
5.6a Proposed Measurement Setup for the NL One-Port Network	151
5.6b Proposed Block Diagram of a NL One-Port Network.....	152
5.7 Noise Measurement Receiver Calibration for the NL One-Port Network	159
5.8 Source Match Calibration for the NL One-Port Network	163
5.9a Proposed Measurement Setup for the NL Two-Port Network.....	166
5.9b Proposed Measurement Setup for the NL Two-Port Network.....	166
5.10 Noise Measurement Receiver Calibration for the NL Two-Port Network.....	172
5.11 Source Match Calibration for the NL Two-Port Network	177

List of Abbreviations

AC	Alternating Current
BPF	Bandpass Filter
Cplr	Coupler
CW	Continuous Wave
dBm	Decibel Power Relative to One Milliwatt
DC	Direct Current
DUT	Device Under Test
ENR	Excess Noise Ratio
F	Noise Factor
G	Gain
KCL	Kirchhoff's Current Law
LSOP	Large-Signal Operating Point
KVL	Kirchhoff's Voltage Law
NCM	Noise Correlation Matrix
NF	Noise Figure
NL	Nonlinear
NVNA	Nonlinear Vector Network Analyzer

PNA-X	Keysight Technology's Performance Network X-Series Analyzer
PSD	Power Spectral Density
RF	Radio Frequency
RMS	Root-Mean-Square
rx	Receiver
S	Small-Signal Scattering Parameter
S	S-parameter (Scattering) Matrix
Src	Source
Si	Silicon
SNR	Signal-to-Noise Ratio
t	Time
T	Temperature in Kelvin
x	Distance
X	Large-Signal Scattering Parameter
X	X-parameter (Scattering) Matrix

List of Symbols

q	Charge of an Electron, Coulombs
\hat{I}_s	Average Shot Noise Current, Ampere
\hat{i}_s	Instantaneous Shot Noise Current, Ampere
$\Delta f_n, B, \text{NBW}$	Noise Bandwidth, Hertz
k	Boltzmann's Constant, Joules/Kelvin
T_o	Reference Temperature of 290K
\hat{V}_t	Thermal Noise Voltage, Volt
T_e, \hat{T}_e	Effective Input Noise Temperature, Kelvin
dB	Decibel
dBm	Absolute Power Relative to 1 Milliwatt
GHz	Gigahertz
MHz	Megahertz
Hz	Hertz
Re	Real
ω	Radian Frequency
γ	Propagation Constant

α	Attenuation Constant, Neper/Length
β	Phase Constant, Radian/Length
j	Complex Number
Z_c	Complex Characteristic Impedance, Ohm
Z_o	Real Characteristic Impedance, Ohm
Z_s	Complex or Real Source Impedance, Ohm
Z_L, Z_l	Complex or Real Load Impedance, Ohm
ϕ	Radians
ν_g	Group Delay, Second
W	Watts
T	Period, Seconds
E	Energy, Joules
P	Power, Watts
P_{av}	Available Power, Watts
$\hat{\Phi}$	Noise Power Spectral Density, Watts/Hertz
Γ	Reflection Coefficient
\mathbb{R}	Set of all Real Numbers
\mathbb{C}	Set of all Complex Numbers
G	Gain
G_{av}	Available Gain
g_r	Measurement Receiver's Transmission Coefficient

G_r	Measurement Receiver's Gain-Bandwidth Product, Hertz
\hat{T}_a	Available Noise Temperature, Kelvin
\hat{T}_s, \hat{T}_{gs}	Noise Temperature of Source Impedance Z_s , Kelvin
\hat{T}_{Hot}	Effective Noise Temperature of Noise Source in On-State, Kelvin
\hat{T}_{Cold}	Noise Temperature of Noise Source in Off-State, Kelvin
$\mathfrak{F}[\cdot]$	Fourier Transform
\dagger	Hermitian
R	Designates Circuit Symbol of a Resistor, Ohm
L	Designates Circuit Symbol of a Inductor, Henry
C	Designates Circuit Symbol of a Capacitor, Farad
G	Designates Circuit Symbol of a Conductance, Mho
\hat{a}	Incident Noise Wave, $\sqrt{W/Hz}$
\hat{b}	Scattered Noise Wave, $\sqrt{W/Hz}$
\hat{b}_s, \hat{b}_{gs}	Generator Noise Wave of Source Impedance Z_s , $\sqrt{W/Hz}$
$\hat{b}_l, \hat{b}_{gl}, \hat{b}_L$	Generator Noise Wave of Load Impedance Z_L , $\sqrt{W/Hz}$
\hat{b}_{gt}	Generator Noise Wave of a Termination, $\sqrt{W/Hz}$
\hat{b}_{gd}	Generator Noise Wave of the Device Under Test, $\sqrt{W/Hz}$
\hat{b}_{ms}	Generator Noise Wave of the Measurement System, $\sqrt{W/Hz}$
\hat{b}_r	Generator Noise Wave of the Measurement Receiver, $\sqrt{W/Hz}$

Chapter 1

Introduction

Receiving systems often require the processing of low level signals in the presence of noise. This noise is added by the system tending to make the weak signal inconspicuous and preventing it from being suitably processed. The ability of a receiving system to process low level signals is commonly described in terms of its sensitivity, bit error ratio, or noise figure. Consequently, to achieve a given receiving system sensitivity, designers will choose components based on their gain and noise figure [1].

Reliable methods have been developed which describe the noise behavior of components and systems under linear (small signal) conditions. Among these, certain techniques represent the network by noise correlation and signal matrices to determine its figures-of-merit including noise figure, effective input noise temperature, and noise parameters [2].

At low frequency, the capacity of a network to deliver noise power to its connecting terminations may be represented by introducing noise voltage and current generators to its ports. Their relationship can be summarized with the noise correlation matrix [2], [3]. When dimensions of the circuit are greater or comparable to the signal frequencies wavelength of operation, a traveling noise wave approach is more suitable [3], [4], [5], [6], [7]. The methods are particularly compatible with scattering and transfer scattering signal representations. In conjunction with noise waves, suitable noise behavioral models representing a stimulus-

response or what is commonly referred as a black-box analysis may be used to assess the network's noise correlation matrix (NCM).

While much attention has been given to predicting noise behavior of networks functioning under small-signal conditions, the same is not true for the large-signal case [8]. Presently absent in practice are comprehensive solutions that link NL network noise modeling with software simulation and hardware measurement capabilities. Despite this, there is motivation for a communication systems architect to quantify the noise behavior of large-signal drive circuits within both its transmitter and receiver chains.

First, to maximize output power and efficiency (PAE) of a communication system's transmitter chain, power amplifiers (PA) often operate within their nonlinear region. Consequently, this tends to lower the gain of the PA thereby degrading the transmitter's signal-to-noise ratio. Thus, having the ability to model the noise behavior of the transmitter chain and/or PA and link this to industry accepted figures-of-merit such as noise figure may offer benefit to the system architect by minimizing design cycle time and cost.

Second, it's not uncommon that due to interfering signals of sufficient strength, receiver performance is reduced. In general, this may occur in the receiver chain due to preamplifier compression and/or or mixer overload. In both cases, it reduces the signal-to-noise ratio of the receiver leading to an increase in noise figure. To have a model that can predict noise behavior of a nonlinear network or chain under similar operating conditions as the application has the potential to be very useful to the designer. By extraction of the NL network's noise correlation matrix through software simulation or hardware measurement, the system architect may use such tools to quantify performance at each stage of the design process.

In response to these industry needs, the goals of this research are to:

- Design a generalized scattered noise behavioral model for time-invariant, nonlinear microwave circuits.

- Demonstrate the scattered noise behavioral model's validity across a network's nonlinear and linear regions of operation.
- Construct an identification method which extracts a nonlinear circuit's noise correlation matrix from its scattered noise behavioral model.
- Express a nonlinear network's noise factor in terms of its extracted noise properties. Propose a formalism consistent with linear network standards.
- Design a proposed hardware measurement setup with supporting algorithms that employ an identification method for extracting a nonlinear network's noise correlation matrix.

The research topics are in chapter five of this thesis.

1.1 Chronological History of Noise Concepts, Modeling, and Measurement

A time sequential evolution of notable discoveries leading to the technical underpinnings governing the field of modern day electronic noise will be offered [3]. Each topic is presented as a highlight emphasizing its contribution to the field rather than delving into the depths of its technical details. Much of the in-depth studies will ensue in the coming chapters. The historical perspective is not all encompassing within the field of electronic noise. Rather, it's directed toward subject matter relevant to the research topic of this thesis. Further, it is subjective in that another author may choose topics which have not been treated with the same emphasis or perhaps omitted all together. Next, the chronological assessment enters efforts of mathematical treatment and modeling of these noise concepts to predict the performance of an associated system to which a device of interest is under consideration. In this case, the subject will be narrowed to distributed systems in the RF/microwave frequency spectrum. Lastly, selected measurement techniques known to exploit the referred to models will be highlighted.

In 1828, botanist Robert Brown [4] published his observations on the subject known today as Brownian motion. In the preceding year, Brown was evaluating under microscope particles of pollen immersed in water. He observed their movement through the water but could not account for the cause of their motion. Nearly a century would pass before Albert Einstein in 1905 presented a mathematical based description explaining the observations made by Brown. Einstein's account described molecular movement in the fluid colliding with the pollen particles thereby resulting in their displacement. It had long been held that matter consisted of atoms and molecules. Einstein formalized this theory [5]. Shortly thereafter, Jean Perrin reinforced Einstein's conclusions through his experimental findings [6].

The first three decades of the twentieth century witnessed significant development in the field of electronic noise theory. The first twenty years focused largely on identifying and classifying noise generating mechanisms; the last decade emphasized development of mathematical frameworks used to describe these experimental observations [3].

Walter Schottky published in 1918 a paper describing what eventually came to be known as the shot effect [7]. He observed current fluctuations in vacuum tubes ultimately arriving at a conclusion that the root-mean-square value of these variations can be described by

$$\hat{i}_{s,rms} = \sqrt{\hat{i}_s^2} = \sqrt{2q|I_s|\Delta f_n} \quad (1.1)$$

where q is the charge of an electron, I_s the average current, and Δf_n the bandwidth that \hat{i}_s is confined. The current fluctuation \hat{i}_s is known today as shot noise.

In 1926 John Johnson of Bell Laboratories first measured what today is known as thermal noise. His findings were first reported in 1927 and further elaborated in his 1928 publication [4]. Johnson shared his measurement results with Harry Nyquist, also of Bell Labs, who substantiated Johnson's observations. His theoretical derivation [8] determined that the root-mean-square value of thermal noise voltage in a conductor exhibiting resistance R is

$$\hat{v}_{t,\text{rms}} = \sqrt{\hat{v}_t^2} = \sqrt{4kTR\Delta f_n} . \quad (1.2)$$

k is Boltzmann's constant, T the physical temperature of the conductor, and Δf_n is the bandwidth to which the thermal noise is restricted. It became understood that this noise placed a lower limit on receiver performance.

In conjunction with the study of electronic noise types, progress was underway to define a suitable figure-of-merit to specify receiver performance. Fredrick Llewellyn in 1931 [9] compared the signal-to-noise ratio at a receiver's output under different input terminal conditions including short circuit and impedance loading. Publications by Williams [10] and Franz [11] built on Llewellyn's innovation by offering analytical treatment of a receiver signal-to-noise ratio (SNR) figure-of-merit. In their work, it was suggested for the first time that a noisy receiver could be modeled by an equivalent signal version of the receiver. This and previous studies were directed to low frequency narrow band applications in telephony.

The advent of World War II brought with it the need for broadband microwave communication systems. This ushered contribution from E.W. Herold [3, 12] in his studies of second stage noise contributions following a low gain first stage as well as his effort to maximize SNR at a receiver output through tuning its input impedance. The demanding requirements for improved system sensitivity presented an impetus for comparing receiver performance. In 1942 Dwight North was the first to define a noise factor [13] as means to describe a systems overall noise behavior. Shortly thereafter, Harold Friis introduced originaive insight to his own definition of system behavior which he termed noise figure leading to the expression [14]

$$F = \left(\frac{S_{\text{in}}}{N_{\text{in}}} \right) \cdot \left(\frac{S_{\text{out}}}{N_{\text{out}}} \right)^{-1} . \quad (1.3)$$

Additionally, Friis was the first to quantify the degradation of receiver noise due to noise generated from its following stages. Today this widely used expression is often referred as the cascade gain equation and is described by [14]

$$F_{\text{tot}} = F_1 + \frac{F_2 - 1}{G_1} + \frac{F_3 - 1}{G_1 G_2} + \dots + \frac{F_n - 1}{G_1 G_2 \dots G_{n-1}} \quad (1.4)$$

where F_n and G_n are the noise figure and gain of the n -th stage respectively. The work of North, Friis, and others advanced standardization related to electronic noise modeling and measurement techniques within the engineering community. D.K. MacDonald showed in his publication of 1944 [15] that North's noise factor and Friis's noise figure are in fact equivalent. Indeed, the IRE Standards Committee of 1952, 1953, and again in 1957 updated industry standards largely formalizing the contributions of North and Friis while aiding the engineering community with a practical framework for addressing state-of-art behavioral noise requirements [3].

To cope with low noise devices, it was believed by some [3, 16] that instead of using noise figure, a more appropriate scale of noise appraisal was effective input noise temperature T_c . The IRE Standards Committee adopted this concept in 1960 [17] using the relation

$$T_c = (F - 1) \cdot T_0 \quad (1.5)$$

where T_0 is a reference temperature of 290 Kelvin. In this way, both concepts were preserved, depending on system requirements one could choose T_c or F .

For distributed networks operating in the RF/microwave frequency spectrum, the wave representation of noise developed by Rothe and Dalke [18], Penfield [19], Bosma [20], and Meyes [21, 22] is particularly useful. Its theoretical tenets will be developed in chapters 2-4. The methods described are particularly compatible with scattering and transfer scattering signal representations.

Within the past two decades CAD-oriented methods of noise analysis have been developed by Dobrowski [23], Wedge and Rutledge [24, 25], Randa [26], and others [27, 28]. The noise behavior is often derived through a variety of methods including a physics-based approach, the use of an equivalent circuit, or through describing equations. The common feature with each

of these approaches is that the internal workings of the device or network need be known from a given perspective.

Within the context of noise, there are also behavioral models requiring no knowledge of the network's internal workings. Behavioral models represent a stimulus-response or what is commonly referred as a black-box approach. S-parameters are perhaps the most well-known behavioral model in the RF/microwave industry having been introduced in the 1960s [29].

Many of the mentioned linear network noise modeling capabilities that were conceived and developed in preceding decades are presently being leveraged and advanced to address modern communication systems that utilize GaN and GaAs HEMT technology [59, 60, 61, 62].

In roughly the past two decades, fueled by an increasing need to balance maximum transmit output power and power added efficiency while preserving a sufficient signal-to-noise ratio, considerable effort has been devoted to predicting nonlinear performance of large-signal driven networks [55, 56, 63, 64].

The progression of noise measurements dates to the early 1940s. In 1942 [3, 14] Friis describes a CW method for determining the noise figure using a signal source. Though accurate in its time, it proved to be somewhat involved in that separate gain and bandwidth measurements needed to be performed on the measurement receiver prior to determining the device's noise factor F . The development of a high frequency broadband source exhibiting a high excess noise ratio is largely credited to Bill Mumford [3, 30] who worked closely with Friis. The theoretical to measurement agreement with respect to excess noise was on the order of $\pm 0.5\text{dB}$ to $\pm 1.0\text{dB}$. From the work of Mumford and others, gradual improvement eventually led to agreement of $\pm 0.1\text{dB}$. The accuracies noted were obtained under tightly controlled conditions orchestrated through what today would be metrology level efforts. Sard showed [3, 31] that the most accurate measurement of T_e in that time was the Y-factor technique. In 1980 the Hewlett-Packard Co. introduced the H8970A noise figure meter. It implemented the Y-factor method [32]. As a commercial based solution, it was widely used by the industry for more than twenty years.

Versions of this approach are implemented today by Keysight Technology's noise figure analyzer and even within its family of signal analyzers. It uses a calibrated noise source presented to the device of interest. This technique offers reasonable levels of accuracy for a wide variety of applications.

In recent times, there has remained an unrelenting pursuit to improve system noise performance. In response, advances in measurement science have been needed to improve accuracy. In 2007, Agilent Technologies in collaboration with University of Leeds professor Roger Pollard introduced a revolutionary cold source method leveraging Agilent's PNA-X vector network analyzer [33]. Using this commercially based technique, noise figure accuracy of $\pm 0.2\text{dB}$ was achieved to 26.5GHz. The cold source technique determines the noise correlation matrix of the device of interest. Taken with its S-parameters, the noise figure of the device may be precisely determined. In 2013 Agilent extended this method to 50 GHz.

At the same time, there has and continues to be advances in measurement science pertaining to NL network noise characterization [65] and modeling [66]. While some progress has been made, much work remains.

1.2 Organization of the Thesis

Chapter 2 is concerned with developing the concepts of noise theory central to quantifying system performance in the RF/microwave spectrum. First, the theory of signal traveling waves is developed and within this context how S-parameters are used to quantify their interaction within distributed systems. Noise-wave concepts are extended from this theory. Important characteristics of noise such as correlation, power spectral density, and noise bandwidth will be highlighted. Finally, network analysis will be used to assess the exchange of noise power between passive terminations.

Chapter 3 focuses on describing the noise behavior of passive and active linear networks through the noise correlation matrix (NCM). First regarding passive, various distributed circuit topologies will be considered each building from the other and culminating with a generalized embedded n -port. The concept of noise temperature will be introduced as an equivalent means for quantifying noise level. Second, in context to active networks, the NCM will be derived for embedded two-port and generalized n -port configurations. It will be shown that from the NCM, figures-of-merit such as noise factor, effective noise temperature, and noise parameters may be derived to describe network performance.

Chapter 4 will derive the NCM of an active network through a series of simulated noise power measurements under varying source termination conditions. This is known as the cold source technique. Noise properties of the source impedance and active noise power measurement receiver will be isolated from the active network of interest using S -parameter representation of the cascaded network. Keysight Technology's Advanced Design System (ADS) simulation software will be used as a verification tool to reinforce the theoretical development and subsequent numerical analysis.

Chapter 5 concentrates on extending the cold source measurement technique to nonlinear networks by use of a relatively new behavioral model known as X -parameters. The chapter opens by describing the familiar S -parameter behavioral model emphasizing its strengths and shortcomings. The X -parameter model will be introduced as a superset to S -parameters addressing the full operational-space of the network. The mathematical framework capturing simultaneous large and small signal responses to input stimuli will be developed. An X -parameter measurement extraction technique of the network employed by a Nonlinear Vector Network Analyzer (NVNA) will be reviewed. With this background, a generalized noise behavioral model for nonlinear (and linear) networks will be derived leveraging X -parameters. Analysis of embedded nonlinear one-port and two-port network configurations are chosen examples to reinforce use of the generalized formalism. Important features such as its reduction to the S -parameter behavioral model thus predicting noise performance within the network's small signal operational-space will be shown. Using ADS, numerical versus experimental results will be

detailed for NL one-port and two-port examples. In context of the two-port case, figures-of-merit including effective noise temperature and noise factor will be determined. Finally, a detailed hardware measurement thought experiment employing an extension of the cold source technique will be developed. Using Keysight's NVNA / PNA-X, measurement and calibration algorithms will be delineated. Specialized hardware requirements for the measurement setup in application of the algorithms will be disclosed. The thought experiments will be offered for both the nonlinear one-port and two-port configurations.

Chapter 6 summarizes the advancements of this work and continues with a suggested road-map for further studies and implementation.

Chapter 2

Signal and Noise-Wave Concepts

To characterize and model the noise behavior of a linear RF/microwave network requires an understanding of noise properties. While under certain conditions noise may share common attributes with deterministic signal types, in general, their properties are quite different. The purpose of this chapter is to highlight those characteristics of noise expected to be central to our purpose of quantifying distributed network noise behavior. In section 2.1, for purpose of developing the concept of traveling waves and scattering parameters, a deterministic signal excitation and response of a distributed network is described. Section 2.2 uses this development to show under proper conditions how traveling noise-waves can be constructed in similar mathematical form to deterministic signal types. In section 2.3 noise characteristics including correlation, auto-correlation, and cross-correlation are reviewed to enhance insight through analysis not only in time but also the frequency domain. Lastly, noise bandwidth will be defined and contrasted to the more common half-power bandwidth. These concepts will be collectively applied in section 2.4 to noise analysis of two one-port terminations connected to a lossless transmission line. The practical implementation of this analysis will be considered.

2.1 Signal Waves and Scattering Parameters

There are two ways microwave energy is transmitted from one location to another [34]. The first is by use of directive antenna aimed at one another whereupon a portion of the radiated energy

transmitted at one end is coupled and delivered to a load at the other. The second is by use of transmission line. A signal source and load typically are matched to their connecting line and separated by its length. In both cases, the transmitted energy can be described as a traveling wave. Within the context of sinusoidal excitation of uniform transmission lines, the concept of traveling waves and their interaction will now be developed.

Maxwell's equations can be used in the analysis of transmission lines. By use of established boundary conditions usually taken at the transmission lines endpoints, signal characteristics can be determined including field pattern and mode of propagation. Alternatively, a distributed electric circuit model of a uniform transmission line can be described. This simpler technique while less comprehensive uses AC circuit theory to describe transmission line impedance and determination of its supported voltage and current propagation characteristics with respect to time and location.

Using a circuit representation as shown in Fig. 2.1, each transmission line section consists of a series resistance R and inductance L , along with shunt conductance G and capacitance C each taken per unit length Δx [35].

AC circuit theory can be employed by choosing Δx to be small compared to the operating wavelength. By applying KVL and KCL to transmission line section - Δx , two differential equations are constructed in the $\lim \Delta x \rightarrow 0$. The first describes the voltage drop across the transmission line due to its series resistance and inductance such that [35]

$$-\frac{\partial v(x,t)}{\partial x} = Ri(x,t) + L \frac{\partial i(x,t)}{\partial t} . \quad (2.1)$$

The second depicts the lessened output current from input due to its shunt conductance and capacitance as shown by [35]

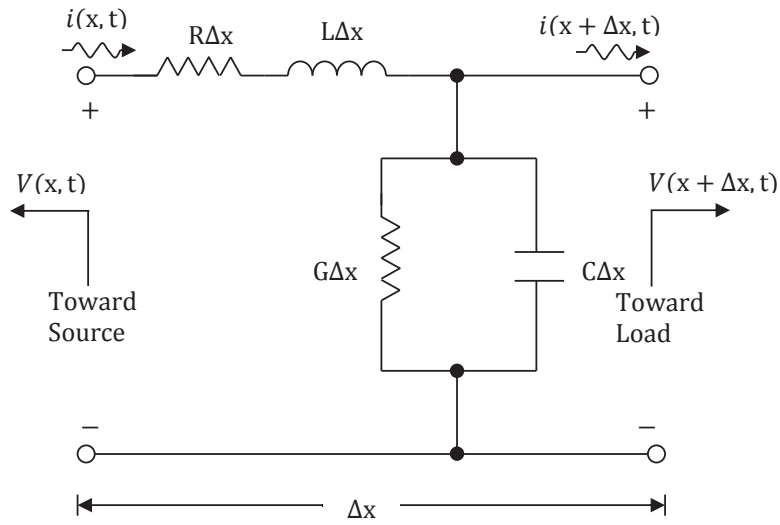


Figure 2.1: Circuit Representation of a Uniform Transmission Line

$$-\frac{\partial i(x, t)}{\partial x} = Gv(x, t) + C \frac{\partial v(x, t)}{\partial t} \quad (2.2)$$

For a sinusoidal stimulus, phasor notation can be applied to (2.1) and (2.2) to solve the steady-state response $v(x, t)$ and $i(x, t)$. The steady-state voltage and current responses along the transmission line will also be sinusoidal and described as a function of position x and time t such that

$$v(x, t) = f(x) \cos(\omega t + \phi_v(x)) \quad (2.3)$$

and

$$i(x, t) = g(x) \cos(\omega t + \phi_i(x)) \quad (2.4)$$

where $f(x)$ and $g(x)$ are real functions [35]. Applying Euler's formula and peak-phasor notation, (2.3) and (2.4) become

$$v(x, t) = \text{Re} \left[f(x) e^{j\phi(x)} e^{j\omega t} \right] = \text{Re} \left[V(x) e^{j\omega t} \right] \quad (2.5)$$

and

$$i(x, t) = \text{Re} \left[g(x) e^{j\phi(x)} e^{j\omega t} \right] = \text{Re} \left[I(x) e^{j\omega t} \right] \quad (2.6)$$

where $V(x)$ and $I(x)$ are phasors describing correspondingly the variation of voltage and current with respect to position along the transmission line [35]. Equations (2.1) and (2.2) can now be expressed in phasor form through substitution of (2.5) and (2.6) such that [36]

$$-\frac{d[V(x)]}{dx} = (R + j\omega L) I(x) \quad (2.7)$$

and

$$-\frac{d[I(x)]}{dx} = (G + j\omega C) V(x). \quad (2.8)$$

Evaluating the derivative of (2.7) with respect to x and substituting (2.8), a second order differential equation in $V(x)$ results in

$$\frac{d^2[V(x)]}{dx^2} = (R + j\omega L)(G + j\omega C)V(x). \quad (2.9)$$

Its solution in phasor form is [36]

$$V(x) = V^+ e^{j\phi^+} e^{-\gamma x} + V^- e^{j\phi^-} e^{\gamma x} \quad (2.10)$$

where V^+ and V^- are real quantities representing peak voltages of the forward and reverse traveling waves respectively. The propagation constant γ is expressed as [36]

$$\gamma = \sqrt{(R + j\omega L)(G + j\omega C)}. \quad (2.11)$$

The propagation constant is typically complex and is written as $\gamma = \alpha + j\beta$ where α is considered the attenuation constant in Np/length and β the phase constant in rad/length.

Referring to Fig. 2.2, a sinusoidal voltage wave $V^+(x) = V^+ e^{j\phi^+} e^{-\gamma x}$ traveling in the positive- x direction is scattered by the load resulting in a sinusoidal voltage wave $V^-(x) = V^- e^{j\phi^-} e^{\gamma x}$ traveling in the negative- x direction [37]. The peak-phasor quantity $V(x)$ is the superposition of $V^+(x)$ and $V^-(x)$ representing the voltage at a specific position x on the transmission line.

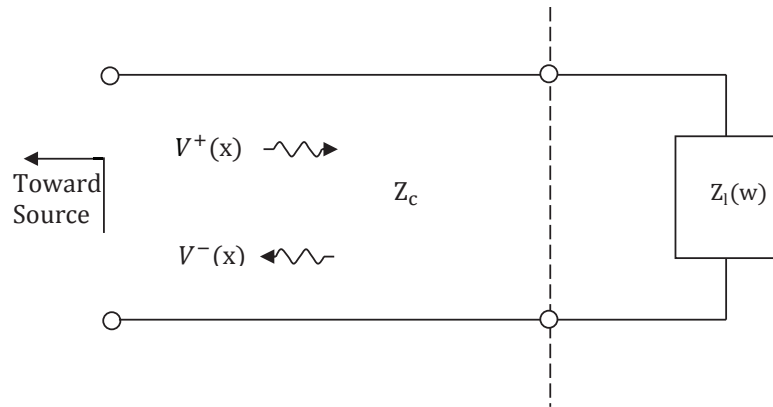


Figure 2.2: Transmission Line Connected to Z_1 with Traveling Waves $V^+(x)$ and $V^-(x)$

Substituting (2.10) into (2.7), evaluating the derivative of $d[V(x)]/dx$ and solving for the current along the transmission line provides the solution [36]

$$I(x) = \frac{1}{Z_c} [V^+(x) - V^-(x)] = I^+(x) - I^-(x). \quad (2.12)$$

Z_c is the complex characteristic impedance of the transmission line and is given as

$$Z_c = \frac{R + j\omega L}{\gamma} = \sqrt{\frac{R + j\omega L}{G + j\omega C}}. \quad (2.13)$$

Z_c is the voltage-to-current ratio of the forward traveling wave (or reverse) and is in units of ohms.

In many practical applications, the loss of the transmission line is considered negligible, i.e. $R = G = 0$. In this case α becomes zero and the propagation constant becomes $\gamma = j\beta$ and $Z_c = Z_o = \sqrt{L/C}$. $V(x)$ in (2.10) and $I(x)$ in (2.12) respectively become

$$V(x) = V^+ e^{j\phi^+} e^{-j\beta x} + V^- e^{j\phi^-} e^{j\beta x} \quad (2.14)$$

and

$$I(x) = \frac{V^+ e^{j\phi^+}}{Z_o} e^{-j\beta x} - \frac{V^- e^{j\phi^-}}{Z_o} e^{j\beta x} \quad (2.15)$$

where $V^+(x) = V^+ e^{j\phi^+} e^{-j\beta x}$ and $V^-(x) = V^- e^{j\phi^-} e^{j\beta x}$ [35].

The time-dependent form of (2.14) and (2.15) are obtained by multiplying phasors $V(x)$ and $I(x)$ respectively by $e^{j\omega t}$ and evaluating the real component thus resulting in [35]

$$v(x, t) = V^+ \cos(\omega t + \phi^+ - \beta x) + V^- \cos(\omega t + \phi^- + \beta x) \quad (2.16)$$

and

$$i(x, t) = \frac{V^+}{Z_o} \cos(\omega t + \phi^+ - \beta x) - \frac{V^-}{Z_o} \cos(\omega t + \phi^- + \beta x). \quad (2.17)$$

The phasor notation described thus far has been in units of peak voltage and current. To consider the average power associated with a traveling wave, the root-mean-square (rms) of the voltage and current is assessed. For a sinusoidal signal, the peak-phasor can be scaled such that [35]

$$V_{rms}(x) = \frac{V(x)}{\sqrt{2}} \quad (2.18)$$

and

$$I_{rms}(x) = \frac{I(x)}{\sqrt{2}} \quad (2.19)$$

Derived from AC circuit theory, the net average (real) power flow at location- x on the transmission line is

$$P(x) = \text{Re} \left[V_{rms}(x) \cdot I_{rms}(x)^* \right] \quad (2.20)$$

where the asterisk symbol "*" is the conjugate of phasor $I_{rms}(x)$ [38]. Similar conclusions may be drawn for power associated with the forward and reverse traveling waves, $P^+(x)$ and $P^-(x)$ respectively. Note, for a lossless line their power is independent of x .

The scattering matrix is an analytic model used to describe the linear behavior of a microwave network [32]. It represents the networks influence through comparison of its incoming and outgoing traveling waves. These waves are typically normalized to the characteristic impedance of the network's connecting transmission lines. The incident normalized voltage wave on a lossy line is defined as [35]

$$a(x) = \frac{V_{rms}^+(x)}{\sqrt{Z_0}} \quad (2.21)$$

and the scattered normalized voltage wave as [35]

$$b(x) = \frac{V_{rms}^-(x)}{\sqrt{Z_0}} \quad (2.22)$$

Described by Fig. 2.3, a lossless transmission line of length- x and characteristic impedance Z_0 is connected on its left by a source and terminated to its right by complex

impedance $Z_1(\omega)$. The source emits incident wave a to its connecting line which then propagates in the $+x$ direction.

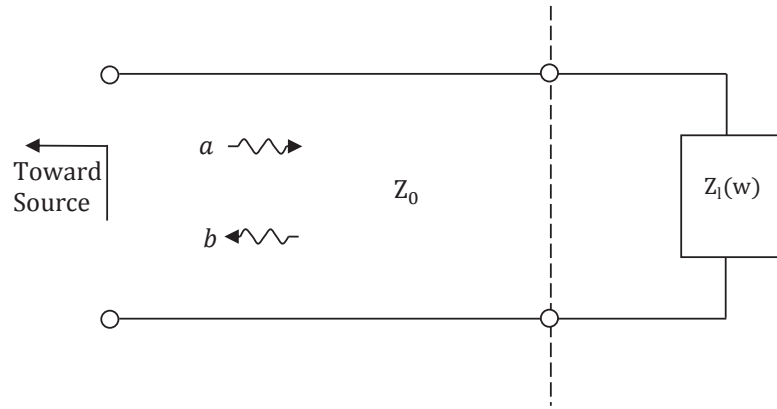


Figure 2.3: Transmission Line Connected to Z_1 with Traveling Waves a and b

Upon reaching Z_1 , the incident wave scatters forming an outgoing b -wave which travels in the minus x direction.

For a lossless line, the wave variables amplitudes are independent of position. The load is described as a one-port network exhibiting a single scattering coefficient defined by [37]

$$b = Sa, \quad (2.23)$$

S is the scattering coefficient describing the mapping of the incident a -wave to the scattered b -wave. Further, it identifies the relationship of the load impedance normalized to its connecting line and given by [37]

$$S(\omega) = \frac{Z_1(\omega) - Z_0}{Z_1(\omega) + Z_0}. \quad (2.24)$$

The a and b -waves represent rms-phasors with units in \sqrt{W} . Since they are normalized to Z_0 , the squared magnitude of their rms values represent their power flow such that

$$P^+ = aa^* = |a|^2 \quad (2.25)$$

and

$$P^- = bb^* = |b|^2. \quad (2.26)$$

To form a complete model of the one-port, the termination noise needs to be included. In the next section, the traveling wave concept will be applied with some modification to analytically describe this noise.

2.2 Traveling Noise-Waves

The one-port model described in Fig. 2.2 does not consider the noise generated by the complex impedance $Z_1(\omega)$. Using traveling wave concepts previously outlined, adaptation of noise to the existing one-port model will now be developed. The results will form a comprehensive signal and noise behavioral model for the one-port which can readily be extended to the general n-port.

The real component of Z_1 is resistive and generates a thermal noise voltage $\hat{v}_t(t)$ as shown in Fig. 2.4. $\hat{v}_t(t)$ is a random process. While measurements from one instant in time to another will generally not repeat, there are statistical properties of the noise which are invariant [35]. First, we observe that its time-average is zero such that

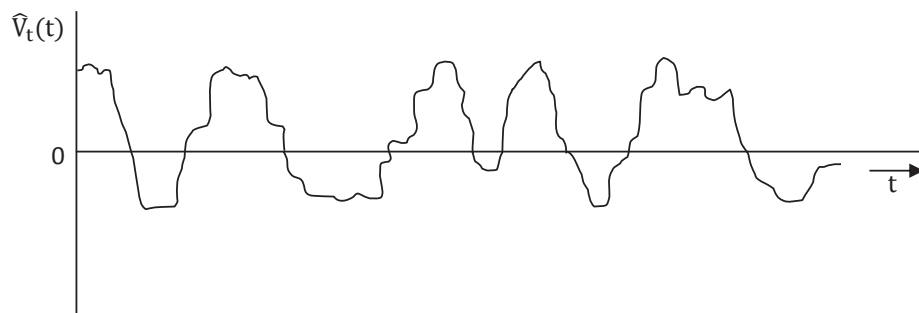


Figure 2.4: Thermal Noise Voltage versus Time [35]

$$\overline{\hat{v}_t} = \lim_{T \rightarrow \infty} \frac{1}{T} \int_{-T/2}^{T/2} \hat{v}_t(t) dt = 0 . \quad (2.27)$$

Second, its time-averaged noise voltage squared is [35]

$$\overline{\hat{v}_t^2} = \lim_{T \rightarrow \infty} \frac{1}{T} \int_{-T/2}^{T/2} \hat{v}_t^2(t) dt = \hat{v}_{t,\text{rms}}^2 . \quad (2.28)$$

At microwave frequencies, the real component of $Z_1(\omega)$ will generate thermal noise which may be represented as a phasor under the condition that the noise is sufficiently restricted to a small bandwidth Δf relative to its center frequency f_c . A description of noise bandwidth requirements is discussed in section 2.4.3. Hence for $\Delta f \ll f_c$, the traveling noise voltage depicted in phasor form is [37]

$$\hat{V}^-(x, t) = \hat{v}^-(t) e^{j\hat{\phi}^-(t)} e^{j\beta x} = \hat{V}^-(t) e^{j\beta x} . \quad (2.29)$$

Referring to (2.29) and Fig. 2.5, it can be seen that $\hat{V}^-(x, t)$ is a traveling noise-wave propagating along a lossless transmission line in the $-x$ direction. In general, it is a function of position x and time t . $\hat{v}^-(t)$ and $\hat{\phi}^-(t)$ are random processes of the noise-wave's amplitude and phase envelope respectively. β is the phase constant at f_c [37]. By use of (2.28) and (2.29), the rms-value of the noise-wave along the lossless transmission line is [35]

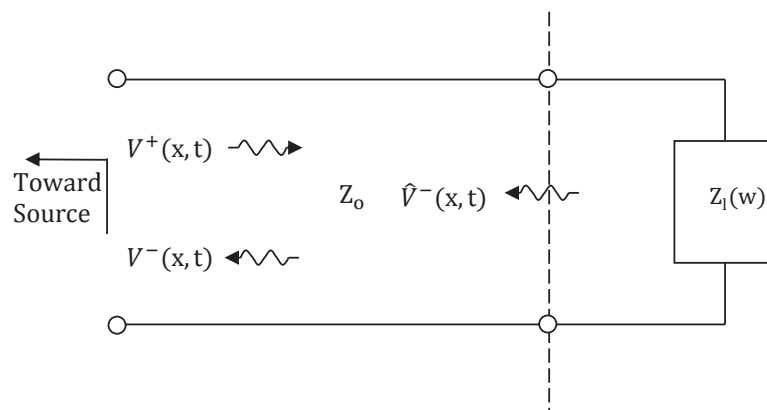


Figure 2.5: One-Port Signal and Noise Model

$$\hat{v}_{\text{rms}}^- = \sqrt{\overline{|\hat{V}^-(x,t)|^2}} = \sqrt{\lim_{T \rightarrow \infty} \frac{1}{T} \int_{-T/2}^{T/2} [\hat{v}^-(t)]^2 dt} \quad (2.30)$$

where the time-averaged magnitude squared of $\hat{V}^-(x,t)$ is $\overline{|\hat{V}^-(x,t)|^2} = \overline{\hat{V}^-(x,t) \cdot \hat{V}^-(x,t)^*}$.

To determine the power associated with (2.29), a normalized noise-wave envelope is defined such that [37, 39]

$$\hat{b}(x,t) = \frac{\hat{V}^-(x,t)}{\sqrt{Z_o}}. \quad (2.31)$$

Multiplying (2.31) on both sides by its complex conjugate yields

$$|\hat{b}(x,t)|^2 = \frac{|\hat{V}^-(x,t)|^2}{Z_o} = \frac{[\hat{v}^-(t)]^2}{Z_o}. \quad (2.32)$$

The time-average of the squared magnitude represents the noise-power associated with $\hat{V}^-(x,t)$ such that [35, 37]

$$\overline{|\hat{b}(x,t)|^2} = \lim_{T \rightarrow \infty} \frac{1}{T} \int_{-T/2}^{T/2} |\hat{b}(x,t)|^2 dt = \frac{1}{Z_o} \lim_{T \rightarrow \infty} \frac{1}{T} \int_{-T/2}^{T/2} [\hat{v}^-(t)]^2 dt. \quad (2.33)$$

$\overline{|\hat{b}(x,t)|^2}$ is the mean-squared value of the noise-wave envelope associated with the traveling noise-wave $\hat{V}^-(x,t)$ normalized to Z_o . The units for $\overline{|\hat{b}(x,t)|^2}$ is watts. It will be shown in section 2.3.4 to be a function of the measurement bandwidth Δf and its center frequency f_c .

The model may now be augmented to include the noise contribution of the load termination as depicted below in Fig. 2.6. The scattered wave now includes both signal and noise

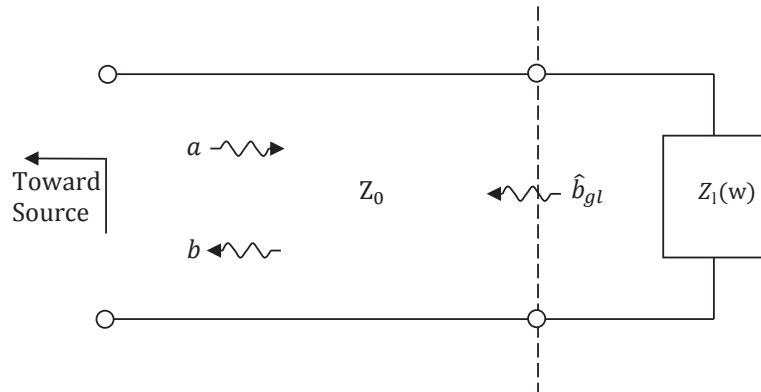


Figure 2.6: Transmission Line Connected to Z_1 and Traveling Waves a , b , and \hat{b}_{gl}

behavior of load termination Z_1 such that [37, 39]

$$b = Sa + \hat{b}_{gl} . \quad (2.34)$$

Thus, the termination's signal behavior is described by S and its generated noise by \hat{b}_{gl} [20, 37].

This concept may readily be extended to an n -port network. However, greater appreciation for this more complicated multiport description can be realized by first acquiring an understanding of noise characteristics including correlation, noise-power spectral density, and noise bandwidth as will be outlined in the forthcoming section.

2.3 Noise-Wave Characteristics

To quantify the strength of a deterministic signal, its peak, mean-square, or root-mean-square value is commonly reported [40]. In a resistive network operating at low frequency, they are mathematically described as amplitude signals where the phase of the signal is of no concern. In most practical applications capacitors and inductors are present, i.e. complex impedances, and phasor notation is used to describe the signals magnitude and phase [40]. This is certainly the

case at higher frequency where the circuits are no longer considered lumped element but treated as distributive networks.

Non-deterministic signals such as noise do not have a peak value. Noise is a random signal and does not possess a mathematically describable function. However, if the signals statistics are known, conclusion may be drawn as to its strength. For noise, the mean-square value or root-mean-square value are commonly used [40]. In the case of distributive networks, it is convenient to describe noise-signal behavior in terms of a phasor involving two random processes, magnitude and phase.

In circuit analysis, there is an occasional need to sum two or more signals simultaneously present at a node or on a transmission line. For deterministic signals, such as sinusoids, the individual functions are summed [40]. That is each signal may be viewed a phasor, i.e. vector, the sum of which represents the aggregate signal. For non-deterministic signals, such as noise, the square root of the mean-square sum of the noise contributors is required [40]. The value of this sum depends on the correlation the noise contributors have with respect to one another. It also depends on the noise bandwidth Δf to which the noise is confined and its center frequency of operation f_c . In the upcoming sections, two important concepts will be developed, correlation and noise bandwidth.

2.3.1 Correlation

Consider two normalized noise voltage-waves \hat{X} and \hat{Y} traveling in the same direction on a given transmission line. The total noise-wave \hat{Z} is [20, 40]

$$\hat{Z} = \hat{X} + \hat{Y} \quad . \quad (2.35)$$

The power associated with noise wave \hat{Z} confined to noise bandwidth Δf is [20, 40]

$$\Delta \hat{P}_z = \overline{\hat{Z}\hat{Z}^*} = \overline{(\hat{X} + \hat{Y}) \cdot (\hat{X} + \hat{Y})^*} . \quad (2.36)$$

If the entirety of the two noise sources is derived by their own physical phenomenon, their amplitude distributions are independent. Being that they share nothing in common, their inner products are $\overline{\hat{X}\hat{Y}^*} = \overline{\hat{Y}\hat{X}^*} = 0$. \hat{X} and \hat{Y} are orthogonal to one another [20, 40]. Noise-waves which are orthogonal are said to be uncorrelated. Thus, the power associated with noise-wave \hat{Z} under this condition may be stated as

$$\Delta \hat{P}_z = \overline{\hat{Z}\hat{Z}^*} = \overline{\hat{X}\hat{X}^*} + \overline{\hat{Y}\hat{Y}^*} \quad (2.37)$$

where $\Delta \hat{P}_z$ represents the sum of the noise-powers of the \hat{X} and \hat{Y} noise waves.

If the amplitude distribution of the two noise-waves are dependent, then a similarity between them is present. Their power will combine but not as the direct sum of their constituent components as in the uncorrelated case. Noise-waves exhibiting dependency are said to cohere. Such waves are produced at least in-part from the same physical phenomenon. The magnitude and phase of the noisy disturbances are related by a complex number known as the correlation factor where [20, 40]

$$C = \frac{\overline{\hat{X}\hat{Y}^*}}{\sqrt{\overline{\hat{X}\hat{X}^*} \cdot \overline{\hat{Y}\hat{Y}^*}}} . \quad (2.38)$$

The correlation factor is a measure of their similarity. Zero represents no correlation and unity full correlation thus the magnitude of C is bounded by the interval $0 \leq |C| \leq 1$

The magnitude of C describes the portion of noise-power which is common to noise-waves \hat{X} and \hat{Y} relative to the square-root of the product of their respective magnitudes. The argument of C describes the relative phase of the portion of \hat{X} and \hat{Y} which are in common.

Since the path two correlated noise-waves take can be different, the relative phase is dependent on the difference of their path lengths [20].

The resultant noise-power of correlated noise-waves \hat{X} and \hat{Y} will generally produce an interference effect. $\Delta\hat{P}_z$ is [20, 40]

$$\begin{aligned}\Delta\hat{P}_z &= \overline{\hat{X}\hat{X}^*} + \overline{\hat{X}\hat{Y}^*} + \overline{\hat{Y}\hat{X}^*} + \overline{\hat{Y}\hat{Y}^*} \\ &= \overline{\hat{X}\hat{X}^*} + \overline{\hat{Y}\hat{Y}^*} + (C+C^*)\sqrt{\overline{\hat{X}\hat{X}^*}\cdot\overline{\hat{Y}\hat{Y}^*}}.\end{aligned}\quad (2.39)$$

Depending on their relative phase, constructive or destructive interference will result due to their coherence. Destructive interference yields a $\Delta\hat{P}_z$ value less than the noise power sum of its constituent components. Constructive interference produces a sum which is greater.

An interesting special case is when the relative phase between correlated noise-waves is $\pm\pi/2$ [20]. The inner product of $\overline{\hat{X}\hat{Y}^*}$ is zero leading to a total noise-wave power $\Delta\hat{P}_z$ which is equal to its constituent components, the same power as in the uncorrelated noise-wave case. In general, the presence of interference will result in variation of the noise-power spectral density with respect to frequency.

2.3.2 Auto-Correlation and Power Spectral Density

So far, attention has been solely directed to the time domain analysis of traveling noise-waves. An understanding of noise-wave characteristics can be augmented through their study in the frequency domain. For example, determining the noise-behavior of a linear multiport involves assessment of the auto- and cross-correlation of its noise-waves. To that end, this involves quantifying their associated noise-power spectral density.

Consider a single normalized noise-voltage wave $\hat{b}_1(t)$ traveling on a lossless transmission line. Due to its nonfinite signal energy [41]

$$E = \int_{-\infty}^{\infty} \hat{b}_1(t) \hat{b}_1(t)^* dt = \infty. \quad (2.40)$$

The squared magnitude of $\hat{b}_1(t)$ evaluated over the time interval $(-\infty, \infty)$ cannot be integrated. Also, its Fourier transform does not exist. An alternative is to determine the noise-power spectral density of the complex function $\hat{b}_1(t)$ through use of its average auto-correlation function $\overline{\varphi_{\hat{b}_1 \hat{b}_1^*}(\tau)}$ [41, 42]. By definition

$$\overline{\varphi_{\hat{b}_1 \hat{b}_1^*}(\tau)} = \lim_{T \rightarrow \infty} \frac{1}{T} \left[\int_{-T/2}^{T/2} \hat{b}_1^*(t) \cdot \hat{b}_1(t + \tau) dt \right] \quad (2.41)$$

where T is the averaging time over which the noise-wave is observed [41]. $\overline{\varphi_{\hat{b}_1 \hat{b}_1^*}(\tau)}$ is the time-averaged energy of noise wave $\hat{b}_1(t)$. By evaluating the Fourier transform of $\overline{\varphi_{\hat{b}_1 \hat{b}_1^*}(\tau)}$, (2.41) becomes [41]

$$\int_{-\infty}^{\infty} \overline{\varphi_{\hat{b}_1 \hat{b}_1^*}(\tau)} e^{-j\omega\tau} d\tau = \int_{-\infty}^{\infty} \left[\lim_{T \rightarrow \infty} \frac{1}{T} \int_{-T/2}^{T/2} \hat{b}_1^*(t) \cdot \hat{b}_1(t + \tau) dt \right] e^{-j\omega\tau} d\tau. \quad (2.42)$$

Re-ordering the integration yields

$$\begin{aligned} &= \lim_{T \rightarrow \infty} \frac{1}{T} \left[\int_{-T/2}^{T/2} \hat{b}_1^*(t) \cdot e^{j\omega t} dt \int_{-T/2}^{T/2} \hat{b}_1(t + \tau) \cdot e^{-j\omega(t+\tau)} d\tau \right] \\ &= \lim_{T \rightarrow \infty} \frac{1}{T} \left\{ \left[\int_{-T/2}^{T/2} \hat{b}_1(t) \cdot e^{-j\omega t} dt \right]^* \left[\int_{-T/2}^{T/2} \hat{b}_1(x) \cdot e^{-j\omega x} dx \right] \right\} \end{aligned}$$

where $x = t + \tau$ and $dx = d\tau$.

Evaluating the Fourier transform of the first and second integrals provides [41]

$$\begin{aligned} \int_{-\infty}^{\infty} \overline{\varphi_{\hat{b}_1 \hat{b}_1^*}(\tau)} e^{-j\omega\tau} d\tau &= \lim_{T \rightarrow \infty} \frac{1}{T} [\hat{B}_1^*(\omega) \hat{B}_1(\omega)] \\ &= \lim_{T \rightarrow \infty} \frac{1}{T} |\hat{B}_{11}(\omega)|^2 . \end{aligned} \quad (2.43)$$

where $\hat{B}_1(\omega)$ is the frequency domain representation of $\hat{b}_1(t)$. Equation (2.43) describes the time-averaged energy spectral density, i.e. power spectral density of noise-wave $\hat{b}_1(t)$.

Parseval's Theorem for finite signal energy whose functions are complex values of t is [41]

$$E = \int_{-\infty}^{\infty} |f(t)|^2 dt = \frac{1}{2\pi} \int_{-\infty}^{\infty} |F(\omega)|^2 d\omega \quad (2.44)$$

For nonfinite energy signals, the energy E is infinite. In (2.43), as the interval $T \rightarrow \infty$, the energy density $|\hat{B}_{11}(\omega)|^2 \rightarrow \infty$. Hence the quantity $|\hat{B}_{11}(\omega)|^2/T$ may approach a limit as in the case of an assumed ergodic process. As such [41]

$$\hat{P} = \text{Total Signal Power} = \frac{1}{2\pi} \lim_{T \rightarrow \infty} \frac{1}{T} \int_{-\infty}^{\infty} |\hat{B}_{11}(\omega)|^2 d\omega . \quad (2.45)$$

Limiting the analysis to a finite bandwidth and noting the two-sidedness of the frequency spectrum yields [41]

$$\begin{aligned} \Delta \hat{P}_{11} &= 2 \cdot \frac{1}{2\pi} \lim_{T \rightarrow \infty} \frac{1}{T} \int_{\omega_1}^{\omega_2} |\hat{B}_{11}(\omega)|^2 d\omega \\ &= 2 \cdot \lim_{T \rightarrow \infty} \frac{1}{T} \int_{f_1}^{f_2} |\hat{B}_{11}(f)|^2 df . \end{aligned} \quad (2.46)$$

$\Delta \hat{P}_{11}$ is the power confined to $\Delta f = f_2 - f_1$. For a sufficiently narrow Δf , the power spectral density may be treated as a constant across its bandwidth such that (2.46) becomes [37, 41]

$$\Delta \hat{P}_{11} = 2 |\hat{B}_{11}(f_c)|^2 \Delta f . \quad (2.47)$$

$\overline{2|\hat{B}_{11}(f_c)|^2}$ is the time-averaged energy spectral density of $\hat{b}_1(t)$ at center frequency f_c and confined to Δf . $\Delta\hat{P}_{11}$ is the noise-power deliverable to a noiseless matched termination due to the $\hat{b}_1(t)$ noise-wave. The noise-power spectral density associated with $\hat{b}_1(t)$ will be represented in the frequency domain by $\overline{\hat{b}_1\hat{b}_1^*}$ such that [37]

$$\overline{\hat{b}_1\hat{b}_1^*} \approx \frac{\Delta\hat{P}_{11}}{\Delta f} = 2\overline{|\hat{B}_{11}(f_c)|^2}. \quad (2.48)$$

It's important to note that the noise bandwidth Δf need be narrow enough such that the noise-power spectral density is treated as a constant across its interval [37]. There are factors which need be considered to ensure this condition. This will be addressed in Section 2.4.3. For now, we assume this condition is true and the above expression valid.

2.3.3 Cross-Correlation and Power Spectral Density

More than one noise-wave may travel on the same transmission line and in the same direction. These noise-waves may or may not be correlated. Subsequently, their dependence will influence the noise-power spectral density at a given frequency. Beginning with the definition of the averaged cross-correlation function [41, 42]

$$\overline{\varphi_{\hat{b}_1\hat{b}_2}(\tau)} = \lim_{T \rightarrow \infty} \frac{1}{T} \left[\int_{-T/2}^{T/2} \hat{b}_1^*(t) \cdot \hat{b}_2(t + \tau) \right] dt \quad (2.49)$$

and applying an analogous approach as outlined in Section 2.3.2, it can be shown that the cross noise-power spectral density between $\hat{b}_1(t)$ and $\hat{b}_2(t)$ is [37]

$$\overline{\hat{b}_1\hat{b}_2^*} \approx \frac{\Delta\hat{P}_{12}}{\Delta f} = 2\overline{\hat{B}_1(f_c)\hat{B}_2^*(f_c)}. \quad (2.50)$$

Equations (2.48) and (2.50) may be combined to form a general expression for relating the comparison of any two noise-waves. Let i represent one noise-wave, and j the second. From this

$$\overline{\hat{b}_i \hat{b}_j^*} \approx \frac{\Delta \hat{P}_{ij}}{\Delta f} = 2 \overline{\hat{B}_i(f_c) \hat{B}_j^*(f_c)} = \hat{\Phi}_{ij}(f_c), \quad (2.51)$$

where $\hat{\Phi}_{ij}(f_c)$ is the noise-power spectral density of two processes, $\hat{B}_i(f_c)$ and $\hat{B}_j(f_c)$, each centered at frequency f_c and within Δf [37]. $\overline{\hat{b}_i \hat{b}_j^*}$ is the self-power spectral density when $i = j$. The cross-power spectral density is the case for which $i \neq j$. Later, we will use (2.51) to analytically define the noise behavior of a linear multiport network in the frequency domain.

In this writing, frequent reference has been made to the noise bandwidth Δf . As shown, the noise-power spectral density is dependent on the bandwidth under which the noise is evaluated. Unlike the half power or -3 dB bandwidth commonly specified for discrete signals, the noise bandwidth of a filter differs in that it's defined for white noise signals. Understanding this difference and how it applies to noise analysis is the subject of the next section.

2.3.4 Noise Bandwidth

It is common that a filter's passband be specified in terms of its -3dB bandwidth. The bandwidth is regarded as a range in frequency over which the filter's transfer function is within half-power of its maximum gain which will be denoted $|H_0|^2$. The filter may be determined through analytical evaluation of its transfer function or in measurement by sweeping a sinusoidal signal frequency and determining its half-power (corner frequency) location(s) [40].

The effective noise bandwidth, heretofore referred to as Δf_n of the filter is different. Its transfer function is regarded as having a "brick-wall" shape with constant gain across its passband. The noise bandwidth is chosen to pass the equivalent noise-power to that of the actual

filter. Thus, it can be used in noise analysis to relate the power measured at the output of the actual filter to the power spectral density of the incoming noise-signal of interest [40]. While a filter's -3 dB bandwidth is commonly used for deterministic signal types, its noise bandwidth is specified for nondeterministic signals such as white noise.

To clarify the meaning of Δf in (2.51), i.e. Δf_n , consider that the noise-power at the output of a filter may be determined by [40]

$$\hat{P}_{o1} = \int_0^{\infty} \hat{\Phi}_{ij}(f) \cdot |H(j2\pi f)|^2 df . \quad (2.52)$$

$\hat{\Phi}_{ij}(f)$ and $|H(j2\pi f)|^2$ are the filter's input noise-power spectral density and transfer function respectively. If the incoming signal's noise-power spectral density is a constant across df then (2.52) becomes [40]

$$\hat{P}_{o1} = \hat{\Phi}_{ij} \int_0^{\infty} |H(j2\pi f)|^2 df . \quad (2.53)$$

Now consider an ideal bandpass filter with constant gain $|H_o|^2$. The total noise-power assessed at its output for the same signal input is [40]

$$\hat{P}_{o2} = \int_0^{\infty} \hat{\Phi}_{ij}(f) |H_o|^2 df . \quad (2.54)$$

Similarly, if the incoming signal's noise-power spectral density is constant across df then (2.54) becomes [40]

$$\hat{P}_{o2} = \hat{\Phi}_{ij} |H_o|^2 \Delta f_n . \quad (2.55)$$

Using (2.53) and (2.55), Δf_n is chosen such that $\hat{P}_{o1} = \hat{P}_{o2}$ yielding a noise bandwidth [40]

$$\Delta f_n = \frac{1}{|H_o|^2} \int_0^{\infty} |H(j2\pi f)|^2 df . \quad (2.56)$$

The noise bandwidth depicts an ideal bandpass filter exhibiting bandwidth Δf_n set such that it will pass the same noise-power as the actual bandpass filter.

Fig. 2.7 compares graphically the transfer function of each. Notice the ideal filter gain is set at maximum $|H_0|^2$ of the actual bandpass. Under these conditions, the area under the two

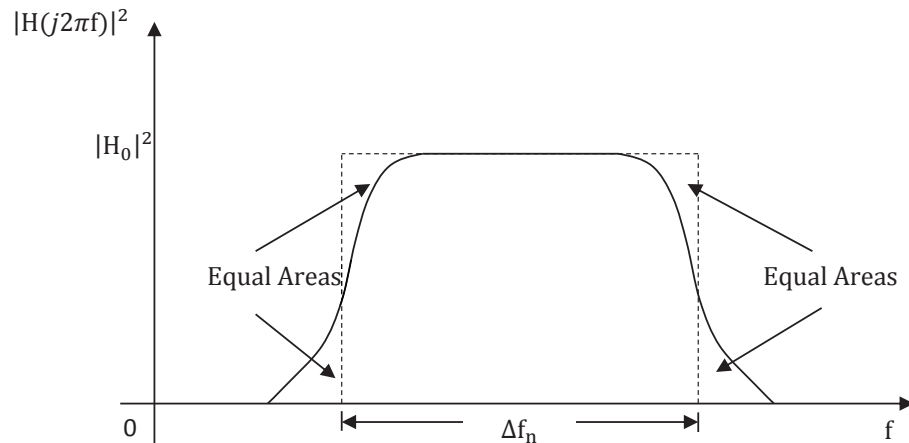


Figure 2.7: Graphical Description of a Bandpass Filter's Noise Bandwidth

curves are equal. In this example, a bandpass filter was chosen to define noise bandwidth. The same approach can be applied for lowpass filtering [40].

Should the input signal's noise-power spectral density be a constant then (2.53), (2.55), and (2.56) apply. In this work, upcoming attention will be given to network analysis through judicious use of noise-power measurements. The noise bandwidth may be determined in calibration by use of a broadband white noise source. In this way, the measurement receiver's gain and bandwidth may be applied in (2.56) to determine Δf_n . Following calibration, (2.51) may be used to assess the noise behavior $\overline{\hat{b}_i \hat{b}_j^*}$ of a device under test.

But first, the measurement system's electrical properties need be considered to ensure that noise-power spectral density of the input signal is a constant across a chosen noise bandwidth. Such criteria will be outlined in the next section by use of an example.

2.4 Network Analysis of Two Noisy Passive One-Ports

Using previously developed concepts, noise-wave equations can be formulated to determine the flow of noise-power within a distributed network. The validity of its implementation can only be justified under restricted conditions. An example of this analysis will be given using two passive one-ports connected by a lossless line. The basis of this development will follow by outlining the required conditions of the measurement system.

2.4.1 Noise-Wave Formalism

Shown in Fig. 2.8 is a lossless transmission line of length L terminated to its left and right by resistive loads R_1 and R_2 respectively [20]. Reference planes for R_1 and R_2 show the location to which the terminations are connected to the line and from it the match that each presents as noted by real reflection coefficients Γ_1 and Γ_2 respectively. Consistent with (2.31), \hat{b}_{gl_1} and \hat{b}_{gl_2} are normalized noise-wave sources produced by passive terminations R_1 and R_2 respectively; each are injected into the transmission line. They will be regarded as uncorrelated to one another.

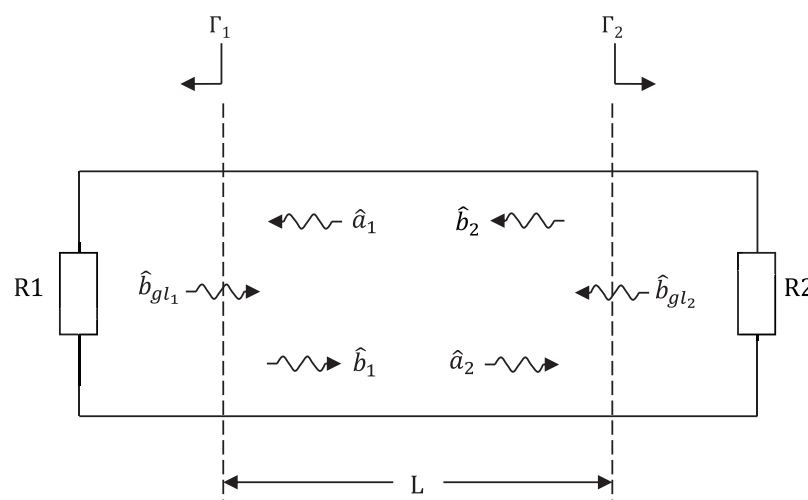


Figure 2.8: Two Passive One-Ports Connected by a Lossless Transmission Line

Consistent with the one-port model described in (2.34) and by inspection of Fig. 2.8, the normalized incident and scattered waves at port 1 are [20]

$$\hat{a}_1 = \hat{b}_2 e^{-j\beta L} \quad (2.57)$$

and

$$\hat{b}_1 = \Gamma_1 \hat{a}_1 + \hat{b}_{gl_1} \quad (2.58)$$

respectively where β is the phase constant taken at f_c . Similarly, the normalized incident and scattered waves at port 2 are

$$\hat{a}_2 = \hat{b}_1 e^{-j\beta L} \quad (2.59)$$

and

$$\hat{b}_2 = \Gamma_2 \hat{a}_2 + \hat{b}_{gl_2} \quad (2.60)$$

Manipulation of (2.57) – (2.60) may be used to express incident and scattered transmission noise-waves at port 1 (or port 2) in terms of noise wave sources \hat{b}_{gl_1} and \hat{b}_{gl_2} such that [20]

$$\hat{a}_1 = \frac{\Gamma_2 e^{-j2\beta L} \hat{b}_{gl_1} + e^{-j\beta L} \hat{b}_{gl_2}}{1 - \Gamma_1 \Gamma_2 e^{-j2\beta L}} \quad (2.61)$$

and

$$\hat{b}_1 = \frac{\hat{b}_{gl_1} + \Gamma_1 e^{-j\beta L} \hat{b}_{gl_2}}{1 - \Gamma_1 \Gamma_2 e^{-j2\beta L}} \quad (2.62)$$

respectively. From (2.61) and (2.62), it's evident that noise-wave sources \hat{b}_{gl_1} and \hat{b}_{gl_2} radiating into the ends of the connecting line each contribute to the construction of transmission noise-

waves \hat{a}_1 and \hat{b}_1 by their interaction with the composite network. These expressions can be used to assess the exchange of noise-power between terminations R1 (port 1) and R2 (port 2).

2.4.2 Exchangeable Noise-Power

The exchangeable noise-power between the one-ports in Fig. 2.8 can be used to determine the portion of noise-power generated by one termination and absorbed in the other. From (2.61), the noise-power per Hertz incident to the one-port on the left-side of Fig. 2-8 is obtained by evaluating the time-averaged product of \hat{a}_1 with its complex conjugate. Multiplying factors and recognizing the noise-wave sources are uncorrelated, i.e. $\overline{\hat{b}_{g1} \hat{b}_{g2}^*} = \overline{\hat{b}_{g2} \hat{b}_{g1}^*} = 0$, yields [20]

$$\hat{\Phi}_{\hat{a}_1} = \overline{\hat{a}_1 \hat{a}_1^*} = \frac{|\Gamma_2|^2 \overline{|\hat{b}_{g1}|^2} + \overline{|\hat{b}_{g2}|^2}}{(1 - \Gamma_1 \Gamma_2 e^{-j2\beta L}) \cdot (1 - \Gamma_1^* \Gamma_2^* e^{j2\beta L})}. \quad (2.63)$$

Evaluated in a 1 Hz noise bandwidth, $\overline{\hat{a}_1 \hat{a}_1^*}$ is equivalent to the noise-power exchanged from right-to-left. If $\Gamma_1 \Gamma_2 e^{-j2\beta L} = 1$, the system will resonate. This condition can be avoided by inserting a small attenuation to the connecting line. In most practical applications, this is the case and is so in our work, therefore in general $\Gamma_1 \Gamma_2 e^{-j2\beta L} \neq 1$.

By similar approach, the power spectral density of scattered wave \hat{b}_1 ascribed at port 1 can be determined using (2.62) resulting in [20]

$$\hat{\Phi}_{\hat{b}_1} = \overline{\hat{b}_1 \hat{b}_1^*} = \frac{\overline{|\hat{b}_{g1}|^2} + |\Gamma_1|^2 \overline{|\hat{b}_{g2}|^2}}{(1 - \Gamma_1 \Gamma_2 e^{-j2\beta L}) \cdot (1 - \Gamma_1^* \Gamma_2^* e^{j2\beta L})}. \quad (2.64)$$

Assessed in a 1 Hz noise bandwidth, $\overline{\hat{b}_1 \hat{b}_1^*}$ is the noise-power exchanged from left-to-right.

The transfer of noise-power generated by one termination and delivered to the second can be determined by use of (2.63) and/or (2.64). For example, the noise-power emitted by termination R1 into its connecting line is $\overline{|\hat{b}_{g1}|^2}$. $\overline{|\hat{b}_{g1}|^2}$ travels left-to-right. At the termination R2 plane a portion of $\overline{|\hat{b}_{g1}|^2}$ is reflected. The remainder is absorbed in the R2 one-port such that [20]

$$\Delta\hat{P}_{21} = \frac{\overline{|\hat{b}_{g1}|^2} (1 - |\Gamma_2|^2)}{(1 - \Gamma_1\Gamma_2 e^{-j2\beta L}) \cdot (1 - \Gamma_1^* \Gamma_2^* e^{j2\beta L})} \cdot \Delta f_n . \quad (2.65)$$

$\Delta\hat{P}_{21}$ is the portion of noise-power confined to a noise bandwidth Δf_n that is generated by R1 and dissipated in R2. If the one-ports are matched to the connecting line, the full $\overline{|\hat{b}_{g1}|^2}$ is dissipated in R2. For an unmatched condition, $\Delta\hat{P}_{21}$ is magnified due to multiple reflections as indicated in the denominator of (2.65).

The noise-power restricted to Δf_n that is emitted by termination R1 and dissipated in R1 is [20]

$$\Delta\hat{P}_{11} = \left(\overline{|\hat{b}_{g1}|^2} \cdot \Delta f_n - \Delta\hat{P}_{21} \right) \cdot (1 - |\Gamma_1|^2) . \quad (2.66)$$

Similar expressions may be generated for the noise-power emitted by the one-port R2 and dissipated in R1 as well as that portion emitted by R2 and dissipated in R2.

Qualifying noise performance of RF/microwave components and systems is central to this work. In practice, it will require evaluating noise-power quantities in a measurement bandwidth $\Delta f_n \gg 1$ Hz. The valid use of the noise-wave formalism described in (2.57) – (2.60) requires that the noise-power spectral density across the measurement bandwidth be constant. Thus, the interference effects due to correlated noise-waves are uniform across Δf_n [20]. To preserve

noise-wave formalism, the measurement system conditions required for a sufficiently narrow Δf_n will now be described.

2.4.3 Constraints on Validity of Analysis

Expression (2.65) describes the portion of noise-power $\Delta \hat{P}_{21}$ generated by resistor R1 in a 1Hz bandwidth that is dissipated in R2. In practical applications, the measurement bandwidth Δf_n will likely be wider than 1Hz. This leads to the question, what constraints need be placed on Δf_n such that (2.65) remain true?

We begin by considering an arbitrary noise-power spectral density $\hat{\Phi}(f)$ over a given frequency range such that

$$\frac{d\hat{P}}{df} = \hat{\Phi}(f) . \quad (2.67)$$

As described in Fig. 2.9, $\hat{\Phi}(f)$ in general varies over Δf_n . The total power confined to this bandwidth is

$$\Delta \hat{P} = \int_{f_1}^{f_2} \hat{\Phi}(f) df \quad (2.68)$$

where $df \ll \Delta f_n$.

In (2.65), $\Delta \hat{P}_{21}$ is expressed in terms of phase constant β . Rewriting the above relation [20],

$$\Delta \hat{P}_{21} = \int_{\beta_1}^{\beta_2} \hat{\Phi}(\beta) d\beta \quad (2.69)$$

where $\beta \equiv 2\pi/\lambda = (2\pi/v_g)f$ and $\lambda \equiv v_g/f$. Re-stating the question, what is the constraint for $\Delta\beta$ over which $\hat{\Phi}_{21}(\beta)$ can be considered a constant, i.e. $\hat{\Phi}_{21}(\beta) \approx \hat{\Phi}_{21}(\bar{\beta})$, and simple integration may be performed such that $\Delta\hat{P}_{21} \approx \hat{\Phi}_{21}(\bar{\beta})\Delta\beta$?

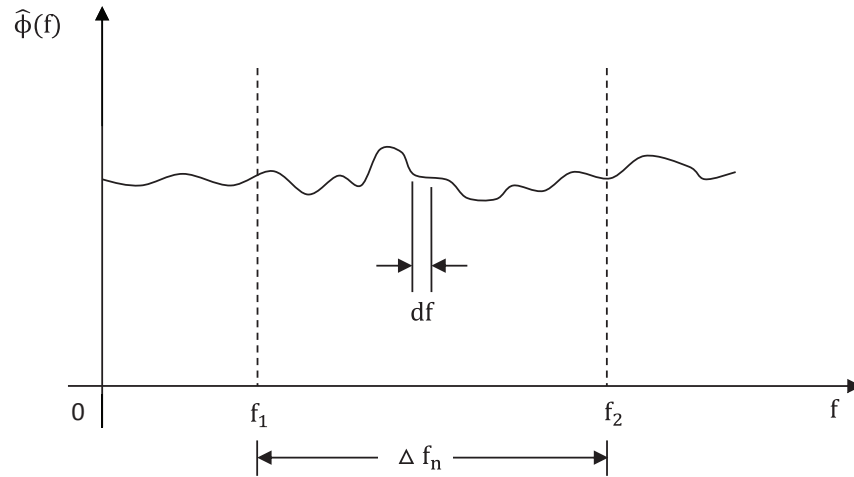


Figure 2.9: Input-Noise Power Spectral Density $\hat{\Phi}(f)$ Across Δf_n

Equation (2.65) describing $\Delta\hat{P}_{21}$ in accordance with Fig. 2.8 can be written as a function of β such that [20]

$$\hat{\Phi}_{21}(\beta) = \frac{d\hat{P}_{21}}{d\beta} = \frac{\overline{|\hat{b}_{g1}|^2} (1 - |\Gamma_2|^2)}{(1 - \Gamma_1 \Gamma_2 e^{-j2\beta L}) \cdot (1 - \Gamma_1^* \Gamma_2^* e^{j2\beta L})} \cdot \quad (2.70)$$

Multiplying denominator factors in (2.70) and noting in this example that Γ_1 and Γ_2 are real quantities, the noise-power density may be stated as [20]

$$\hat{\Phi}_{21}(\beta) = \frac{\overline{|\hat{b}_{g1}|^2} (1 - |\Gamma_2|^2)}{1 - 2\Gamma_1 \Gamma_2 \cos 2\beta L + |\Gamma_1|^2 |\Gamma_2|^2} \quad (2.71)$$

where Euler's equation is used in its determination.

The magnitude of the relative variation of $\hat{\Phi}_{21}(\beta)$ can be determined by evaluating the derivative of (2.71) with respect to β and ratioing it to $\hat{\Phi}_{21}(\beta)$ such that [20]

$$\left| \frac{\Delta \hat{\Phi}_{21}(\beta)}{\hat{\Phi}_{21}(\beta)} \right| = \left| \frac{2\Gamma_1\Gamma_2 \sin 2\beta L}{1 - 2\Gamma_1\Gamma_2 \cos 2\beta L + |\Gamma_1|^2 |\Gamma_2|^2} \right| \cdot 2L\Delta\beta \quad (2.72)$$

where $\Delta\beta$ is the variation of β over Δf_n .

The first factor to the right-hand side of (2.72) attains a maximum value when β satisfies

$$\cos 2\beta L = \frac{2\Gamma_1\Gamma_2}{1 + |\Gamma_1|^2 |\Gamma_2|^2} . \quad (2.73)$$

Substituting (2.73) into (2.72), an inequality applying to all values of β is algebraically reduced to form [20]

$$\left| \frac{\Delta \hat{\Phi}_{21}(\beta)}{\hat{\Phi}_{21}(\beta)} \right| \leq \left| \frac{2\Gamma_1\Gamma_2}{1 - |\Gamma_1|^2 |\Gamma_2|^2} \right| \cdot 2L\Delta\beta . \quad (2.74)$$

A relative variation of $\Delta \hat{\Phi}_{21}(\beta)$ better than epsilon is required such that the variation of $\Delta\beta$ is restricted by [20]

$$\left| \frac{\Delta \hat{\Phi}_{21}(\beta)}{\hat{\Phi}_{21}(\beta)} \right| \leq \left| \frac{2\Gamma_1\Gamma_2}{1 - |\Gamma_1|^2 |\Gamma_2|^2} \right| \cdot 2L\Delta\beta < \varepsilon . \quad (2.75)$$

ε is defined over the interval $0 < \varepsilon \ll 1$. Substituting the relation $\Delta\beta = (2\pi/v_g)\Delta f_n$ into (2.75) and solving the inequality for the effective noise bandwidth yields [20]

$$\Delta f_n < \frac{\varepsilon}{2\pi} \left| \frac{1 - |\Gamma_1|^2 |\Gamma_2|^2}{4\Gamma_1\Gamma_2} \right| \cdot \frac{v_g}{L} . \quad (2.76)$$

The boundary condition established in (2.76) is known as the spot noise criterion [20]. The measurement system used to judge a device's noise behavior needs to adhere to the above inequality. As $|\Gamma_1|^2 |\Gamma_2|^2$ approaches one, Δf_n must be very small. Alternatively, if $|\Gamma_1|^2 |\Gamma_2|^2 \ll 1$ then Δf_n can be broadband and still satisfy the spot noise criterion. This condition for $\Gamma_1 \Gamma_2$ is known as a quasi-match [20].

For example, with respect to Fig. 2.8, consider a measurement system with resistors R1 and R2 presenting a 20dB return loss relative to their connected 50 ohm teflon-based transmission line of length $L = 2\text{m}$. Assuming an epsilon of 0.1, the spot noise criterion is satisfied for an effective noise bandwidth up to $\approx 40\text{MHz}$. Generally, this is easily satisfied in practice given that common noise-power measurements conducted by modern instrumentation are typically confined to an effective noise bandwidth Δf_n of 4MHz.

Let n denote the number of significant reflections posed by the measurement system such that [20]

$$n = \left| \frac{4\Gamma_1\Gamma_2}{1 - |\Gamma_1|^2 |\Gamma_2|^2} \right|. \quad (2.77)$$

Further, the system's coherence length Δl is related to the group velocity set by the transmission line and divided into $2\pi\Delta f_n$ [37]. Substituting the expression for Δl into (2.76) we arrive at a conclusion that [37]

$$nL \ll \Delta l. \quad (2.78)$$

That is, the distance traveled by the noise-waves due to significant subsequent reflections by the measurement system need be much smaller than the coherence length of the system. Observing this inequality ensures that a fixed phase relationship of correlated noise-waves is maintained across Δf_n . In fact, adherence to the spot noise criterion permits use of the noise-wave theory developed in sections 2.2 and 2.3 [20].

Returning to Fig. 2-8, noise-waves \hat{a}_1 and \hat{b}_1 can be used to determine the overall noise performance of the network, including exchangeable noise-power densities $\overline{\hat{a}_1 \hat{a}_1^*}$ and $\overline{\hat{b}_1 \hat{b}_1^*}$, their correlation $\overline{\hat{a}_1 \hat{b}_1^*}$, as well as the noise-power per Hertz dissipated in the connecting line's terminations. If the measurement system is quasi-matched, then (2.63) and (2.64) reduce to [20]

$$\overline{\hat{a}_1 \hat{a}_1^*} = |\Gamma_2|^2 \overline{|\hat{b}_{gl_1}|^2} + \overline{|\hat{b}_{gl_2}|^2} \in \mathbb{R} \quad (2.79)$$

$$\overline{\hat{b}_1 \hat{b}_1^*} = \overline{|\hat{b}_{gl_1}|^2} + |\Gamma_1|^2 \overline{|\hat{b}_{gl_2}|^2} \in \mathbb{R} \quad (2.80)$$

respectively and their correlation is

$$\overline{\hat{a}_1 \hat{b}_1^*} = \Gamma_2 e^{-j2\beta L} \overline{|\hat{b}_{gl_1}|^2} + \Gamma_1^* \overline{|\hat{b}_{gl_2}|^2} \in \mathbb{C}. \quad (2.81)$$

If R1 and R2 terminations are matched to their connecting transmission line, then the noise-power density $\overline{\hat{a}_1 \hat{a}_1^*}$ generated by R2 and dissipated in R1 is $\overline{|\hat{b}_{gl_2}|^2}$. Also, the noise-power density $\overline{\hat{b}_1 \hat{b}_1^*}$ generated by R1 and delivered to R2 is $\overline{|\hat{b}_{gl_1}|^2}$. From (2.81), it's evident that for a matched network condition no correlation between noise waves \hat{a}_1 and \hat{b}_1 exists.

Chapter 3

Linear Network Noise Behavioral Modeling

Within the RF/microwave frequency spectrum, the noise behavior of a distributed network may completely be described by use of its scattering wave representation. That is, by expressing the network's scattered noise-waves in terms of a weighted linear combination of its incident noise-waves and noise-wave sources (that emanate even in absence of a stimulus), a noise behavioral model of the network may be formulated. In section 3.1.1, an attribute of this model known as the noise correlation matrix (NCM) will be defined within the framework of the network's S-parameters. Embedded one-, two-, and n-port cases will be investigated under which generalized noise-power flow equations are constructed. The expressions will be applied to passive networks in section 3.1.2. Overall system considerations including thermodynamics and the termination network behavior are considered in the process of deriving the NCM of the embedded network of interest. The subject of noise temperature will be introduced in section 3.1.3 and related to the wave description of noise-power spectral density. The generalized noise-power flow formulation will then be applied to active networks in section 3.2.1, including two- and n-port configurations; in each case the network's NCM will be extracted. Lastly, section 3.2.2 will use the network's NCM to describe figures-of-merit including noise factor, effective noise temperature, and noise parameters.

3.1 Passive Components

3.1.1 Network Representation using S-parameters and Noise-Waves

3.1.1.1 One-Port Network

A noisy one-port will inject its energy into a transmission line to which it's connected [20]. This energy may be considered a noise source. The time-average of the energy is power and will be a function of the connecting line's impedance and frequency of operation. As described in the previous chapter, a transmission line stimulated by a noise source will introduce a response which may be described as a traveling noise-wave [34]. Should the transmission line and its load impedance not be matched, a portion or all the traveling wave's noise-power will be reflected. Further, if the one-port is not matched to its connecting line, the reflected noise-power will be re-reflected, in this way, multiple reflections may occur.

From this and earlier development in Chapter 2, the one-port can be modeled as shown

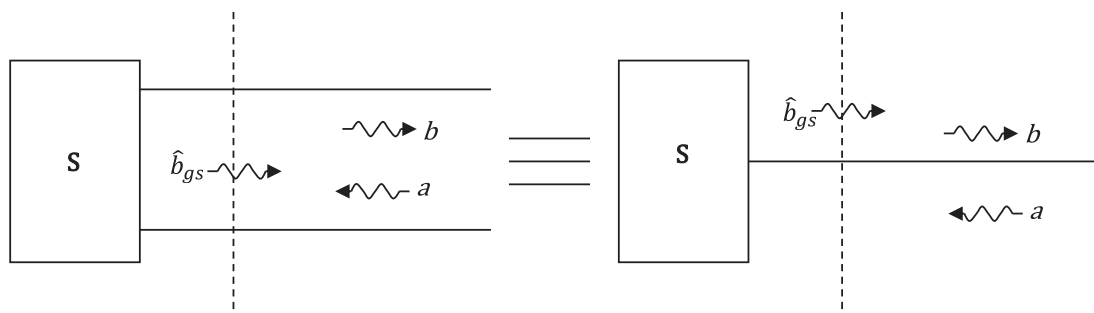


Figure 3.1: Noisy One-Port Connected to a Lossless Transmission Line

in Fig. 3.1 [20]. The one-port's signal and noise properties are represented as the sum of the scattered wave Sa and noise-wave source \hat{b}_{gs} such that

$$b = Sa + \hat{b}_{gs} . \quad (3.1)$$

Transmission signal-waves a and b may support simultaneous presence of deterministic and non-deterministic signal-types or non-deterministic only. The subscript “ gs ” in noise-wave source \hat{b}_{gs} denotes the characteristic noise generated by the one-port.

The reference plane is established at the physical location to which the one-port is connected to the transmission line and is distinguished in Fig. 3.1 by a dashed vertical line. Beside the one-port itself, the scattering coefficient “ S ” is dependent on the impedance of its connecting line and the location of the reference plane [20].

The separation of the one-port’s signal and noise behavior is a significant model attribute. It suggests that for linear systems, the signal and noise representation can be evaluated separately [20, 37].

Referring to Fig. 3.1, the noise-power spectral density associated with noise-wave source \hat{b}_{gs} is $\overline{\hat{b}_{gs}\hat{b}_{gs}^*}$. Assuming this quantity is constant across a chosen effective noise bandwidth of Δf_n , the noise-power of \hat{b}_{gs} is satisfied by simple integration such that

$$\Delta \hat{P}_{\hat{b}_{gs}} = \overline{\hat{b}_{gs}\hat{b}_{gs}^*} \cdot \Delta f_n \quad (3.2)$$

Consider Fig. 3.1 to consist of no deterministic signals. For the case of the noisy one-port terminated in a matched, passive, noiseless load via its connecting line, (3.2) represents the noise-power delivered to this load. We may deduce from it and (3.1) that [24, 37]

$$\overline{\hat{b}\hat{b}^*} = \overline{\hat{b}_{gs}\hat{b}_{gs}^*} = \Delta \hat{P}_{\hat{b}_{gs}} / \Delta f_n \quad (3.3)$$

where $\overline{\hat{a}\hat{a}^*} = 0$. In practical terms, unless the passive load is at absolute zero temperature, it will generate thermal noise forming a traveling noise-wave \hat{a} incident to the one-port [24]. Within context of network noise analysis, these practical considerations will be outlined in section 3.1.2. At this juncture, the salient point is that the noise behavior of the one-port is defined by (3.3).

3.1.1.2 Multi-Port Network

Like the one-port, a signal and noise representation for a generalized noisy n-port may be constructed. Referring to Fig. 3.2 [20], the noisy multipoint is connected at each of its ports to a

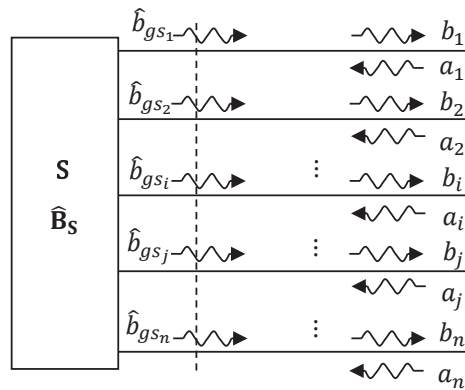


Figure 3.2: Noisy Multipoint Connected to Lossless Z_0 Transmission Lines

lossless transmission line. The network signal behavior will be defined based on its S-parameters and noise-wave sources $\hat{b}_{gs_1}, \hat{b}_{gs_2}, \dots, \hat{b}_{gs_n}$ emitted from its respective ports. The subscript denotes the port number to which each noise-wave source is assigned. The vertical dashed line is the reference plane marking the physical location to which the multipoint is connected to its lines. The definition for the incident and scattered transmission waves a and b respectively are unchanged from the one-port model description. The generalized n-port signal and noise behavior can be modeled in matrix form by [20, 39, 43]

$$\mathbf{b} = \mathbf{S}\mathbf{a} + \hat{\mathbf{b}}_{gs} \tag{3.4}$$

or more explicitly as

$$\begin{bmatrix} b_1 \\ b_2 \\ \cdot \\ \cdot \\ b_n \end{bmatrix} = \begin{bmatrix} S_{11} & S_{12} & \cdot & \cdot & S_{1n} \\ S_{21} & S_{22} & \cdot & \cdot & S_{2n} \\ \cdot & \cdot & \cdot & \cdot & \cdot \\ \cdot & \cdot & \cdot & \cdot & \cdot \\ S_{n1} & S_{n2} & \cdot & \cdot & S_{nn} \end{bmatrix} \begin{bmatrix} a_1 \\ a_2 \\ \cdot \\ \cdot \\ a_n \end{bmatrix} + \begin{bmatrix} \hat{b}_{gs_1} \\ \hat{b}_{gs_2} \\ \cdot \\ \cdot \\ \hat{b}_{gs_n} \end{bmatrix} . \quad (3.5)$$

The S-parameters represent the multiport influence on the incident a waves applied to its ports. This influence results in the formation of the scattered b waves. That is, the S-parameters represent a mapping of the a waves to the b waves. Finally, with respect to the multiport, vector \hat{b}_{gs} comprises n- noise wave sources generated by the network and assigned to each of its ports.

Consistent with (2.48) and (3.2), the noise-power density emitted by the network's noise-wave source at its i-th port and confined to Δf_n is [20, 37]

$$\overline{\hat{b}_{gs_i} \hat{b}_{gs_i}^*} = \Delta \hat{P}_{\hat{b}_{gs_i} \hat{b}_{gs_i}^*} / \Delta f_n . \quad (3.6)$$

Each noise-wave source is generated by one or more physical phenomenon within the multiport. Thus, to an extent, each may be common depending on the distribution of noise properties within the network. The complex noise-power density describing the correlation of the i-th and j-th noise-wave sources is [20, 37]

$$\overline{\hat{b}_{gs_i} \hat{b}_{gs_j}^*} = \Delta \hat{P}_{\hat{b}_{gs_i} \hat{b}_{gs_j}^*} / \Delta f_n . \quad (3.7)$$

Equation (3.6) is the correlation of noise-wave source i with itself; (3.7) is the correlation of noise-wave source i with noise-wave source j .

A NCM $\hat{\mathbf{B}}_s$ can be formulated collectively to describe the multiport's self- and cross-port noise correlation behavior by multiplying the noise-wave source vector $\hat{\mathbf{b}}_{gs}$ by its Hermitian. That is [20, 37, 44]

$$\hat{\mathbf{B}}_s = \overline{\hat{\mathbf{b}}_{gs} \hat{\mathbf{b}}_{gs}^\dagger} = \begin{bmatrix} \hat{b}_{gs_1} \\ \hat{b}_{gs_2} \\ \cdot \\ \hat{b}_{gs_n} \end{bmatrix} \begin{bmatrix} \hat{b}_{gs_1} \\ \hat{b}_{gs_2} \\ \cdot \\ \hat{b}_{gs_n} \end{bmatrix}^\dagger = \begin{bmatrix} \overline{\hat{b}_{gs_1} \hat{b}_{gs_1}^*} & \overline{\hat{b}_{gs_1} \hat{b}_{gs_2}^*} & \cdot & \cdot & \overline{\hat{b}_{gs_1} \hat{b}_{gs_n}^*} \\ \overline{\hat{b}_{gs_2} \hat{b}_{gs_1}^*} & \overline{\hat{b}_{gs_2} \hat{b}_{gs_2}^*} & \cdot & \cdot & \overline{\hat{b}_{gs_2} \hat{b}_{gs_n}^*} \\ \cdot & \cdot & \cdot & \cdot & \cdot \\ \cdot & \cdot & \cdot & \cdot & \cdot \\ \overline{\hat{b}_{gs_n} \hat{b}_{gs_1}^*} & \overline{\hat{b}_{gs_n} \hat{b}_{gs_2}^*} & \cdot & \cdot & \overline{\hat{b}_{gs_n} \hat{b}_{gs_n}^*} \end{bmatrix}. \quad (3.8)$$

The symbol \dagger refers to Hermitian. The Hermitian involves two mathematical operations, first by taking the transpose of a matrix and second by applying the complex conjugate to its elements [44]. Thus $\hat{\mathbf{b}}_{gs}^\dagger$ is the Hermitian matrix of $\hat{\mathbf{b}}_{gs}$.

S-parameters provide a full signal-state behavior representation of an n-port network. The NCM $\hat{\mathbf{B}}_s$ offers a complete description of its noise behavior. Consistent with the one-port description in (3.2), the diagonal elements of (3.8) are real quantities representing the noise-power per Hz delivered to a passive, noise-free termination matched to its connecting line. However, with a multiport there are off-diagonal elements that are complex and describe the correlation of the noise-wave sources to one another. Recall from (2.51) that the time-averaged cross-correlation of noise-waves \hat{b}_{g_i} to \hat{b}_{g_j} may be expressed as

$$\overline{\hat{b}_{g_i} \hat{b}_{g_j}^*} = \lim_{T \rightarrow \infty} \frac{1}{T} \int_{-T/2}^{T/2} \hat{b}_{g_i}^*(t) \hat{b}_{g_j}(t + \tau) dt \approx \Delta \hat{P}_{\hat{b}_{g_i} \hat{b}_{g_j}^*} / \Delta f_n = \hat{\Phi}_{ij}(f_c) \quad (3.9)$$

where the approximation becomes equal in the limit for a constant $\hat{\Phi}_{ij}(f_c)$ across the noise bandwidth Δf_n .

Together, \mathbf{S} and $\hat{\mathbf{B}}_s$ provide a comprehensive description of a generalized n-port's signal and noise representation. In practice, a passive noise-free termination is generally not easily realized. Therefore, in section 3.1.2, the NCM of the generalized multiport will be derived as an embedded network, that is as one connected to a second multiport acting as its termination network. In this case, the termination network will be treated as passive, reflective, and noisy.

3.1.2 Passive Component Network Analysis

Attention is now directed to deriving the noise correlation matrix of a multiport network connected to noisy, reflective, passive load terminations. This represents a set of conditions typically encountered in practice. Figure 3.3 shows the noisy multiport of interest to the left with S-parameter and noise correlation matrices \mathbf{S} and $\hat{\mathbf{B}}_s$ respectively. To the right is a passive, noisy, reflective load termination network also described by its S-parameter and noise correlation matrices \mathbf{L} and $\hat{\mathbf{B}}_L$ in that order. The matrices are of $n \times n$ dimension. In practice, cables used to

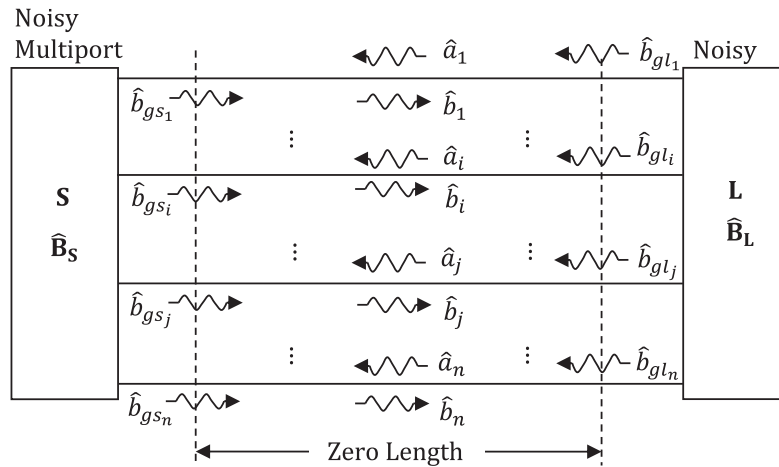


Figure 3.3: Noisy Multiport Network-S Embedded in a Terminations Network-L [20]

join the two multi-ports are considered part of the termination network. It's understood in Fig. 3.3 that all traveling waves are non-deterministic.

From the above diagram, the scattered and incident noise-wave vectors are correspondingly expressed as

$$\hat{\mathbf{b}} = \mathbf{S}\hat{\mathbf{a}} + \hat{\mathbf{b}}_{gs} \tag{3.10}$$

and

$$\hat{\mathbf{a}} = \mathbf{L}\hat{\mathbf{b}} + \hat{\mathbf{b}}_{gl} . \quad (3.11)$$

Substituting (3.11) into (3.10) permits expression of $\hat{\mathbf{b}}$ in terms of $\hat{\mathbf{b}}_{gs}$ and $\hat{\mathbf{b}}_{gl}$. Applying matrix manipulation [20, 26]

$$\hat{\mathbf{b}} = (\mathbf{I} - \mathbf{S}\mathbf{L})^{-1} (\mathbf{S}\hat{\mathbf{b}}_{gl} + \hat{\mathbf{b}}_{gs}) \quad (3.12)$$

where \mathbf{I} is the identity matrix.

Similarly, by substituting (3.10) into (3.11) we have $\hat{\mathbf{a}}$ in terms of $\hat{\mathbf{b}}_{gs}$ and $\hat{\mathbf{b}}_{gl}$ such that

$$\hat{\mathbf{a}} = (\mathbf{I} - \mathbf{L}\mathbf{S})^{-1} (\mathbf{L}\hat{\mathbf{b}}_{gs} + \hat{\mathbf{b}}_{gl}) . \quad (3.13)$$

The noise-power spectral density of the incident and scattered noise-waves with respect to network-S is

$$\overline{\hat{\mathbf{a}}\hat{\mathbf{a}}^\dagger} = (\mathbf{I} - \mathbf{L}\mathbf{S})^{-1} (\hat{\mathbf{B}}_L + \mathbf{L}\hat{\mathbf{B}}_S\mathbf{L}^\dagger) (\mathbf{I} - \mathbf{L}\mathbf{S})^{-1\dagger} \quad (3.14)$$

and

$$\overline{\hat{\mathbf{b}}\hat{\mathbf{b}}^\dagger} = (\mathbf{I} - \mathbf{S}\mathbf{L})^{-1} (\hat{\mathbf{B}}_S + \mathbf{S}\hat{\mathbf{B}}_L\mathbf{S}^\dagger) (\mathbf{I} - \mathbf{S}\mathbf{L})^{-1\dagger} \quad (3.15)$$

where $\hat{\mathbf{B}}_S = \overline{\hat{\mathbf{b}}_{gs}\hat{\mathbf{b}}_{gs}^\dagger}$ and $\hat{\mathbf{B}}_L = \overline{\hat{\mathbf{b}}_{gl}\hat{\mathbf{b}}_{gl}^\dagger}$. In the derivation of (3.14) and (3.15) it's understood that the internally generated noise of network's-S and $-\mathbf{L}$ are uncorrelated leading to the conclusion that their time-averaged product $\overline{\hat{\mathbf{b}}_{gs}\hat{\mathbf{b}}_{gl}^\dagger}$ and $\overline{\hat{\mathbf{b}}_{gl}\hat{\mathbf{b}}_{gs}^\dagger}$ are both equal to zero.

For a known Δf_n , the use of (3.14) may be used to determine the power $\overline{\hat{a}_i\hat{a}_i^*}$ of noise-wave \hat{a}_i at the i -th port. A similar approach can be taken by (3.15) to determine the power $\overline{\hat{b}_i\hat{b}_i^*}$

of noise-wave \hat{b}_i . The trace of matrix $\overline{\hat{a}\hat{a}^\dagger} \cdot \Delta f_n$ represents the total noise-power exchanged from termination network-L to the multiport network-S. Similar application to matrix $\overline{\hat{b}\hat{b}^\dagger}$ is the total noise-power exchanged from network-S to -L [20]. The off-diagonal elements in matrix $\overline{\hat{a}\hat{a}^\dagger}$, i.e., $\overline{\hat{a}_i\hat{a}_j^*}$, of the i -th and j -th ports describe the cross-port correlation of the two noise-waves. A similar description can be made for the off-diagonal elements in matrix $\overline{\hat{b}\hat{b}^\dagger}$.

Regarding (3.15), the first-term to the right of the equal sign is the noise of $\overline{\hat{b}\hat{b}^\dagger}$ due to network-S. This network generates noise described by its correlation matrix $\hat{\mathbf{B}}_S$ which undergoes a transformation due to its interaction with the overall network. The second-term is the noise of $\overline{\hat{b}\hat{b}^\dagger}$ originating from network-L. Thus, the termination network produces noise defined by $\hat{\mathbf{B}}_L$ which undergoes its own transformation. The sum of the two transformations form the full-insitu scattered noise matrix $\overline{\hat{b}\hat{b}^\dagger}$.

To elaborate on the interpretation of (3.14) and (3.15), consider the special case where the terminations of network-L are noise-free. The correlation matrix $\hat{\mathbf{B}}_L = 0$ and matrices $\overline{\hat{a}\hat{a}^\dagger}$ and $\overline{\hat{b}\hat{b}^\dagger}$ reduce to [20, 26]

$$\overline{\hat{a}\hat{a}^\dagger} = (\mathbf{I} - \mathbf{L}\mathbf{S})^{-1} \mathbf{L}\hat{\mathbf{B}}_S\mathbf{L}^\dagger (\mathbf{I} - \mathbf{L}\mathbf{S})^{-1\dagger} \quad (3.16)$$

and

$$\overline{\hat{b}\hat{b}^\dagger} = (\mathbf{I} - \mathbf{S}\mathbf{L})^{-1} \hat{\mathbf{B}}_S (\mathbf{I} - \mathbf{S}\mathbf{L})^{-1\dagger} . \quad (3.17)$$

Additionally, should the terminations be uncoupled and matched to their connecting lines then $\overline{\hat{a}\hat{a}^\dagger} = 0$ and $\overline{\hat{b}\hat{b}^\dagger} = \hat{\mathbf{B}}_S$. In practice, the condition of a noise-free termination is not easily attained. All resistive loads produce thermal noise unless cooled to absolute zero. Further, should a measurement system consisting of network-L be used to extract the NCM $\hat{\mathbf{B}}_S$, its terminations will be quasi-matched at best. Therefore, equations (3.14) and (3.15) apply and to solve for $\hat{\mathbf{B}}_S$

will require a-priori knowledge of $\hat{\mathbf{B}}_L$ and the scattering parameters of networks-S and -L [20, 26].

As a generalized expression, (3.15) can be used to extract the noise performance $\hat{\mathbf{B}}_S$ of passive and active device-types. The remainder of this section will be devoted to passive component noise analysis using this expression in context to one-, two-, and multi-port ($n>2$) modeling examples.

Shown in Fig. 3.4 is a passive noisy one-port connected to a noisy, matched, termination. The passive one-port behavior is represented by single-value parameters assigned to \mathbf{S} and $\hat{\mathbf{B}}_S$. The device's complex reflection coefficient Γ_S equals \mathbf{S} and its noise spectral density $\overline{\hat{b}_{gs}\hat{b}_{gs}^*}$ present at its connecting line is $\hat{\mathbf{B}}_S$. As depicted, the entire system comprising networks-S and -L is at uniform temperature T. The goal is to use (3.15) to extract the NCM $\hat{\mathbf{B}}_S$ of the embedded network-S.

From (3.15) and the stated conditions described in Fig. 3.4, the noise-power density of the scattered \hat{b} wave is

$$\overline{\hat{b}\hat{b}^*} = \overline{\hat{b}_{gs}\hat{b}_{gs}^*} + \Gamma_S \overline{\hat{b}_{gl}\hat{b}_{gl}^*} \Gamma_S^* \quad (3.18)$$

where $\mathbf{L} = \Gamma_l = 0$ and $\hat{\mathbf{B}}_L = \overline{\hat{b}_{gl}\hat{b}_{gl}^*}$. It should be noted that each Hermitian symbol in (3.15) has been replaced with a conjugate character and their replacement is valid only for the one-port network configuration.

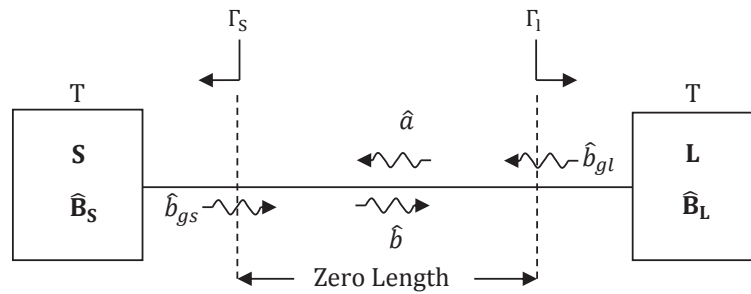


Figure 3.4: Embedded Passive One-Port Network-S. System is at Uniform Temperature T

Given the composite network is at uniform temperature, the second law of thermodynamics dictates that $\overline{\hat{a}\hat{a}^*} = \overline{\hat{b}\hat{b}^*}$ [8, 20, 24]. If this were not the case network-S would heat or cool relative to network-L and the system would not remain at uniform temperature.

Since the one-port is matched to its connecting line $\overline{\hat{a}\hat{a}^*} = \overline{\hat{b}_{gl}\hat{b}_{gl}^*}$. Therefore, solving (3.15) for the NCM of network-S results in

$$\hat{\mathbf{B}}_S = \overline{\hat{b}_{gs}\hat{b}_{gs}^*} = \overline{\hat{b}\hat{b}^*} (1 - \Gamma_s \Gamma_s^*) . \quad (3.19)$$

The NCM of the one-port is a single-value time-averaged real number representing the internally generated noise-power density $\overline{\hat{b}_{gs}\hat{b}_{gs}^*}$ sited at its connecting line.

As a second example, consider the two-port case shown in Fig. 3.5. In this scenario, the passive terminations presented to network - S from - L are noisy, matched, and uncoupled.

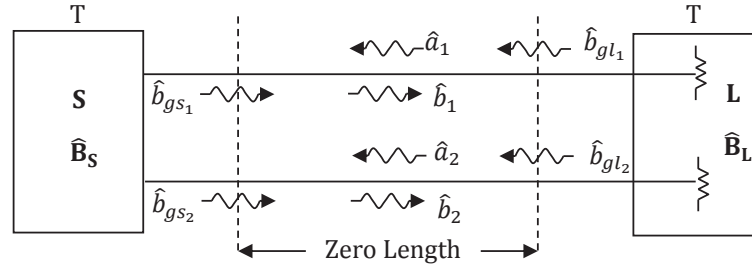


Figure 3.5: Embedded Passive Two-Port Network-S. System is at Uniform Temperature T [20]

Equation (3.15) becomes

$$\overline{\hat{b}\hat{b}^\dagger} = \overline{\hat{b}_{gs}\hat{b}_{gs}^\dagger} + \overline{\mathbf{S}\hat{b}_{gl}\hat{b}_{gl}^\dagger\mathbf{S}^\dagger} \quad (3.20)$$

where each quantity in (3.20) is a 2x2 matrix.

For a passive system at thermal equilibrium, $\overline{\hat{a}\hat{a}^\dagger} = \overline{\hat{b}\hat{b}^\dagger}$. Additionally, since the termination network is matched to its connecting lines we conclude that $\overline{\hat{a}\hat{a}^\dagger} = \overline{\hat{b}_{gl}\hat{b}_{gl}^\dagger}$. Given that network-L's terminations are isolated, the incident-wave matrix $\overline{\hat{a}\hat{a}^\dagger}$ is diagonal, and hence, so is the scattered wave matrix $\overline{\hat{b}\hat{b}^\dagger}$ and NCM $\overline{\hat{b}_{gl}\hat{b}_{gl}^\dagger}$. Therefore, solving for $\overline{\hat{b}_{gs}\hat{b}_{gs}^\dagger}$ in (3.20) and applying it to the stated conditions leads to [20]

$$\begin{aligned} \hat{\mathbf{B}}_S &= \overline{\hat{b}_{gs}\hat{b}_{gs}^\dagger} = \overline{\hat{b}\hat{b}^\dagger} - \overline{\mathbf{S}\hat{b}\hat{b}^\dagger\mathbf{S}^\dagger} \\ &= \overline{\hat{b}\hat{b}^\dagger} (\mathbf{I} - \mathbf{S}\mathbf{S}^\dagger) . \end{aligned} \quad (3.21)$$

The noise-power per line emerging and entering the uncoupled passive terminations is equal. Thus $\overline{\hat{b}\hat{b}^\dagger} = \overline{|\hat{b}|^2} \cdot \mathbf{I}$ where $\overline{|\hat{b}|^2}$ is a scalar quantity multiplied against the identity matrix \mathbf{I} . Like the one-port, the NCM of network-S is determined by the noise density of its scattered waves and S-parameters. Calculating elements of the NCM using (3.21) yields [20, 24, 37]

$$\hat{\mathbf{B}}_s = \begin{bmatrix} \overline{|\hat{b}_{gs_1}|^2} & \overline{\hat{b}_{gs_1} \hat{b}_{gs_2}^*} \\ \overline{\hat{b}_{gs_2} \hat{b}_{gs_1}^*} & \overline{|\hat{b}_{gs_2}|^2} \end{bmatrix} = \overline{|\hat{b}|^2} \cdot \begin{bmatrix} 1 - |S_{11}|^2 - |S_{12}|^2 & -S_{11}S_{21}^* - S_{12}S_{22}^* \\ -S_{21}S_{11}^* - S_{22}S_{12}^* & 1 - |S_{21}|^2 - |S_{22}|^2 \end{bmatrix}. \quad (3.22)$$

Noise-power densities $\overline{|\hat{b}_{gs_1}|^2}$ and $\overline{|\hat{b}_{gs_2}|^2}$ are engendered by network-S at port-1 and port-2 respectively. Since noise-waves \hat{b}_{gs_1} and \hat{b}_{gs_2} may originate in-part from identical noise-sources within network-S, it's expected that the two will correlate to some extent. However, the scattered waves $\hat{\mathbf{S}}\hat{\mathbf{a}}$ combine with $\overline{\hat{b}_{gs_1} \hat{b}_{gs_2}^*}$ canceling the effects of correlation, thus $\overline{\hat{b}_1 \hat{b}_2^*} = 0$ [37]. If there was correlation between \hat{b}_1 and \hat{b}_2 then the noise-power delivered to the terminations would be other than $\overline{|\hat{b}|^2}$ and the system could not maintain thermal equilibrium [37].

Per the configuration of network-L in Fig. 3.5, the balance of exchangeable noise-power flow is maintained per connecting line, i.e., $\overline{\hat{b}_i \hat{b}_i^*} - \overline{\hat{a}_i \hat{a}_i^*} = 0$ at the i -th port. The second law of thermodynamics under thermal equilibrium does not require this condition. It does require that the total net exchange of noise-power be zero [20]. Mathematically this can be written as [20]

$$\text{trace}(\overline{\hat{\mathbf{b}}\hat{\mathbf{b}}^\dagger} - \overline{\hat{\mathbf{a}}\hat{\mathbf{a}}^\dagger}) = 0. \quad (3.23)$$

The fact that the net exchange of noise-power flow per connecting line is zero is a consequence of network-L reciprocity. The balance of exchangeable power per line cannot be maintained for nonreciprocal networks [20]. The configuration of network-L in Fig. 3.5 was chosen because it approximates the conditions of a noise measurement system used in commercial practice – a subject reserved for Chapter 4.

The method employed in derivation of a NCM for the passive two-port case in (3.21) can readily be used to extend to n -ports by increasing the dimensions of its matrices to $n \times n$. Fig. 3.6

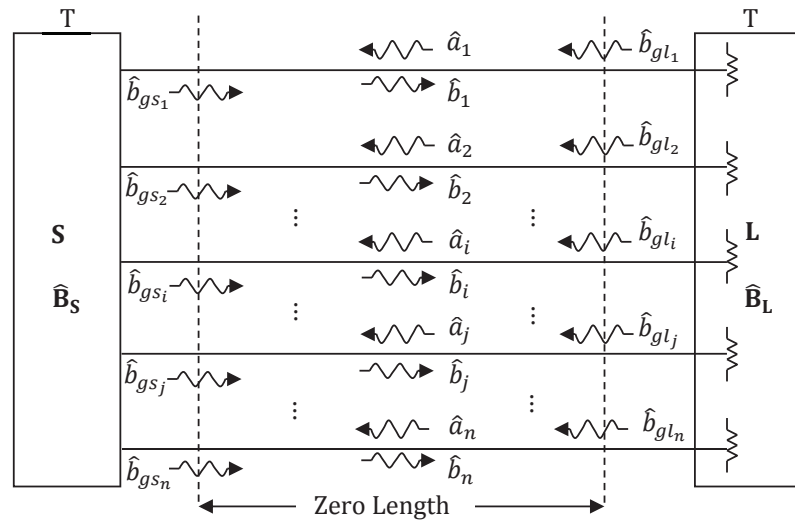


Figure 3.6: Embedded Passive N-port Network-S. System at Temperature Equilibrium T [20]

shows a diagram of the n-port connected to its terminations. In conclusion, a passive device's NCM can be determined by its S-parameters and the time-averaged noise-power density $\overline{\hat{b}\hat{b}^\dagger}$ of its scattered waves.

It has been demonstrated that the NCM of a passive device embedded in a system shown by Fig. 3.6 can be derived through the noise-power density equation of (3.15) and within context of thermodynamic arguments. So far noise-power and noise-power spectral density have been described in terms of traveling noise-waves. The upcoming section outlines the use of noise-temperature as an equivalent means to describe the flow of noise-power.

3.1.3 Noise Temperature

Consider in Fig. 3.7 two conductors each joined at the ends of a long dispersive transmission line. The line's length $L \gg \lambda$ where λ is the wavelength of operation. Conductors R1 and R2 are

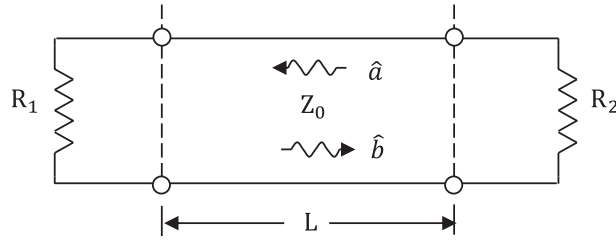


Figure 3.7: Passive System at Temperature Equilibrium [20]

matched to the characteristic impedance Z_0 of the transmission line, i.e., $Z_0 = R1 = R2$. Accordingly, there is no reflection of traveling-waves \hat{a} and \hat{b} . Consider the passive system to be at temperature T exhibiting time-averaged noise-power densities $\overline{\hat{a}\hat{a}^*}$ and $\overline{\hat{b}\hat{b}^*}$ of waves \hat{a} and \hat{b} respectively.

The noise-energy \hat{E}_{21} transferred from left-to-right and right-to-left is [20]

$$\overline{\hat{b}\hat{b}^*} = \hat{\Phi}_{21}(f_c) = \frac{\Delta \hat{P}_{21}(f_c)}{\Delta f_n} = \hat{E}_{21}(f_c) \quad (3.24)$$

and

$$\overline{\hat{a}\hat{a}^*} = \hat{\Phi}_{12}(f_c) = \frac{\Delta \hat{P}_{12}(f_c)}{\Delta f_n} = \hat{E}_{12}(f_c) \quad (3.25)$$

respectively. Under the stated condition of thermal equilibrium, (3.24) and (3.25) are equal. Consequently, they may be expressed in terms of Planck's Formula producing the relation [8, 20, 45]

$$\hat{E}_{12}(f_c) = \hat{E}_{21}(f_c) = hf \cdot \left(e^{\frac{hf}{kT}} - 1 \right)^{-1} . \quad (3.26)$$

Expressing $e^{(hf/k\hat{T})}$ in its power-series form and recognizing for this application that $hf \ll k\hat{T}$, it follows that

$$\hat{E}_{12}(f_c) = \hat{E}_{21}(f_c) = k\hat{T} . \quad (3.27)$$

From (3.27), it's evident that each conductor generates thermal noise-energy $k\hat{T}$. Under the condition that the system is at thermal equilibrium,

$$\overline{\hat{a}\hat{a}^*} = \overline{\hat{b}\hat{b}^*} = k\hat{T} \quad (3.28)$$

in accordance with (3.24) and (3.25). The available noise-power generated by each resistor can be determined by multiplying its noise-energy against the effective noise bandwidth Δf_n to which it's confined. This is the maximum noise-power which may be delivered to a conjugate matched load at temperature T as outlined in Fig. 3.7 [20, 24].

Returning to (3.22), the NCM of a passive two-port device operating at physical temperature T is [20]

$$\hat{\mathbf{B}}_s = k\hat{T}(\mathbf{I} - \mathbf{S}\mathbf{S}^\dagger) \quad (3.29)$$

where the elements in $\hat{\mathbf{B}}_s$ are in units of W/Hz . In accordance with Fig. 3.5, the total available noise-power $\Delta\hat{P}_{21}$ and $\Delta\hat{P}_{12}$ emerging from network-S and network-L respectively is

$$\Delta\hat{P}_{21}(f_c) = \text{trace}(\overline{\hat{\mathbf{b}}\hat{\mathbf{b}}^\dagger}) \cdot \Delta f_n = \text{trace}\left(k\hat{T}\begin{bmatrix} 1 & 0 \\ 0 & 1 \end{bmatrix}\right) \cdot \Delta f_n = \text{trace}(k\hat{T}\mathbf{I}) \cdot \Delta f_n \quad (3.30)$$

and

$$\Delta\hat{P}_{12}(f_c) = \text{trace}(\overline{\hat{\mathbf{a}}\hat{\mathbf{a}}^\dagger}) \cdot \Delta f_n = \text{trace}\left(k\hat{T}\begin{bmatrix} 1 & 0 \\ 0 & 1 \end{bmatrix}\right) \cdot \Delta f_n = \text{trace}(k\hat{T}\mathbf{I}) \cdot \Delta f_n . \quad (3.31)$$

To maintain thermal equilibrium in context with Fig. 3.5, (3.30) is the noise-power delivered to network-L and (3.31) is its equivalent absorbed by network-S.

In the next section on active devices, it will become clear that the physical interpretation of noise temperature is not always straight-forward. For example, the off-diagonal elements of the NCM are complex numbers which can be assigned a noise-temperature [20]. Further, it will be shown that the use of noise-temperature need not be dedicated to describing thermal noise alone.

3.2 Active Components

3.2.1 Network Representation using S-parameters and Noise-Waves

In section 3.1, an exchangeable noise-power flow equation between a generalized noisy multiport and its connected termination network was derived. This relationship, described in (3.15), was then applied to the passive component case where it was determined that in conjunction with thermodynamic arguments the component's NCM could be determined. In the analysis, both multiport and termination networks were treated as passive; the noise-waves were strictly comprised of thermal noise.

Use of the exchangeable noise-power flow expressions are applicable to passive as well as active device-types. The noise-waves need not be solely due to thermal effects. In an active network, thermal and shot noise (the physical source of this noise largely originating from semiconductors) are typically expected.

This section makes use of scattered noise-waves emanating from an active device in order that its NCM may be determined. The NCM will then be used to determine figures-of-merit including noise factor, effective input noise temperature, and noise parameters.

3.2.1.1 Two-Port Network

To illustrate the use of (3.15), we will use it to calculate the output scattered noise density $\overline{\hat{b}_2 \hat{b}_2^*}$ of an active two-port. The system is shown in Fig. 3.8 [20] where network-S is the active two-port and network-L the termination network to which it's connected. Active device port-one is the input, port-two the output. The active network noise is modeled by two correlated noise-wave sources \hat{b}_{gs_1} and \hat{b}_{gs_2} emerging from its input and output ports respectively.

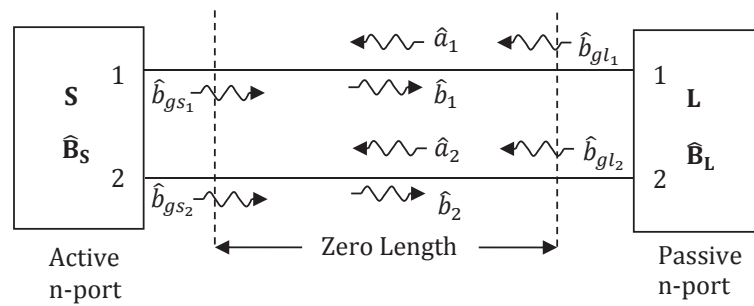


Figure 3.8: Active Two-Port Network-S Connected to Passive Termination Network-L

From (3.15) and Fig. 3.8, the full-insitu scattered noise density matrix $\overline{\hat{b}\hat{b}^\dagger}$ of the active two-port can be written in (3.32) as

$$\overline{\hat{b}\hat{b}^\dagger} = (\mathbf{I} - \mathbf{S}\mathbf{L})^{-1} (\hat{\mathbf{B}}_S + \mathbf{S}\hat{\mathbf{B}}_L\mathbf{S}^\dagger) (\mathbf{I} - \mathbf{S}\mathbf{L})^{-1\dagger} \quad (3.32)$$

where

$$\overline{\hat{b}\hat{b}^\dagger} = \begin{bmatrix} \overline{\hat{b}_1 \hat{b}_1^*} & \overline{\hat{b}_1 \hat{b}_2^*} \\ \overline{\hat{b}_2 \hat{b}_1^*} & \overline{\hat{b}_2 \hat{b}_2^*} \end{bmatrix}, \quad (3.32a)$$

$$\mathbf{S} = \begin{bmatrix} S_{11} & S_{12} \\ S_{21} & S_{22} \end{bmatrix}, \quad (3.32b)$$

$$\mathbf{L} = \begin{bmatrix} L_{11} & L_{12} \\ L_{21} & L_{22} \end{bmatrix}, \quad (3.32c)$$

$$\hat{\mathbf{B}}_S = \overline{\hat{\mathbf{b}}_{gs} \hat{\mathbf{b}}_{gs}^\dagger} = \begin{bmatrix} \overline{\hat{b}_{gs_1} \hat{b}_{gs_1}^*} & \overline{\hat{b}_{gs_1} \hat{b}_{gs_2}^*} \\ \overline{\hat{b}_{gs_2} \hat{b}_{gs_1}^*} & \overline{\hat{b}_{gs_2} \hat{b}_{gs_2}^*} \end{bmatrix}, \quad (3.32d)$$

and

$$\hat{\mathbf{B}}_L = \overline{\hat{\mathbf{b}}_{gl} \hat{\mathbf{b}}_{gl}^\dagger} = \begin{bmatrix} \overline{\hat{b}_{gl_1} \hat{b}_{gl_1}^*} & \overline{\hat{b}_{gl_1} \hat{b}_{gl_2}^*} \\ \overline{\hat{b}_{gl_2} \hat{b}_{gl_1}^*} & \overline{\hat{b}_{gl_2} \hat{b}_{gl_2}^*} \end{bmatrix}. \quad (3.32e)$$

Through matrix multiplication of (3.32), four linear equations describing the relationship of the embedded active network's scattered noise-waves can be produced. Expressions related to the diagonal elements $\overline{\hat{b}_1 \hat{b}_1^*}$ and $\overline{\hat{b}_2 \hat{b}_2^*}$ represent the noise density present at port's one and two respectively and those for the off-diagonal entries $\overline{\hat{b}_1 \hat{b}_2^*}$ and $\overline{\hat{b}_2 \hat{b}_1^*}$ signify the correlation between scattered noise-waves \hat{b}_1 at port-one and \hat{b}_2 at port-two.

Having performed matrix algebra on (3.32), it's evident that the output scattered noise density $\overline{\hat{b}_2 \hat{b}_2^*}$ expression is written in terms of the elements comprising the active network's NCM. With the goal in mind of extracting these elements either through simulation or measurement we consider the following. First, termination network-L will approximate a typical measurement system interface to the active network such that its ports are uncoupled and well matched at port-two. Therefore, $L_{12} = L_{21} = 0$ and $L_{22} \approx 0$. L_{11} is the source match presented to the active network from its port-one frame-of-reference. Hence the complex source reflection coefficient Γ_s is assigned to L_{11} . Since ports one and two of the termination network are uncoupled, their noise-wave sources \hat{b}_{gl_1} and \hat{b}_{gl_2} are uncorrelated yielding $\overline{\hat{b}_{gl_1} \hat{b}_{gl_2}^*} = \overline{\hat{b}_{gl_2} \hat{b}_{gl_1}^*} = 0$. As for the active network, it will be represented as an amplifier under the condition that \hat{b}_{gl_2}

offers a negligible contribution to the total output noise-power ascribed to noise-wave \hat{b}_2 [46]. Further, let the amplifier exhibit high isolation, i.e., $S_{12} \approx 0$, and a moderately matched output such that $\overline{\hat{b}_{g_{s_2}} \hat{b}_{g_{s_2}}^*} \gg S_{22} S_{22}^* \overline{\hat{b}_{g_{l_2}} \hat{b}_{g_{l_2}}^*}$. With these conditions imposed, (3.32) reduces to

$$\overline{|\hat{b}_2|^2} = \left| \frac{\Gamma_S S_{21}}{1 - \Gamma_S S_{11}} \right|^2 \left(\overline{|\hat{b}_{g_{s_1}}|^2} + |S_{11}|^2 \overline{|\hat{b}_{g_{l_1}}|^2} \right) + |S_{21}|^2 \overline{|\hat{b}_{g_{l_1}}|^2} + \overline{|\hat{b}_{g_{s_2}}|^2} + 2 \operatorname{Re} \left\{ \frac{\Gamma_S S_{21}}{1 - \Gamma_S S_{11}} \left(\overline{\hat{b}_{g_{s_1}} \hat{b}_{g_{s_2}}^*} + S_{11} S_{21}^* \overline{|\hat{b}_{g_{l_1}}|^2} \right) \right\} \quad (3.33)$$

Separating the noise output terms due to the input termination noise $\hat{b}_{g_{l_1}}$ and that by the active two-port leads to

$$\overline{|\hat{b}_2|^2} = \left(\left| \frac{\Gamma_S S_{21}}{1 - \Gamma_S S_{11}} \right|^2 |S_{11}|^2 + 2 \operatorname{Re} \left\{ \frac{\Gamma_S S_{11}}{1 - \Gamma_S S_{11}} \right\} + 1 \right) |S_{21}|^2 \overline{|\hat{b}_{g_{l_1}}|^2} + \left(\left| \frac{\Gamma_S S_{21}}{1 - \Gamma_S S_{11}} \right|^2 \overline{|\hat{b}_{g_{s_1}}|^2} + \overline{|\hat{b}_{g_{s_2}}|^2} + 2 \operatorname{Re} \left\{ \frac{\Gamma_S S_{21}}{1 - \Gamma_S S_{11}} \overline{\hat{b}_{g_{s_1}} \hat{b}_{g_{s_2}}^*} \right\} \right). \quad (3.34)$$

The first-term to the right-side of the equals sign in (3.34) may be simplified by expanding its present form, identifying a common denominator, and summing its terms. The result can be substituted into (3.34) to form

$$\overline{|\hat{b}_2|^2} = \frac{|S_{21}|^2}{|1 - \Gamma_S S_{11}|^2} \overline{|\hat{b}_{g_{l_1}}|^2} + \left(\left| \frac{\Gamma_S S_{21}}{1 - \Gamma_S S_{11}} \right|^2 \overline{|\hat{b}_{g_{s_1}}|^2} + \overline{|\hat{b}_{g_{s_2}}|^2} + 2 \operatorname{Re} \left\{ \frac{\Gamma_S S_{21}}{1 - \Gamma_S S_{11}} \overline{\hat{b}_{g_{s_1}} \hat{b}_{g_{s_2}}^*} \right\} \right). \quad (3.35)$$

Equation (3.35) is the amplifier's scattered noise power density \hat{b}_2 at its output port-two. Multiplying both sides of (3.35) by Δf_n results in the total noise-power confined to an effective noise bandwidth that's entering its connecting transmission line [26].

The second-term to the right-side of the equal sign in (3.35) may be contracted [37] and substituted into (3.35) resulting in

$$\overline{|\hat{b}_2|^2} = \frac{|S_{21}|^2}{|1 - \Gamma_S S_{11}|^2} \overline{|\hat{b}_{g1}|^2} + \overline{\left| \frac{\Gamma_S S_{21}}{1 - \Gamma_S S_{11}} \hat{b}_{g1} + \hat{b}_{g2} \right|^2}. \quad (3.36)$$

The first-term is the characteristic noise-out due to noise-in. The second-term is the characteristic noise-out due to the amplifier. The second-term is a function of the time-averaged noise density $\overline{|\hat{b}_{g1}|^2}$ and $\overline{|\hat{b}_{g2}|^2}$ present at port-one and port-two respectively, as well as the time-averaged noise-wave products describing their correlation, that is $\overline{\hat{b}_{g1} \hat{b}_{g2}^*}$ and $\overline{\hat{b}_{g2} \hat{b}_{g1}^*}$. These four quantities comprise the NCM of the amplifier. To determine the elements, the active two-port's forward S-parameters and its time-averaged input noise density $\overline{|\hat{b}_{g1}|^2}$ need be determined. Lastly, four independent equations related to (3.36), each in terms of a distinct Γ_S may be produced whereupon the four elements of the NCM may be extracted.

If the assumptions outlined in deriving (3.36) do not apply, the complete form of (3.32, 3.32a-e) may be used. This equation is lengthy but calculations can be expedited through Matlab or Keysight's Advanced Design System (ADS) software.

From section 3.1.3 and equation (3.36), the noise density $\overline{|\hat{b}_2|^2}$ at port-two of the amplifier may be expressed as a noise-temperature \hat{T}_2 such that [26, 35]

$$\overline{|\hat{b}_2|^2} = k\hat{T}_2 = k\hat{T}_{2_{av}} \left(1 - |S'_{22}|^2\right). \quad (3.37)$$

Per (3.37), the available (actual equivalent) noise temperature $\hat{T}_{2_{av}}$ at the output port is related to its available noise power density. It can be seen from (3.37) that the noise-power injected into its connecting transmission line is related to the port's available noise-power reduced by the quantity $\left(1 - |S'_{22}|^2\right)$ where S'_{22} is the complex match "looking into" the amplifier's output port-two with its input port terminated in Γ_S . If a complex conjugate match exists between the

output and its connected load, the available noise-power will be delivered to the termination. Using noise-temperature, a more compact form is realized such that [26]

$$\hat{T}_2 = \hat{T}_{2av} \left(1 - |S'_{22}|^2\right). \quad (3.38)$$

Unlike a passive device, the available noise-temperature associated with an active device will generally not be represented by its physical temperature.

Consistent with the noise-temperature concept, one may assign noise-temperatures to represent the elements comprising the amplifier's NCM by letting [21, 46]

$$\overline{|\hat{b}_{gs_1}|^2} = k\hat{T}_{gs_1}, \quad (3.39a)$$

$$\overline{|\hat{b}_{gs_2}|^2} = k\hat{T}_{gs_2}, \quad (3.39b)$$

and

$$\overline{\hat{b}_{gs_1} \hat{b}_{gs_2}^*} = k\hat{T}_{gs_{12}} e^{j\hat{\phi}_{gs_{12}}} \quad (3.39c)$$

where $\hat{b}_{gs_1} = \sqrt{k\hat{T}_{gs_1}} e^{j\hat{\phi}_{gs_1}}$, $\hat{b}_{gs_2} = \sqrt{k\hat{T}_{gs_2}} e^{j\hat{\phi}_{gs_2}}$, $\hat{T}_{gs_{12}} = \sqrt{\hat{T}_{gs_1} \hat{T}_{gs_2}}$, and $\hat{\phi}_{gs_{12}} = \frac{1}{2} \cdot (\hat{\phi}_{gs_1} - \hat{\phi}_{gs_2}) \cdot \hat{T}_{gs_1}$, \hat{T}_{gs_2} , $\hat{T}_{gs_{12}}$, and $\hat{\phi}_{gs_{12}}$ are real quantities. Thus, noise-wave generators \hat{b}_{gs_1} and \hat{b}_{gs_2} of the active two-port are assigned complex amplitudes which can be related to their spectral densities [28].

The total characteristic noise temperature \hat{T}_2 present at output port-two of the amplifier due to its internally generated noise may be determined by direct substitution of (3.39a-c) into the second-term of (3.35) forming

$$\hat{T}_2 = \left(\left| \frac{\Gamma_S S_{21}}{1 - \Gamma_S S_{11}} \right|^2 \hat{T}_{gs_1} + \hat{T}_{gs_2} + 2 \operatorname{Re} \left\{ \frac{\Gamma_S S_{21}}{1 - \Gamma_S S_{11}} \hat{T}_{gs_{12}} e^{j\hat{\phi}_{gs_{12}}} \right\} \right). \quad (3.40)$$

Meyes [21] and Kanaglekar et al [46] describe an approach that determines $\hat{T}_{g_{s_1}}$, $\hat{T}_{g_{s_2}}$, $\hat{T}_{g_{s_{12}}}$, and $\hat{\varphi}_{g_{s_{12}}}$ by setting the reflection coefficient Γ_s to four distinct states, generating four independent linear equations and solving for each of the unknowns.

Referring to Fig. 3.8, the noise-power density of wave generator $\hat{b}_{g_{l_1}}$ due to the passive termination connected at port-one of our amplifier may be expressed as [20, 26]

$$\overline{|\hat{b}_{g_{l_1}}|^2} = k\hat{T}_{L1} = k\hat{T}_{L1_{av}}(1 - |\Gamma_s|^2). \quad (3.41)$$

$\hat{T}_{L1_{av}}$ is the available noise temperature at port-one of the termination network. Because termination L1 is passive, its available noise-temperature $\hat{T}_{L1_{av}}$ is represented by its physical temperature. This termination is the amplifier's source impedance exhibiting a source reflection coefficient Γ_s presented to its input port. The reduced or characteristic noise temperature assigned to L1 is \hat{T}_{L1} .

3.2.1.2 Multi-Port Network

The two-port network theory may be extended to the generalized n-port. The dimensions for matrices (3.32a-e) are expanded to nxn and substituted into (3.32) providing a full-insitu noise matrix expression for the multi-port. From (3.32), the total noise-power present at a selected output port will account for noise contribution from each of its input ports as well as the network's internally generated noise [26].

No single figure-of-merit adequately describes the noise behavior of a device for all systems it may be used [36]. In some applications, noise factor is preferred, for others it may be noise temperature, or the often-referred noise parameters. Regardless of format, each may be

derived from knowledge of the device's S-parameter and noise correlation matrices. The first of these to be addressed is noise factor.

3.2.2 Figures-of-Merit

3.2.2.1 Noise Factor

Noise factor F quantifies the noise appraisal of a network. It's defined as the ratio of the total available noise power at a network's output to the total available noise power at the output due to the input termination's thermal noise [1]. That is [1, 35]

$$F = \frac{\hat{P}_{av,net} + \hat{P}_{av,in} G_{av}}{\hat{P}_{av,in} G_{av}} \quad (3.42)$$

where $\hat{P}_{av,net}$ and $\hat{P}_{av,in}$ are the available noise power at the output due to the internally generated noise added by the network and from the input termination respectively. G_{av} is the network's available gain. It may be described as the ratio of available signal-power out, P_{av,sig_out} , to available signal-power in, P_{av,sig_in} , such that [1, 35]

$$G_{av} = \frac{P_{av,sig_out}}{P_{av,sig_in}} \quad (3.43)$$

The expression for F in (3.42) may be written as [1, 35]

$$F = \frac{\hat{P}_{av,out}}{\hat{P}_{av,in} G_{av}} \quad (3.44)$$

where $\hat{P}_{av,out}$ is the total available noise power present at the network's output port. Substituting (3.43) into (3.44), it's evident that noise factor describes the available signal-to-noise ratio degradation from the input to output port of the network. That is [1, 35]

$$F = \left(\frac{P_{av, sig}}{\hat{P}_{av}} \right)_{in} / \left(\frac{P_{av, sig}}{\hat{P}_{av}} \right)_{out} \quad (3.45)$$

Figure 3.9 [35] depicts a two-port network having available gain G_{av} and noise factor F connected to a passive termination R_s at its input and Z_l at its output. The network's input and

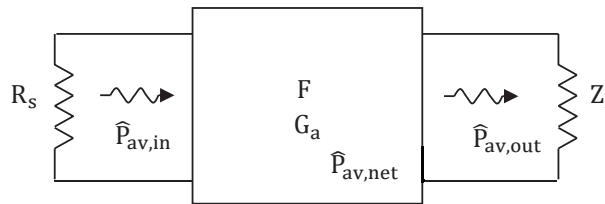


Figure 3.9: Two-Port Network Connected to Input and Output Terminations

output available noise-power is $\hat{P}_{av, in}$ and $\hat{P}_{av, out}$ respectively. An alternative view of the noise factor concept may be offered through inspection of (3.42) and re-writing it in the form of

$$F = 1 + \frac{\hat{P}_{av, net}}{\hat{P}_{av, in} G_{av}} \quad (3.46)$$

Industry standards establish an input termination reference temperature of $T_0 = 290K$ [47]. Thus (3.46) may be expressed as

$$F = 1 + \frac{\hat{P}_{av, net}}{kT_0 G_{av}} \quad (3.47)$$

where $\hat{P}_{av, in} = kT_0 \Delta f_n = kT_0$ for an effective noise bandwidth of 1Hz. From (3.47), a conclusion is drawn that noise factor is a measure of output available noise-power the network adds compared to the output available noise power due to the reference input termination at physical temperature T_0 . Per (3.47), should a device contribute zero noise, its minimum noise factor F

presents a numerical value of unity. Under such condition, there is no degradation of signal-to-noise ratio from the input-to-output port as demonstrated by (3.45).

Industry standards define noise factor [47] for the two-port case. From (3.35), the total noise-power emerging from an active two-port was described. Further, it was noted in (3.37) that the output match “looking-into” the network’s output port is S'_{22} with a source reflection coefficient of Γ_s connected to its input. From this, the noise-power $\overline{|\hat{b}_{2,net}|^2}$ added by the amplifier may be described by [35]

$$\overline{|\hat{b}_{2,net}|^2} = \hat{P}_{av,net} (1 - |S'_{22}|^2) \quad (3.48)$$

The second-term of (3.35) is also the noise-power added by the network. Equating this to (3.48) and solving for the available noise-power added by the two-port network results in

$$\hat{P}_{av,net} = \left| \frac{\Gamma_s S_{21}}{1 - \Gamma_s S_{11}} \right|^2 \frac{\overline{|\hat{b}_{gs1}|^2}}{1 - |S'_{22}|^2} + \frac{\overline{|\hat{b}_{gs2}|^2}}{1 - |S'_{22}|^2} + 2 \operatorname{Re} \left\{ \frac{\Gamma_s S_{21}}{1 - \Gamma_s S_{11}} \frac{\overline{\hat{b}_{gs1} \hat{b}_{gs2}^*}}{1 - |S'_{22}|^2} \right\}. \quad (3.49)$$

Through use of signal flow graphs and application of Mason’s Rule [35], the available gain G_{av} of the two-port network is

$$G_{av} = \frac{|S_{21}|^2 (1 - |\Gamma_s|^2)}{|1 - \Gamma_s S_{11}|^2 (1 - |S'_{22}|^2)}. \quad (3.50)$$

Substituting (3.49) and (3.50) into (3.47), the noise factor of the two-port amplifier may be written as [37]

$$F = 1 + \frac{|\Gamma_s|^2 \overline{|\hat{b}_{gs1}|^2} + 2 \operatorname{Re} \left\{ \frac{\Gamma_s (1 - \Gamma_s S_{11})^*}{S_{21}^*} \overline{\hat{b}_{gs1} \hat{b}_{gs2}^*} \right\} + \frac{|1 - \Gamma_s S_{11}|^2}{|S_{21}|^2} \overline{|\hat{b}_{gs2}|^2}}{kT_o (1 - |\Gamma_s|^2)} \quad (3.51)$$

$$= 1 + \frac{\overline{\left[\Gamma_S \hat{b}_{g_{s_1}} + \frac{1 - \Gamma_S S_{11}}{S_{21}} \hat{b}_{g_{s_2}} \right]^2}}{kT_o (1 - |\Gamma_S|^2)} . \quad (3.52)$$

A more compact form of (3.52) can be described in matrix form by [37]

$$F = 1 + \frac{\begin{bmatrix} \Gamma_S & \frac{1 - \Gamma_S S_{11}}{S_{21}} \end{bmatrix} \cdot \begin{bmatrix} \overline{\hat{b}_{g_{s_1}}^2} & \overline{\hat{b}_{g_{s_1}} \hat{b}_{g_{s_2}}^*} \\ \overline{\hat{b}_{g_{s_2}} \hat{b}_{g_{s_1}}^*} & \overline{\hat{b}_{g_{s_2}}^2} \end{bmatrix} \cdot \begin{bmatrix} \Gamma_S^* \\ \frac{1 - \Gamma_S^* S_{11}^*}{S_{21}^*} \end{bmatrix}}{kT_o (1 - |\Gamma_S|^2)} \quad (3.53)$$

$$= 1 + \frac{\boldsymbol{\beta} \hat{\mathbf{B}}_S \boldsymbol{\beta}^\dagger}{kT_o (1 - |\Gamma_S|^2)} . \quad (3.54)$$

$\boldsymbol{\beta}$ is a 1x2 matrix described by $\left[\Gamma_S \quad (1 - \Gamma_S S_{11})/S_{21} \right]$ and $\hat{\mathbf{B}}_S$ is the NCM of the two-port amplifier. Collective knowledge of the two-port's NCM, forward S-parameters, and input termination reflection coefficient permits determination of its noise factor F .

IEEE standards do not define noise factor for the multiport case [26]. However, an assessment is possible by substitution of the terms comprising the scattered noise matrix expression of (3.15) into (3.47). Further, by defining the relation

$$\overline{\hat{b}_{g_{l_i}} \hat{b}_{g_{l_j}}^*} = kT_o \overline{\hat{b}_{g_{l_i}}^\Psi \hat{b}_{g_{l_j}}^{\Psi*}} , \quad (3.55)$$

the elements of matrix $\hat{\mathbf{B}}_L^\Psi$ are introduced as ratios of the noise waves (or their equivalent noise temperature) incident to the DUT's ports divided by kT_o . Thus, $\hat{\mathbf{B}}_L = kT_o \hat{\mathbf{B}}_L^\Psi$. Consideration of (3.15) and (3.55) within the context of (3.47) yields [26]

$$F_i = 1 + \frac{\left\{ [\mathbf{I} - \mathbf{S}\mathbf{L}]^{-1} \hat{\mathbf{B}}_S [\mathbf{I} - \mathbf{S}\mathbf{L}]^{-1\dagger} \right\}_{ii}}{kT_o \left\{ [\mathbf{I} - \mathbf{S}\mathbf{L}]^{-1} \hat{\mathbf{S}} \hat{\mathbf{B}}_L^\Psi \hat{\mathbf{S}}^\dagger [\mathbf{I} - \mathbf{S}\mathbf{L}]^{-1\dagger} \right\}_{ii}} \quad (3.56)$$

where i represents the i -th output port and ii is a diagonal element of the matrix within brackets. Equation (3.56) evaluates the available noise at the i -th output due to the noise generated by the multiport and ratios it to that portion of available noise out due to all incident noise.

Noise matrix $\hat{\mathbf{B}}_L^v$ retains the correlation each incident noise wave source exhibits to the other. Should the connecting network's ports be isolated and present a noise temperature T_0 to the DUT's ports, $\hat{\mathbf{B}}_L^v$ reduces to the identity matrix and $\hat{\mathbf{B}}_L = kT_0\mathbf{I}$. Further, (3.55) supports assessment of the DUT's noise factor for the more general scenario where different input termination noise temperatures are presented to its ports.

The above expression is a generalized form. In accordance with (3.52), it reduces to the two-port case, i.e. $i = 2$, with input termination temperature set at T_0 .

3.2.2.2 Effective Noise Temperature

There are applications such as those involving satellite receivers where the noise factor is very small. For such cases, to better address the noise appraisal, an effective input noise temperature, \hat{T}_e , is preferred. If a resistor is heated to temperature \hat{T}_e , the available noise-power $\hat{P}_{av,res}$ it will generate is [1]

$$\hat{P}_{av,res} = k\hat{T}_e\Delta f_n \quad (3.57)$$

Equation (3.54) may be used to describe an effective noise-temperature of an active device as the temperature an input resistor would need be heated to produce the equivalent output noise-power of an active noise-free device. This may be expressed as [1]

$$F = 1 + \frac{k\hat{T}_e\Delta f_n}{kT_0\Delta f_n} = 1 + \frac{k\hat{T}_e}{kT_0} \quad (3.58)$$

Equating (3.54) and (3.58) results in the active two-port's effective noise-temperature being [37]

$$k\hat{T}_e = \frac{\beta\hat{B}_s\beta^\dagger}{(1-|\Gamma_s|^2)}. \quad (3.59)$$

Consider a satellite application [36] with an input noise temperature of 20K. From (3.58)

$$\hat{T}_e = T_o(F-1). \quad (3.60)$$

Let the noise factor of an amplifier used in this application be 1.2. Therefore, \hat{T}_e is 58 K. Even though the noise factor of the amplifier is very low, it's immediately apparent that for an input noise-temperature of 20K, that the noise of the amplifier is the dominant source [36]. For applications, such as satellite receivers where the input noise-temperature is low, specifying noise appraisal in terms of effective noise-temperature is generally more insightful.

Perhaps second to noise factor and its equivalent effective input noise temperature, noise parameters are the most common means by which the noise behavior of a microwave network is assessed. The next section will address this important figure-of-merit.

3.2.2.3 Noise Parameters

So far it has been shown that advanced knowledge of a linear network's NCM and scattering parameters can lead to quantifying its noise factor and effective noise-temperature. Each of these figures-of-merit are a function of the source impedance to which the network is connected. It's common practice for manufacturers to report a transistor's minimum achievable noise factor, the complex source reflection coefficient corresponding to the minimum, and its effective noise-resistance. These noise parameters are used by the amplifier designer to optimize noise performance or obtain the best tradeoff between low noise-high gain behaviors as a function of

source match. In this section, we will clarify the meaning of noise parameters and determine their relationship to the elements comprising the NCM.

A common form describing the noise factor in terms of a linear two-port's noise parameters is derived by Gonzalez [35] resulting in

$$F = F_{\min} + 4\hat{r}_n \frac{|\Gamma_S - \Gamma_{\text{OPT}}|^2}{|1 + \Gamma_{\text{OPT}}|^2 (1 - |\Gamma_S|^2)} \quad (3.61)$$

where

F_{\min} = the minimum noise factor,

Γ_{OPT} = the optimum source reflection coefficient yielding F_{\min} , and

$\hat{r}_n = \frac{\hat{R}_n}{Z_o}$ = the normalized equivalent noise resistance.

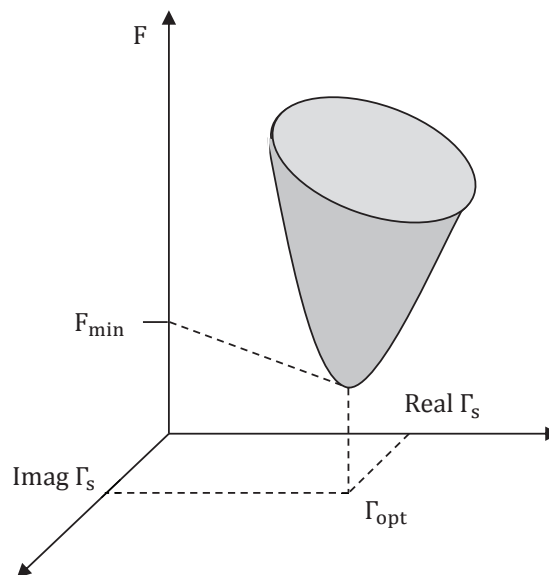


Figure 3.10: 3D Representation of Noise Factor versus Source Impedance [48]

F_{\min} and $\hat{\Gamma}_n$ are real numbers and Γ_{OPT} is complex. Equation (3.61) is graphically presented in Fig. 3.10 [48].

The noise parameters can be determined experimentally. The traditional approach [35] is to tune the reflection coefficient Γ_S of the source termination until F_{\min} is achieved. A noise figure meter and a vector network analyzer are used to measure F_{\min} and Γ_{OPT} respectively. The normalized equivalent noise-resistance $\hat{\Gamma}_n$ dictates the sensitivity of the device's noise factor as a function of source impedance. The larger $\hat{\Gamma}_n$ is, the more rapidly the noise factor will increase for a difference in change of Γ_S from Γ_{OPT} . To determine $\hat{\Gamma}_n$, the source reflection coefficient Γ_S is set to zero and noise factor F is measured. From (3.61) [35]

$$\hat{\Gamma}_n = (F|_{\Gamma_S=0} - F_{\min}) \frac{|1 + \Gamma_{\text{OPT}}|^2}{4|\Gamma_{\text{OPT}}|^2} \cdot \quad (3.62)$$

The effective noise-temperature may be described in terms of a two-port's noise parameters by substitution of (3.61) into (3.58) yielding [37]

$$k\hat{T}_e = k\hat{T}_{\min} + 4kT_0\hat{\Gamma}_n \frac{|\Gamma_S - \Gamma_{\text{OPT}}|^2}{|1 + \Gamma_{\text{OPT}}|^2 (1 - |\Gamma_S|^2)} \cdot \quad (3.63)$$

The elements comprising the NCM of an active two-port network may be expressed in terms of its noise and scattering parameters. We begin with the network's noise-wave model described in Fig. 3.11.

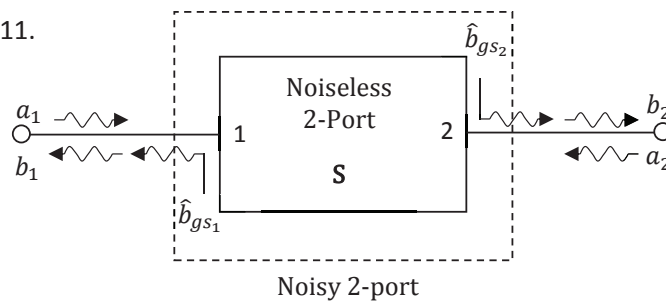


Figure 3.11: Scattered Noise-Wave Model of an Active Noisy Two-Port Amplifier

Scattered noise-wave generators \hat{b}_{gs_1} and \hat{b}_{gs_2} of a noisy two-port amplifier are assigned respectively to input port-one and output port-two of a noise-free, otherwise electrical equivalent network exhibiting behavior defined by its S-parameters. As previously discussed and repeated here for convenience, the NCM $\hat{\mathbf{B}}_s$ consists in the two-port case of four elements $\overline{|\hat{b}_{gs_1}|^2}$, $\overline{|\hat{b}_{gs_2}|^2}$, $\overline{\hat{b}_{gs_1}\hat{b}_{gs_2}^*}$, and $\overline{\hat{b}_{gs_2}\hat{b}_{gs_1}^*}$ where

$$\hat{\mathbf{B}}_s = \begin{bmatrix} \overline{|\hat{b}_{gs_1}|^2} & \overline{\hat{b}_{gs_1}\hat{b}_{gs_2}^*} \\ \overline{\hat{b}_{gs_2}\hat{b}_{gs_1}^*} & \overline{|\hat{b}_{gs_2}|^2} \end{bmatrix}. \quad (3.64)$$

The elements of the amplifier's NCM can be expressed in terms of its noise parameters by equating (3.59) and (3.63) [37]. Multiplying both of its sides by $1-|\Gamma_s|^2$ results in

$$|\Gamma_s|^2 \overline{|\hat{b}_{gs_1}|^2} + 2 \operatorname{Re} \left\{ \Gamma_s^* \left(\frac{1-\Gamma_s S_{11}}{S_{21}} \right) \overline{\hat{b}_{gs_1}\hat{b}_{gs_2}^*} \right\} + \left| \frac{1-\Gamma_s S_{11}}{S_{21}} \right|^2 \overline{|\hat{b}_{gs_2}|^2} = k\hat{T}_{\min} (1-|\Gamma_s|^2) + kt \frac{|\Gamma_s - \Gamma_{\text{OPT}}|^2}{|1 + \Gamma_{\text{OPT}}|^2} \quad (3.65)$$

where the normalized temperature-energy of the two-port is [37]

$$kt = \frac{4kT_0 \hat{R}_n}{Z_o}. \quad (3.66)$$

By introducing different values of Γ_s at the device's input, (3.65) can be used to extract expressions for each of the noise-wave elements comprising $\hat{\mathbf{B}}_s$ in terms of its noise parameters.

For example, to determine $\overline{|\hat{b}_{gs_2}|^2}$, Γ_s can be set to zero resulting in [27, 37]

$$\overline{|\hat{b}_{gs_2}|^2} = |S_{21}|^2 \left(k\hat{T}_{\min} + kt \frac{|\Gamma_{\text{OPT}}|^2}{|1 + \Gamma_{\text{OPT}}|^2} \right). \quad (3.67)$$

A-priori knowledge of noise parameters $\hat{\Gamma}_{\min}$, Γ_{OPT} , and \hat{R}_n along with forward gain S_{21} allows calculation of the amplifier's output noise-power due to scattered wave $\hat{b}_{g_{s_2}}$.

The noise-power of the input-port's scattered wave $\hat{b}_{g_{s_1}}$ can be determined by setting $\Gamma_s = \frac{1}{S_{11}}$, substituting it into (3.65), and solving for $\overline{|\hat{b}_{g_{s_1}}|^2}$. This leads to [27, 37]

$$\overline{|\hat{b}_{g_{s_1}}|^2} = k\hat{\Gamma}_{\min}(|S_{11}|^2 - 1) + kt \frac{|1 - S_{11}\Gamma_{\text{OPT}}|^2}{|1 + \Gamma_{\text{OPT}}|^2}. \quad (3.68)$$

The remaining two unknowns, $\overline{\hat{b}_{g_{s_1}}\hat{b}_{g_{s_2}}^*}$ and $\overline{\hat{b}_{g_{s_2}}\hat{b}_{g_{s_1}}^*}$, may be solved by constructing two equations, one by establishing an open-circuit as viewed from the device input, i.e. $\Gamma_s = 1$, and a second by tuning the input match to a short-circuit such that $\Gamma_s = -1$. By substitution of (3.67) and (3.68) into these equations, and solving for the correlation of noise-wave $\hat{b}_{g_{s_2}}$ compared to $\hat{b}_{g_{s_1}}$, we are left with [27, 37]

$$\overline{\hat{b}_{g_{s_1}}\hat{b}_{g_{s_2}}^*} = \frac{-S_{21}^*\Gamma_{\text{OPT}}^*kt}{|1 + \Gamma_{\text{OPT}}|^2} + \frac{S_{11}}{S_{21}}\overline{|\hat{b}_{g_{s_2}}|^2} \quad (3.69)$$

where $\overline{|\hat{b}_{g_{s_2}}|^2}$ is shown in (3.67). Equations (3.67-3.69) are used to convert from the network's noise parameters to its equivalent noise-wave description. In the case of our amplifier example, knowledge of the device's forward S-parameters is also required to complete the translation.

Next is to address the inverse conversion formulas. This set of expressions relates the noise parameters of a linear two-port as a function of its noise-wave description (NCM). Continuing with our amplifier example, to obtain its minimum achievable noise factor (or effective noise temperature), consider (3.59) relating a network's effective noise temperature to its noise wave quantities and input source match. Assuming the noise waves are known a-priori,

the question to be posed is, what is the optimum source match which yields the network's minimum effective noise temperature?

We begin by recognizing that the source match is comprised of real and imaginary components such that $\Gamma_s = \Gamma_{s_r} + j\Gamma_{s_i}$. Substituting into (3.59), $k\hat{T}_e$ is written as a function of two independent variables, Γ_{s_r} and Γ_{s_i} . To locate coordinates in the Γ_s - plane that correspond to the extrema of the circular-paraboloid shown in Fig. 3.10, two first-order partial derivatives of $k\hat{T}_e$ with respect to Γ_{s_r} and Γ_{s_i} are set zero. Their results produce two equations which are solved simultaneously yielding expressions for Γ_{s_r} and Γ_{s_i} . To locate the absolute minimum effective noise temperature $k\hat{T}_{\min}$, all extrema yielding values of $k\hat{T}_e$ as a function of $(\Gamma_{s_r}, \Gamma_{s_i})$ are compared. The optimum ordered pair yielding the absolute minimum is denoted $(\Gamma_{s_{\text{opt}_r}}, \Gamma_{s_{\text{opt}_i}})$. Lastly, the network's optimum source match $\Gamma_{s_{\text{opt}}}$ is obtained by combining the optimum real and imaginary components forming (3.70) and (3.71) such that [37]

$$\Gamma_{\text{OPT}} = \frac{\eta}{2} \left(1 - \sqrt{1 - \frac{4}{|\eta|^2}} \right) \quad (3.70)$$

where the complex number η is

$$\eta = \frac{\overline{S_{21}\hat{b}_{g_{s_1}} - S_{11}\hat{b}_{g_{s_2}}} + \overline{\hat{b}_{g_{s_2}}}}{S_{11}\overline{\hat{b}_{g_{s_2}}} - S_{21}\overline{\hat{b}_{g_{s_1}}\hat{b}_{g_{s_2}}^*}} \quad (3.71)$$

By direct substitution of (3.70 – 3.71) into (3.51), the minimum achievable noise factor of the active two-port amplifier can be stated as

$$F_{\min} = 1 + \frac{k\hat{T}_{\min}}{kT_o} \quad (3.72)$$

where [37]

$$k\hat{T}_{\min} = \frac{\overline{|\hat{b}_{g_{s_2}}|^2} - \overline{|\hat{b}_{g_{s_1}} S_{21} - \hat{b}_{g_{s_2}} S_{11}|^2} |\Gamma_{\text{OPT}}|^2}{|S_{21}|^2 (1 + |\Gamma_{\text{OPT}}|^2)} . \quad (3.73)$$

The fourth and remaining noise parameter to be acquired is the device's equivalent noise-resistance \hat{R}_n . Setting its input source match Γ_S to a short-circuit and substituting this into (3.65), one may conclude the two-port's normalized temperature-energy kt [37] is

$$kt = \overline{\left| \hat{b}_{g_{s_1}} - \frac{(1 + S_{11})}{S_{21}} \hat{b}_{g_{s_2}} \right|^2} . \quad (3.74)$$

From kt , the equivalent noise-resistance \hat{R}_n can be calculated from (3.66).

The complexity of the conversion formulas is due to the different definitions associated with noise-wave and noise parameters in (3.59) and (3.63) respectively [37]. Equation (3.59) shows a simplified relation for the effective noise-temperature of the active two-port when its source-match is terminated, i.e., $\Gamma_S = 0$. That is [37]

$$k\hat{T}_e = \frac{\overline{|\hat{b}_{g_{s_2}}|^2}}{|S_{21}|^2} \quad (3.75)$$

where only the output scattered noise-wave $\hat{b}_{g_{s_2}}$ contributes to the noise appraisal of the two-port. By contrast, per (3.63), a simplified expression for the effective noise-temperature is attained when the source-match is tuned to Γ_{OPT} . Under such conditions, the effective noise-temperature is at its minimum achievable value \hat{T}_{\min} .

By use of S-parameters and noise-wave theory, noise models for passive- and active-type n-ports embedded within a passive termination network have been derived. From these models, the n-port's NCM was extracted. It has been shown that use of a network's S-parameters and

NCM enables quantification of its noise behavior in accordance with industry standards, including noise factor, effective noise-temperature, and noise parameters.

In practice, it's often encountered that noise analysis performed on a device be conducted in the presence of a measurement receiver. The two networks are typically arranged in cascade, the first-stage being the device under test (DUT) followed second by a low-noise active measurement receiver. Both networks generate noise. To extract the DUT's NCM will require assessing the cascaded (overall) network noise and that of the measurement receiver. Aided by noise-wave theory and use of the cascade network's S-parameters, the details of the NCM de-embedding process will be developed in Chapter 4.

Chapter 4

Characterization and De-embedding a Linear Network's Noise Matrix

In practice, to characterize the noise behavior of a network requires the introduction of a second network connected to it in cascade. The first-stage is typically the device under test (DUT) followed by a second- representing an active noise measurement receiver. Generally, literature written on this subject [28, 49] uses scattering transfer parameters (T-parameters) and noise wave theory to de-embed, i.e. separate, the noise properties of a two-port DUT from its active receiver. The IEEE standards, previously outlined in Chapter 3, define noise figure in context of a two-port device. It follows that T-parameters are used because of their convenience in the analysis of cascaded connections [35]. However, a truly generalized noise behavioral model shall accommodate multi-port DUTs, i.e. $n \geq 2$, serving a wide range of network topologies and applications. Additionally, it's advantageous that such a model can predict behavior across its linear *and* nonlinear functional regions. For these reasons, Chapter 4 will use the S-parameter linear network representation. Later in Chapter 5, to accommodate for a network's performance over its full operating-space (linear *and* nonlinear), X-parameters will be the representation of choice. X-parameters are considered a mathematical superset of S-parameters, thereby reducing to a network's S-parameters within its small-signal (linear) operative space.

Pertaining to Chapter 4, section 4.1, an innovative derivation uses noise wave theory and S-parameters to de-embed the noise properties of a DUT from its overall network. Sections 4.2 and 4.3 build on the use of this novel mathematical framework to extract the DUTs NCM through a series of practical measurements. To re-enforce the concepts, an example network will be

analyzed using Keysight Technology's Advanced Design System (ADS) software. Model validation will be attained by comparison of independent numerical versus simulated results.

4.1 Two-Port Device Noise Measurement Model

Figure 4.1 shows two linear two-port networks connected in cascade; the first is the DUT and the second is an active noise measurement receiver. Both first- and second-stage networks are represented by their scattering and noise-wave parameters [28, 49]. From the DUT's frame of reference, its input and output ports are terminated in passive impedance Z_s and active noise receiver respectively. The incident and scattered waves of the DUT are strictly nondeterministic (noise). To de-embed the noise properties of the DUT from the overall network, noise-wave models for each stage may be devised. From these models, signal-flow equations can be constructed and ultimately used to solve for the DUT's NCM.

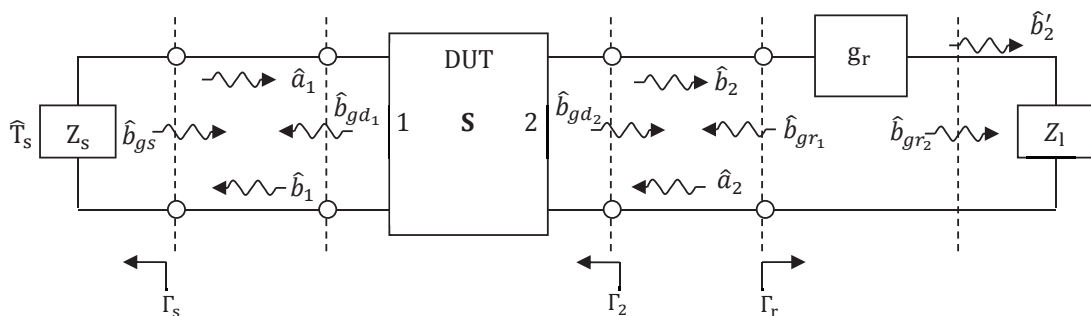


Figure 4.1: Two-Port Network Noise-Wave Model Connected To Passive Z_s And Noise Receiver

To that end, we begin with the scattered noise-wave model of an embedded n-port described by (3.12). Applying the two-port-case to (3.12), the DUT's scattered noise-wave \hat{b}_2 at its output port is solved whereby in (4.1)

$$\hat{b}_2 = \frac{S_{21}\hat{b}_{gs} + (\Gamma_s S_{12} S_{21} - \Gamma_s S_{11} S_{22} + S_{22})\hat{b}_{gr1} + \Gamma_s S_{21}\hat{b}_{gd1} + (1 - \Gamma_s S_{11})\hat{b}_{gd2}}{(1 - \Gamma_s S_{11})(1 - \Gamma_r S_{22}) - \Gamma_s \Gamma_r S_{12} S_{21}} \quad (4.1)$$

From (4.1), it's evident that the noise properties \hat{b}_{gs} of the source, \hat{b}_{gr1} of the receiver, and \hat{b}_{gd1} , \hat{b}_{gd2} of the DUT contribute to \hat{b}_2 . Each noise-generator undergoes a transformation due to its interaction with the overall network. This interaction is represented in (4.1) by the noise-generator's coefficient. A more intuitive form of (4.1) is realized by considering the DUT's output port-two match Γ_2 as shown in Fig. 4.1 under the condition its input port is terminated in Z_s and presented with reflection coefficient Γ_s . Using signal flow analysis, it can be shown that [35]

$$\Gamma_2 = S_{22} + \frac{\Gamma_s S_{12} S_{21}}{1 - \Gamma_s S_{11}} \quad (4.2)$$

Substituting (4.2) into (4.1), the DUT's scattered noise-wave evaluated at its output port becomes

$$\hat{b}_2 = \frac{S_{21}\hat{b}_{gs} + \Gamma_2(1 - \Gamma_s S_{11})\hat{b}_{gr1} + \Gamma_s S_{21}\hat{b}_{gd1} + (1 - \Gamma_s S_{11})\hat{b}_{gd2}}{(1 - \Gamma_s S_{11})(1 - \Gamma_r \Gamma_2)} \quad (4.3)$$

The noise-power density of the scattered wave can be obtained by evaluating the time-averaged product of \hat{b}_2 with its complex conjugate resulting in

$$\overline{\hat{b}_2 \hat{b}_2^*} = \frac{|S_{21}|^2 \overline{|\hat{b}_{gs}|^2} + |\Gamma_2|^2 |1 - \Gamma_s S_{11}|^2 \overline{|\hat{b}_{gr1}|^2} + |\Gamma_s|^2 |S_{21}|^2 \overline{|\hat{b}_{gd1}|^2} + \Gamma_s S_{21} (1 - \Gamma_s S_{11})^* \overline{\hat{b}_{gd1} \hat{b}_{gd2}^*} + \Gamma_s^* S_{21} (1 - \Gamma_s S_{11}) \overline{\hat{b}_{gd1}^* \hat{b}_{gd2}} + |1 - \Gamma_s S_{11}|^2 \overline{|\hat{b}_{gd2}|^2}}{|1 - \Gamma_s S_{11}|^2 |1 - \Gamma_r \Gamma_2|^2} \quad (4.4)$$

where use is made that the noise generated by source, receiver, and DUT are uncorrelated to one another. By inspection of (4.4), it's evident that the four elements comprising the DUT's NCM are present.

The DUT's scattered noise-wave present at its output port is also the incident noise-wave introduced to the input port of the receiver. As shown in Fig. 4.1, the receiver will influence its incident noise-wave \hat{b}_2 by its gain g_r , noise-bandwidth which we will assume to be unity for now, and the internally generated noise-wave \hat{b}_{gr_2} emerging from its output port. That is, the noise-wave \hat{b}'_2 imparted across the receiver's load Z_1 can be determined by accounting for the amplification g_r of the receiver's incident noise-wave \hat{b}_2 and the always present outgoing noise-wave \hat{b}_{gr_2} such that [28, 49, 58]

$$\hat{b}'_2 = \left(\frac{S_{21}\hat{b}_{gs} + \Gamma_2(1 - \Gamma_s S_{11})\hat{b}_{gr_1} + \Gamma_s S_{21}\hat{b}_{gd_1} + (1 - \Gamma_s S_{11})\hat{b}_{gd_2}}{(1 - \Gamma_s S_{11})(1 - \Gamma_r \Gamma_2)} \right) \cdot g_r + \hat{b}_{gr_2}. \quad (4.5)$$

To make noise-power measurements with the receiver is equivalent to assessing the noise-power associated with the instantaneous noise-wave \hat{b}'_2 .

4.2 Noise-Power Measurement

The two-port noise measurement model described in (4.5) is the foundation from which a received noise-power measurement expression may be formulated that relates noise-power measured in terms of the noise properties and S-parameters of the source, receiver, and DUT. We begin by assessing the noise-power density $\hat{\Phi}_r$ of the instantaneous noise-wave \hat{b}'_2 presented across the receiver's load. By taking the product of \hat{b}'_2 in (4.5) with its complex conjugate and evaluating its time-averaged quantity, we are left with the expression

$$\hat{\Phi}_r = \overline{\hat{b}'_2 \hat{b}_2^*} = \frac{|S_{21}|^2 |g_r|^2}{|1 - \Gamma_s S_{11}|^2 |1 - \Gamma_r \Gamma_2|^2} \overline{|\hat{b}_{gs}|^2} + \frac{|\Gamma_2|^2 |g_r|^2}{|1 - \Gamma_r \Gamma_2|^2} \overline{|\hat{b}_{gr1}|^2} + \frac{\Gamma_2 g_r}{1 - \Gamma_r \Gamma_2} \overline{\hat{b}_{gr1} \hat{b}_{gr2}^*} + \frac{\Gamma_2^* g_r}{(1 - \Gamma_r \Gamma_2)^*} \overline{\hat{b}_{gr1}^* \hat{b}_{gr2}} + \overline{|\hat{b}_{gr2}|^2} +$$

$$\frac{|\Gamma_s|^2 |S_{21}|^2 |g_r|^2}{|1 - \Gamma_s S_{11}|^2 |1 - \Gamma_r \Gamma_2|^2} \overline{|\hat{b}_{gd1}|^2} + \frac{\Gamma_s S_{21} |g_r|^2}{(1 - \Gamma_s S_{11}) |1 - \Gamma_r \Gamma_2|^2} \overline{\hat{b}_{gd1} \hat{b}_{gd2}^*} + \frac{\Gamma_s^* S_{21} |g_r|^2}{(1 - \Gamma_s S_{11})^* |1 - \Gamma_r \Gamma_2|^2} \overline{\hat{b}_{gd1}^* \hat{b}_{gd2}} + \frac{|g_r|^2}{|1 - \Gamma_r \Gamma_2|^2} \overline{|\hat{b}_{gd2}|^2}.$$

(4.6)

The first-term to the right of the second equal sign is the noise-density appearing at the receiver's output due to the source termination Z_s . The next four-terms are related to the receiver's internally generated noise. The remaining terms describing the receiver's output are from the internally generated noise of the two-port DUT. Thus, the noise generated by the measurement system comprises the first five-terms in (4.6) while the remaining four encompass the noise properties of the two-port DUT.

Practical measurement receivers provide a bandwidth $\Delta f_n \gg 1\text{Hz}$. The total measured noise-power \hat{P}_m confined to the receiver's noise-bandwidth that's delivered to its load Z_l can be attained by multiplying both sides of (4.6) by Δf_n . Having performed this operation, all terms in (4.6) involving noise-wave generation within the source, DUT, and the reflected version of receiver noise-density $\overline{|\hat{b}_{gs}|^2}$ include a gain-bandwidth product $|g_r|^2 \cdot \Delta f_n$ in their coefficients. This is defined as [58]

$$G_r \equiv |g_r|^2 \cdot \Delta f_n. \quad (4.7)$$

For this consideration, along with substitution of (3.41) into the source related term $\overline{|\hat{b}_{gs}|^2}$ of (4.6), the noise-power expression \hat{P}_m delivered to the receiver becomes

$$\hat{P}_m = \frac{|S_{21}|^2 k\hat{T}_s (1-|\Gamma_s|^2) G_r}{|1-\Gamma_s S_{11}|^2 |1-\Gamma_r \Gamma_2|^2} + \frac{|\Gamma_2|^2 G_r}{|1-\Gamma_r \Gamma_2|^2} \overline{|\hat{b}_{gr1}|^2} + \frac{\Gamma_2 \mathbf{g}_r \cdot \Delta \mathbf{f}_n}{1-\Gamma_r \Gamma_2} \overline{\hat{b}_{gr1} \hat{b}_{gr2}^*} + \frac{\Gamma_2^* \mathbf{g}_r^* \cdot \Delta \mathbf{f}_n}{(1-\Gamma_r \Gamma_2)^*} \overline{\hat{b}_{gr1}^* \hat{b}_{gr2}} + \overline{|\hat{b}_{gr2}|^2} \cdot \Delta \mathbf{f}_n +$$

$$\frac{|\Gamma_s|^2 |S_{21}|^2 G_r}{|1-\Gamma_s S_{11}|^2 |1-\Gamma_r \Gamma_2|^2} \overline{|\hat{b}_{gd1}|^2} + \frac{\Gamma_s S_{21} G_r}{(1-\Gamma_s S_{11}) |1-\Gamma_r \Gamma_2|^2} \overline{\hat{b}_{gd1} \hat{b}_{gd2}^*} + \frac{\Gamma_s^* S_{21}^* G_r}{(1-\Gamma_s S_{11})^* |1-\Gamma_r \Gamma_2|^2} \overline{\hat{b}_{gd1}^* \hat{b}_{gd2}} + \frac{G_r}{|1-\Gamma_r \Gamma_2|^2} \overline{|\hat{b}_{gd2}|^2}$$

(4.8)

where \hat{T}_s is the available (physical) noise-temperature of the passive source impedance Z_s .

Through a series of noise-power measurements, (4.8) can be used to de-embed, i.e. isolate, the noise properties of the two-port DUT from the measurement system's generated noise; this is the subject of Section 4.3.

4.3 Linear Network Noise Extraction from its Cascaded Network

To separate the noise generated by the DUT from the noise generated by the measurement system, it's fitting to group the terms of (4.8) in matrix form such that [28, 49, 58]

$$\hat{P}_m = \left[\begin{array}{cccc} \frac{k\hat{T}_s (1-|\Gamma_s|^2) |S_{21}|^2}{|1-\Gamma_s S_{11}|^2 |1-\Gamma_r \Gamma_2|^2} & \frac{|\Gamma_2|^2}{|1-\Gamma_r \Gamma_2|^2} & \frac{\Gamma_2}{1-\Gamma_r \Gamma_2} & \frac{\Gamma_2^*}{(1-\Gamma_r \Gamma_2)^*} \end{array} \right] \cdot \left[\begin{array}{c} G_r \\ G_r \cdot \overline{|\hat{b}_{gr1}|^2} \\ \mathbf{g}_r \cdot \Delta \mathbf{f}_n \cdot \overline{\hat{b}_{gr1} \hat{b}_{gr2}^*} \\ \mathbf{g}_r^* \cdot \Delta \mathbf{f}_n \cdot \overline{\hat{b}_{gr1}^* \hat{b}_{gr2}} \\ \Delta \mathbf{f}_n \cdot \overline{|\hat{b}_{gr2}|^2} \end{array} \right] +$$

$$G_r \cdot \begin{bmatrix} \frac{|\Gamma_s|^2 |S_{21}|^2}{|1 - \Gamma_s S_{11}|^2 |1 - \Gamma_r \Gamma_2|^2} & \frac{\Gamma_s S_{21}}{(1 - \Gamma_s S_{11}) |1 - \Gamma_r \Gamma_2|^2} & \frac{\Gamma_s^* S_{21}^*}{(1 - \Gamma_s S_{11})^* |1 - \Gamma_r \Gamma_2|^2} & \frac{1}{|1 - \Gamma_r \Gamma_2|^2} \end{bmatrix} \cdot \begin{bmatrix} \overline{|\hat{b}_{gd1}|^2} \\ \overline{\hat{b}_{gd1} \hat{b}_{gd2}^*} \\ \overline{\hat{b}_{gd2} \hat{b}_{gd1}^*} \\ \overline{|\hat{b}_{gd2}|^2} \end{bmatrix}. \quad (4.9)$$

The 5x1 column matrix in (4.9) are calibration coefficients related to the measurement receiver. Beside the gain-bandwidth product G_r , there are the four elements comprising the receiver's noise correlation matrix $\hat{\mathbf{B}}_R$ which will be defined as [28, 49, 58]

$$\hat{\mathbf{B}}_R \equiv \begin{bmatrix} \hat{r}_{11} & \hat{r}_{12} \\ \hat{r}_{21} & \hat{r}_{22} \end{bmatrix} = \begin{bmatrix} G_r \overline{|\hat{b}_{gr1}|^2} & g_r \cdot \Delta f_n \cdot \overline{\hat{b}_{gr1} \hat{b}_{gr2}^*} \\ g_r^* \cdot \Delta f_n \cdot \overline{\hat{b}_{gr1}^* \hat{b}_{gr2}} & \Delta f_n \cdot \overline{|\hat{b}_{gr2}|^2} \end{bmatrix}. \quad (4.10)$$

In (4.10), g_r is incorporated into the receiver's noise-wave parameters. This eliminates the need for determining the phase of g_r and thus simplifies the receiver calibration process. The unit of measure for the elements involving $\hat{\mathbf{B}}_R$ is watts.

The 4x1 column matrix in (4.9) are the four elements encompassing the two-port DUT's NCM $\hat{\mathbf{B}}_D$. Consistent in form to that present in (3.53, 3.54), it's defined to be

$$\hat{\mathbf{B}}_D \equiv \begin{bmatrix} \hat{d}_{11} & \hat{d}_{12} \\ \hat{d}_{21} & \hat{d}_{22} \end{bmatrix} = \begin{bmatrix} \overline{|\hat{b}_{gd1}|^2} & \overline{\hat{b}_{gd1} \hat{b}_{gd2}^*} \\ \overline{\hat{b}_{gd1}^* \hat{b}_{gd2}} & \overline{|\hat{b}_{gd2}|^2} \end{bmatrix} \quad (4.11)$$

with a unit of measure in W/Hz.

Substituting (4.10) and (4.11) into (4.9):

$$\hat{\mathbf{P}}_m = \begin{bmatrix} \frac{k\hat{\Gamma}_s(1-|\Gamma_s|^2)|S_{21}|^2}{|1-\Gamma_s S_{11}|^2|1-\Gamma_r\Gamma_2|^2} & \frac{|\Gamma_2|^2}{|1-\Gamma_r\Gamma_2|^2} & \frac{\Gamma_2}{1-\Gamma_r\Gamma_2} & \frac{\Gamma_2^*}{(1-\Gamma_r\Gamma_2)^*} & 1 \end{bmatrix} \cdot \begin{bmatrix} G_r \\ \hat{r}_{11} \\ \hat{r}_{12} \\ \hat{r}_{21} \\ \hat{r}_{22} \end{bmatrix} + G_r \cdot \begin{bmatrix} \frac{|\Gamma_s|^2|S_{21}|^2}{|1-\Gamma_s S_{11}|^2|1-\Gamma_r\Gamma_2|^2} & \frac{\Gamma_s S_{21}}{(1-\Gamma_s S_{11})|1-\Gamma_r\Gamma_2|^2} & \frac{\Gamma_s^* S_{21}^*}{(1-\Gamma_s S_{11})^*|1-\Gamma_r\Gamma_2|^2} & \frac{1}{|1-\Gamma_r\Gamma_2|^2} \end{bmatrix} \cdot \begin{bmatrix} \hat{d}_{11} \\ \hat{d}_{12} \\ \hat{d}_{21} \\ \hat{d}_{22} \end{bmatrix}. \quad (4.12)$$

The first-term in (4.12) is related to the influence of noise generation due to the source and receiver while the second-term is the consequence of noise generation due to the two-port DUT. Should $\hat{\Gamma}_s$, G_r , and $\hat{\mathbf{B}}_R$ be known through calibration, then the linear equation of (4.12) comprises four remaining unknowns each representing the noise-wave parameters of $\hat{\mathbf{B}}_D$.

By performing four noise-power measurements, each performed at a distinct source match Γ_s , four independent linear equations may be constructed whereby the elements of NCM $\hat{\mathbf{B}}_D$ may be attained. Once $\hat{\mathbf{B}}_D$ is known, (3.54) and (3.59) may be solved for the noise factor and effective noise-temperature respectively of the two-port DUT for any input reflection coefficient Γ_s which is presented at its input port.

Equation (4.12) may be composed in a more compact form by introducing column matrices [28, 46, 49]

$$\boldsymbol{\alpha}_R = [\alpha_{r1} \quad \alpha_{r2}] = \begin{bmatrix} \frac{\Gamma_2}{1-\Gamma_r\Gamma_2} & 1 \end{bmatrix} \quad (4.13)$$

and

$$\boldsymbol{\alpha}_D = [\alpha_{d1} \quad \alpha_{d2}] = \begin{bmatrix} \frac{\Gamma_s S_{21}}{1 - \Gamma_s S_{11}} & 1 \end{bmatrix} \quad (4.14)$$

such that

$$\hat{P}_m = k\hat{T}_s (1 - |\Gamma_s|^2) \left(\frac{|S_{21}|^2 G_r}{|1 - \Gamma_s S_{11}|^2 |1 - \Gamma_r \Gamma_2|^2} \right) + \boldsymbol{\alpha}_D \hat{\mathbf{B}}_D \boldsymbol{\alpha}_D^\dagger \left(\frac{G_r}{|1 - \Gamma_r \Gamma_2|^2} \right) + \boldsymbol{\alpha}_R \hat{\mathbf{B}}_R \boldsymbol{\alpha}_R^\dagger. \quad (4.15)$$

$\boldsymbol{\alpha}_D$ translates the devices noise signals appearing at its input and output ports to their output equivalent, thus $\alpha_{d2} = 1$. $\boldsymbol{\alpha}_R$ accomplishes the same purpose for the receiver's noise signals. By inspection of (4.15), it's evident that noise generated by the source, DUT, and receiver undergo a linear transformation appearing at the composite network's output. The transformations are due to the interaction of the embedded component's noise-waves with its connected network including multiplication by the gain due to subsequent devices in the transmission signal path. Consequently, each noise-wave generator in the cascade network contributes to the noise-power \hat{P}_m detected at the receiver's output.

In our case, we seek to determine the NCM $\hat{\mathbf{B}}_D$ of the two-port DUT. To solve for $\hat{\mathbf{B}}_D$ in (4.15), we will need to know the absolute noise-temperature (physical temperature) \hat{T}_s of the passive source impedance and the receiver's characteristics including its gain-bandwidth product G_r and NCM $\hat{\mathbf{B}}_R$. Their values will be determined in calibration.

4.3.1 Noise Receiver Calibration

The purpose for calibrating the noise receiver is to determine its gain-bandwidth product and NCM, G_r and $\hat{\mathbf{B}}_R$ respectively. This is a prerequisite to testing the DUT to distinguish its noise from the noise contributors of the measurement system.

To calibrate the noise receiver, a noise source will be directly connected to its input. The noise source Z_s shown in Fig. 4.2 will introduce various effective noise-temperatures and [58]

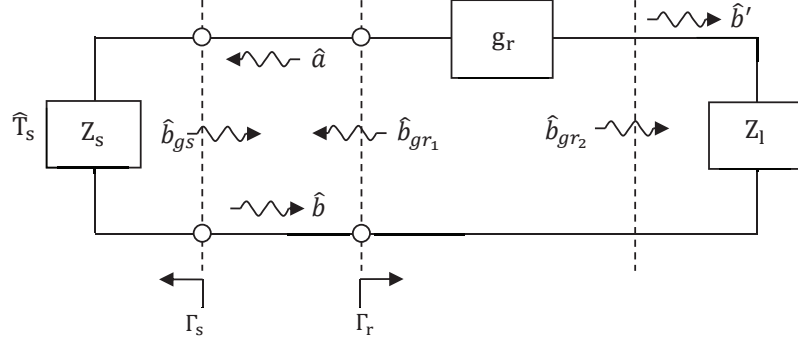


Figure 4.2: Noise Receiver Calibration – Noise Source Connected To Noise Receiver

reflection coefficients $\hat{\Gamma}_s$ and Γ_s respectively to the receiver's input in order that \mathbf{G}_r and $\hat{\mathbf{B}}_R$ be determined.

By inspection of Fig. 4.2, two equations related to the network's transmission noise-waves \hat{a} and \hat{b} are evident, that is

$$\hat{b} = \Gamma_s \hat{a} + \hat{b}_{gs} \quad (4.16)$$

and

$$\hat{a} = \Gamma_r \hat{b} + \hat{b}_{gr1} \quad (4.17)$$

Substituting (4.17) into (4.16) and solving for the scattered noise-wave \hat{b} incident to the receiver's input yields

$$\hat{b} = \frac{1}{1 - \Gamma_s \Gamma_r} \left(\Gamma_s \hat{b}_{gr1} + \hat{b}_{gs} \right) \quad (4.18)$$

Referencing Fig. 4.2, the noise-wave \hat{b}' incident to the receiver's load Z_1 is determined by two observations. First, noise-wave \hat{b} imposed at the receiver's input undergoes a linear transformation g_r . Second, the output noise-wave \hat{b}_{gr_2} of the receiver is directly presented to Z_1 . Given the receiver's output termination is matched, the noise-wave \hat{b}' detected by the receiver is

$$\hat{b}' = \frac{\Gamma_s g_r}{1 - \Gamma_s \Gamma_r} \hat{b}_{gr_1} + \frac{g_r}{1 - \Gamma_s \Gamma_r} \hat{b}_{gs} + \hat{b}_{gr_2} \quad (4.19)$$

The noise-power $\hat{P}_{r,cal}$ detected by the receiver (measured) at Z_1 is obtained by multiplying noise-wave \hat{b}' by its complex conjugate and evaluating its time-averaged product. Recognizing the noise generated by the source is uncorrelated with that produced by the receiver,

$$\hat{P}_{r,cal} = \overline{\hat{b}' \hat{b}'^*} \cdot \Delta f_n = \frac{|g_r|^2 \Delta f_n}{|1 - \Gamma_s \Gamma_r|^2} \overline{|\hat{b}_{gs}|^2} + \frac{|\Gamma_s|^2 |g_r|^2 \Delta f_n}{|1 - \Gamma_s \Gamma_r|^2} \overline{|\hat{b}_{gr_1}|^2} + \frac{\Gamma_s g_r \Delta f_n}{1 - \Gamma_s \Gamma_r} \overline{\hat{b}_{gr_1} \hat{b}_{gr_2}^*} + \frac{\Gamma_s^* g_r^* \Delta f_n}{1 - \Gamma_s^* \Gamma_r^*} \overline{\hat{b}_{gr_1}^* \hat{b}_{gr_2}} + \Delta f_n \overline{|\hat{b}_{gr_2}|^2} \quad (4.20)$$

Equation (4.20) can be expressed in matrix form such that

$$\hat{P}_{r,cal} = \begin{bmatrix} \frac{\overline{|\hat{b}_{gs}|^2}}{|1 - \Gamma_s \Gamma_r|^2} & & & & \\ & \frac{|\Gamma_s|^2}{|1 - \Gamma_s \Gamma_r|^2} & & & \\ & & \frac{\Gamma_s}{1 - \Gamma_s \Gamma_r} & & \\ & & & \frac{\Gamma_s^*}{1 - \Gamma_s^* \Gamma_r^*} & \\ & & & & 1 \end{bmatrix} \cdot \begin{bmatrix} |g_r|^2 \cdot \Delta f_n \\ |g_r|^2 \cdot \Delta f_n \cdot \overline{|\hat{b}_{gr_1}|^2} \\ g_r \cdot \Delta f_n \cdot \overline{\hat{b}_{gr_1} \hat{b}_{gr_2}^*} \\ g_r^* \cdot \Delta f_n \cdot \overline{\hat{b}_{gr_1}^* \hat{b}_{gr_2}} \\ \Delta f_n \cdot \overline{|\hat{b}_{gr_2}|^2} \end{bmatrix} \quad (4.21)$$

Use of (4.7) and (4.10) in (4.21) results in (4.22) where

$$\hat{\mathbf{P}}_{r, \text{cal}} = \begin{bmatrix} \frac{|\hat{b}_{gs}|^2}{|1 - \Gamma_s \Gamma_r|^2} & \frac{|\Gamma_s|^2}{|1 - \Gamma_s \Gamma_r|^2} & \frac{\Gamma_s}{1 - \Gamma_s \Gamma_r} & \frac{\Gamma_s^*}{1 - \Gamma_s^* \Gamma_r^*} & 1 \end{bmatrix} \cdot \begin{bmatrix} \mathbf{G}_r \\ \hat{r}_{11} \\ \hat{r}_{12} \\ \hat{r}_{21} \\ \hat{r}_{22} \end{bmatrix}. \quad (4.22)$$

There are three observations worth highlighting in (4.22). First, the five unknowns related to the receiver are delineated in the column matrix. Second, determining the phase of transmission coefficient g_r is not necessary, only its gain $|g_r|^2$. g_r and its conjugate are embedded in the receiver's NCM elements \hat{r}_{12} and \hat{r}_{21} respectively. This is convenient within the context of modern noise measurement system hardware architecture. Finally, by choosing a minimum of five distinct source settings, i.e. combination of $|\hat{b}_{gs}|^2$ and Γ_s , five independent linear equations may be generated and used to solve for \mathbf{G}_r and $\hat{\mathbf{B}}_R$.

To that end, inspection of (4.22) offers some clues to appropriate source settings (standards) used for calibration of the receiver. For example, if $\Gamma_s = 0$, two terms remain. Should a noise source offer two distinct effective noise-temperature values, two unknowns in \mathbf{G}_r and \hat{r}_{22} may be solved. Next, a standard with $\Gamma_s = 1$ will distinguish itself from row matrix entries one and five. Finally, two additional high reflection standards with a suitable phase shift will illuminate row matrix entries two through four. The equations formed from these remaining three standards will enable a solution for \hat{r}_{11} , \hat{r}_{12} , and \hat{r}_{21} .

A diode-based noise source may be used as a suitable calibration standard capable of offering two distinct effective noise-temperature conditions. The noise source in its "on" state produces a calibrated level of noise-power at a specific frequency while thermal noise is generated when operating in its "off" state. The noise power, described by its excess noise ratio (ENR) is defined as [1]

$$\text{ENR} \equiv 10 \log_{10} \left(\frac{\hat{T}_{\text{hot}} - \hat{T}_{\text{cold}}}{290} \right) \quad (4.23)$$

where compensation needs to be applied to \hat{T}_{cold} in (4.23) if $\hat{T}_{\text{room}} \neq \hat{T}_{\text{cold}} = 290\text{K}$. The ENR describes the effective noise-temperature \hat{T}_{hot} a resistor would need be heated to generate an equivalent noise-power delivered to a connected fifty ohm load. Solving for \hat{T}_{hot} in (4.23) and assuming $\hat{T}_{\text{room}} = \hat{T}_{\text{cold}} = 290\text{K}$,

$$\hat{T}_{\text{hot}} = 290 \left(10^{\frac{\text{ENR}}{10}} + 1 \right) . \quad (4.24)$$

The effective noise-temperature is related to the source's available noise-power by [1]

$$k\hat{T}_{\text{hot}}\Delta f_n = \hat{P}_{\text{av}} \left(1 - |\Gamma_{\text{hot}}|^2 \right) . \quad (4.25)$$

Γ_{hot} represents the reflection coefficient of the noise source in its "on" state. Comparing (4.25) with (3.41), it's evident that

$$\overline{|\hat{b}_{gs}|^2} = \overline{|\hat{b}_{hot}|^2} = k\hat{T}_{\text{hot}} . \quad (4.26)$$

Substituting (4.26) into (4.22),

$$\hat{P}_{\text{hot}} = \left[\begin{array}{cccc} \frac{k\hat{T}_{\text{hot}}}{|1 - \Gamma_{\text{hot}}\Gamma_r|^2} & \frac{|\Gamma_{\text{hot}}|^2}{|1 - \Gamma_{\text{hot}}\Gamma_r|^2} & \frac{\Gamma_{\text{hot}}}{1 - \Gamma_{\text{hot}}\Gamma_r} & \frac{\Gamma_{\text{hot}}^*}{1 - \Gamma_{\text{hot}}^*\Gamma_r^*} \\ & & & 1 \end{array} \right] \cdot \begin{bmatrix} \mathbf{G}_r \\ \hat{\Gamma}_{11} \\ \hat{\Gamma}_{12} \\ \hat{\Gamma}_{21} \\ \hat{\Gamma}_{22} \end{bmatrix} ; \quad (4.27)$$

equation (4.27) is applicable when the noise source is operating in its "on" state.

The noise source in its “off” state operates as a passive termination, thus (4.22) takes the form

$$\hat{\mathbf{P}}_{\text{cold}} = \begin{bmatrix} \frac{k\hat{T}_{\text{room}}(1-|\Gamma_{\text{cold}}|^2)}{|1-\Gamma_{\text{cold}}\Gamma_r|^2} & \frac{|\Gamma_{\text{cold}}|^2}{|1-\Gamma_{\text{cold}}\Gamma_r|^2} & \frac{\Gamma_{\text{cold}}}{1-\Gamma_{\text{cold}}\Gamma_r} & \frac{\Gamma_{\text{cold}}^*}{1-\Gamma_{\text{cold}}^*\Gamma_r^*} & 1 \end{bmatrix} \cdot \begin{bmatrix} \mathbf{G}_r \\ \hat{r}_{11} \\ \hat{r}_{12} \\ \hat{r}_{21} \\ \hat{r}_{22} \end{bmatrix} \quad (4.28)$$

where \hat{T}_{room} is the ambient temperature in Kelvin. \hat{T}_{hot} , Γ_{hot} , and Γ_{cold} are calibrated values of the noise source.

Three additional calibration standards are required. The standards chosen will be passive terminations exhibiting reflection coefficients, $\Gamma_{s,1}$, $\Gamma_{s,2}$, and $\Gamma_{s,3}$. The corresponding noise-power delivered to the receiver will be $\hat{P}_{r,1}$, $\hat{P}_{r,2}$, and $\hat{P}_{r,3}$.

To solve for the receiver's gain-bandwidth product G_r and NCM $\hat{\mathbf{B}}_R$, a matrix expression is formed from (4.22), (4.27), and (4.28) such that

$$\begin{bmatrix} \hat{\mathbf{P}}_{\text{hot}} \\ \hat{\mathbf{P}}_{\text{cold}} \\ \hat{\mathbf{P}}_{r,1} \\ \hat{\mathbf{P}}_{r,2} \\ \hat{\mathbf{P}}_{r,3} \end{bmatrix} = \begin{bmatrix} \frac{k\hat{\mathbf{T}}_{\text{hot}}}{|1-\Gamma_{\text{hot}}\Gamma_r|^2} & \frac{|\Gamma_{\text{hot}}|^2}{|1-\Gamma_{\text{hot}}\Gamma_r|^2} & \frac{\Gamma_{\text{hot}}}{1-\Gamma_{\text{hot}}\Gamma_r} & \frac{\Gamma_{\text{hot}}^*}{1-\Gamma_{\text{hot}}^*\Gamma_r^*} & 1 \\ \frac{k\hat{\mathbf{T}}_{\text{room}}(1-|\Gamma_{\text{cold}}|^2)}{|1-\Gamma_{\text{cold}}\Gamma_r|^2} & \frac{|\Gamma_{\text{cold}}|^2}{|1-\Gamma_{\text{cold}}\Gamma_r|^2} & \frac{\Gamma_{\text{cold}}}{1-\Gamma_{\text{cold}}\Gamma_r} & \frac{\Gamma_{\text{cold}}^*}{1-\Gamma_{\text{cold}}^*\Gamma_r^*} & 1 \\ \frac{k\hat{\mathbf{T}}_{\text{room}}(1-|\Gamma_{s,1}|^2)}{|1-\Gamma_{s,1}\Gamma_r|^2} & \frac{|\Gamma_{s,1}|^2}{|1-\Gamma_{s,1}\Gamma_r|^2} & \frac{\Gamma_{s,1}}{1-\Gamma_{s,1}\Gamma_r} & \frac{\Gamma_{s,1}^*}{1-\Gamma_{s,1}^*\Gamma_r^*} & 1 \\ \frac{k\hat{\mathbf{T}}_{\text{room}}(1-|\Gamma_{s,2}|^2)}{|1-\Gamma_{s,2}\Gamma_r|^2} & \frac{|\Gamma_{s,2}|^2}{|1-\Gamma_{s,2}\Gamma_r|^2} & \frac{\Gamma_{s,2}}{1-\Gamma_{s,2}\Gamma_r} & \frac{\Gamma_{s,2}^*}{1-\Gamma_{s,2}^*\Gamma_r^*} & 1 \\ \frac{k\hat{\mathbf{T}}_{\text{room}}(1-|\Gamma_{s,3}|^2)}{|1-\Gamma_{s,3}\Gamma_r|^2} & \frac{|\Gamma_{s,3}|^2}{|1-\Gamma_{s,3}\Gamma_r|^2} & \frac{\Gamma_{s,3}}{1-\Gamma_{s,3}\Gamma_r} & \frac{\Gamma_{s,3}^*}{1-\Gamma_{s,3}^*\Gamma_r^*} & 1 \end{bmatrix} \cdot \begin{bmatrix} G_r \\ \hat{\Gamma}_{11} \\ \hat{\Gamma}_{12} \\ \hat{\Gamma}_{21} \\ \hat{\Gamma}_{22} \end{bmatrix}. \quad (4.29)$$

In (4.29), the detected noise-power column matrix to the left-side of the equal sign will be assigned matrix variable $\hat{\mathbf{P}}_{\mathbf{R},\text{Cal}}$. To the right-side of this expression, the 5x5 dimensioned matrix will be designated as β_{Cal} . As such, equation (4.29) may be summarized in the form,

$$\hat{\mathbf{P}}_{\mathbf{R},\text{Cal}} = \beta_{\text{Cal}} \cdot \begin{bmatrix} G_r \\ \hat{\Gamma}_{11} \\ \hat{\Gamma}_{12} \\ \hat{\Gamma}_{21} \\ \hat{\Gamma}_{22} \end{bmatrix}. \quad (4.30)$$

Pre-multiplying both sides of (4.30) by the inverse of β_{Cal} , the measurement receiver's gain-bandwidth product G_r and the elements of its NCM $\hat{\mathbf{B}}_{\mathbf{R}}$ are solved for by the expression

$$\begin{bmatrix} G_r \\ \hat{\Gamma}_{11} \\ \hat{\Gamma}_{12} \\ \hat{\Gamma}_{21} \\ \hat{\Gamma}_{22} \end{bmatrix} = \beta_{\text{Cal}}^{-1} \hat{\mathbf{P}}_{\mathbf{R},\text{Cal}}. \quad (4.31)$$

The receiver noise model described by (4.31) is validated using ADS. Figure 4.3 depicts the receiver as an amplifier with assigned signal (S-parameters) and noise parameters. Source impedance states defined by noise-temperature \hat{T}_s and complex reflection coefficient Γ_s are sequentially presented to the receiver's input at a fixed frequency.

The noise-power P_{del_W} delivered to the receiver's load at each corresponding source impedance state is delineated in Table 4.1. The power is assessed by simulated measurement of the rms noise-voltage v_2 presented across the receiver's output load Z_1 , squaring this result, and dividing it by fifty ohms.

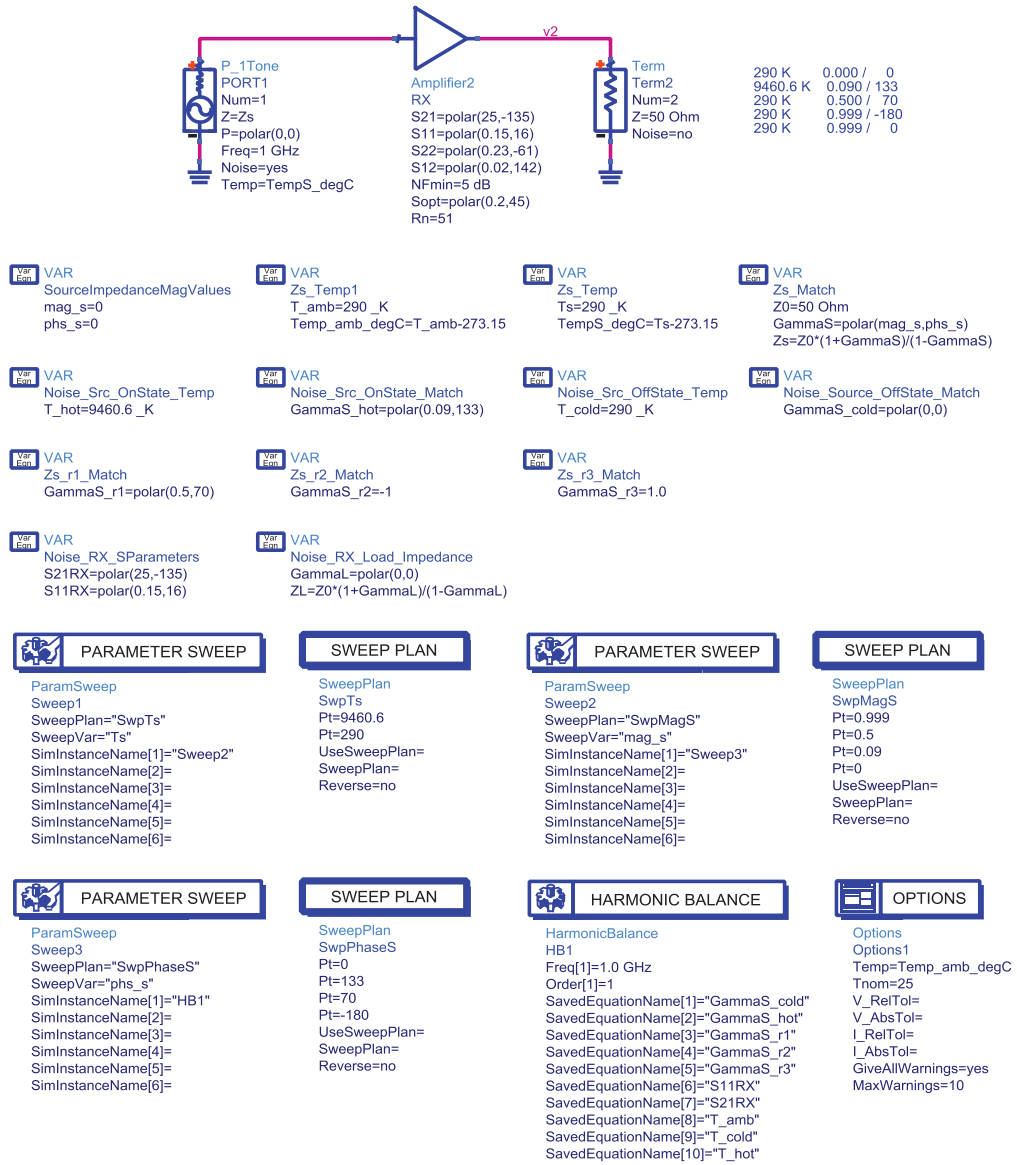


Figure 4.3: Schematic Representation of the Receiver.

Included in Table 4.1 is the receiver's noise figure $nf(2)$ and effective noise temperature $te(2)$, both of which are referred at output port two.

☼	phs_s	nf(2)[0]	te(2)[0]	Pdel_W
	Ts=290.000, mag_s=0.000			
	-180.000	5.166	662.838	8.222E-18
	0.000	5.166	662.838	8.222E-18
	70.000	5.166	662.838	8.222E-18
	133.000	5.166	662.838	8.222E-18
	Ts=290.000, mag_s=0.090			
	-180.000	5.303	693.389	8.203E-18
	0.000	5.096	647.480	8.236E-18
	70.000	5.066	641.013	7.982E-18
	133.000	5.196	669.301	8.024E-18
	Ts=290.000, mag_s=0.500			
	-180.000	6.934	1141.566	8.058E-18
	0.000	5.767	804.253	8.221E-18
	70.000	5.574	756.740	6.807E-18
	133.000	6.361	964.586	7.159E-18
	Ts=290.000, mag_s=0.999			
	-180.000	33.098	591502.015	7.789E-18
	0.000	30.677	338643.470	7.961E-18
	70.000	30.195	303026.730	5.224E-18
	133.000	31.995	458832.783	6.190E-18
	Ts=9.461E3, mag_s=0.000			
	-180.000	5.166	662.838	8.736E-17
	0.000	5.166	662.838	8.736E-17
	70.000	5.166	662.838	8.736E-17
	133.000	5.166	662.838	8.736E-17
	Ts=9.461E3, mag_s=0.090			
	-180.000	5.303	693.389	8.470E-17
	0.000	5.096	647.480	8.881E-17
	70.000	5.066	641.013	8.661E-17
	133.000	5.196	669.301	8.473E-17
	Ts=9.461E3, mag_s=0.500			
	-180.000	6.934	1141.566	5.968E-17
	0.000	5.767	804.253	7.712E-17
	70.000	5.574	756.740	6.645E-17
	133.000	6.361	964.586	5.949E-17
	Ts=9.461E3, mag_s=0.999			
	-180.000	33.098	591502.015	7.910E-18
	0.000	30.677	338643.470	8.177E-18
	70.000	30.195	303026.730	5.382E-18
	133.000	31.995	458832.783	6.314E-18

Table 4.1: Results of the Receiver's Noise Figure, Effective Noise Temperature, and Delivered Noise Power with respect to Source Temperature and Source Reflection Coefficient

In Fig. 4.3, the receiver's load impedance is matched to the amplifier and is regarded noise-free. This condition emulates the noise receiver hardware architecture of Keysight's PNA-

X; the load is realized in digital signal processing following analog-to-digital conversion of the detected noise voltage [33]. In this example, the receiver's bandwidth is set to unity. In practice the noise bandwidth is adjustable but typically set at 4 MHz.

A results comparison summary of the simulated detected noise-power measured at the receiver's load against independent numeric calculation (expected values) is shown in Table 4.2.

Source Impedance Z_s		$P_{del_W} \times 10^{-18}$		
Noise Temperature	Gamma S	Simulated	Indep. Calc.	% Error <
9460.6	$0.09e^{j133^\circ}$	84.73	85.37	0.8
290	0	8.222	8.214	0.1
290	$0.5e^{j70^\circ}$	6.807	6.819	0.2
290	-1	7.789	7.782	0.1
290	1	7.961	7.949	0.2

Table 4.2: The Receiver's Delivered Noise Power Spectral Density - Simulation versus Independent Numeric Calculation

Using (4.29), P_{del_W} is evaluated at each of five source impedance states (\hat{T}_s, Γ_s) including (9460.6K, $0.09e^{j133^\circ}$), (290K, 0), (290K, $0.5e^{j70^\circ}$), (290K, -1) and (290K, 1). The two approaches leverage identical noise and S-parameters assigned to the receiver as shown in Fig. 4.3. Results by numeric calculation are obtained as follows; first, the receiver's noise parameters are converted to the elements comprising its NCM [27]. Along with the receiver's S-parameters and use of (4.7) and (4.10), this enables calculation of G_r , \hat{r}_{11} , \hat{r}_{12} , \hat{r}_{21} , and \hat{r}_{22} . Second, each row of matrix β_{Cal} in (4.29) corresponds to a source impedance state defined by its noise-temperature and reflection coefficient. As such, P_{del_W} is calculated for \hat{P}_{hot} , \hat{P}_{cold} , $\hat{P}_{r,1}$, $\hat{P}_{r,2}$, and $\hat{P}_{r,3}$. Both simulated and calculated results of P_{del_W} are presented in Table 4.2. Their comparison agrees to less than a one percent error.

To validate (4.31), the simulated noise-power values in Table 4.2 are assigned to $\hat{\mathbf{P}}_{R,Cal}$. Their coefficients explicitly described in (4.29) are post-processed in ADS to form β_{Cal} . Shown in (4.31), pre-multiplication of matrix inverse β_{Cal} with $\hat{\mathbf{P}}_{R,Cal}$ produces simulated results for the receiver's gain-bandwidth product G_r and its noise-wave parameters, $\hat{\Gamma}_{11}$, $\hat{\Gamma}_{12}$, $\hat{\Gamma}_{21}$, $\hat{\Gamma}_{22}$. Table 4.3 summarizes simulation and numerically calculated values indicating conformance to less than or equal one percent error.

G_r		$\hat{\mathbf{B}}_R$			
		$\hat{\Gamma}_{11} \times 10^{-18}$	$\hat{\Gamma}_{12} \times 10^{-18}$	$\hat{\Gamma}_{21} \times 10^{-18}$	$\hat{\Gamma}_{22} \times 10^{-18}$
Simulated	619.8	2.192	$1.355e^{j101.2^\circ}$	$1.355e^{-j101.2^\circ}$	5.741
Indep. Calc.	625	2.212	$1.354e^{j101.4^\circ}$	$1.354e^{-j101.4^\circ}$	5.711
% Error <	0.9	1.0	0.1	0.1	0.6

Table 4.3: The Receiver's Gain-Bandwidth Product & NCM - Simulation versus Independent Numeric Calculation

4.3.2 Noise Matrix Characterization of a Linear Two-Port Device

With a calibrated measurement system (receiver and source), the device under test may be evaluated to extract its noise properties. The technique is similar in approach to determining the receiver's NCM $\hat{\mathbf{B}}_R$. Referring to Fig. 4.1, a reflection coefficient Γ_s of source impedance Z_s is presented to the two-port DUT's input. The corresponding noise-power delivered to Z_1 of the receiver is assessed. The relationship between Γ_s and the measured noise-power is governed by (4.12). Beside the previously determined calibration coefficients, (4.12) is expressed in terms of the elements composing the DUT's NCM $\hat{\mathbf{B}}_D$. It's clear that unknowns \hat{d}_{11} , \hat{d}_{12} , \hat{d}_{21} , and \hat{d}_{22} are present. To solve for these, four distinct noise-power measurements can be made. Each measurement is to correspond to a unique Γ_s state. The impedance states presented to the DUT

will be passive. Having generated four independent linear equations, matrix mathematics will be used in an expanded version of (4.12) to solve the four unknowns. Once $\hat{\mathbf{B}}_D$ is determined, (3.54) and (3.59) may respectively be used to acquire the noise factor and effective noise-temperature of the two-port DUT for any Γ_s presented to its input port.

To construct an expanded version of (4.12), the value of \hat{P}_m is replaced with a 4x1 column matrix comprising four distinct noise-power measurements $\hat{P}_{m,1}$ through $\hat{P}_{m,4}$; each measurement will correspond to a distinct source impedance state $\Gamma_{s,1}$ through $\Gamma_{s,4}$. This matrix will be described by

$$\hat{\mathbf{P}}_M = \begin{bmatrix} \hat{P}_{m,1} \\ \hat{P}_{m,2} \\ \hat{P}_{m,3} \\ \hat{P}_{m,4} \end{bmatrix}. \quad (4.32)$$

The measured noise-power readings are the result of the combined influence of noise generation from the source $\hat{\mathbf{P}}_S$, DUT $\hat{\mathbf{P}}_D$, and receiver $\hat{\mathbf{P}}_R$.

Consistent with the above description, the source-related entry in (4.12) may be expanded to form a 4x1 column vector $\hat{\mathbf{P}}_S$ described as

$$\hat{\mathbf{P}}_{\mathbf{S}} = \left(k \hat{\mathbf{T}}_{\text{room}} |S_{21}|^2 \mathbf{G}_r \right) \begin{bmatrix} \frac{1 - |\Gamma_{s,1}|^2}{|1 - \Gamma_{s,1} S_{11}|^2 |1 - \Gamma_{2,1} \Gamma_r|^2} \\ \frac{1 - |\Gamma_{s,2}|^2}{|1 - \Gamma_{s,2} S_{11}|^2 |1 - \Gamma_{2,2} \Gamma_r|^2} \\ \frac{1 - |\Gamma_{s,3}|^2}{|1 - \Gamma_{s,3} S_{11}|^2 |1 - \Gamma_{2,3} \Gamma_r|^2} \\ \frac{1 - |\Gamma_{s,4}|^2}{|1 - \Gamma_{s,4} S_{11}|^2 |1 - \Gamma_{2,4} \Gamma_r|^2} \end{bmatrix} . \quad (4.33)$$

Each source impedance state $\Gamma_{s,x} \mid_{x=1 \rightarrow 4}$ contributes a distinct noise-power to the aggregate measured at Z_1 . In effect, there is a linear transformation from the source noise $\hat{\mathbf{T}}_{\text{room}}$ to Z_1 that may be described as $\hat{\mathbf{P}}_{\mathbf{S}} = k \hat{\mathbf{T}}_{\text{room}} \boldsymbol{\beta}_{\mathbf{S}}$. Here, $\boldsymbol{\beta}_{\mathbf{S}}$ is a linear transformation matrix describing the relationship between the source noise $k \hat{\mathbf{T}}_{\text{room}}$ and its contribution to the overall noise-power appearing at Z_1 . Equation (4.33) describes the interaction the source noise experiences as it propagates through the overall network from input to output for each of the four measurements being conducted.

The receiver-related terms in (4.12) may be extended to account for multiple measurements forming a 4x4 matrix multiplied by a column vector comprising the elements of $\hat{\mathbf{B}}_{\mathbf{R}}$. This is shown in (4.34) to be

$$\hat{\mathbf{P}}_{\mathbf{R}} = \begin{bmatrix} \frac{|\Gamma_{2,1}|^2}{|1-\Gamma_{2,1}\Gamma_r|^2} & \frac{\Gamma_{2,1}}{1-\Gamma_{2,1}\Gamma_r} & \frac{\Gamma_{2,1}^*}{1-\Gamma_{2,1}^*\Gamma_r^*} & 1 \\ \frac{|\Gamma_{2,2}|^2}{|1-\Gamma_{2,2}\Gamma_r|^2} & \frac{\Gamma_{2,2}}{1-\Gamma_{2,2}\Gamma_r} & \frac{\Gamma_{2,2}^*}{1-\Gamma_{2,2}^*\Gamma_r^*} & 1 \\ \frac{|\Gamma_{2,3}|^2}{|1-\Gamma_{2,3}\Gamma_r|^2} & \frac{\Gamma_{2,3}}{1-\Gamma_{2,3}\Gamma_r} & \frac{\Gamma_{2,3}^*}{1-\Gamma_{2,3}^*\Gamma_r^*} & 1 \\ \frac{|\Gamma_{2,4}|^2}{|1-\Gamma_{2,4}\Gamma_r|^2} & \frac{\Gamma_{2,4}}{1-\Gamma_{2,4}\Gamma_r} & \frac{\Gamma_{2,4}^*}{1-\Gamma_{2,4}^*\Gamma_r^*} & 1 \end{bmatrix} \cdot \begin{bmatrix} \hat{\Gamma}_{11} \\ \hat{\Gamma}_{12} \\ \hat{\Gamma}_{21} \\ \hat{\Gamma}_{22} \end{bmatrix}, \quad (4.34)$$

where $\hat{\mathbf{P}}_{\mathbf{R}} = \boldsymbol{\beta}_{\mathbf{R}} \begin{bmatrix} \hat{\Gamma}_{11} \\ \hat{\Gamma}_{12} \\ \hat{\Gamma}_{21} \\ \hat{\Gamma}_{22} \end{bmatrix}$. $\boldsymbol{\beta}_{\mathbf{R}}$ is the linear transformation matrix of the receiver's noise-power

delivered to its load Z_1 .

The remaining term in (4.12) is related to the DUT. Its expanded version may be accounted using a similar approach as outlined above in (4.34). Let the noise-power appearing at the receiver's load due to the DUT for each of four impedance states be accounted for by column vector $\hat{\mathbf{P}}_{\mathbf{D}}$, such that

$$\hat{\mathbf{P}}_{\mathbf{D}} = \mathbf{G}_r \begin{bmatrix} \frac{|\Gamma_{s,1}|^2 |S_{21}|^2}{|1 - \Gamma_{s,1} S_{11}|^2 |1 - \Gamma_{2,1} \Gamma_r|^2} & \frac{\Gamma_{s,1} S_{21}}{(1 - \Gamma_{s,1} S_{11}) |1 - \Gamma_{2,1} \Gamma_r|^2} & \frac{\Gamma_{s,1}^* S_{21}^*}{(1 - \Gamma_{s,1}^* S_{11}^*) |1 - \Gamma_{2,1} \Gamma_r|^2} & \frac{1}{|1 - \Gamma_{2,1} \Gamma_r|^2} \\ \frac{|\Gamma_{s,2}|^2 |S_{21}|^2}{|1 - \Gamma_{s,2} S_{11}|^2 |1 - \Gamma_{2,2} \Gamma_r|^2} & \frac{\Gamma_{s,2} S_{21}}{(1 - \Gamma_{s,2} S_{11}) |1 - \Gamma_{2,2} \Gamma_r|^2} & \frac{\Gamma_{s,2}^* S_{21}^*}{(1 - \Gamma_{s,2}^* S_{11}^*) |1 - \Gamma_{2,2} \Gamma_r|^2} & \frac{1}{|1 - \Gamma_{2,2} \Gamma_r|^2} \\ \frac{|\Gamma_{s,3}|^2 |S_{21}|^2}{|1 - \Gamma_{s,3} S_{11}|^2 |1 - \Gamma_{2,3} \Gamma_r|^2} & \frac{\Gamma_{s,3} S_{21}}{(1 - \Gamma_{s,3} S_{11}) |1 - \Gamma_{2,3} \Gamma_r|^2} & \frac{\Gamma_{s,3}^* S_{21}^*}{(1 - \Gamma_{s,3}^* S_{11}^*) |1 - \Gamma_{2,3} \Gamma_r|^2} & \frac{1}{|1 - \Gamma_{2,3} \Gamma_r|^2} \\ \frac{|\Gamma_{s,4}|^2 |S_{21}|^2}{|1 - \Gamma_{s,4} S_{11}|^2 |1 - \Gamma_{2,4} \Gamma_r|^2} & \frac{\Gamma_{s,4} S_{21}}{(1 - \Gamma_{s,4} S_{11}) |1 - \Gamma_{2,4} \Gamma_r|^2} & \frac{\Gamma_{s,4}^* S_{21}^*}{(1 - \Gamma_{s,4}^* S_{11}^*) |1 - \Gamma_{2,4} \Gamma_r|^2} & \frac{1}{|1 - \Gamma_{2,4} \Gamma_r|^2} \end{bmatrix} \begin{bmatrix} \hat{d}_{11} \\ \hat{d}_{12} \\ \hat{d}_{21} \\ \hat{d}_{22} \end{bmatrix} \quad (4.35)$$

The first matrix on the right-side of (4.35) is the linear transformation matrix describing the mapping of the DUT's noise properties to the measurement receiver's load Z_1 . Equation (4.35) written in abbreviated form is

$$\hat{\mathbf{P}}_{\mathbf{D}} = \boldsymbol{\beta}_{\mathbf{D}} \begin{bmatrix} \hat{d}_{11} \\ \hat{d}_{12} \\ \hat{d}_{21} \\ \hat{d}_{22} \end{bmatrix} \quad (4.36)$$

The 4x1 column vectors $\hat{\mathbf{P}}_{\mathbf{S}}$, $\hat{\mathbf{P}}_{\mathbf{D}}$, and $\hat{\mathbf{P}}_{\mathbf{R}}$ may be summed in accordance with (4.12) yielding the overall noise-power measured for each source impedance state $\Gamma_{s,x} \big|_{x=1 \rightarrow 4}$. Thus, (4.12) becomes

$$\hat{\mathbf{P}}_{\mathbf{M}} = \hat{\mathbf{P}}_{\mathbf{S}} + \hat{\mathbf{P}}_{\mathbf{D}} + \hat{\mathbf{P}}_{\mathbf{R}} \quad (4.37)$$

Solving for $\hat{\mathbf{P}}_{\mathbf{D}}$ and substituting (4.36) yields

$$\beta_{\mathbf{D}} \begin{bmatrix} \hat{d}_{11} \\ \hat{d}_{12} \\ \hat{d}_{21} \\ \hat{d}_{22} \end{bmatrix} = \hat{\mathbf{P}}_{\mathbf{M}} - \hat{\mathbf{P}}_{\mathbf{S}} - \hat{\mathbf{P}}_{\mathbf{R}} . \quad (4.38)$$

Pre-multiplication of inverse matrix $\beta_{\mathbf{D}}$ to (4.38) yields the elements comprising the DUT's NCM $\hat{\mathbf{B}}_{\mathbf{D}}$ such that

$$\begin{bmatrix} \hat{d}_{11} \\ \hat{d}_{12} \\ \hat{d}_{21} \\ \hat{d}_{22} \end{bmatrix} = \beta_{\mathbf{D}}^{-1} (\hat{\mathbf{P}}_{\mathbf{M}} - \hat{\mathbf{P}}_{\mathbf{S}} - \hat{\mathbf{P}}_{\mathbf{R}}) . \quad (4.39)$$

To validate the noise model described by (4.39), a cascaded network experiment circuit is constructed in ADS consisting of a DUT joined to a passive tunable source termination and noise receiver at its input and output ports respectively. The intent is to demonstrate that collective knowledge of the source and receiver noise properties along with the S-parameters of the DUT and its connected networks enables extraction of the DUT's NCM.

The schematic in Fig. 4.4 presents the network (S-parameters) and noise parameters for the source, DUT, and noise receiver. The noise receiver is functionally identical to that shown in Fig. 4.2. Its pre-determined noise properties and gain-bandwidth product are described in the schematic of Fig. 4.3 along with the source termination's noise-temperature. The key to this simulation is to sequentially tune the source reflection coefficient and assess the noise-power delivered to the receiver's load. Four distinct source reflection coefficient $\Gamma_{\mathbf{s}}$ settings and their corresponding Pdel_W are used in order that a system of four independent linear equations be formed from which the elements of the DUT's NCM $\hat{\mathbf{B}}_{\mathbf{D}}$ may be extracted.

To establish a baseline, the noise parameters of the DUT are converted to the elements comprising its NCM [27]. Substituting into (4.12) the noise properties of the source, DUT, and

receiver, along with the DUT and receiver's S-parameters, the noise-power expected to be measured by the receiver is numerically calculated at a prescribed Γ_s . In this experiment a 290K source temperature is chosen. The expected Pdel_W is calculated for each of four Γ_s settings. The source impedance states are selected to be widely distributed across the Smith Chart including 0, $0.5e^{j70^\circ}$, -1 , and 1.

Having established our reference (expected) data, the simulation is then performed in ADS with results shown in Table 4.4.

Table 4.5 compares the results of Pdel_W obtained through independent numeric computation against the simulated results acquired from ADS. Comparison was made at each of the four Γ_s settings. Overall agreement is less than 0.3 percent error.

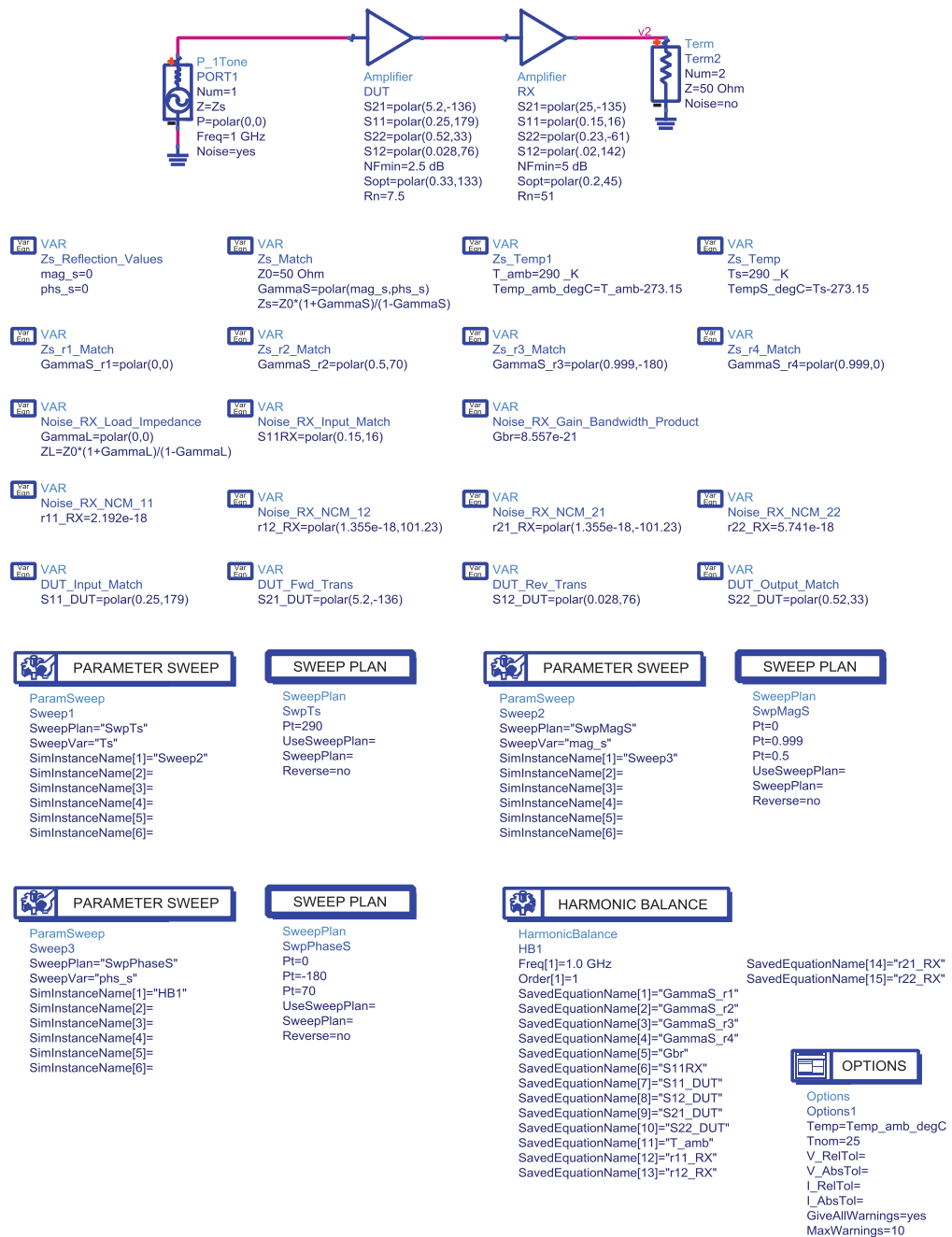


Figure 4.4: Schematic Representation of the DUT Embedded in a Cascaded Network

phs_s	nf(2)[0]	te(2)[0]	Pdel_W	
Ts=290.000, mag_s=0.000	-180.000	2.896	274.921	1.459E-16
	0.000	2.896	274.921	1.459E-16
	70.000	2.896	274.921	1.459E-16
Ts=290.000, mag_s=0.500	-180.000	3.037	293.544	1.447E-16
	0.000	4.163	466.256	1.175E-16
	70.000	3.296	329.450	1.107E-16
Ts=290.000, mag_s=0.999	-180.000	25.064	92771.903	8.147E-17
	0.000	28.850	222241.609	7.563E-17
	70.000	26.167	119688.321	5.190E-17

Table 4.4: Results of the Cascaded Network's Noise Figure, Effective Noise Temperature and Pdel_W versus Source Reflection Coefficient and Noise Temperature. Simulation Performed in ADS.

Source Impedance Z_s		$P_{del_W} \times 10^{-16}$		
Noise Temperature	Gamma S	Simulated	Indep. Calc.	% Error <
290	0	1.459	1.458	0.1
290	$0.5e^{j70^\circ}$	1.107	1.108	0.1
290	-1	0.8147	0.8123	0.3
290	1	0.563	0.7553	0.2

Table 4.5: The Cascade Network's Delivered Noise Power Spectral Density in Simulation versus Independent Numeric Calculation

By use of (4.32-4.34), matrices $\hat{\mathbf{P}}_M$, $\hat{\mathbf{P}}_S$, and $\hat{\mathbf{P}}_R$ are post-processed in ADS as well as β_D from (4.35). The elements of these matrices are known given collective knowledge of the S-parameters and noise properties of source and receiver as well as S-parameters of the DUT. Substituting these into (4.39), further processing yields the elements comprising the NCM $\hat{\mathbf{B}}_D$ of

the DUT. Table 4.6 summarizes the simulated versus expected results offering a percent error of 8.2, 1.0, 1.0, and 1.9 for NCM elements $\overline{\hat{b}_{gd_1} \hat{b}_{gd_1}^*}$, $\overline{\hat{b}_{gd_1} \hat{b}_{gd_2}^*}$, $\overline{\hat{b}_{gd_1}^* \hat{b}_{gd_2}}$, and $\overline{\hat{b}_{gd_2} \hat{b}_{gd_2}^*}$ respectively.

	$\hat{\mathbf{B}}_D$			
	$\overline{\hat{b}_{gd_1} \hat{b}_{gd_1}^*} \times 10^{-21}$	$\overline{\hat{b}_{gd_1} \hat{b}_{gd_2}^*} \times 10^{-21}$	$\overline{\hat{b}_{gd_1}^* \hat{b}_{gd_2}} \times 10^{-21}$	$\overline{\hat{b}_{gd_2} \hat{b}_{gd_2}^*} \times 10^{-21}$
Simulated	0.3188	$4.708e^{-j129.8^\circ}$	$4.708e^{j129.8^\circ}$	96.69
Indep. Calc.	0.3471	$4.664e^{-j130.3^\circ}$	$4.664e^{j130.3^\circ}$	94.96
% Error <	8.2	1.0	1.0	1.9

Table 4.6: The DUT's Extracted NCM $\hat{\mathbf{B}}_D$ in Simulation versus Independent Numeric Calculation

Lastly, having determined the NCM $\hat{\mathbf{B}}_D$, (3.59) may be used to assess the effective noise-temperature of the two-port DUT for any impedance presented to its input terminals. The simulated effective noise-temperature was evaluated over a diverse Γ_s range. Contrasted with numeric calculations, a two percent worst case error was realized. Table 4.7 summarizes these results taken at four distinct Γ_s settings.

Source Impedance Z_s		$T_{e, DUT}$		
Noise Temperature	Gamma S	Simulated	Indep. Calc.	% Error <
290	0	258.99	254.35	1.9
290	$0.5e^{j70^\circ}$	304.23	299.18	1.7
290	-1	87781.4	87040.7	0.9
290	1	207593	205751.4	0.9

Table 4.7: The DUT's Effective Noise Temperature - Simulation versus Numeric Calculation

From the following simulation exercises, it has been shown that the S-parameter derived noise model in (4.39) can be used as a valid technique to de-embed (extract) the DUT's NCM from its cascaded network.

While noise-power flow expressions in this chapter have been developed within the context of a two-port network, (3.15) may be generalized to accommodate for an n-port DUT. Indeed, one purpose for choosing S-parameters as the preferred network representation, unlike for example T-parameters, is its applicability to the generalized n-port case. Though industry standards define noise factor for the two-port network only, a multiport noise factor assessment based on the scattering noise matrix has been theoretically developed and suggested by Randa [26]. The evolution of low noise complex integrated system development may facilitate its future use. The underpinnings of his derivation use (3.15). For the two-port case, this generalized formulism reduces to the more familiar expressions outlined above.

To develop an expression deriving a nonlinear RF/microwave network's NCM requires a model which can accommodate additional frequency components including harmonics and intermodulation products as a function of large signal drive conditions. The X-parameter behavioral network representation satisfies this requirement. Further, X-parameters are the correct mathematical extension of S-parameters for the time-invariant nonlinear network condition. That is, under small signal drive conditions, the X-parameter formulism reduces to the familiar S-parameter network representation. Further, X-parameters applicability to existing software simulation and hardware measurement methodologies permit a means to noise model validation. In consideration to these justifications, focus will now be directed in the upcoming chapter to a NCM derivation of the time-invariant nonlinear network scenario.

Chapter 5

Nonlinear Network Noise Behavioral Modeling

This chapter presents a generalized scattered noise behavioral model for time-invariant nonlinear microwave circuits. The formalism uses noise waves and large-signal scattering functions known as X-parameters to extract a multi-port network's noise correlation matrix. From this, expressions representing the network's effective input noise temperature and noise factor will be established. Within the small-signal space, it will be demonstrated that the behavioral model reduces to a familiar form describing noise wave influence governed by the network's S-parameter functions. Using the generalized form, two examples given in context of embedded nonlinear one-port and two-port configurations are offered with each presented with matched termination networks. Both cases use a passive source and load in the analysis. Numerical versus simulated results will be compared. Results in the two-port case yield its noise factor. Lastly, hardware noise measurement thought experiments for one- and two-port nonlinear network scenarios will be designed to determine their noise properties.

Given the nonlinear network noise behavioral model is represented as a function of its X-parameters, and as such, capable of describing performance across its nonlinear (and linear) operating-regions, it's prudent to begin with a review of the X-parameter (and S-parameter) formulation in context to deterministic signals.

5.1 Linear and Nonlinear (Time-Invariant) Network Behavioral Modeling

5.1.1 Linear Network Behavioral Modeling using S-parameters

While a linear system exhibits an output response proportional to its input stimulus, this description does not fully embody the concept of linearity. Essentially, linearity implies two properties known as superposition and homogeneity. To develop their meaning, we begin by stating that if input stimuli [41, 50]

$$a_1(t) \rightarrow b_1(t) \quad (5.1)$$

and

$$a_2(t) \rightarrow b_2(t) \quad (5.2)$$

then

$$a_1(t) + a_2(t) \rightarrow b_1(t) + b_2(t) . \quad (5.3)$$

In other words, each stimulus $a_1(t)$ and $a_2(t)$ produces a corresponding response $b_1(t)$ and $b_2(t)$; the sum of their stimuli produce the sum of their responses. The total response due to all stimuli presented simultaneously can be determined by introducing each stimulus individually, with all others zero, evaluating their corresponding responses and summing their total. This system property is known as superposition.

Now let us scale an input stimulus $a(t)$ by a constant (real or complex) c . If

$$ca(t) \rightarrow cb(t) \quad (5.4)$$

then the system is considered homogenous. Thus, linearity implies two properties, superposition and homogeneity (scaling). Both properties can be combined to form a single property known as generalized superposition [50]. That is, if

$$c_1 a_1(t) \rightarrow c_1 b_1(t) \quad (5.5)$$

and

$$c_2 a_2(t) \rightarrow c_2 b_2(t) \quad (5.6)$$

then

$$c_1 a_1(t) + c_2 a_2(t) \rightarrow c_1 b_1(t) + c_2 b_2(t) . \quad (5.7)$$

If (5.7) applies, the system exhibits generalized superposition and is regarded linear. As such, there is no need to individually confirm superposition and homogeneity, expressions (5.3) and (5.4) respectively.

Described in the time domain, equations (5.1–5.7) exhibit identical properties in the frequency domain. Taking the Fourier transform of the incident (cause) and scattered (effect) waves yields their complex amplitude (phasor) representation. The application of incident waves $a_k(\omega)$ to a linear n-port network are modified by the network, each contributing to the total response forming a scattered wave $b_i(\omega)$ where subscripts k and i represent the network's input and output ports respectively. The modification or translation of the incident to scattered waves of a linear network is commonly described by its scattering parameters (S-parameters). This relationship or mapping of incident to scattered waves of a linear n-port can be described in the form of a weighted linear combination such that [51]

$$b_i(\omega) = \sum_{k=1}^n S_{ik}(\omega) \cdot a_k(\omega) \quad (5.8)$$

where the network's S-parameters S_{ik} are complex coefficients. Equation (5.8) preserves the linear network's properties of superposition and scaling. It's important to note that the sinusoidal description of the incident waves $a_k(\omega)$ exhibit a complex peak amplitude sufficiently small such that higher-order (frequency) terms in the scattered waves $b_i(\omega)$ are considered negligible in

comparison to the fundamental frequency component. As such, to preserve the condition of linearity, the amplitude of the incident waves, while they may be scaled, are restricted to a range that ensures linear operation of the network.

For now, we assume the linear network is noise-free, as such, the set of generalized linear equations described in (5.8) may be used to form the S-parameter matrix model of the linear n-port illustrated in (3.5).

Equations (3.5) or (5.8) can be used to form an S-parameter model of a mismatch-embedded linear two-port network. In this case, each of two scattered waves emanating from the network's input and output ports is each written as a sum of its responses to the network's incident waves thus forming two equations in (5.9) and (5.10) such that

$$b_1 = S_{11}a_1 + S_{12}a_2 \quad (5.9)$$

and

$$b_2 = S_{21}a_1 + S_{22}a_2 . \quad (5.10)$$

Combining (5.9) and (5.10) in matrix form yields

$$\begin{bmatrix} b_1 \\ b_2 \end{bmatrix} = \begin{bmatrix} S_{11} & S_{12} \\ S_{21} & S_{22} \end{bmatrix} \begin{bmatrix} a_1 \\ a_2 \end{bmatrix} . \quad (5.11)$$

To obtain a solution, four independent linear equations need be constructed. For the linear two-port, a minimum of two experiments is needed to acquire the full set of S-parameters. In the first experiment, a stimulus a_1 is applied to port-one whereupon the network's response to the excitation is measured on both its ports. A second experiment can be conducted by re-directing the stimulus in the reverse direction to port-two and repeating the measurements of the network's responses. The set of equations comprising (5.9) and (5.10) are valid if the S-parameters of the network are independent of the assigned stimulus port. Such behavior is typically true of linear networks. The measured results from each of the two stimulus/response

experiments may be incorporated into the framework of (5.11) by augmenting its incident and scattered wave vectors such that [52]

$$\begin{bmatrix} b_1^{fwd} & b_1^{rev} \\ b_2^{fwd} & b_2^{rev} \end{bmatrix} = \begin{bmatrix} S_{11} & S_{12} \\ S_{21} & S_{22} \end{bmatrix} \begin{bmatrix} a_1^{fwd} & a_1^{rev} \\ a_2^{fwd} & a_2^{rev} \end{bmatrix}. \quad (5.12)$$

The two-port network's S-parameters are attained by post-multiplication on both sides of (5.12) by the incident-wave matrix inverse thereby yielding the solution

$$\begin{bmatrix} S_{11} & S_{12} \\ S_{21} & S_{22} \end{bmatrix} = \begin{bmatrix} b_1^{fwd} & b_1^{rev} \\ b_2^{fwd} & b_2^{rev} \end{bmatrix} \begin{bmatrix} a_1^{fwd} & a_1^{rev} \\ a_2^{fwd} & a_2^{rev} \end{bmatrix}^{-1}. \quad (5.13)$$

Figure 5.1 shows a typical hardware measurement setup. The PNA-X's source-one may be directed to test port-one, thus stimulating the network under test in the forward direction. The reference and test receivers positioned behind test ports-one and -two measure the resulting "a" and "b" waves of the network. The source-one stimulus is then reversed in direction, now being presented to test port-two. Subsequently the receiver's once again measure the corresponding waves. Once the process is complete, the measured waves are used to extract the S-parameters of the linear network.

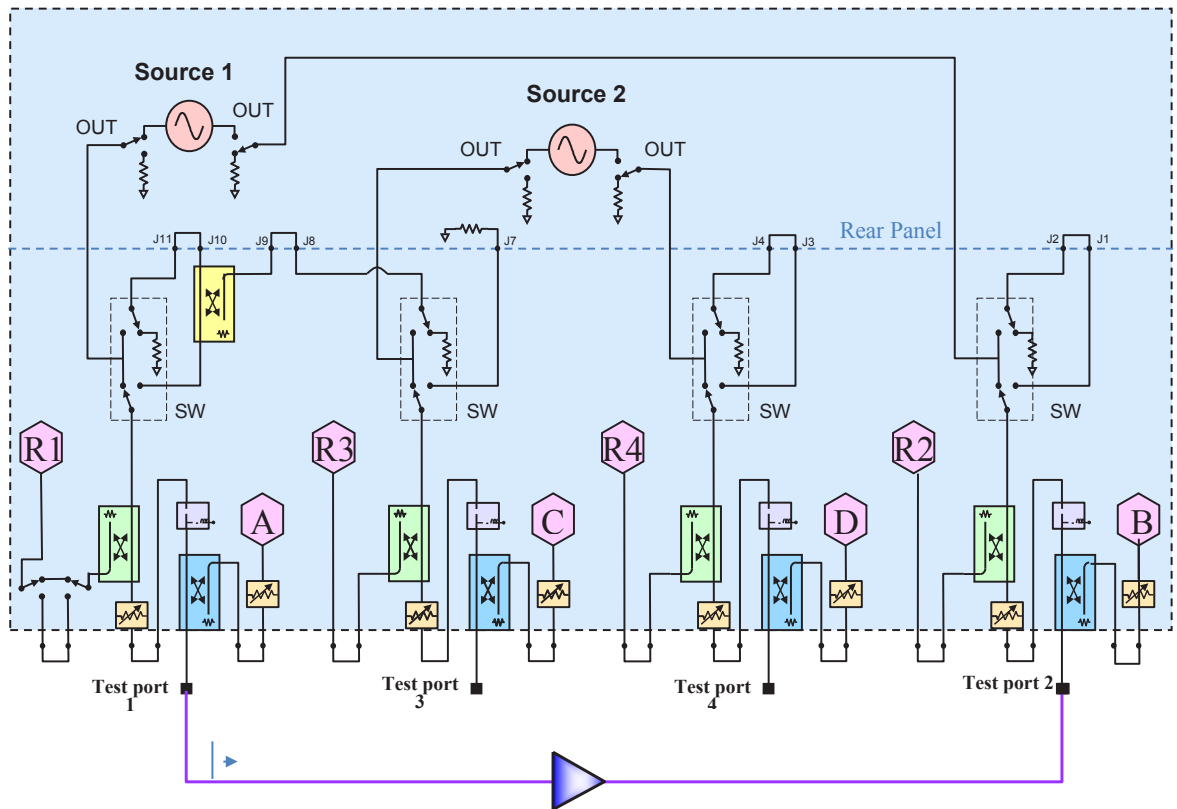


Figure 5.1: Modern Vector Network Analyzer Block Diagram (4-Port PNA-X) [53]

Time-invariance is an important property common to a wide variety of linear (and nonlinear) devices of passive- and active-type classification. Signifying these devices or any arrangement thereof as a network, the property states that if a network acts on input stimulus $a(t)$ forming a response $b(t)$ such that [50, 51]

$$b(t) = O[a(t)], \quad (5.14)$$

then the network is time-invariant if the input stimulus is delayed by time τ resulting in

$$b(t - \tau) = O[a(t - \tau)] \quad \tau \in \mathbb{R}. \quad (5.15)$$

The operator O describes the network's transformation from its input stimulus to its output response. Equations (5.14) and (5.15) are identical with the exception that they are time delayed versions of one another. From (5.15), a time delay τ initiated by the stimulus yields the same delay in response; a network exhibiting this characteristic is regarded as time-invariant. Resistors, inductors, capacitors, diodes, and transistors typically exhibit this property. Oscillators are one example of a time-varying network whereupon (5.14) and (5.15) characteristically do not apply.

The S-parameter model conforms to the property of time-invariance. This can be shown by use of the Fourier transform in relation to (5.8) [51].

$$\mathfrak{F}[b_i(t)] = b_i^{(pk)}(\omega) = \sum_{k=1}^n S_{ik} \mathfrak{F}[a_k(t)] \quad (5.16)$$

where the Fourier transform $\mathfrak{F}[\cdot]$ of response $b_i(t)$ at port i yields its frequency domain representation expressed in units of peak (complex amplitude). By delaying all input stimuli in (5.16) by time τ , the time-domain response at port i becomes [51]

$$\begin{aligned} \mathfrak{F}^{-1} \left\{ \sum_{k=1}^n S_{ik} \mathfrak{F}[a_k(t - \tau)] \right\} &= \mathfrak{F}^{-1} \left\{ \sum_{k=1}^n S_{ik} \mathfrak{F}[a_k(t)] e^{j\omega\tau} \right\} = \mathfrak{F}^{-1} \left[\sum_{k=1}^n S_{ik} a_k^{(pk)}(\omega) e^{j\omega\tau} \right] \\ &= \mathfrak{F}^{-1} [b_i^{(pk)}(\omega) e^{j\omega\tau}] = b_i(t - \tau). \end{aligned} \quad (5.17)$$

Any network modeled by its S-parameters obeys the property of time-invariance.

To describe a relationship between a network's incident and scattered waves that's applicable to its linear and nonlinear regions requires a more generalized behavioral model than the S-parameter formulation. For example, returning to our two-port network, as the input

stimulus amplitude is increased, several behavioral changes may ensue. First, the network's input and output match may not necessarily remain unchanged. Second, comprised within the incident and scattered waves there may be the presence of additional spectral components beyond the fundamental order. These characteristics are common to large-signal stimulated networks where the principles of linearity are no longer strictly adhered. As such, the S-parameter model described by (5.8) or (5.9-5.10) is no longer valid. A more comprehensive model is required, one which faithfully predicts the network's properties across its large- (and small-) signal operating-space while continuing to obey in accordance with (5.15) the property of time-invariance. One such model is known as X-parameters.

5.1.2 Nonlinear (and Linear) Network Behavioral Modeling using X-parameters

A network operating in its small-input signal region can be faithfully modeled through a set of equations described by (5.8). Within this operating space, the S-parameters remain independent of the incident signal's amplitude. Continued increase in amplitude eventually leads to multiple output frequency components due to the network's nonlinear behavior. Consequently, the nonlinear network's reflection and transmission characteristics now become a function of the large-input (drive) signal. Hence, the S-parameter model is no longer valid and a new model that embodies both nonlinear and linear network behavior is necessary. Equation (5.18) illustrates such a model [51].

$$B_{ij} = X_{ij}^{(F)} (\text{LSOP}) P^j + \sum_{\text{all } kl} \left[X_{ij,kl}^{(S)} (\text{LSOP}) P^{j-1} a_{kl} + X_{ij,kl}^{(T)} (\text{LSOP}) P^{j+1} a_{kl}^* \right] \quad (5.18)$$

where

i = output port index

j = output frequency index

k = input port index

l = input frequency index

LSOP = Large-Signal Operating Point $\equiv |A_{mn}|$

m = large-signal input port index

n = large-signal input frequency index

and

$$P = e^{j\theta(A_{mn})} .$$

Equation (5.18) uses large-signal scattering coefficients known as X-parameters. The X-parameter formulation is founded on the theory of Poly-Harmonic Distortion modeling [55].

In general, the scattered waves B_{ij} are composed of the sum of large- and small-signal responses. The $X_{ij}^{(F)}$ terms represent the large-signal responses at port i - harmonic j for a nonlinear network match-terminated at all its ports [51]. $X_{ij,kl}^{(S)}$ and $X_{ij,kl}^{(T)}$ are related to the small-signal responses and describe the nonlinear network's sensitivity to mismatch at port i -harmonic j [51]. Unlike S-parameters, the small-signal responses are proportional to both a_{kl} and a_{kl}^* . The total small-signal response is obtained by summing the independent small-signal response contributors due to $X_{ij,kl}^{(S)} a_{kl}$ and $X_{ij,kl}^{(T)} a_{kl}^*$ across all input ports k - harmonics l . The X-parameters are a function of the network's LSOP which in this case is defined by $|A_{11}|$ as a single, CW, large-signal tone incident to port-one at the fundamental frequency of operation. The large-signal responses in (5.18) are not ratio terms unlike the small-signal responses which are related to small-signal incident stimuli a_{kl} and their conjugates. The small-signal incident waves are regarded to have sufficiently small amplitude to not appreciably alter the network's LSOP. As such, the total small-signal responses are superimposed on those of the large- across the harmonic-grid for all ij . Through the summation symbol, the formulation indicates that each

small-signal incident wave across all k contributes to the formation of a small signal (total) response at ij . Analogous to S-parameters, the nonlinear network's gain and match at the fundamental frequency can be described through its X-parameters. But, due to the cross-frequency terms, there are typically more X-parameters than S-parameters needed to provide a full behavioral description of the network. For example, the ratio of the nonlinear network's small-signal fundamental response emerging from port-two and the second harmonic incident to its port-one is $X_{21,12}$.

Unlike the S-parameter formulation, a more generalized model embodying nonlinear (and linear) behavior does not inherently conform to the property of time-invariance described by (5.15). Therefore, to properly represent its incoming and outgoing waves, the time-invariance property is deliberately incorporated into the X-parameter formulism. The P terms present in (5.18) for both large- and small-signal responses enforce the property of time-invariance consistent with (5.15). Without their inclusion, the model is inherently incorrect and may lead in some cases to unacceptable inaccuracies [51].

To demonstrate the applicability of equation (5.18) within the network's linear operating space, consider the condition where the large-signal amplitude $|A_{11}| \rightarrow 0$. First, the large-signal responses described by the $X^{(F)}$ terms approach zero. Second, all harmonic content above the fundamental order becomes negligible and therefore the input and output harmonic indices l and j equal one and are dropped from the expression. Third, the small-signal responses related to $X^{(T)}$ approach zero in the small-signal region of the network. Lastly, the remaining X-parameter coefficients are no longer a function of a LSOP and as such become independent of the small-signal stimuli a_k . As an example, applying the stated conditions to a linear two-port, (5.18) becomes

$$b_i = \sum_{k=1}^2 [X_{i,k}^{(S)} a_k] = \sum_{k=1}^2 [S_{ik} a_k] \quad (5.19)$$

where $X_{ij,kl}^{(S)} P^{j-1} \Big|_{|A_{11}| \rightarrow 0} = X_{i,k}^{(S)} = S_{ik}$. Equation (5.19) reduces to two expressions describing the linear two-port's scattered waves b_1 and b_2 consistent with those previously described by (5.9) and (5.10).

To illustrate the X-parameter identification process, the use of (5.18) will be exercised within context of a quasi-match embedded nonlinear two-port network with a LSOP defined by the large-signal amplitude $|A_{11}|$. In this example, analysis is restricted to the fundamental order with no higher-order harmonics applied or emerging from the two-port. Directing these restrictions to (5.18), the scattered waves of the two-port become

$$B_i = X_i^{(F)}(|A_{11}|)P + \sum_{k=1}^2 \left[X_{i,k}^{(S)}(|A_{11}|)a_k + X_{i,k}^{(T)}P^2(|A_{11}|)a_k^* \right] \quad (5.20)$$

where port indices $1 = j = 1$ have been removed from the expression. The nonlinear network's scattered waves B_1 and B_2 emanating from its input and output ports respectively form (5.21) and (5.22) such that

$$B_1 = X_1^{(F)}P(|A_{11}|) + X_{1,1}^{(S)}(|A_{11}|)a_1 + X_{1,1}^{(T)}P^2(|A_{11}|)a_1^* + X_{1,2}^{(S)}(|A_{11}|)a_2 + X_{1,2}^{(T)}P^2(|A_{11}|)a_2^* \quad (5.21)$$

and

$$B_2 = X_2^{(F)}P(|A_{11}|) + X_{2,1}^{(S)}(|A_{11}|)a_1 + X_{2,1}^{(T)}P^2(|A_{11}|)a_1^* + X_{2,2}^{(S)}(|A_{11}|)a_2 + X_{2,2}^{(T)}P^2(|A_{11}|)a_2^* . \quad (5.22)$$

Combining (5.21) and (5.22) in matrix form produces

$$\begin{bmatrix} B_1 \\ B_2 \end{bmatrix} = \begin{bmatrix} X_1^{(F)}P \\ X_2^{(F)}P \end{bmatrix} + \begin{bmatrix} X_{1,1}^{(S)} & X_{1,1}^{(T)}P^2 & X_{1,2}^{(S)} & X_{1,2}^{(T)}P^2 \\ X_{2,1}^{(S)} & X_{2,1}^{(T)}P^2 & X_{2,2}^{(S)} & X_{2,2}^{(T)}P^2 \end{bmatrix} \begin{bmatrix} a_1 \\ a_1^* \\ a_2 \\ a_2^* \end{bmatrix} . \quad (5.23)$$

The two equations comprise ten unknowns. To extract (solve) the network's X-parameters, a series of five experiments will be conducted with defined stimuli and corresponding response quantities assessed and incorporated within the framework of (5.23).

First, a large-signal with amplitude $|A_{11}|$ is applied to the network's input port thereby establishing a desired LSOP. Large-signal responses $B_{1m}^{(LS)}$ and $B_{2m}^{(LS)}$ are then measured at its input and output ports respectively. The subscript m will be used to denote a measured quantity, in this case a measured large-signal response. The measured responses will be used in post-process to determine the $X^{(F)}$ terms reported in (5.23) [51]. Next, while the large-signal stimulus remains incident to the network's input port, a small-signal stimulus a is introduced to the network. To solve for the remaining eight unknowns, a set of four experiments is conducted. While the LSOP of the network is maintained, a small-signal stimulus a_1 is first directed to the input port and the response on both ports is measured. The phase of the a_1 stimulus is then altered by $\pi/2$ (quadrature) and the responses are once again assessed. The small-signal stimulus is then re-directed to the network's output port, now referred as a_2 , whereupon the process is repeated. The stimuli and response vectors in (5.23) may now be augmented to include the measured quantities procured from each of the five experiments thus forming (5.24) [52].

$$\begin{bmatrix} B_{1m}^{fwd} & B_{1m}^{fwd\frac{\pi}{2}} & B_{1m}^{rev} & B_{1m}^{rev\frac{\pi}{2}} \\ B_{2m}^{fwd} & B_{2m}^{fwd\frac{\pi}{2}} & B_{2m}^{rev} & B_{2m}^{rev\frac{\pi}{2}} \end{bmatrix} = \begin{bmatrix} B_{1m}^{(LS)} & B_{1m}^{(LS)} & B_{1m}^{(LS)} & B_{1m}^{(LS)} \\ B_{2m}^{(LS)} & B_{2m}^{(LS)} & B_{2m}^{(LS)} & B_{2m}^{(LS)} \end{bmatrix} + \begin{bmatrix} X_{1,1}^{(S)} & X_{1,1}^{(T)}P^2 & X_{1,2}^{(S)} & X_{1,2}^{(T)}P^2 \\ X_{2,1}^{(S)} & X_{2,1}^{(T)}P^2 & X_{2,2}^{(S)} & X_{2,2}^{(T)}P^2 \end{bmatrix} \cdot \begin{bmatrix} a_{1m}^{fwd} & a_{1m}^{fwd\frac{\pi}{2}} & a_{1m}^{rev} & a_{1m}^{rev\frac{\pi}{2}} \\ a_{1m}^{fwd*} & a_{1m}^{fwd*\frac{\pi}{2}} & a_{1m}^{rev*} & a_{1m}^{rev*\frac{\pi}{2}} \\ a_{2m}^{fwd} & a_{2m}^{fwd\frac{\pi}{2}} & a_{2m}^{rev} & a_{2m}^{rev\frac{\pi}{2}} \\ a_{2m}^{fwd*} & a_{2m}^{fwd*\frac{\pi}{2}} & a_{2m}^{rev*} & a_{2m}^{rev*\frac{\pi}{2}} \end{bmatrix}$$

(5.24)

The nonlinear two-port's small-signal responses from each of the four experiments can be calculated by subtracting the large-signal responses from the total responses resulting in

$$\begin{bmatrix} b_1^{fwd} & b_1^{fwd \frac{\pi}{2}} & b_1^{rev} & b_1^{rev \frac{\pi}{2}} \\ b_2^{fwd} & b_2^{fwd \frac{\pi}{2}} & b_2^{rev} & b_2^{rev \frac{\pi}{2}} \end{bmatrix} = \begin{bmatrix} B_{1m}^{fwd} & B_{1m}^{fwd \frac{\pi}{2}} & B_{1m}^{rev} & B_{1m}^{rev \frac{\pi}{2}} \\ B_{2m}^{fwd} & B_{2m}^{fwd \frac{\pi}{2}} & B_{2m}^{rev} & B_{2m}^{rev \frac{\pi}{2}} \end{bmatrix} - \begin{bmatrix} B_{1m}^{(LS)} & B_{1m}^{(LS)} & B_{1m}^{(LS)} & B_{1m}^{(LS)} \\ B_{2m}^{(LS)} & B_{2m}^{(LS)} & B_{2m}^{(LS)} & B_{2m}^{(LS)} \end{bmatrix} = \\
 \begin{bmatrix} X_{1,1}^{(S)} & X_{1,1}^{(T)}P^2 & X_{1,2}^{(S)} & X_{1,2}^{(T)}P^2 \\ X_{2,1}^{(S)} & X_{2,1}^{(T)}P^2 & X_{2,2}^{(S)} & X_{2,2}^{(T)}P^2 \end{bmatrix} \cdot \begin{bmatrix} a_{1m}^{fwd} & a_{1m}^{fwd \frac{\pi}{2}} & a_{1m}^{rev} & a_{1m}^{rev \frac{\pi}{2}} \\ a_{1m}^{fwd*} & a_{1m}^{fwd* \frac{\pi}{2}} & a_{1m}^{rev*} & a_{1m}^{rev* \frac{\pi}{2}} \\ a_{2m}^{fwd} & a_{2m}^{fwd \frac{\pi}{2}} & a_{2m}^{rev} & a_{2m}^{rev \frac{\pi}{2}} \\ a_{2m}^{fwd*} & a_{2m}^{fwd* \frac{\pi}{2}} & a_{2m}^{rev*} & a_{2m}^{rev* \frac{\pi}{2}} \end{bmatrix} \cdot \quad (5.25)$$

The X-parameter matrix summarizing the nonlinear network's mapping of the small-signal stimuli to their corresponding responses is solved by post-multiplying both sides of (5.25) by the small-signal stimuli matrix inverse thereby producing the desired result

$$\begin{bmatrix} X_{1,1}^{(S)} & X_{1,1}^{(T)}P^2 & X_{1,2}^{(S)} & X_{1,2}^{(T)}P^2 \\ X_{2,1}^{(S)} & X_{2,1}^{(T)}P^2 & X_{2,2}^{(S)} & X_{2,2}^{(T)}P^2 \end{bmatrix} = \begin{bmatrix} b_1^{fwd} & b_1^{fwd \frac{\pi}{2}} & b_1^{rev} & b_1^{rev \frac{\pi}{2}} \\ b_2^{fwd} & b_2^{fwd \frac{\pi}{2}} & b_2^{rev} & b_2^{rev \frac{\pi}{2}} \end{bmatrix} \cdot \begin{bmatrix} a_{1m}^{fwd} & a_{1m}^{fwd \frac{\pi}{2}} & a_{1m}^{rev} & a_{1m}^{rev \frac{\pi}{2}} \\ a_{1m}^{fwd*} & a_{1m}^{fwd* \frac{\pi}{2}} & a_{1m}^{rev*} & a_{1m}^{rev* \frac{\pi}{2}} \\ a_{2m}^{fwd} & a_{2m}^{fwd \frac{\pi}{2}} & a_{2m}^{rev} & a_{2m}^{rev \frac{\pi}{2}} \\ a_{2m}^{fwd*} & a_{2m}^{fwd* \frac{\pi}{2}} & a_{2m}^{rev*} & a_{2m}^{rev* \frac{\pi}{2}} \end{bmatrix}^{-1} \quad (5.26)$$

With the $X^{(S)}$, and $X^{(T)}P^2$ related terms extracted, they can be applied to the large-signal response measurements, i.e. $B_{1m}^{(LS)}$ and $B_{2m}^{(LS)}$, to extract the match-embedded nonlinear two-port network's large-signal responses $X_1^{(F)}P$ and $X_2^{(F)}P$ thus completing the X-parameter extraction (ten unknowns) process for the set of equations described in (5.23) [51].

In this example, analysis was restricted to a two-port operating at its fundamental frequency. The X-parameter formulism supports the generalized n-port, m-harmonic condition. In such a case, the number of measurements can be increased to assess both large- and small-signal stimulus/response conditions to solve for the X-parameter matrix. As such, the matrix will

be larger in dimension to accommodate for an increase to port and harmonic count. Multiple harmonics introduces cross-frequency coefficients to the formulism. The X-parameter extraction process is like that used in our two-port example with exception that the small-signal stimulus is to be sequentially applied at each of the m -harmonics on a given port and then repeated at the remaining $n-1$ ports.

The Keysight Technologies PNA-X network analyzer may be used to derive X-parameter models using nonlinear vector network analyzer (NVNA) software. A measurement sequence consistent with that previously described, may be implemented in hardware per Fig. 5.2. During the measurement sequence, a large-signal is applied only to the PNA-X's port-one via source-one. Simultaneously with the large-signal applied, a small-signal at the fundamental frequency is introduced to port-one via source-two and the combiner. The stimulus and response of the network, i.e. the " a " and " b " waves, are measured using the test and reference receivers positioned at the PNA-X's port-one and port-three signal paths. The phase of the small-signal is then rotated, and the measurement process repeated. If specified by the user, the small-signal is then sequentially tuned to each harmonic frequency and the stimulus/response measurements on the DUT are repeated. Lastly, while the large-signal remains on port-one, the small-signal is reversed in direction thus being applied to the network's output port via the PNA-X's source-two/test port-three signal path. The small-signal is exercised at its fundamental and harmonics (if specified). At each stimulus frequency/phase setting, stimulus/response measurements are performed on the network. Once the measurement sequences have concluded, the measured waves are used to extract the X-parameters of the network.

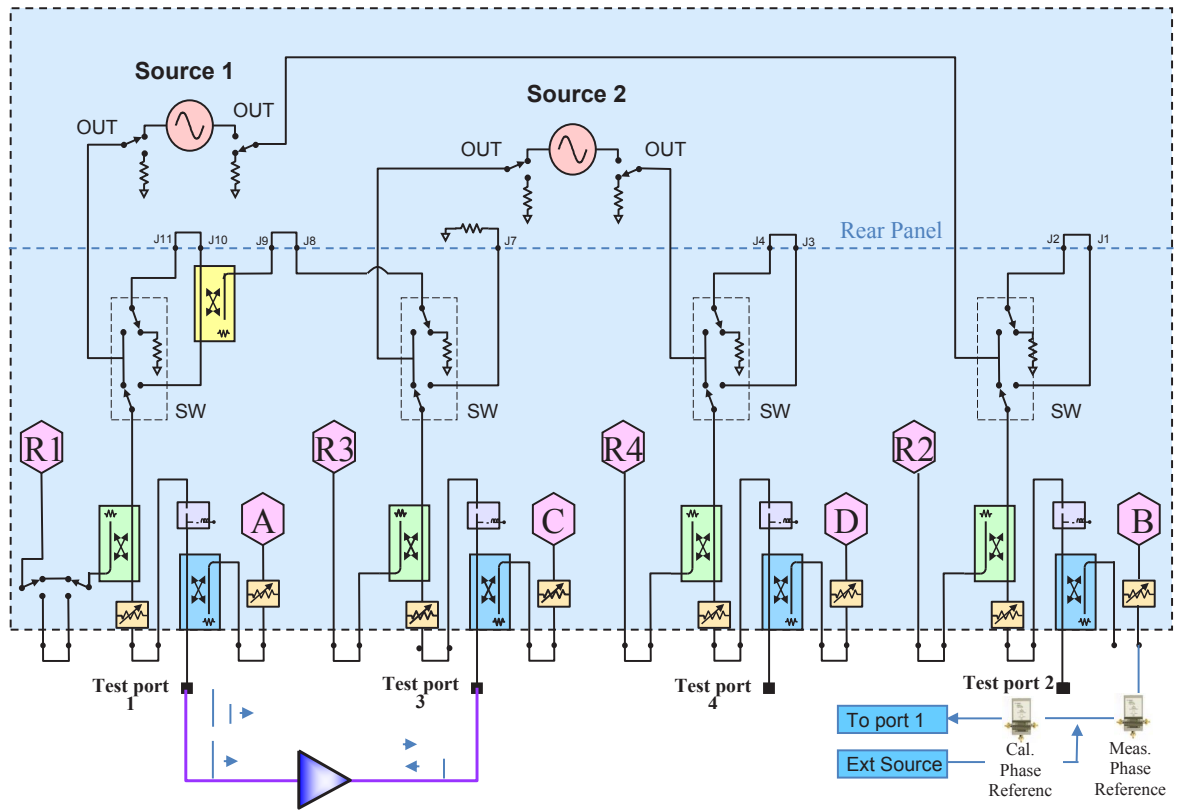


Figure 5.2: The Keysight PNA-X Architecture with NVNA Application to Extract X-parameters [53]

5.2 Nonlinear Network Noise Modeling Using X-parameters

While much attention has been given to predicting network noise behavior under small-signal operation, the same is not true for the large-signal case [54]. It's not uncommon that interfering signals of sufficient amplitude may compromise receiver performance. In current practice, at the time of this writing, there are limited reliable methods for characterization, modeling, and simulation of noise behavior associated with nonlinear networks [65, 66].

Presented in this section is a generalized noise behavioral model for embedded nonlinear (and linear) time-invariant microwave circuits. Using large-signal scattering functions known as X-parameters [51] in conjunction with noise wave theory, the model will be derived in terms of the nonlinear network's noise correlation matrix. Important features will be shown, such as its reduction to the S-parameter behavioral model thus predicting noise performance within the network's small-signal operating-space. Lastly, in terms of the nonlinear network's noise matrix (or noise correlation matrix), relationships describing its noise factor and effective noise temperature will be developed. Using the generalized form, two examples given in context of embedded nonlinear one-port and two-port configurations are offered with each presented with matched termination networks. Numerical versus simulated results will be compared. Lastly, a hardware-based measurement approach will be developed for deriving the noise correlation matrix of a nonlinear two-port network.

5.2.1 General Theory

As described earlier, performing noise characterization on a distributed linear network in the RF/microwave frequency spectrum commonly employs its S-parameters to describe mapping of the network's incident to scattered noise waves. Through their collective use, a comprehensive noise behavioral model for embedded linear networks can be derived.

Should the network experience an input signal of sufficient amplitude leading to operation beyond its linear region, its S-parameters no longer provide a viable predictor of its signal behavior, including noise. In practice, large-signal conditions generate higher-order harmonic and distortion products within a network's response which cannot be captured with the S-parameter framework. Further, S-parameters are independent of drive signal amplitude, a condition not applicable within the nonlinear operating region of the network.

In recent years, a behavioral model known as X-parameters was developed principally by Verspecht and Root [51, 55, 56] to capture a network's discrete response not only at the fundamental frequency but higher-order spectral components associated with a large-input stimulus. The behavior of the device, described by its X-parameters is dependent on the network's large signal operating point (LSOP). X-parameters are a mathematically correct extension of S-parameters. That is, should the large-input signal amplitude be reduced such that the network operates in its linear-space, the X-parameter formulism relating the incident to scattered noise waves reduces to the familiar S-parameter network representation. Thus, the X-parameter behavioral model may be used to predict behavior across the network's entire input-signal space.

It's proposed in this work that X-parameters be utilized to derive a comprehensive noise behavioral model to predict a nonlinear network's noise performance. To be valid, the network's noise will be treated as a small-signal to not alter the LSOP collectively established by application of DC and, in this case, a discrete single CW RF input tone. Thus, the small-signal mapping of incident to scattered noise waves described by the network's X-parameters is superimposed on its deterministic signal response.

5.2.1.1 Noise Correlation Matrix

Consider Fig. 5.3(a) consisting of a noisy nonlinear n-port network evaluated over m-harmonics operating at an LSOP. The network's signal and noise behavior will be represented by its X-

parameters and equivalent internal noise wave generator array $\hat{\mathbf{b}}_{gd}$ respectively. The $m \times n$ elements forming column vector $\hat{\mathbf{b}}_{gd}$ exist at each of the device's ports and their respective harmonics described in units of square root watts per Hz. The i, j -th element of $\hat{\mathbf{b}}_{gd}$ is noise wave $\hat{b}_{gd_{ij}}$ where lower subscripts i and j are the output port-harmonic index respectively. The power spectral densities of the noise waves are designated by their time-averaged magnitude squared normalized to a 1Hz bandwidth. This is the characteristic noise power density which would be delivered to a matched, noise-free termination.

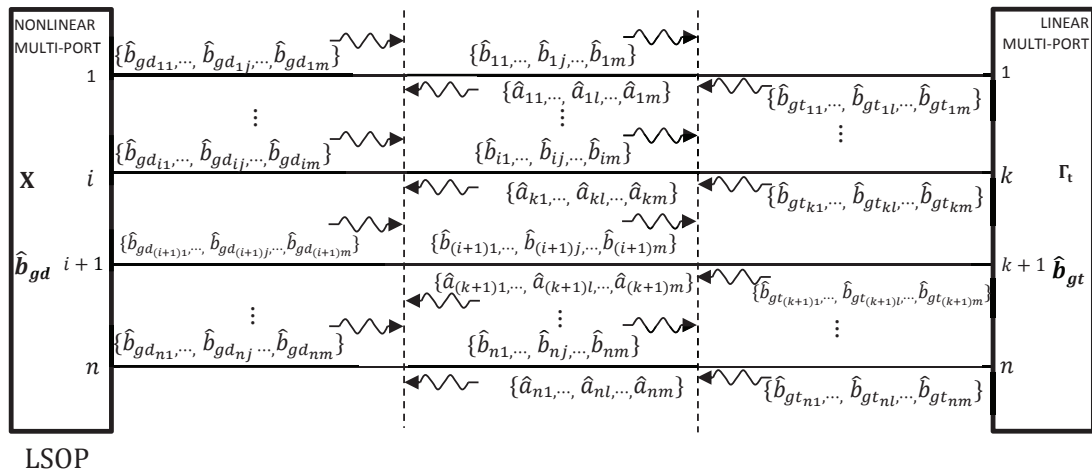


Figure 5.3(a): Two connected noisy multi-ports, the nonlinear (n-port, m-harmonic) device and its linear termination network

As depicted in Fig. 5.3(a), each port of the nonlinear network is terminated in a passive, reflective, noisy load. The termination network considered will be linear and generalized to account for coupling between its ports as described by its S-parameters matrix. In its simplest form, the off-diagonal elements are zero indicating infinite isolation to its adjacent ports and elements along its diagonal are reflection coefficients presented to each of the nonlinear network's ports. The

amplitudes of the termination network's noise wave generators are accounted in column vector $\hat{\mathbf{b}}_{gt}$. The k, l -th element of $\hat{\mathbf{b}}_{gt}$ is noise wave $\hat{b}_{gt_{kl}}$ where lower subscripts k and l represent the input port-harmonic index.

The nonlinear network's incident and scattered noise waves are ordered in column vectors $\hat{\mathbf{a}}$ and $\hat{\mathbf{b}}$ respectively; in turn their elements will be stated \hat{a}_{kl} and \hat{b}_{ij} . Fig. 5.3(b) is the

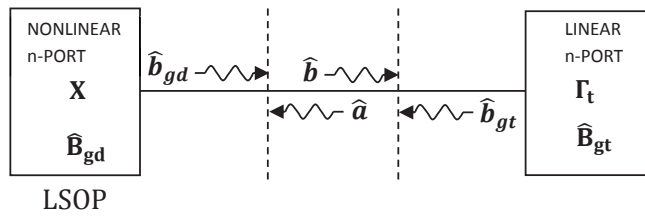


Figure 5.3(b): Two connected noisy n-ports.
Noise wave equations in matrix form can readily be devised by inspection.

corresponding matrix representation of Fig. 5.3(a). Its inspection yields two expressions related to the noise-wave vectors. First, the incident noise vector $\hat{\mathbf{a}}$ can be expressed as shown in (5.27).

$$\hat{\mathbf{a}} = \Gamma_t \hat{\mathbf{b}} + \hat{\mathbf{b}}_{gt} \quad (5.27)$$

where Γ_t is a square matrix with dimension $[m * n, m * n]$. From (5.27), incident noise wave \hat{a}_{kl} may be written in (5.28) as

$$\hat{a}_{kl} = \sum_{i=1}^n \sum_{j=1}^m (\Gamma_{t_{kl,ij}} \hat{b}_{ij}) + \hat{b}_{gt_{kl}} \quad (5.28)$$

for all $l = j$, else $\Gamma_{t_{kl,ij}} = 0$.

Consistent with X-parameter theory, a second expression, also from Fig. 5.3(b), describes the scattered noise wave vector $\hat{\mathbf{b}}$ of a noisy NL n-port with total response

$$\hat{\mathbf{b}} = \mathbf{X}^{(S)}(DC, |A_{11}|) \otimes \mathbf{P}^{(S)} \hat{\mathbf{a}} + \mathbf{X}^{(T)}(DC, |A_{11}|) \otimes \mathbf{P}^{(T)} \hat{\mathbf{a}}^* + \hat{\mathbf{b}}_{gd} \quad (5.29)$$

The character “ \otimes ” indicates the operation-type is multiplication and the “ $\cdot \otimes$ ” is an element-by-element matrix multiplication. In (5.29), there are two small-signal responses initiated by incident noise vector $\hat{\mathbf{a}}$ in the formation of $\hat{\mathbf{b}}$, S- and T-type. The distinct contribution of each incident noise wave \hat{a}_{kl} to this response is described by scattering matrices $\mathbf{X}^{(S)}$ and $\mathbf{X}^{(T)}$ each of dimension $[m * n, m * n]$. Equation (5.29) shows these contributions have complex values which are functions of the LSOP defined by bias and the magnitude of the large-signal $|A_{11}|$. The significance of $\mathbf{P}^{(S)}$ and $\mathbf{P}^{(T)}$ is that it enforces the property of time-invariance by re-aligning in time the response with the stimulus.

From (5.29), outgoing noise wave \hat{b}_{ij} is described by

$$\hat{b}_{ij} = \sum_{k=1}^n \sum_{l=1}^m \left[X_{ij,kl}^{(S)}(DC, |A_{11}|) P^{(j-1)} \hat{a}_{kl} + X_{ij,kl}^{(T)}(DC, |A_{11}|) P^{(j+1)} \hat{a}_{kl}^* \right] + \hat{b}_{gd_{ij}} \quad (5.30)$$

where elements in matrices $\mathbf{P}^{(S)}$ and $\mathbf{P}^{(T)}$ are correspondingly depicted by $P^{(j-1)}$ and $P^{(j+1)}$.

Substituting (5.27) into (5.29) and organizing the scattered noise wave vector $\hat{\mathbf{b}}$ - and $\hat{\mathbf{b}}^*$ - terms produces

$$\left(\mathbf{I} - \mathbf{X}^{(S)} \cdot \otimes \mathbf{P}^{(S)} \Gamma_{\mathbf{t}} \right) \hat{\mathbf{b}} - \mathbf{X}^{(T)} \cdot \otimes \mathbf{P}^{(T)} \Gamma_{\mathbf{t}}^* \hat{\mathbf{b}}^* = \mathbf{X}^{(S)} \cdot \otimes \mathbf{P}^{(S)} \hat{\mathbf{b}}_{gt} + \mathbf{X}^{(T)} \cdot \otimes \mathbf{P}^{(T)} \hat{\mathbf{b}}_{gt}^* + \hat{\mathbf{b}}_{gd} \quad (5.31)$$

where \mathbf{I} is the identity matrix. Taking the complex conjugate of (5.31) generates a second equation from which scattered noise wave vectors $\hat{\mathbf{b}}$ and $\hat{\mathbf{b}}^*$ are organized in an aggregate matrix and solved resulting in the expression shown in (5.32).

$$\begin{bmatrix} \hat{\mathbf{b}} \\ \hat{\mathbf{b}}^* \end{bmatrix} = \begin{bmatrix} (\mathbf{I} - \mathbf{X}^{(S)} \cdot \otimes \mathbf{P}^{(S)} \Gamma_t) & -\mathbf{X}^{(T)} \cdot \otimes \mathbf{P}^{(T)} \Gamma_t^* \\ -\mathbf{X}^{(T)*} \cdot \otimes \mathbf{P}^{(T)*} \Gamma_t & (\mathbf{I} - \mathbf{X}^{(S)} \cdot \otimes \mathbf{P}^{(S)} \Gamma_t)^* \end{bmatrix}^{-1} \begin{bmatrix} \mathbf{X}^{(S)} \cdot \otimes \mathbf{P}^{(S)} \hat{\mathbf{b}}_{gt} + \mathbf{X}^{(T)} \cdot \otimes \mathbf{P}^{(T)} \hat{\mathbf{b}}_{gd} + \hat{\mathbf{b}}_{gd} \\ \mathbf{X}^{(S)*} \cdot \otimes \mathbf{P}^{(S)*} \hat{\mathbf{b}}_{gt}^* + \mathbf{X}^{(T)*} \cdot \otimes \mathbf{P}^{(T)*} \hat{\mathbf{b}}_{gd}^* + \hat{\mathbf{b}}_{gd}^* \end{bmatrix} \quad (5.32)$$

The correlation of the embedded nonlinear network's scattered waves is defined by noise matrix $\hat{\mathbf{B}}$ such that

$$\hat{\mathbf{B}} \equiv \overline{\begin{bmatrix} \hat{\mathbf{b}} \\ \hat{\mathbf{b}}^* \end{bmatrix} \begin{bmatrix} \hat{\mathbf{b}} \\ \hat{\mathbf{b}}^* \end{bmatrix}^\dagger} \quad (5.33)$$

where the symbol “ \dagger ” implies Hermitian and the bar illustrates the time-average of an assumed ergodic process. $\hat{\mathbf{B}}$ is the connected system's full in-situ noise matrix. The diagonal elements of $\hat{\mathbf{B}}$ represent the characteristic noise power spectral density $\overline{|\hat{b}_{ij}|^2}$ of the nonlinear network's scattered waves at each port i - harmonic j index. Its correspondence to the available noise power density is specified by $\overline{|\hat{b}_{ij}|^2} = \overline{|\hat{b}_{j,av}|^2} (1 - |\Gamma_{ij}|^2)$. The off-diagonal elements are the cross port-harmonic correlation of each scattered wave to the other.

Noise matrix $\hat{\mathbf{B}}$ can be expressed in terms of the signal and noise properties of the nonlinear n-port and its connecting terminations. Use of (5.32, 5.33) yields (5.34) such that

$$\overline{\begin{bmatrix} \hat{\mathbf{b}} \\ \hat{\mathbf{b}}^* \end{bmatrix} \begin{bmatrix} \hat{\mathbf{b}} \\ \hat{\mathbf{b}}^* \end{bmatrix}^\dagger} = \begin{bmatrix} (\mathbf{I} - \mathbf{X}^{(S)} \cdot \otimes \mathbf{P}^{(S)} \Gamma_t) & -\mathbf{X}^{(T)} \cdot \otimes \mathbf{P}^{(T)} \Gamma_t^* \\ -\mathbf{X}^{(T)*} \cdot \otimes \mathbf{P}^{(T)*} \Gamma_t & (\mathbf{I} - \mathbf{X}^{(S)} \cdot \otimes \mathbf{P}^{(S)} \Gamma_t)^* \end{bmatrix}^{-1} \cdot \left\{ \begin{bmatrix} \mathbf{X}^{(S)} \cdot \otimes \mathbf{P}^{(S)} & \mathbf{X}^{(T)} \cdot \otimes \mathbf{P}^{(T)} \\ \mathbf{X}^{(T)*} \cdot \otimes \mathbf{P}^{(T)*} & \mathbf{X}^{(S)*} \cdot \otimes \mathbf{P}^{(S)*} \end{bmatrix} \cdot \overline{\begin{bmatrix} \hat{\mathbf{b}}_{gt} \\ \hat{\mathbf{b}}_{gt}^* \end{bmatrix} \begin{bmatrix} \hat{\mathbf{b}}_{gt} \\ \hat{\mathbf{b}}_{gt}^* \end{bmatrix}^\dagger} \cdot \begin{bmatrix} \mathbf{X}^{(S)} \cdot \otimes \mathbf{P}^{(S)} & \mathbf{X}^{(T)} \cdot \otimes \mathbf{P}^{(T)} \\ \mathbf{X}^{(T)*} \cdot \otimes \mathbf{P}^{(T)*} & \mathbf{X}^{(S)*} \cdot \otimes \mathbf{P}^{(S)*} \end{bmatrix}^\dagger + \overline{\begin{bmatrix} \hat{\mathbf{b}}_{gd} \\ \hat{\mathbf{b}}_{gd}^* \end{bmatrix} \begin{bmatrix} \hat{\mathbf{b}}_{gd} \\ \hat{\mathbf{b}}_{gd}^* \end{bmatrix}^\dagger} \right\} \cdot \begin{bmatrix} (\mathbf{I} - \mathbf{X}^{(S)} \cdot \otimes \mathbf{P}^{(S)} \Gamma_t) & -\mathbf{X}^{(T)} \cdot \otimes \mathbf{P}^{(T)} \Gamma_t^* \\ -\mathbf{X}^{(T)*} \cdot \otimes \mathbf{P}^{(T)*} \Gamma_t & (\mathbf{I} - \mathbf{X}^{(S)} \cdot \otimes \mathbf{P}^{(S)} \Gamma_t)^* \end{bmatrix}^{-1\dagger} \quad (5.34)$$

where noise generated by the comprising networks are treated as uncorrelated to one another. From (5.34), the NCM summarizing the intrinsic noise properties generated by the NL-device $\hat{\mathbf{B}}_{gd}$ and its connected terminations $\hat{\mathbf{B}}_{gt}$ will be defined as

$$\hat{\mathbf{B}}_{gd} \equiv \begin{bmatrix} \hat{\mathbf{b}}_{gd} \\ \hat{\mathbf{b}}_{gd}^* \end{bmatrix} \cdot \begin{bmatrix} \hat{\mathbf{b}}_{gd} \\ \hat{\mathbf{b}}_{gd}^* \end{bmatrix}^{\dagger} \text{ and } \hat{\mathbf{B}}_{gt} \equiv \begin{bmatrix} \hat{\mathbf{b}}_{gt} \\ \hat{\mathbf{b}}_{gt}^* \end{bmatrix} \cdot \begin{bmatrix} \hat{\mathbf{b}}_{gt} \\ \hat{\mathbf{b}}_{gt}^* \end{bmatrix}^{\dagger} . \quad (5.35a,b)$$

Pertaining to (5.34), the full in-situ NCM of the scattered noise waves is expressed as a transformation sum of the noise properties associated with that of the nonlinear network and its connecting terminations. This noise transformation leading to its contribution to the scattered waves is the result of its interaction with the composing network's scattering functions (X- and S-parameters). Thus, knowledge of these scattering functions and the noise correlation matrices in (5.35) enables calculation of the full in-situ scattered noise matrix $\hat{\mathbf{B}}$.

While (5.34) can be validated in software simulation the same is not true in hardware. Practical limitations in measurement exist due to superposition of large- (discrete) and small-signal noise responses present across the harmonic grid. Inability to sufficiently separate the signals precludes an accurate assessment of the noise.

Alternatively, a more generalized approach may be taken whereupon the NL network's scattered noise response is measured at a small offset frequency above and/or below the harmonic grid while preserving the LSOP. While this technique offers benefit given the perturbation frequency of the noise is now distinct from the drive tone frequency, it's not without a potential restriction. The method assumes that the X-parameters evaluated on the harmonic grid are unchanged at the established offset frequency. NL network's exhibiting moderate to strong memory effects may not satisfy this criterion [51]. In this work, such effects exhibited by the network of interest will be assumed negligible.

Equation (5.27) may be adapted to accommodate for a finite frequency offset condition above and below the harmonic grid forming two expressions in

$$\hat{\mathbf{a}}' = \Gamma_{\dagger} \hat{\mathbf{b}}' + \hat{\mathbf{b}}'_{gd} \quad (5.36)$$

and

$$\hat{\mathbf{a}}'' = \Gamma_{\dagger} \hat{\mathbf{b}}'' + \hat{\mathbf{b}}''_{gd} \quad (5.37)$$

where “ ’ ” and “ ’ ’ ” correspondingly signify positive and negative frequency offsets.

Equation (5.29) is modified to describe the NL-network’s scattered noise vectors residing above and below the spectral components comprising its large-signal response. The scattered noise waves positioned above the spectral locations defining the harmonic grid are

$$\hat{\mathbf{b}}' = \mathbf{X}^{(S)}(DC, |A_{11}|) \cdot \otimes \mathbf{P}^{(S)} \hat{\mathbf{a}}' + \mathbf{X}^{(T)}(DC, |A_{11}|) \cdot \otimes \mathbf{P}^{(T)} \hat{\mathbf{a}}'^* + \hat{\mathbf{b}}'_{gd} \quad (5.38)$$

while those below are

$$\hat{\mathbf{b}}'' = \mathbf{X}^{(S)}(DC, |A_{11}|) \cdot \otimes \mathbf{P}^{(S)} \hat{\mathbf{a}}'' + \mathbf{X}^{(T)}(DC, |A_{11}|) \cdot \otimes \mathbf{P}^{(T)} \hat{\mathbf{a}}''^* + \hat{\mathbf{b}}''_{gd} . \quad (5.39)$$

Substitution of (5.36) and (5.37) into (5.38) returns in (5.40)

$$\left(\mathbf{I} - \mathbf{X}^{(S)} \cdot \otimes \mathbf{P}^{(S)} \Gamma_{\dagger} \right) \hat{\mathbf{b}}' - \mathbf{X}^{(T)} \cdot \otimes \mathbf{P}^{(T)} \Gamma_{\dagger}^* \hat{\mathbf{b}}''^* = \mathbf{X}^{(S)} \cdot \otimes \mathbf{P}^{(S)} \hat{\mathbf{b}}'_{gd} + \mathbf{X}^{(T)} \cdot \otimes \mathbf{P}^{(T)} \hat{\mathbf{b}}''_{gd} + \hat{\mathbf{b}}'_{gd} . \quad (5.40)$$

Taking the complex conjugate of (5.40), a second equation is created from which unknowns $\hat{\mathbf{b}}'$ and $\hat{\mathbf{b}}''^*$ may be solved. Analogous in procedure to (5.31) - (5.34), a full in-situ noise matrix bounded across the harmonic grid may be computed resulting in

$$\begin{aligned} \overline{\begin{bmatrix} \hat{b}' \\ \hat{b}'' \end{bmatrix}} \cdot \overline{\begin{bmatrix} \hat{b}' \\ \hat{b}'' \end{bmatrix}}^\dagger &= \begin{bmatrix} (\mathbf{I} - \mathbf{X}^{(s)} \otimes \mathbf{P}^{(s)} \Gamma_t) & -\mathbf{X}^{(r)} \otimes \mathbf{P}^{(r)} \Gamma_t^* \\ -\mathbf{X}^{(r)*} \otimes \mathbf{P}^{(r)*} \Gamma_t & (\mathbf{I} - \mathbf{X}^{(s)} \otimes \mathbf{P}^{(s)} \Gamma_t)^* \end{bmatrix}^{-1} \\ &\left\{ \begin{bmatrix} \mathbf{X}^{(s)} \otimes \mathbf{P}^{(s)} & \mathbf{X}^{(r)} \otimes \mathbf{P}^{(r)} \\ \mathbf{X}^{(r)*} \otimes \mathbf{P}^{(r)*} & \mathbf{X}^{(s)*} \otimes \mathbf{P}^{(s)*} \end{bmatrix} \cdot \overline{\begin{bmatrix} \hat{b}'_{gt} \\ \hat{b}''_{gt} \end{bmatrix}} \cdot \overline{\begin{bmatrix} \hat{b}'_{gt} \\ \hat{b}''_{gt} \end{bmatrix}}^\dagger \cdot \begin{bmatrix} \mathbf{X}^{(s)} \otimes \mathbf{P}^{(s)} & \mathbf{X}^{(r)} \otimes \mathbf{P}^{(r)} \\ \mathbf{X}^{(r)*} \otimes \mathbf{P}^{(r)*} & \mathbf{X}^{(s)*} \otimes \mathbf{P}^{(s)*} \end{bmatrix}^\dagger + \overline{\begin{bmatrix} \hat{b}'_{gd} \\ \hat{b}''_{gd} \end{bmatrix}} \cdot \overline{\begin{bmatrix} \hat{b}'_{gd} \\ \hat{b}''_{gd} \end{bmatrix}}^\dagger \right\} \\ &\begin{bmatrix} (\mathbf{I} - \mathbf{X}^{(s)} \otimes \mathbf{P}^{(s)} \Gamma_t) & -\mathbf{X}^{(r)} \otimes \mathbf{P}^{(r)} \Gamma_t^* \\ -\mathbf{X}^{(r)*} \otimes \mathbf{P}^{(r)*} \Gamma_t & (\mathbf{I} - \mathbf{X}^{(s)} \otimes \mathbf{P}^{(s)} \Gamma_t)^* \end{bmatrix}^{-1\dagger} \end{aligned} \quad (5.41)$$

For purpose of brevity, (5.41) is written as

$$\begin{aligned} \hat{\mathbf{B}}''' &= \begin{bmatrix} (\mathbf{I} - \mathbf{X}^{(s)} \otimes \mathbf{P}^{(s)} \Gamma_t) & -\mathbf{X}^{(r)} \otimes \mathbf{P}^{(r)} \Gamma_t^* \\ -\mathbf{X}^{(r)*} \otimes \mathbf{P}^{(r)*} \Gamma_t & (\mathbf{I} - \mathbf{X}^{(s)} \otimes \mathbf{P}^{(s)} \Gamma_t)^* \end{bmatrix}^{-1} \\ &\left\{ \begin{bmatrix} \mathbf{X}^{(s)} \otimes \mathbf{P}^{(s)} & \mathbf{X}^{(r)} \otimes \mathbf{P}^{(r)} \\ \mathbf{X}^{(r)*} \otimes \mathbf{P}^{(r)*} & \mathbf{X}^{(s)*} \otimes \mathbf{P}^{(s)*} \end{bmatrix} \cdot \hat{\mathbf{B}}'''_{gt} \cdot \begin{bmatrix} \mathbf{X}^{(s)} \otimes \mathbf{P}^{(s)} & \mathbf{X}^{(r)} \otimes \mathbf{P}^{(r)} \\ \mathbf{X}^{(r)*} \otimes \mathbf{P}^{(r)*} & \mathbf{X}^{(s)*} \otimes \mathbf{P}^{(s)*} \end{bmatrix}^\dagger + \hat{\mathbf{B}}'''_{gd} \right\} \\ &\begin{bmatrix} (\mathbf{I} - \mathbf{X}^{(s)} \otimes \mathbf{P}^{(s)} \Gamma_t) & -\mathbf{X}^{(r)} \otimes \mathbf{P}^{(r)} \Gamma_t^* \\ -\mathbf{X}^{(r)*} \otimes \mathbf{P}^{(r)*} \Gamma_t & (\mathbf{I} - \mathbf{X}^{(s)} \otimes \mathbf{P}^{(s)} \Gamma_t)^* \end{bmatrix}^{-1\dagger} \end{aligned} \quad (5.42)$$

where the “'''” symbolizes matrix elements comprising noise wave quantities residing at upper and lower sidebands, “'” and “''” respectively.

The time-averaged noise matrix $\hat{\mathbf{B}}'''$ consists of two parts. The first term is the characteristic noise power emanating from the NL network's ports due to incident noise matrix $\hat{\mathbf{B}}'''_{gt}$ being modified through its interaction with the composing network [26]. The second term is the characteristic noise power emerging from the NL network's ports due to its own intrinsic noise matrix $\hat{\mathbf{B}}'''_{gd}$ [26]. That is, the noise of the device undergoes its own alteration. Thus, the scattered noise power at the NL network's ports is the sum of two transformations.

Of interest is that the noise performance of the nonlinear multi-port network is entirely described by its scattering parameter \mathbf{X} and noise correlation $\hat{\mathbf{B}}_{gd}'''$ matrices. Collectively, they explain as evidence in (5.41) the behavior of the device in relation to its connecting networks. The elements of \mathbf{X} and $\hat{\mathbf{B}}_{gd}'''$ need be determined from measurement or numerical calculation [20].

To re-enforce its applicability across the network's entire input signal-space, equation (5.41) will be employed for embedded one- and two-port examples in sections 5.2.2 and 5.2.3 respectively.

5.2.1.2 Noise Factor

Noise factor, and equivalently, noise figure quantifies the noise appraisal of a two-port network. It's defined as the ratio of total available noise power at a network's output to total available noise power at the output due to the input termination's thermal noise [1, 35]. IEEE industry standards establish an input termination reference temperature T_0 at 290K [47]. From this, the conclusion is drawn that noise factor is a measure of output available noise power the network adds compared to the output available noise power due to the reference input termination at physical temperature T_0 . Accordingly, should the device contribute zero noise, its minimum noise factor F presents a numerical value of unity.

Industry standards define noise factor [47] for a two-port network case but do not extend it to the generalized multi-port, i.e. $n > 2$, network condition. However, an assessment is possible by use of the terms comprising the scattering noise wave matrix expression for $\hat{\mathbf{B}}'''$ given by (5.42) and its use within context of the definition for F . Through their use, the upper sideband spot noise factor F'_{ij} can be presented as

$$F_{ij}'' = 1 + \frac{1}{kT_0} \frac{\left\{ \left[\begin{array}{cc} (I - X^{(s)} \cdot \otimes P^{(s)} \Gamma_t) & -X^{(r)} \cdot \otimes P^{(r)} \Gamma_t^* \\ -X^{(r)*} \cdot \otimes P^{(r)*} \Gamma_t & (I - X^{(s)} \cdot \otimes P^{(s)} \Gamma_t)^* \end{array} \right]^{-1} \hat{\mathbf{B}}_{gd}'' \left[\begin{array}{cc} (I - X^{(s)} \cdot \otimes P^{(s)} \Gamma_t) & -X^{(r)} \cdot \otimes P^{(r)} \Gamma_t^* \\ -X^{(r)*} \cdot \otimes P^{(r)*} \Gamma_t & (I - X^{(s)} \cdot \otimes P^{(s)} \Gamma_t)^* \end{array} \right]^{-1 \dagger} \right\}_{\text{diag}(ij-ij)'}}{\left\{ \left[\begin{array}{cc} (I - X^{(s)} \cdot \otimes P^{(s)} \Gamma_t) & -X^{(r)} \cdot \otimes P^{(r)} \Gamma_t^* \\ -X^{(r)*} \cdot \otimes P^{(r)*} \Gamma_t & (I - X^{(s)} \cdot \otimes P^{(s)} \Gamma_t)^* \end{array} \right]^{-1} \left[\begin{array}{cc} X^{(s)} \cdot \otimes P^{(s)} & X^{(r)} \cdot \otimes P^{(r)} \\ X^{(r)*} \cdot \otimes P^{(r)*} & X^{(s)*} \cdot \otimes P^{(s)*} \end{array} \right]^{-1} \hat{\mathbf{B}}_{gt}'' \left[\begin{array}{cc} X^{(s)} \cdot \otimes P^{(s)} & X^{(r)} \cdot \otimes P^{(r)} \\ X^{(r)*} \cdot \otimes P^{(r)*} & X^{(s)*} \cdot \otimes P^{(s)*} \end{array} \right] \left[\begin{array}{cc} (I - X^{(s)} \cdot \otimes P^{(s)} \Gamma_t) & -X^{(r)} \cdot \otimes P^{(r)} \Gamma_t^* \\ -X^{(r)*} \cdot \otimes P^{(r)*} \Gamma_t & (I - X^{(s)} \cdot \otimes P^{(s)} \Gamma_t)^* \end{array} \right]^{-1 \dagger} \right\}_{\text{diag}(ij-ij)'}}$$

(5.43)

where $(ij)'$ represents the ij -th output port-harmonic at its upper sideband frequency location and $\text{diag}(ij-ij)'$ is a diagonal element of the matrix within brackets [26]. The above expression evaluates the upper sideband noise power out due to noise added by the nonlinear network and ratios it to the portion of upper sideband noise power out due to the incident noise presented to all its input ports. In (5.43), the nonlinear network's terminations are referenced to available noise power density kT_0 . This condition is enforced by defining the expression $\hat{\mathbf{B}}_{gt}'' = kT_0 \hat{\mathbf{B}}_{gt}''$ and its use in the denominator of (5.43). Noise matrix $\hat{\mathbf{B}}_{gt}''$ retains the correlation each incident noise wave source exhibits to the other. Should the DUT's connecting terminations be passive, isolated, and present a noise temperature T_0 to all its ports, $\hat{\mathbf{B}}_{gt}''$ reduces to the identity matrix. Further, use of $\hat{\mathbf{B}}_{gt}''$ supports analysis of the DUT's noise factor for the more general scenario where different input termination noise temperatures are presented to its ports [26].

The lower sideband spot noise factor F_{ij}'' can be assessed using (5.43) by replacing $\text{diag}(ij-ij)'$ with $\text{diag}(ij-ij)''$. As such, the diagonal elements in the numerator and denominator correspond exclusively to the $(ij)''$ port-harmonic indices.

Equation (5.43) is a generalized formulism supporting a nonlinear network consisting of n -ports across m -harmonics. In section 5.2.3, through use of an example, it will be shown that

the expression can be reduced to the two-port fundamental frequency case, with input termination reference temperature T_0 .

5.2.2 Noise Analysis of a Nonlinear One-Port Network

Through the full in-situ scattered noise matrix [26] expression of (5.41), the noise performance of a nonlinear multiport is described in relation to its connecting networks. This section is devoted to clarifying as well as confirming in-part this generalized formalism through analysis of a match-terminated nonlinear one-port network. Calculated numerical results for specific levels of noise under various large-signal drive tone operating conditions will be examined and compared with computer simulation of an example circuit using ADS software.

The nonlinear one-port is composed in simulation of an npn Si transistor operating within a single-stage common-emitter circuit configuration. In this example, the transistor's load is connected to its collector terminal. The one-port's incoming and outgoing RF signals will be accessed at the transistor's base terminal. Circuit elements are chosen in order that negligible memory effects are introduced. The circuit's response, large-signal or large-signal plus noise are separately analyzed in simulation by turning its noise generators off and on respectively.

The one-port's connected network delivers a single CW RF drive tone to its input contributing to creation of its LSOP. This network also acts as the one-port's termination through its source impedance, in this case being passive, matched, and noisy.

In the experiment, noise analysis is restricted to the fundamental frequency and its bounded offsets. For (5.38) and (5.39) to remain valid, the source impedance, from the one-port's frame of reference, will be noise-free and matched at frequencies corresponding to higher order harmonics. To impose this condition, a bandpass filter is inserted in the signal path to eliminate incident noise located at frequencies corresponding to the upper harmonic-grid. Hence, the filter's out-of-band characteristics are absorptive, i.e. matched. Figure 5.4 emulates the

schematic of the noisy nonlinear one-port circuit and its connected source/termination network used to conduct the experiment. The noisy X-parameter model of the nonlinear one-port network is represented by the X-parameter representation of its noise-free otherwise electrical equivalent circuit summed with its own complex noise values versus time. To construct this model, two simulations are performed prior to this experiment; the first is to create an X-parameter behavioral model from the original albeit noise-free nonlinear one-port circuit, and second to acquire a data base of complex noise emanating from the noisy one-port versus time. Separation of these experiments is required due to X-parameters not presently supporting noise analysis in ADS. Lastly, the combiner's S-parameters are chosen to preserve the same input match as the original noisy nonlinear one-port network.

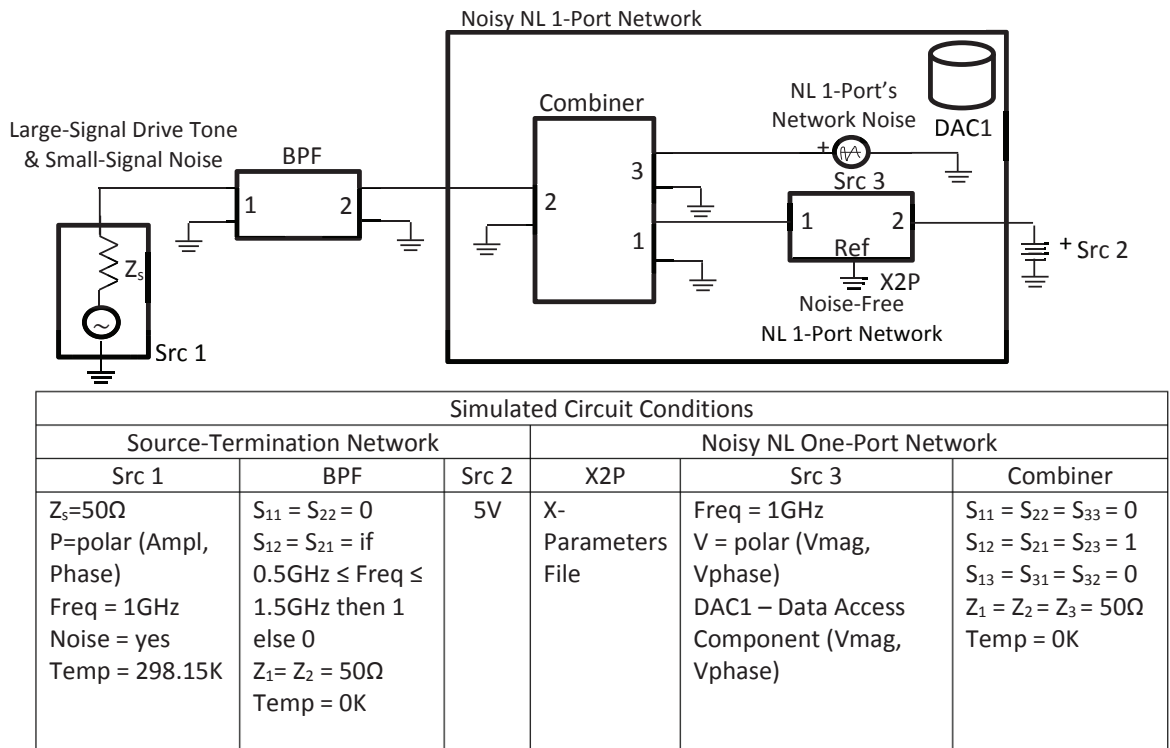


Figure 5.4: Simulation of a Noisy Nonlinear One-Port Match Embedded with its Source-Termination Network

With experiment conditions now defined, the generalized scattered noise matrix expression in (5.41) is constituted by

$$\begin{bmatrix} \overline{\hat{b}'_{11}} & \overline{\hat{b}'_{11}} \\ \overline{\hat{b}''_{11}} & \overline{\hat{b}''_{11}} \end{bmatrix}^\dagger = \begin{bmatrix} 1 & 0 \\ 0 & 1 \end{bmatrix}^{-1} \left\{ \begin{bmatrix} X_{11,11}^{(S)} P^0 & X_{11,11}^{(T)} P^2 \\ X_{11,11}^{(T)*} P^{-2} & X_{11,11}^{(S)*} P^0 \end{bmatrix} \begin{bmatrix} \overline{\hat{b}'_{gs_{11}}} & \overline{\hat{b}'_{gs_{11}}} \\ \overline{\hat{b}''_{gs_{11}}} & \overline{\hat{b}''_{gs_{11}}} \end{bmatrix}^\dagger \begin{bmatrix} X_{11,11}^{(S)} P^0 & X_{11,11}^{(T)} P^2 \\ X_{11,11}^{(T)*} P^{-2} & X_{11,11}^{(S)*} P^0 \end{bmatrix}^\dagger + \begin{bmatrix} \overline{\hat{b}'_{gd_{11}}} & \overline{\hat{b}'_{gd_{11}}} \\ \overline{\hat{b}''_{gd_{11}}} & \overline{\hat{b}''_{gd_{11}}} \end{bmatrix}^\dagger \right\} \begin{bmatrix} 1 & 0 \\ 0 & 1 \end{bmatrix}^{-1\dagger} \quad (5.44)$$

where $\Gamma_{S_{11}} = 0$ and $P = e^{j\theta_{A_{11}}}$.

Multiplying the time-averaged scattered, incident, and intrinsic noise vectors [26] in (5.44) by their respective Hermitian's returns

$$\begin{bmatrix} \overline{\hat{b}'_{11}\hat{b}'_{11}} & \overline{\hat{b}'_{11}\hat{b}''_{11}} \\ \overline{\hat{b}''_{11}\hat{b}'_{11}} & \overline{\hat{b}''_{11}\hat{b}''_{11}} \end{bmatrix} = \begin{bmatrix} X_{11,11}^{(S)} P^0 & X_{11,11}^{(T)} P^2 \\ X_{11,11}^{(T)*} P^{-2} & X_{11,11}^{(S)*} P^0 \end{bmatrix} \begin{bmatrix} \overline{\hat{b}'_{gs_{11}}\hat{b}'_{gs_{11}}} & \overline{\hat{b}'_{gs_{11}}\hat{b}''_{gs_{11}}} \\ \overline{\hat{b}''_{gs_{11}}\hat{b}'_{gs_{11}}} & \overline{\hat{b}''_{gs_{11}}\hat{b}''_{gs_{11}}} \end{bmatrix} \begin{bmatrix} X_{11,11}^{(S)} P^0 & X_{11,11}^{(T)} P^2 \\ X_{11,11}^{(T)*} P^{-2} & X_{11,11}^{(S)*} P^0 \end{bmatrix}^\dagger + \begin{bmatrix} \overline{\hat{b}'_{gd_{11}}\hat{b}'_{gd_{11}}} & \overline{\hat{b}'_{gd_{11}}\hat{b}''_{gd_{11}}} \\ \overline{\hat{b}''_{gd_{11}}\hat{b}'_{gd_{11}}} & \overline{\hat{b}''_{gd_{11}}\hat{b}''_{gd_{11}}} \end{bmatrix}. \quad (5.45)$$

The intrinsic NCM of the nonlinear one-port device describes the auto- and cross-correlation of noise waves $\hat{b}'_{gd_{11}}$ and $\hat{b}''_{gd_{11}}$. The noise power spectral density, i.e., auto-correlation, of the two noise waves are described along its diagonal elements while their cross-correlation is described at its off-diagonal locations.

The passive termination's noise source's processes $\hat{b}'_{gs_{11}}$ and $\hat{b}''_{gs_{11}}$ operate at differing frequencies and thus are uncorrelated. Consequently, their time-averaged cross-correlation noise products, $\overline{\hat{b}'_{gs_{11}}\hat{b}''_{gs_{11}}}$ and $\overline{\hat{b}''_{gs_{11}}\hat{b}'_{gs_{11}}}$ are zero.

The four in-situ time-averaged scattered noise properties in (5.45) are expressed in (5.46) as the sum of the incident noise power, suitably modified by the nonlinear one-port, and its unmodified intrinsic noise power under a match-terminated condition. Applying matrix multiplication in (5.45) results in

$$\overline{\hat{b}'_{11}\hat{b}'_{11}{}^*} = X_{11,11}^{(S)} \overline{\hat{b}'_{gs_{11}}\hat{b}'_{gs_{11}}{}^*} X_{11,11}^{(S)*} + X_{11,11}^{(T)} \overline{\hat{b}''_{gs_{11}}\hat{b}''_{gs_{11}}{}^*} X_{11,11}^{(T)*} + \overline{\hat{b}'_{gd_{11}}\hat{b}'_{gd_{11}}{}^*} \in \mathfrak{R}_+, \quad (5.46a)$$

$$\overline{\hat{b}'_{11}\hat{b}''_{11}} = X_{11,11}^{(S)} \overline{\hat{b}'_{gs_{11}}\hat{b}'_{gs_{11}}{}^*} X_{11,11}^{(T)} P^2 + X_{11,11}^{(T)} P^2 \overline{\hat{b}''_{gs_{11}}\hat{b}''_{gs_{11}}{}^*} X_{11,11}^{(S)} + \overline{\hat{b}'_{gd_{11}}\hat{b}''_{gd_{11}}} \in \mathbb{C}, \quad (5.46b)$$

$$\overline{\hat{b}''_{11}\hat{b}'_{11}{}^*} = X_{11,11}^{(T)*} P^{-2} \overline{\hat{b}'_{gs_{11}}\hat{b}'_{gs_{11}}{}^*} X_{11,11}^{(S)*} + X_{11,11}^{(S)*} \overline{\hat{b}''_{gs_{11}}\hat{b}''_{gs_{11}}{}^*} X_{11,11}^{(T)*} P^{-2} + \overline{\hat{b}''_{gd_{11}}\hat{b}'_{gd_{11}}{}^*} \in \mathbb{C}, \quad (5.46c)$$

and

$$\overline{\hat{b}''_{11}\hat{b}''_{11}{}^*} = X_{11,11}^{(T)*} \overline{\hat{b}'_{gs_{11}}\hat{b}'_{gs_{11}}{}^*} X_{11,11}^{(T)} + X_{11,11}^{(S)*} \overline{\hat{b}''_{gs_{11}}\hat{b}''_{gs_{11}}{}^*} X_{11,11}^{(S)} + \overline{\hat{b}''_{gd_{11}}\hat{b}''_{gd_{11}}{}^*} \in \mathfrak{R}_+ \quad (5.46d)$$

where the diagonal and off-diagonal elements are described by (5.46a,d) and (5.46b,c) respectively.

Slight simplification to (5.46a-d) is made by observing that for a passive source termination, $\overline{\hat{b}'_{gs_{11}}\hat{b}'_{gs_{11}}{}^*} = \overline{\hat{b}''_{gs_{11}}\hat{b}''_{gs_{11}}{}^*} = k\hat{T}_s$ where \hat{T}_s is its physical temperature.

It's important to remember that the scattered noise properties of the nonlinear network are a function of its LSOP. Should a reduction in amplitude of drive tone A_{11} be sufficient that the device operates within its small-signal region, this dependency no longer exists. The time-averaged cross-frequency terms $\overline{\hat{b}'_{gd_{11}}\hat{b}''_{gd_{11}}}$ and $\overline{\hat{b}''_{gd_{11}}\hat{b}'_{gd_{11}}}$ both diminish to zero and X-parameters $X_{11,11}^{(S)}$ and $X_{11,11}^{(T)}$ reduce to S_{11} and zero respectively [51]. As the amplitude of A_{11} approaches zero, the scattered noise properties of the combined network described in (5.46a-d) correspondingly becomes

$$\overline{\hat{b}'_1\hat{b}'_1{}^*} = S_{11} \overline{\hat{b}'_{gs1}\hat{b}'_{gs1}{}^*} S_{11}^* + \overline{\hat{b}'_{gd1}\hat{b}'_{gd1}{}^*} \in \mathfrak{R}_+, \quad (5.47a)$$

$$\overline{\hat{b}'_1\hat{b}''_1} = 0, \quad (5.47b)$$

$$\overline{\hat{b}''_1\hat{b}'_1{}^*} = 0, \quad (5.47c)$$

and

$$\overline{\hat{b}_1^{n*} \hat{b}_1^n} = S_{11}^* \overline{\hat{b}_{gs1}^{n*} \hat{b}_{gs1}^n} S_{11} + \overline{\hat{b}_{gd1}^{n*} \hat{b}_{gd1}^n} \in \mathfrak{R}_+ \quad (5.47d)$$

where, consistent with S-parameter notation, only port number subscript designators remain in the formalism.

To determine operation space from which the experiment in Fig. 5.4 is to be performed, a harmonic balance power sweep simulation is conducted on the one-port network. The rate in harmonic amplitude change versus drive-tone input power $|A_{11}|^2$ is assessed. From this analysis, five operating points are chosen spanning an input-signal space across the network's linear (-35 dBm), compression (-25, -20 dBm), and saturation (-15, -10 dBm) behavioral regions.

Large-Signal Incident And Scattered Waves \sqrt{W}		Large-Signal Incident Power dBm	One-Port Network X-Parameters		Simulated Scattered PSD, dBm/Hz		Numerical Calculation Scattered PSD, dBm/Hz	
A_{11}	B_{11}		$ A_{11} ^2$	$X_{11,11}^{(S)}$	$X_{11,11}^{(T)}$	Upper Offset	Lower Offset	Upper Offset
$5.623 \times 10^{-4}/0^\circ$	$2.41 \times 10^{-4}/-4.3^\circ$	-35	$0.4329e^{-j4.3^\circ}$	$0.0043e^{-j3.03^\circ}$	$\overline{\hat{b}_{11}' \hat{b}_{11}^{I*}}$	$\overline{\hat{b}_{11}^{II*} \hat{b}_{11}^{II}}$	$\overline{\hat{b}_{11}' \hat{b}_{11}^{I*}}$	$\overline{\hat{b}_{11}^{II*} \hat{b}_{11}^{II}}$
$5.623 \times 10^{-4}/0^\circ$	$2.41 \times 10^{-4}/-4.3^\circ$	-35	$0.4329e^{-j4.3^\circ}$	$0.0043e^{-j3.03^\circ}$	-175.691	-175.734	-175.738	-175.716
$1.778 \times 10^{-3}/0^\circ$	$8.243 \times 10^{-3}/-4.2^\circ$	-25	$0.4982e^{-j4.1^\circ}$	$0.0347e^{-j3.03^\circ}$	-175.341	-175.359	-175.341	-175.321
$3.162 \times 10^{-3}/0^\circ$	$1.653 \times 10^{-3}/-4.1^\circ$	-20	$0.5902e^{-j3.9^\circ}$	$0.0676e^{-j3.02^\circ}$	-174.752	-174.791	-174.751	-174.734
$5.623 \times 10^{-3}/0^\circ$	$3.423 \times 10^{-3}/-3.9^\circ$	-15	$0.6836e^{-j3.8^\circ}$	$0.0749e^{-j2.98^\circ}$	-174.161	-174.106	-174.153	-174.138
$10.000 \times 10^{-3}/0^\circ$	$6.838 \times 10^{-3}/-3.8^\circ$	-10	$0.7377e^{-j3.7^\circ}$	$0.0540e^{-j2.90^\circ}$	-173.704	-173.772	-173.821	-173.807

Table 5.1: Conditions - Fundamental Freq. = 1GHz, Source Impedance Temperature = 298.15K, Source Impedance Reflection Coefficient $\Gamma_{s11} = 0$. Lower Offset Frequency = Fundamental Frequency -1MHz, Upper Offset Frequency = Fundamental Frequency +1MHz.

To validate expressions (5.46a, d) and (5.47a, d) at prescribed LSOPs, two experiments are performed whereupon their resulting scattered noise PSD are compared. Referencing Table 5.1, experiment one will be referred as “Simulated Scattered PSD”, experiment two as “Numerical Calculation Scattered PSD”.

In the first experiment, a circuit envelope (CE) simulation is performed on the noisy NL one-port common-emitter network. The simulation samples the instantaneous port noise voltage and noise current of the nonlinear network from zero to 10ms in 0.125us steps. Post-processing within ADS, the sampled port noise voltage and current are expressed as a linear combination forming the NL network's instantaneous incident and scattered traveling noise waves [Withington, Hecken, Root et al]. These time dependent complex quantities are expressed in units of square root watts. A Z-transform is applied to the incident and scattered noise wave data forming their frequency domain representation. In this case, the data is centered at a frequency of 1GHz (in accordance with CE it's reported at a baseband of zero hertz) and distributed across a +/- 4MHz frequency span with a 100Hz frequency resolution. The frequency span and resolution are controlled respectively by the 0.125us sampling time interval and the 10ms time duration both invoked during the simulation. As such, the resulting complex frequency domain data is represented as the instantaneous noise energy spectral density. Its units are square root watts per Hz. Using this, the instantaneous power spectral density of the NL network's incoming and outgoing noise waves is acquired by multiplying each with their respective complex conjugate thus forming units in (real) power, watts per Hz. By integration of this result across lower (-1MHz +/- 0.5MHz) and upper (+1MHz +/- 0.5MHz) sidebands relative to large-signal response B_{11} and dividing each by a 1MHz noise bandwidth, we conclude with the NL one-port's simulated scattered PSD $\overline{\hat{b}_{11}'' \hat{b}_{11}''^*}$ and $\overline{\hat{b}_{11}' \hat{b}_{11}'^*}$ respectively. Within each bandwidth there are 10,001 data points; this is a sufficient sample size to ensure the averaging process converges to its mean. The limits of the lower and upper sidebands are chosen to avoid anticipated phase noise modulation on the large-signal incident A_{11} and scattered response B_{11} . Though not present in simulation, it's expected to exist in practice. Consequently, for hardware measurements, the limits chosen are based on phase noise specifications of Keysight's PNA-X source. Indeed, depending on NL-network characteristics and spectral purity of the large-signal stimulus, these limits may be subject to change.

In the second experiment, we refer to Fig. 5.4 and its mathematical model described by expressions (5.46a, d) and (5.47a, d). We first note that the PSD of the NL one-port's incoming noise waves $\overline{\hat{b}_{g_{s_{11}}}'' \hat{b}_{g_{s_{11}}}''^*}$ and $\overline{\hat{b}_{g_{s_{11}}}' \hat{b}_{g_{s_{11}}}'^*}$ are known from experiment one. Next, at each LSOP, with the one-port connected to a matched noise-free termination, a test of its (internally generated) outgoing noise waves are assessed. Using a procedure analogous to that described above, $\overline{\hat{b}_{g_{d_{11}}}'' \hat{b}_{g_{d_{11}}}''^*}$ and $\overline{\hat{b}_{g_{d_{11}}}'' \hat{b}_{g_{d_{11}}}''^*}$ are obtained. Collectively, these quantities in conjunction with the NL one-port's X-parameters define the components comprising Fig. 5.4. Using this information, numerical computation of the NL one-port's scattered noise PSD is implemented using (5.46a, d). Within the linear operating space of the network, (5.47a, d) is employed. Computer simulations are summarized and compared with independent numerical calculations in Table 5.1. Close agreements suggest that within the stipulated conditions, the scattered noise wave expressions are in fact valid and may be used to predict the noise behavior of a match-terminated nonlinear one-port network across its entire input signal space.

Using Fig. 5.4 and (5.42), a scattered noise wave expression under the mismatch-terminated condition, i.e. within an $0 \leq |\Gamma_{s_{11}}| \leq 1$ interval, has been derived and is reserved for future work. This is shown in Appendix A.

There is however, much greater applicability in assessing two-port network noise behavior, the subject of section 5.2.3.

5.2.3 Noise Analysis of a Nonlinear Two-Port Network

The generalized full in-situ scattered noise matrix [26] expression of (5.42) is applicable to an embedded large (or small)-signal stimulated network of interest exhibiting an arbitrary number of ports- n with each port described across m -harmonics. Section 5.2.3 concentrates on applying the generalized formalism to a match-embedded nonlinear two-port network as means to extract

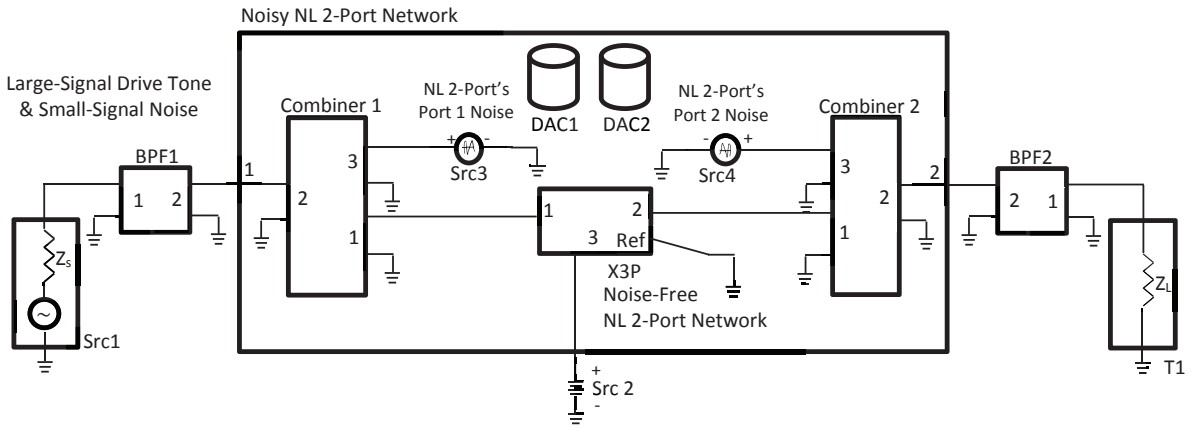
its intrinsic noise matrix. Additionally, the nonlinear two-port's noise factor will be determined from this extraction. Consistent in approach with section 5.2.2, calculated numerical results for specific levels of noise under various large-signal drive tone operating conditions will be examined and compared to computer simulation of an experiment circuit using ADS software.

In simulation, the nonlinear two-port is defined by an npn Si transistor operating within a single-stage common-emitter circuit configuration. The network's incoming and outgoing RF signals will be accessed at its input and output ports corresponding to the transistor's base and collector terminals respectively. Circuit elements exhibit negligible memory effects in this example. The circuit's response, large-signal and large-signal plus noise are separately analyzed in simulation by turning its noise generators off and on in that order.

The two-port's connected network delivers a single CW RF drive tone to its input contributing to creation of its LSOP. Additionally, this network presents isolated passive source and load terminations correspondingly to the nonlinear network's input and output ports. Both terminations are treated as matched and noisy.

In the experiment, noise analysis is restricted to the fundamental frequency and its bounded offsets. For (5.38) and (5.39) to remain valid, the source and load impedance, from the two-port's frame of reference, will be noise-free and matched at frequencies corresponding to higher order harmonics. To impose this condition, bandpass filters are inserted along the incoming and outgoing signal paths of the nonlinear network. Its incident noise at frequencies located on the upper harmonic-grid are eliminated by the filter's absorptive, i.e., matched, out-of-band characteristics. Figure 5.5 mimics the schematic of the noisy nonlinear two-port experiment circuit and its connected termination network. The noisy nonlinear two-port is signified by the X-parameter representation of its noise-free otherwise electrical equivalent circuit summed with its own partially correlated time-dependent complex noise values emanating from its input and output ports. To create this model, two simulations are performed prior to this experiment; the first is to create an X-parameter behavioral model from the original

albeit noise-free nonlinear two-port circuit, and second to acquire data bases of complex noise versus time emanating from each of its ports.



Simulated Circuit Conditions							
Source-Termination Network				Noisy NL One Port Network			
Src 1	BPF1/2	Src 2	T1	X3P	Src3	Src4	Combiner 1/2
$Z_s = 50\Omega$ P=polar (Ampl, Phase) Freq = 1GHz Noise = yes Temp = 298.15K	$S_{11} = S_{22} = 0$ $S_{12} = S_{21} = \text{if}$ $0.5\text{GHz} \leq \text{Freq} \leq 1.5\text{GHz}$ then 1 else 0 $Z_1 = Z_2 = 50\Omega$ Temp = 0K	5V	$Z_L = 50\Omega$ Noise = yes Temp = 298.15K	X-Parameters File	Freq = 1GHz V1 = polar (Vmag1, Vphase1) DAC1 – Data Access Component (Vmag1, Vphase1)	Freq = 1GHz V2 = polar (Vmag2, Vphase2) DAC2 – Data Access Component (Vmag2, Vphase2)	$S_{11} = S_{22} = S_{33} = 0$ $S_{12} = S_{21} = S_{23} = 1$ $S_{13} = S_{31} = S_{32} = 0$ $Z_1 = Z_2 = Z_3 = 50\Omega$ Temp = 0K

Figure 5.5: Simulation of a Noisy Nonlinear Two-Port Match Embedded with its Source-Termination Network

Under the stated conditions enacted in Fig. 5.5, the generalized scattered noise matrix expression in (5.41) becomes

$$\begin{bmatrix} \widehat{b}'_{11} & \widehat{b}'_{21} \\ \widehat{b}''_{11} & \widehat{b}''_{21} \end{bmatrix}^{\dagger} = \mathbf{I}^{-1} \begin{bmatrix} X_{11,11}^{(S)} P^0 & X_{11,21}^{(S)} P^0 & X_{11,11}^{(T)} P^2 & X_{11,21}^{(T)} P^2 \\ X_{21,11}^{(S)} P^0 & X_{21,21}^{(S)} P^0 & X_{21,11}^{(T)} P^2 & X_{21,21}^{(T)} P^2 \\ X_{11,11}^{(T)*} P^{-2} & X_{11,21}^{(T)*} P^{-2} & X_{11,11}^{(S)*} P^0 & X_{11,21}^{(S)*} P^0 \\ X_{21,11}^{(T)*} P^{-2} & X_{21,21}^{(T)*} P^{-2} & X_{21,11}^{(S)*} P^0 & X_{21,21}^{(S)*} P^0 \end{bmatrix} \begin{bmatrix} \widehat{b}'_{g_{s11}} & \widehat{b}'_{g_{s21}} \\ \widehat{b}''_{g_{s11}} & \widehat{b}''_{g_{s21}} \end{bmatrix}^{\dagger} + \begin{bmatrix} X_{11,11}^{(S)} P^0 & X_{11,21}^{(S)} P^0 & X_{11,11}^{(T)} P^2 & X_{11,21}^{(T)} P^2 \\ X_{21,11}^{(S)} P^0 & X_{21,21}^{(S)} P^0 & X_{21,11}^{(T)} P^2 & X_{21,21}^{(T)} P^2 \\ X_{11,11}^{(T)*} P^{-2} & X_{11,21}^{(T)*} P^{-2} & X_{11,11}^{(S)*} P^0 & X_{11,21}^{(S)*} P^0 \\ X_{21,11}^{(T)*} P^{-2} & X_{21,21}^{(T)*} P^{-2} & X_{21,11}^{(S)*} P^0 & X_{21,21}^{(S)*} P^0 \end{bmatrix} \begin{bmatrix} \widehat{b}'_{g_{d11}} & \widehat{b}'_{g_{d21}} \\ \widehat{b}''_{g_{d11}} & \widehat{b}''_{g_{d21}} \end{bmatrix}^{\dagger} \mathbf{I}^{-1\dagger} \quad (5.48)$$

where $\Gamma_{s_{11}} = \Gamma_{l_{21}} = 0$ and $P = e^{j\theta_{A_1}}$.

Multiplying the time-averaged noise vectors in (5.48) yields scattered, incident, and intrinsic (device of interest) noise correlation matrices each comprising auto- and cross-correlation entries related to their respective noise waves. Thus

$$\begin{bmatrix} \overline{\widehat{b}'_{11} \widehat{b}''_{11}} & \overline{\widehat{b}'_{11} \widehat{b}''_{21}} & \overline{\widehat{b}'_{11} \widehat{b}''_{11}} & \overline{\widehat{b}'_{11} \widehat{b}''_{21}} \\ \overline{\widehat{b}'_{21} \widehat{b}''_{11}} & \overline{\widehat{b}'_{21} \widehat{b}''_{21}} & \overline{\widehat{b}'_{21} \widehat{b}''_{11}} & \overline{\widehat{b}'_{21} \widehat{b}''_{21}} \\ \overline{\widehat{b}''_{11} \widehat{b}'_{11}} & \overline{\widehat{b}''_{11} \widehat{b}'_{21}} & \overline{\widehat{b}''_{11} \widehat{b}'_{11}} & \overline{\widehat{b}''_{11} \widehat{b}'_{21}} \\ \overline{\widehat{b}''_{21} \widehat{b}'_{11}} & \overline{\widehat{b}''_{21} \widehat{b}'_{21}} & \overline{\widehat{b}''_{21} \widehat{b}'_{11}} & \overline{\widehat{b}''_{21} \widehat{b}'_{21}} \end{bmatrix} = \begin{bmatrix} X_{11,11}^{(S)} & X_{11,21}^{(S)} & X_{11,11}^{(T)} P^2 & X_{11,21}^{(T)} P^2 \\ X_{21,11}^{(S)} & X_{21,21}^{(S)} & X_{21,11}^{(T)} P^2 & X_{21,21}^{(T)} P^2 \\ X_{11,11}^{(T)*} P^{-2} & X_{11,21}^{(T)*} P^{-2} & X_{11,11}^{(S)*} & X_{11,21}^{(S)*} \\ X_{21,11}^{(T)*} P^{-2} & X_{21,21}^{(T)*} P^{-2} & X_{21,11}^{(S)*} & X_{21,21}^{(S)*} \end{bmatrix} \cdot \begin{bmatrix} \overline{\widehat{b}'_{g_{s11}} \widehat{b}''_{g_{s11}}} & 0 & 0 & 0 \\ 0 & \overline{\widehat{b}'_{g_{s21}} \widehat{b}''_{g_{s21}}} & 0 & 0 \\ 0 & 0 & \overline{\widehat{b}''_{g_{s11}} \widehat{b}'_{g_{s11}}} & 0 \\ 0 & 0 & 0 & \overline{\widehat{b}''_{g_{s21}} \widehat{b}'_{g_{s21}}} \end{bmatrix} \cdot \begin{bmatrix} X_{11,11}^{(S)} & X_{11,21}^{(S)} & X_{11,11}^{(T)} P^2 & X_{11,21}^{(T)} P^2 \\ X_{21,11}^{(S)} & X_{21,21}^{(S)} & X_{21,11}^{(T)} P^2 & X_{21,21}^{(T)} P^2 \\ X_{11,11}^{(T)*} P^{-2} & X_{11,21}^{(T)*} P^{-2} & X_{11,11}^{(S)*} & X_{11,21}^{(S)*} \\ X_{21,11}^{(T)*} P^{-2} & X_{21,21}^{(T)*} P^{-2} & X_{21,11}^{(S)*} & X_{21,21}^{(S)*} \end{bmatrix} + \begin{bmatrix} \overline{\widehat{b}'_{g_{d11}} \widehat{b}''_{g_{d11}}} & \overline{\widehat{b}'_{g_{d11}} \widehat{b}''_{g_{d21}}} & \overline{\widehat{b}'_{g_{d21}} \widehat{b}''_{g_{d11}}} & \overline{\widehat{b}'_{g_{d11}} \widehat{b}''_{g_{d21}}} \\ \overline{\widehat{b}'_{g_{d21}} \widehat{b}''_{g_{d11}}} & \overline{\widehat{b}'_{g_{d21}} \widehat{b}''_{g_{d21}}} & \overline{\widehat{b}''_{g_{d21}} \widehat{b}'_{g_{d11}}} & \overline{\widehat{b}'_{g_{d21}} \widehat{b}''_{g_{d21}}} \\ \overline{\widehat{b}''_{g_{d11}} \widehat{b}'_{g_{d11}}} & \overline{\widehat{b}''_{g_{d11}} \widehat{b}'_{g_{d21}}} & \overline{\widehat{b}''_{g_{d11}} \widehat{b}'_{g_{d11}}} & \overline{\widehat{b}''_{g_{d11}} \widehat{b}'_{g_{d21}}} \\ \overline{\widehat{b}''_{g_{d21}} \widehat{b}'_{g_{d11}}} & \overline{\widehat{b}''_{g_{d21}} \widehat{b}'_{g_{d21}}} & \overline{\widehat{b}''_{g_{d21}} \widehat{b}'_{g_{d11}}} & \overline{\widehat{b}''_{g_{d21}} \widehat{b}'_{g_{d21}}} \end{bmatrix}. \quad (5.49)$$

The intrinsic NCM of the nonlinear two-port device describes auto- and cross-correlation of its noise waves $\widehat{b}'_{g_{d11}}$, $\widehat{b}''_{g_{d11}}$, $\widehat{b}'_{g_{d21}}$, and $\widehat{b}''_{g_{d21}}$. The auto-correlation, i.e., noise power spectral density, of the device's noise waves are real quantities described along its diagonal elements whereas their cross-correlation is complex and portrayed at its off-diagonal locations.

The incident noise correlation matrix in (5.49) is diagonal in form for two reasons. First, the cross-frequency time-averaged products of the noise waves engendered by a passive

termination are uncorrelated to one another. For example, regarding source and load impedances, $\overline{\hat{b}'_{g^{s_{11}}} \hat{b}''_{g^{s_{11}}}}$ and $\overline{\hat{b}'_{g^{l_{21}}} \hat{b}''_{g^{l_{21}}}}$ correspondingly are zero. Second, in this case, the impedances presented by the termination network to the nonlinear two-port device of interest are isolated from one another. As such, the cross-port time-averaged product of noise waves generated by isolated loads is also uncorrelated. A case in point is $\overline{\hat{b}'_{g^{s_{11}}} \hat{b}'_{g^{l_{21}}}}$. In fact, any cross-frequency and/or cross-port related product time-averaged quantity related to noise waves $\hat{b}'_{g^{s_{11}}}$, $\hat{b}''_{g^{s_{11}}}$, $\hat{b}'_{g^{l_{21}}}$, $\hat{b}''_{g^{l_{21}}}$ are zero. The remaining elements along the diagonal represent the auto-correlation, i.e., noise power density, for each of the four incident noise waves.

From (5.49), sixteen equations may be computed. Each illustrates a scattered noise property of the nonlinear network expressed in terms of the incident noise, appropriately altered by the composite network, and the unmodified noise of the match-embedded nonlinear two-port device.

Of practical interest are expressions relating the auto- and cross-correlation terms for output port scattered noise waves \hat{b}'_{21} and \hat{b}''_{21} . Referring to the scattered noise matrix in (5.49), it's evident there are four expressions relating these output noise waves. Their computation yields

$$\overline{\hat{b}'_{21} \hat{b}'_{21}} = X_{21,11}^{(S)} \overline{\hat{b}'_{g^{s_{11}}} \hat{b}'_{g^{s_{11}}}} X_{21,11}^{(S)*} + X_{21,21}^{(S)} \overline{\hat{b}'_{g^{l_{21}}} \hat{b}'_{g^{l_{21}}}} X_{21,21}^{(S)*} + X_{21,11}^{(T)} P^2 \overline{\hat{b}''_{g^{s_{11}}} \hat{b}''_{g^{s_{11}}}} X_{21,11}^{(T)*} P^{-2} + X_{21,21}^{(T)} P^2 \overline{\hat{b}''_{g^{l_{21}}} \hat{b}''_{g^{l_{21}}}} X_{21,21}^{(T)*} P^{-2} + \overline{\hat{b}'_{gd_{21}} \hat{b}'_{gd_{21}}} \in \Re_+, \quad (5.50a)$$

$$\overline{\hat{b}'_{21} \hat{b}''_{21}} = X_{21,11}^{(S)} \overline{\hat{b}'_{g^{s_{11}}} \hat{b}''_{g^{s_{11}}}} X_{21,11}^{(T)} P^2 + X_{21,21}^{(S)} \overline{\hat{b}'_{g^{l_{21}}} \hat{b}''_{g^{l_{21}}}} X_{21,21}^{(T)} P^2 + X_{21,11}^{(T)} P^2 \overline{\hat{b}''_{g^{s_{11}}} \hat{b}'_{g^{s_{11}}}} X_{21,11}^{(S)} + X_{21,21}^{(T)} P^2 \overline{\hat{b}''_{g^{l_{21}}} \hat{b}'_{g^{l_{21}}}} X_{21,21}^{(S)} + \overline{\hat{b}'_{gd_{21}} \hat{b}''_{gd_{21}}} \in \mathbb{C}, \quad (5.50b)$$

$$\overline{\hat{b}''_{21} \hat{b}''_{21}} = X_{21,11}^{(T)*} P^{-2} \overline{\hat{b}'_{g^{s_{11}}} \hat{b}'_{g^{s_{11}}}} X_{21,11}^{(S)*} + X_{21,21}^{(T)*} P^{-2} \overline{\hat{b}'_{g^{l_{21}}} \hat{b}'_{g^{l_{21}}}} X_{21,21}^{(S)*} + X_{21,11}^{(S)*} \overline{\hat{b}''_{g^{s_{11}}} \hat{b}''_{g^{s_{11}}}} X_{21,11}^{(T)*} P^{-2} + X_{21,21}^{(S)*} \overline{\hat{b}''_{g^{l_{21}}} \hat{b}''_{g^{l_{21}}}} X_{21,21}^{(T)*} P^{-2} + \overline{\hat{b}''_{gd_{21}} \hat{b}''_{gd_{21}}} \in \mathbb{C}, \quad (5.50c)$$

and

$$\overline{\hat{b}_{21}'' \hat{b}_{21}''} = X_{21,11}^{(T)*} P^{-2} \overline{\hat{b}'_{gs11} \hat{b}'_{gs11}} X_{21,11}^{(T)} P^2 + X_{21,21}^{(T)*} P^{-2} \overline{\hat{b}'_{gl21} \hat{b}'_{gl21}} X_{21,21}^{(T)} P^2 + X_{21,11}^{(S)*} \overline{\hat{b}''_{gs11} \hat{b}''_{gs11}} X_{21,11}^{(S)} + X_{21,21}^{(S)*} \overline{\hat{b}''_{gl21} \hat{b}''_{gl21}} X_{21,21}^{(S)} + \overline{\hat{b}''_{gd21} \hat{b}''_{gd21}} \in \mathfrak{R}_+. \quad (5.50d)$$

The noise power spectral density presented to the input-output ports of the nonlinear network by its passive source and load impedances is $k\hat{T}_s$ and $k\hat{T}_l$ respectively. Assuming the connected network is at a uniform physical temperature, $\overline{\hat{b}'_{gs11} \hat{b}'_{gs11}} = \overline{\hat{b}''_{gs11} \hat{b}''_{gs11}} = \overline{\hat{b}'_{gl21} \hat{b}'_{gl21}} = \overline{\hat{b}''_{gl21} \hat{b}''_{gl21}} = k\hat{T}_t$ where \hat{T}_t is the termination network's physical temperature. Therefore, a somewhat simplified form of (5.50a-d) can be established.

As previously stated, the scattered noise properties of the nonlinear network are a function of its LSOP. Sufficient reduction in drive tone amplitude A_{11} causes device operation within its small-signal region thus removing this dependency. Further, the time-averaged cross-frequency terms ascribed to the device's intrinsic NCM reduce to zero. As the amplitude of A_{11} approaches zero, the device's scattered noise properties described in (5.50a-d) correspondingly become

$$\overline{\hat{b}'_2 \hat{b}'_2} = S_{21} \overline{\hat{b}'_{gs1} \hat{b}'_{gs1}} S_{21}^* + S_{22} \overline{\hat{b}'_{gl2} \hat{b}'_{gl2}} S_{22}^* + \overline{\hat{b}'_{gd2} \hat{b}'_{gd2}} \in \mathfrak{R}_+, \quad (5.51a)$$

$$\overline{\hat{b}'_2 \hat{b}''_2} = 0, \quad (5.51b)$$

$$\overline{\hat{b}''_2 \hat{b}''_2} = 0, \quad (5.51c)$$

$$\overline{\hat{b}''_2 \hat{b}'_2} = S_{21} \overline{\hat{b}''_{gs1} \hat{b}'_{gs1}} S_{21}^* + S_{22} \overline{\hat{b}''_{gl2} \hat{b}'_{gl2}} S_{22}^* + \overline{\hat{b}''_{gd2} \hat{b}'_{gd2}} \in \mathfrak{R}_+ \quad (5.51d)$$

where the frequency index is dropped and only port number designation is retained in the formalism.

Recall, the resulting expressions of (5.51a, d) are derived under the condition that the two-port DUT's input and output ports are connected to match-embedded passive terminations (not an active receiver). To re-enforce (5.51a, d), we refer to (4.12) and impose the same

embedding network conditions leading to $\Gamma_s = \Gamma_l = 0$, and $\hat{\Gamma}_{12} = \hat{\Gamma}_{21} = \hat{\Gamma}_{22} = 0$. Their substitution into (4.12) leads to the important conclusion that for the same terminating conditions, the linear network's scattered noise power spectral density expression described in (4.12) is identical to (5.51a, d).

The simulation circuit in Fig. 5.5 is used to validate (5.50a, d) and (5.51a, d). To implement the experiment, a-priori knowledge of the network's cross-over point from linear to nonlinear operation is necessary. To satisfy this requirement, a harmonic balance power sweep simulation is performed on the network. Assessed at its output port, the rate in change of the network's harmonic amplitude versus drive-tone input power $|A_{11}|^2$ is evaluated. Five operating points are chosen spanning an input-signal space across the network's linear (-35dBm), compression (-25, -20dBm), and saturation (-15, -10dBm) behavioral regions.

To validate expressions (5.50a, d) and (5.51a, d) at prescribed LSOPs, two experiments are performed whereupon their resulting scattered noise PSD are compared. Referencing Table 5.2, experiment one will be referred as "Simulated Scattered PSD", experiment two as "Numerical Calculation Scattered PSD".

In the first experiment, a circuit envelope (CE) simulation is performed on the noisy NL two-port common-emitter network. The simulation samples the instantaneous port noise voltage and noise current of the nonlinear network from zero to 10ms in 0.125us steps. Post-processing within ADS, the sampled port noise voltage and current are expressed as a linear combination forming the NL network's instantaneous incident and scattered traveling noise waves [Withington, Hecken, Root et al]. These time dependent complex quantities are expressed in units of square root watts. A Z-transform is applied to the incident and scattered noise wave data forming their frequency domain representation. In this case, the data is centered at a frequency of 1GHz (in accordance with CE it's reported at a baseband of zero hertz) and distributed across a +/- 4MHz frequency span with a 100Hz frequency resolution. The frequency span and resolution are controlled respectively by the 0.125us sampling time interval and the

10ms time duration both invoked during the simulation. As such, the resulting complex frequency domain data is represented as the instantaneous noise energy spectral density. Its units are square root watts per Hz. Using this, the instantaneous power spectral density of the NL network's incoming and outgoing noise waves is acquired by multiplying each with their respective complex conjugate thus forming units in (real) power, watts per Hz. By integration of this result across lower (-1MHz +/- 0.5MHz) and upper (+1MHz +/- 0.5MHz) sidebands relative to large-signal response B_{21} and dividing each by a 1MHz noise bandwidth, we conclude with the NL two-port's simulated scattered PSD $\overline{\hat{b}_{21}'' \hat{b}_{21}''^*}$ and $\overline{\hat{b}_{21}' \hat{b}_{21}'^*}$ respectively. Within each bandwidth there are 10,001 data points; this is a sufficient sample size to ensure the averaging process converges to its mean. The limits of the lower and upper sidebands are chosen to avoid anticipated phase noise modulation on the large-signal incident A_{11} and scattered response B_{21} . Though not present in simulation, it's expected to exist in practice. Consequently, for hardware measurements, the limits chosen are based on phase noise specifications of Keysight's PNA-X source. Indeed, depending on NL-network characteristics and spectral purity of the large-signal stimulus, these limits may be subject to change.

In the second experiment, we refer to Fig. 5.5 and its mathematical model described by expressions (5.50a, d) and (5.51a, d). We first note that the PSD of the NL two-port's incoming noise waves $\overline{\hat{b}_{g_{s11}}'' \hat{b}_{g_{s11}}''^*}$, $\overline{\hat{b}_{g_{s11}}' \hat{b}_{g_{s11}}'^*}$, $\overline{\hat{b}_{g_{l21}}'' \hat{b}_{g_{l21}}''^*}$, and $\overline{\hat{b}_{g_{l21}}' \hat{b}_{g_{l21}}'^*}$ are known from experiment one. Next, at each LSOP, with the two-port connected to matched noise-free terminations, a test of its (internally generated) outgoing noise waves are assessed. Using a procedure analogous to that described above, $\overline{\hat{b}_{gd21}'' \hat{b}_{gd21}''^*}$ and $\overline{\hat{b}_{gd21}' \hat{b}_{gd21}'^*}$ are obtained. Collectively, these quantities in conjunction with the NL two-port's X-parameters define the components comprising Fig. 5.5. Using this information, numerical computation of the NL two-port's scattered noise PSD is implemented using (5.50a, d). Within the linear operating space of the network, (5.51a, d) is carried-out. Computer simulations are summarized and compared with independent numerical calculations in Table 5.2. Close agreements suggest that within the stipulated conditions, the scattered noise

wave expressions are in fact valid and may be used to predict the noise behavior of a match-terminated nonlinear two-port network across its entire input signal space.

Large-Signal Incident And Scattered Waves \sqrt{W}		Large - Signal Incident Power dBm	Two-Port Network X-Parameters				Simulated Scattered PSD, dBm/Hz		Numerical Calculation Scattered PSD, dBm/Hz	
							Upper Offset	Lower Offset	Upper Offset	Lower Offset
A_{11}	B_{21}	$ A_{11} ^2$	$X_{21,11}^{(S)}$	$X_{21,11}^{(T)}$	$X_{21,21}^{(S)}$	$X_{21,21}^{(T)}$	$\overline{\hat{b}'_{21} \hat{b}'_{21}}$	$\overline{\hat{b}''_{21} \hat{b}''_{21}}$	$\overline{\hat{b}'_{21} \hat{b}''_{21}}$	$\overline{\hat{b}''_{21} \hat{b}'_{21}}$
$5.623 \times 10^{-4}/0^\circ$	$1.226 \times 10^{-2}/177.8^\circ$	-35	$21.557e^{j177.8^\circ}$	$0.2534e^{-j2.3^\circ}$	$0.0157e^{-j90.9^\circ}$	0	-145.544	-145.621	-145.571	-145.584
$1.778 \times 10^{-3}/0^\circ$	$3.516 \times 10^{-2}/177.8^\circ$	-25	$17.762e^{j177.9^\circ}$	$2.012e^{-j2.3^\circ}$	$0.0157e^{-j90.9^\circ}$	≈ 0	-146.611	-146.570	-146.610	-146.599
$3.162 \times 10^{-3}/0^\circ$	$5.180 \times 10^{-2}/177.9^\circ$	-20	$12.532e^{j177.9^\circ}$	$3.848e^{-j2.3^\circ}$	$0.0157e^{-j90.9^\circ}$	≈ 0	-148.005	-147.949	-148.034	-148.002
$5.623 \times 10^{-3}/0^\circ$	$6.488 \times 10^{-2}/177.9^\circ$	-15	$7.372e^{j178^\circ}$	$4.166e^{-j2.2^\circ}$	$0.0157e^{-j90.9^\circ}$	≈ 0	-149.368	-149.289	-149.378	-149.335
$10.000 \times 10^{-3}/0^\circ$	$7.386 \times 10^{-2}/178^\circ$	-10	$4.417e^{j178.1^\circ}$	$2.972e^{-j2.16^\circ}$	$0.0157e^{-j90.9^\circ}$	≈ 0	-150.075	-150.015	-150.103	-150.054

Table 5.2: Conditions - Fundamental Freq. = 1GHz, Source and Load Impedance Temperature = 298.15K, Source Impedance Reflection Coefficient $\Gamma_{s11} = 0$, Load Impedance Coefficient $\Gamma_{l21} = 0$. Lower Offset Frequency = Fundamental Frequency -1MHz, Upper Offset Frequency = Fundamental Frequency +1MHz.

Recall that (5.42) and the IEEE definition of noise factor [47] were used to derive a generalized noise factor expression resulting in (5.43). This expression can be exercised across the nonlinear network's full operating space accounting for m-harmonics residing at each of its n-ports.

Applying (5.43) enables noise factor appraisal of the match-embedded nonlinear two-port network example described in Fig. 5.5. In this case, noise factor F'_{21} and F''_{21} are both assessed at the network's port-2 output respectively bounding upper and lower offset locations relative to the fundamental frequency of operation. The spot noise factor at the upper offset location is

$$F'_{21} = 1 + \frac{\overline{\hat{b}'_{gd21} \hat{b}'_{gd21*}}}{kT_o \left(|X_{21,11}^{(S)}|^2 + |X_{21,11}^{(T)}|^2 + |X_{21,21}^{(S)}|^2 + |X_{21,21}^{(T)}|^2 \right)} \approx 1 + \frac{\overline{\hat{b}'_{gd21} \hat{b}'_{gd21*}}}{kT_o \left(|X_{21,11}^{(S)}|^2 + |X_{21,11}^{(T)}|^2 \right)} \quad (5.52)$$

where noise contribution from the network's output port termination, in this example, can be regarded negligible compared to that connected to its input.

The conclusion from (3.59) and (5.52) is that the upper offset effective input noise temperature of the match-embedded nonlinear two-port network is

$$kT'_{e_{21}} = \frac{\overline{\hat{b}'_{gd_{21}} \hat{b}'^*_{gd_{21}}}}{|X_{21,11}^{(S)}|^2 + |X_{21,11}^{(T)}|^2} \quad (5.53)$$

Analogous to (5.52, 5.53), there are complementary expressions at the lower frequency offset location corresponding with the network's port-2 noise factor F''_{21} and effective input noise temperature $T''_{e_{21}}$.

Expressions (5.52, 5.53) and their complement reduce to the familiar form [57] within the network's small-signal (linear) operating space.

With respect to (5.53), as the magnitude of the large-signal drive tone $|A_{11}| \rightarrow 0$, it's expected that $X_{21,11}^{(S)} \rightarrow S_{21}$ and $X_{21,11}^{(T)} \rightarrow 0$. Their substitution into (5.53) reduces its form to (3.59), the effective input noise temperature of a linear two-port. Thus, in the linear functional-space of a network, (3.59) and (5.53) are equivalent.

Recall from Table 4.7, for the match-embedded case, the effective input noise temperature of the linear two-port was computed from simulated results using (3.59). This could just as well be determined using the linear network reduced form of (5.53).

Referring to Fig. 5.5, consider the nonlinear two-port simulated circuit operating at an LSOP corresponding to -25dBm. A prior simulation on the nonlinear two-port, operating at this established LSOP was conducted to assess its X-parameters. Then, measuring the bounded in-situ scattered noise power density [26] in simulation and employing (5.50a, d) the nonlinear network's extracted output noise power density $\overline{\hat{b}'_{gd_{21}} \hat{b}'^*_{gd_{21}}}$ and $\overline{\hat{b}''^*_{gd_{21}} \hat{b}''_{gd_{21}}}$ are determined. The spot noise factor and effective input noise temperature at lower and upper offsets are summarized in Table 5.3.

It should be recognized in this case that the NL two-port network amplifier is operating in compression. Thus, (3.59) or the reduced for of (5.53) are not applicable. To compute the effective input noise temperature $T'_{e_{21}}$ of a driven NL network requires the use of its X-parameters (not S-parameters) as presented in (5.53) and Table 5.3.

Large-Signal Incident And Scattered Waves \sqrt{W}		Large-Signal Incident Power dBm	Two-Port Network X-Parameters		Extracted Device Generated Output Noise PSD, W/Hz		Noise Factor		Effective Output Noise Temperature, K	
					Upper Offset	Lower Offset	Upper Offset	Lower Offset	Upper Offset	Lower Offset
A_{11}	B_{21}	$ A_{11} ^2$	$X_{21,11}^{(S)}$	$X_{21,11}^{(T)}$	$\widehat{b}'_{gd_{21}} \widehat{b}'_{gd_{21}*}$	$\widehat{b}''_{gd_{21}} \widehat{b}''_{gd_{21}*}$	F'_{21}	F''_{21}	$T'_{e_{21}}$	$T''_{e_{21}}$
$1.778 \times 10^{-3}/0^0$	$3.516 \times 10^{-2}/177.8^0$	-25	$17.762e^{j177.9^0}$	$2.012e^{-j2.3^0}$	8.600×10^{-19}	8.702×10^{-19}	1.672	1.680	194.9	197.3

Table 5.3: Conditions - Fundamental Freq. = 1GHz, Source and Load Impedance Temperature = 298.15K, Source Impedance Reflection Coefficient $\Gamma_{s_{11}} = 0$, Load Impedance Coefficient $\Gamma_{l_{21}} = 0$. Lower Offset Frequency = Fundamental Frequency -1MHz, Upper Offset Frequency = Fundamental Frequency +1MHz.

Within context of a mismatch-embedded nonlinear two-port, use of (5.42) and the stated conditions imposed in Fig. 5.5 have been applied to derive expressions for the output noise power spectral density assigned to its scattered waves \widehat{b}''_{21} and \widehat{b}'_{21} . This is shown in Appendix B.

5.2.4 Hardware Measurement Thought Experiment

It is proposed that the generalized nonlinear network noise behavioral model previously introduced and validated through computer simulation of an experiment circuit can also be realized in the physical realm. In this section, hardware noise measurement thought experiments for one- and two-port nonlinear network scenarios will be designed to determine their respective noise properties. Practical considerations will include tailoring of the constituent expressions originating from the model to account for the noise generated by the measurement system's active receiver. Having distinguished the noise generated terms of the measurement system's

source and receiver from the nonlinear device under test, calibration methods will be devised to quantify the measurement system's noise properties. Lastly, with the DUT inserted in the measurement system's signal path, its noise output will be measured and NCM extracted.

5.2.4.1 Nonlinear One-Port Network

By the full in-situ scattered noise matrix [26] expression of (5.41), the noise performance of a nonlinear multiport is described in relation to its connecting networks. Through a hardware measurement and analysis thought experiment, this generalized formalism will now be applied to a mismatch-terminated nonlinear one-port network with purpose to extract its NCM. Evaluation will be restricted to the fundamental frequency and its bounded offsets.

A proposed hardware measurement setup shown in Fig. 5.6a uses the Keysight PNA-X

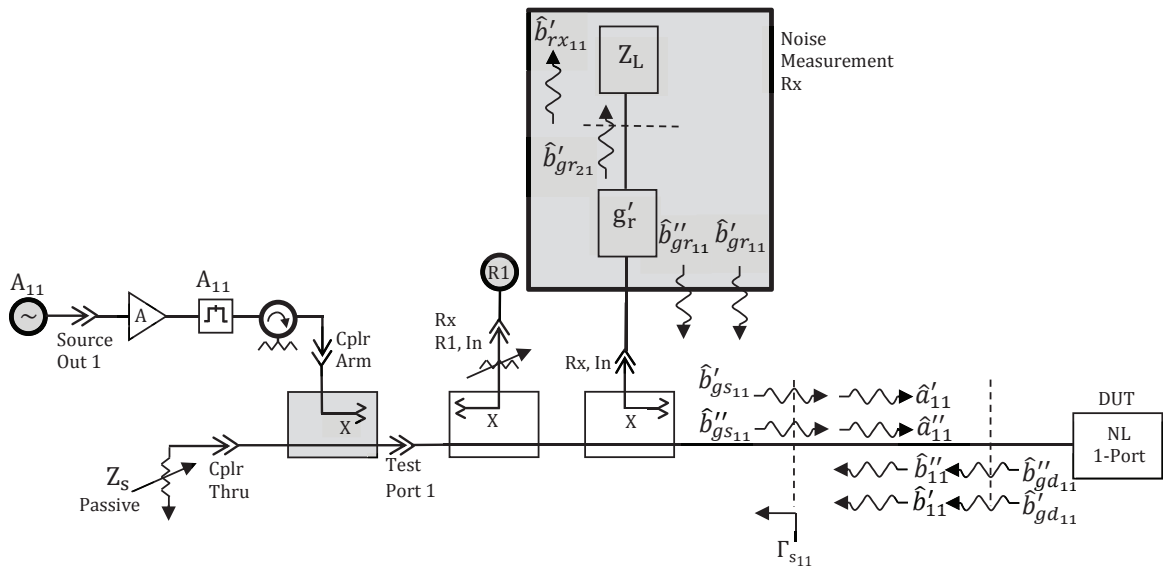


Figure 5.6a: Proposed Measurement Setup for the NL One-Port Network

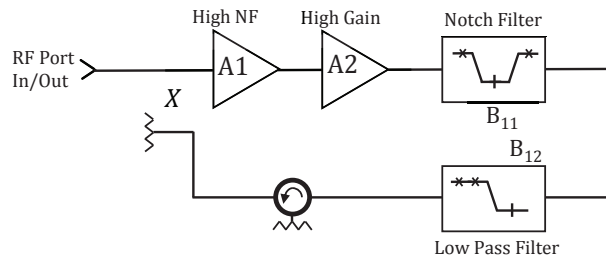


Figure 5.6b: Proposed Block Diagram of a NL One-Port Network

Network Analyzer equipped with a noise measurement receiver. Analogous to the approach described in chapter four, the instrument will be used to perform a series of calibrated noise power readings of the nonlinear one-port network while it undergoes a source-pull. The gray and white components within the diagram distinguish those which are internal and external to the PNA-X respectively. In the figure, the A_{11} stimulus is generated by the PNA-X, summed with the thermal noise produced by source impedance Z_S via an in-line coupler, and then collectively introduced as the incident signal (plus noise) to the DUT. The NL network's incident drive-tone A_{11} is assessed by a reference receiver "R1" coupled to the network analyzer's test port-one signal path. Accompanying A_{11} are incident noise waves \hat{a}'_{11} and \hat{a}''_{11} . The noise power ascribed to the DUTs scattered waves \hat{b}'_{11} and \hat{b}''_{11} are evaluated by the noise measurement receiver. The noise receiver, being active, produces its own noise waves \hat{b}'_{gr11} and \hat{b}''_{gr11} emanating from its input while \hat{b}'_{gr21} and \hat{b}''_{gr21} are dissipated in the receiver's matched load Z_L . The noise waves emerging from the input port of the receiver are not expected to appreciably influence the overall measured noise power due to the "high" two-way loss of the transmission coupling factor between the receiver and the NL one-port DUT. The two vertical dashed lines are separated by zero length in the physical setup; they are introduced in the diagram this way to distinguish the presence of the DUT's incident and scattered noise waves from its internally generated noise waves \hat{b}'_{gd11} , \hat{b}''_{gd11} , and the source impedance noise waves \hat{b}'_{gs11} , \hat{b}''_{gs11} originating from Z_S of the

measurement system. The dashed lines define the measurement plane. Since the DUT will be undergoing a source-pull, minimizing signal path loss between it and Z_S is important to maximize the useable range which $\Gamma_{S_{11}}$ may be exercised.

The proposed NL one-port DUT illustrated in Fig. 5.6b will be comprised of a high gain/noise figure amplifier such that the noise waves are of sufficient amplitude to overcome the inherent losses between it and the noise measurement receiver. A notch filter is used to remove the fundamental A_{11} component while the low-pass filter rejects harmonics. The offset noise, shown by the x-marks, is intended to pass with minimal attenuation. The isolator attenuates the A_{11} signal mitigating its presence on the coupled arm. The X-parameters of the NL one-port will need be of sufficient strength to ensure the noise engendered by Z_S notably influences its scattered waves. As such, a proper balancing of noise contributors is necessary in order that all terms are exercised in the model. If the coupler between the DUT and noise receiver prevents this due to its relatively high loss, the coupler may potentially be replaced by a circulator. Lastly, to impose fundamental frequency only analysis, the noise generated by Z_S at the higher-order harmonics, i.e., $\hat{b}'_{g^{s_{12}}}$, $\hat{b}''_{g^{s_{12}}}$, $\hat{b}'_{g^{s_{13}}}$, $\hat{b}''_{g^{s_{13}}}$..., $\hat{b}'_{g^{s_{1m}}}$, and $\hat{b}''_{g^{s_{1m}}}$, incident to the NL one-port shall not appreciably contribute to its scattered noise waves \hat{b}'_{11} and \hat{b}''_{11} . For this to be true, the NL one-port's cross-frequency X-parameters (S- and T-type) need be at least an order of magnitude less than its self-frequency, fundamental only description. Another way of stating this is that the chosen NL one-port DUT will need to exhibit X-parameters which satisfy the inequalities $X_{11,11}^{(S)} \gg X_{11,1m}^{(S)}$ and $X_{11,11}^{(T)} \gg X_{11,1m}^{(T)}$ for any positive integer value $m \neq 1$. Otherwise, the higher-order X-parameter terms cannot be excluded from the model.

Within context of the defined experimental conditions of the measurement setup and the connected NL one-port DUT, (5.41) can be used to model the power spectral densities of the DUTs scattered noise waves \hat{b}'_{11} and \hat{b}''_{11} as well as their correlation to one another. This yields

$$\begin{aligned} \overline{\begin{bmatrix} \hat{b}'_{11} \\ \hat{b}''_{11} \end{bmatrix} \begin{bmatrix} \hat{b}'_{11} \\ \hat{b}''_{11} \end{bmatrix}^\dagger} &= \begin{bmatrix} (1-\Gamma_{s_{11}} X_{11,11}^{(S)}) & -\Gamma_{s_{11}}^* X_{11,11}^{(T)} P^2 \\ -\Gamma_{s_{11}} X_{11,11}^{(T)*} P^{-2} & (1-\Gamma_{s_{11}} X_{11,11}^{(S)})^* \end{bmatrix}^{-1} \cdot \left\{ \begin{bmatrix} X_{11,11}^{(S)} P^0 & X_{11,11}^{(T)} P^2 \\ X_{11,11}^{(T)*} P^{-2} & X_{11,11}^{(S)*} P^0 \end{bmatrix} \overline{\begin{bmatrix} \hat{b}'_{gs_{11}} \\ \hat{b}''_{gs_{11}} \end{bmatrix} \begin{bmatrix} \hat{b}'_{gs_{11}} \\ \hat{b}''_{gs_{11}} \end{bmatrix}^\dagger} \begin{bmatrix} X_{11,11}^{(S)} P^0 & X_{11,11}^{(T)} P^2 \\ X_{11,11}^{(T)*} P^{-2} & X_{11,11}^{(S)*} P^0 \end{bmatrix}^\dagger + \overline{\begin{bmatrix} \hat{b}'_{gd_{11}} \\ \hat{b}''_{gd_{11}} \end{bmatrix} \begin{bmatrix} \hat{b}'_{gd_{11}} \\ \hat{b}''_{gd_{11}} \end{bmatrix}^\dagger} \right\} \\ &\quad \cdot \begin{bmatrix} (1-\Gamma_{s_{11}} X_{11,11}^{(S)}) & -\Gamma_{s_{11}}^* X_{11,11}^{(T)} P^2 \\ -\Gamma_{s_{11}} X_{11,11}^{(T)*} P^{-2} & (1-\Gamma_{s_{11}} X_{11,11}^{(S)})^* \end{bmatrix}^{-1\dagger} \cdot \end{aligned} \quad (5.54)$$

Shown in Fig. 5.6a, with the measurement receiver tuned to the upper fundamental frequency offset, the scattered power spectral density of its incident noise wave \hat{b}'_{11} is multiplied by the receiver's gain $|g'_r|^2$ and summed with its internally generated output noise density $\overline{\hat{b}'_{g'_{r21}} \hat{b}''_{g'_{r21}}}$. By calculating the expression of $\overline{\hat{b}'_{11} \hat{b}''_{11}}$ from (5.54), magnifying each of its incident terms by $|g'_r|^2$, and summing this with the output noise internally generated by the receiver, the total noise power density $\overline{\hat{b}'_{rx_{11}} \hat{b}''_{rx_{11}}}$ presented to the receiver's load is

$$\begin{aligned} \overline{\hat{b}'_{rx_{11}} \hat{b}''_{rx_{11}}} &= \frac{|g'_r|^2 |X_{11,11}^{(S)} (1-\Gamma_{s_{11}} X_{11,11}^{(S)})^* + \Gamma_{s_{11}}^* |X_{11,11}^{(T)}|^2 \overline{\hat{b}'_{gs_{11}} \hat{b}''_{gs_{11}}} + |g'_r|^2 |X_{11,11}^{(T)}|^2 \overline{\hat{b}''_{gs} \hat{b}'_{gs}}}{\left(|1-\Gamma_{s_{11}} X_{11,11}^{(S)}|^2 - |\Gamma_{s_{11}} X_{11,11}^{(T)}|^2 \right)^2} + \\ &\quad \frac{|g'_r|^2 |1-\Gamma_{s_{11}} X_{11,11}^{(S)}|^2 \overline{\hat{b}'_{gd_{11}} \hat{b}''_{gd_{11}}} + |g'_r|^2 (1-\Gamma_{s_{11}} X_{11,11}^{(S)})^* \Gamma_{s_{11}} X_{11,11}^{(T)*} P^{-2} \overline{\hat{b}'_{gd_{11}} \hat{b}''_{gd_{11}}}}{\left(|1-\Gamma_{s_{11}} X_{11,11}^{(S)}|^2 - |\Gamma_{s_{11}} X_{11,11}^{(T)}|^2 \right)^2} + \\ &\quad \frac{|g'_r|^2 (1-\Gamma_{s_{11}} X_{11,11}^{(S)}) \Gamma_{s_{11}}^* X_{11,11}^{(T)} P^2 \overline{\hat{b}''_{gd_{11}} \hat{b}'_{gd_{11}}} + |g'_r|^2 |\Gamma_{s_{11}} X_{11,11}^{(T)}|^2 \overline{\hat{b}''_{gd_{11}} \hat{b}'_{gd_{11}}}}{\left(|1-\Gamma_{s_{11}} X_{11,11}^{(S)}|^2 - |\Gamma_{s_{11}} X_{11,11}^{(T)}|^2 \right)^2} + \overline{\hat{b}'_{g'_{r21}} \hat{b}''_{g'_{r21}}} \cdot \end{aligned} \quad (5.55)$$

In the calculation of (5.55), the noise generated by the source, receiver, and DUT are treated independent (uncorrelated) from one another.

To extract the noise properties of the DUT, it's convenient to group the terms in (5.55) into two categories, the noise generators of the measurement system and those of the NL one-port. Re-writing (5.55) in matrix form yields,

$$\overline{\hat{b}'_{rx_{11}} \hat{b}''_{rx_{11}}} = \left[\frac{\left(\left| X_{11,11}^{(S)} \left(1 - \Gamma_{s_{11}} X_{11,11}^{(S)} \right)^* + \Gamma_{s_{11}}^* \left| X_{11,11}^{(T)} \right|^2 + \left| X_{11,11}^{(T)} \right|^2 \right) kT_s \left(1 - \left| \Gamma_{s_{11}} \right|^2 \right)}{\left(\left| 1 - \Gamma_{s_{11}} X_{11,11}^{(S)} \right|^2 - \left| \Gamma_{s_{11}} X_{11,11}^{(T)} \right|^2 \right)^2} \right] \cdot \left[\frac{\left| g'_r \right|^2}{\hat{b}'_{g'_{r21}} \hat{b}''_{g'_{r21}}} \right] +$$

$$\left[\frac{\left| g'_r \right|^2 \left| 1 - \Gamma_{s_{11}} X_{11,11}^{(S)} \right|^2}{\left(\left| 1 - \Gamma_{s_{11}} X_{11,11}^{(S)} \right|^2 - \left| \Gamma_{s_{11}} X_{11,11}^{(T)} \right|^2 \right)^2} \quad \frac{\left| g'_r \right|^2 \left(1 - \Gamma_{s_{11}} X_{11,11}^{(S)} \right)^* \Gamma_{s_{11}} X_{11,11}^{(T)*} P^{-2}}{\left(\left| 1 - \Gamma_{s_{11}} X_{11,11}^{(S)} \right|^2 - \left| \Gamma_{s_{11}} X_{11,11}^{(T)} \right|^2 \right)^2} \quad \frac{\left| g'_r \right|^2 \left(1 - \Gamma_{s_{11}} X_{11,11}^{(S)} \right) \Gamma_{s_{11}}^* X_{11,11}^{(T)} P^2}{\left(\left| 1 - \Gamma_{s_{11}} X_{11,11}^{(S)} \right|^2 - \left| \Gamma_{s_{11}} X_{11,11}^{(T)} \right|^2 \right)^2} \quad \frac{\left| g'_r \right|^2 \left| \Gamma_{s_{11}} X_{11,11}^{(T)} \right|^2}{\left(\left| 1 - \Gamma_{s_{11}} X_{11,11}^{(S)} \right|^2 - \left| \Gamma_{s_{11}} X_{11,11}^{(T)} \right|^2 \right)^2} \right] \cdot \begin{bmatrix} \hat{b}'_{gd_{11}} \hat{b}''_{gd_{11}} \\ \hat{b}'_{gd_{11}} \hat{b}''_{gd_{11}} \\ \hat{b}''_{gd_{11}} \hat{b}'_{gd_{11}} \\ \hat{b}''_{gd_{11}} \hat{b}'_{gd_{11}} \end{bmatrix} \quad (5.56)$$

where the passive source impedance Z_s is known to generate a constant broadband thermal noise proportional to its physical temperature T_s . The characteristic noise density of the source is $\overline{\hat{b}'_{g'_{s11}} \hat{b}''_{g'_{s11}}} = \overline{\hat{b}''_{g'_{s11}} \hat{b}'_{g'_{s11}}} = kT_s \left(1 - \left| \Gamma_{s_{11}} \right|^2 \right)$. The terms related to the first and second matrix operations in (5.56) are specific to the measurement system and DUT respectively.

The noise measured by the PNA-X receiver is typically confined to a 4MHz noise bandwidth [58]. A variation to the receiver's bandwidth is considered negligible as the receiver is tuned across the lower to upper offset interval bounding a frequency on the harmonic grid, in this case the fundamental frequency. Therefore, with the receiver tuned to either the lower or upper offset frequency, the receiver's noise bandwidth will be reported by the variable B in units of Hertz. Under these conditions, the noise power measured by the receiver when tuned to the upper offset frequency is

$$\hat{p}'_{rx_{11}} = \overline{\hat{b}'_{rx_{11}} \hat{b}'_{rx_{11}}*} \mathbf{B} = \left[\frac{\left(\left| \mathbf{X}_{11,11}^{(S)} (1 - \Gamma_{s_{11}} \mathbf{X}_{11,11}^{(S)})^* + \Gamma_{s_{11}}^* \left| \mathbf{X}_{11,11}^{(T)} \right|^2 \right|^2 + \left| \mathbf{X}_{11,11}^{(T)} \right|^2 \right) kT_s (1 - |\Gamma_{s_{11}}|^2)}{\left(\left| 1 - \Gamma_{s_{11}} \mathbf{X}_{11,11}^{(S)} \right|^2 - \left| \Gamma_{s_{11}} \mathbf{X}_{11,11}^{(T)} \right|^2 \right)^2} \right] \mathbf{1} \cdot \left[\frac{|\mathbf{g}'_r|^2 \mathbf{B}}{\hat{b}'_{r_{21}} \hat{b}'_{r_{21}}*} \mathbf{B} \right] +$$

$$\left[\frac{|\mathbf{g}'_r|^2 \mathbf{B} \left| 1 - \Gamma_{s_{11}} \mathbf{X}_{11,11}^{(S)} \right|^2}{\left(\left| 1 - \Gamma_{s_{11}} \mathbf{X}_{11,11}^{(S)} \right|^2 - \left| \Gamma_{s_{11}} \mathbf{X}_{11,11}^{(T)} \right|^2 \right)^2} \quad \frac{|\mathbf{g}'_r|^2 \mathbf{B} (1 - \Gamma_{s_{11}} \mathbf{X}_{11,11}^{(S)})^* \Gamma_{s_{11}} \mathbf{X}_{11,11}^{(T)*} \mathbf{P}^{-2}}{\left(\left| 1 - \Gamma_{s_{11}} \mathbf{X}_{11,11}^{(S)} \right|^2 - \left| \Gamma_{s_{11}} \mathbf{X}_{11,11}^{(T)} \right|^2 \right)^2} \quad \frac{|\mathbf{g}'_r|^2 \mathbf{B} (1 - \Gamma_{s_{11}} \mathbf{X}_{11,11}^{(S)}) \Gamma_{s_{11}}^* \mathbf{X}_{11,11}^{(T)} \mathbf{P}^2}{\left(\left| 1 - \Gamma_{s_{11}} \mathbf{X}_{11,11}^{(S)} \right|^2 - \left| \Gamma_{s_{11}} \mathbf{X}_{11,11}^{(T)} \right|^2 \right)^2} \quad \frac{|\mathbf{g}'_r|^2 \mathbf{B} \left| \Gamma_{s_{11}} \mathbf{X}_{11,11}^{(T)} \right|^2}{\left(\left| 1 - \Gamma_{s_{11}} \mathbf{X}_{11,11}^{(S)} \right|^2 - \left| \Gamma_{s_{11}} \mathbf{X}_{11,11}^{(T)} \right|^2 \right)^2} \right] \cdot \begin{bmatrix} \hat{b}'_{gd_{11}} \hat{b}'_{gd_{11}}* \\ \hat{b}'_{gd_{11}} \hat{b}'_{gd_{11}} \\ \hat{b}'_{gd_{11}}* \hat{b}'_{gd_{11}} \\ \hat{b}'_{gd_{11}} \hat{b}'_{gd_{11}} \end{bmatrix} \quad (5.57)$$

With the receiver tuned to the upper offset frequency, we define its gain-bandwidth product G'_r as

$$G'_r \equiv |\mathbf{g}'_r|^2 \mathbf{B} \quad (5.58)$$

Lastly, substitution of (5.58) into (5.57) results in the final expression

$$\hat{p}'_{rx_{11}} = \overline{\hat{b}'_{rx_{11}} \hat{b}'_{rx_{11}}*} \mathbf{B} = \left[\frac{\left(\left| \mathbf{X}_{11,11}^{(S)} (1 - \Gamma_{s_{11}} \mathbf{X}_{11,11}^{(S)})^* + \Gamma_{s_{11}}^* \left| \mathbf{X}_{11,11}^{(T)} \right|^2 \right|^2 + \left| \mathbf{X}_{11,11}^{(T)} \right|^2 \right) kT_s (1 - |\Gamma_{s_{11}}|^2)}{\left(\left| 1 - \Gamma_{s_{11}} \mathbf{X}_{11,11}^{(S)} \right|^2 - \left| \Gamma_{s_{11}} \mathbf{X}_{11,11}^{(T)} \right|^2 \right)^2} \right] \mathbf{1} \cdot \left[\frac{G'_r}{\hat{b}'_{r_{21}} \hat{b}'_{r_{21}}*} \mathbf{B} \right] +$$

$$\left[\frac{G'_r \left| 1 - \Gamma_{s_{11}} \mathbf{X}_{11,11}^{(S)} \right|^2}{\left(\left| 1 - \Gamma_{s_{11}} \mathbf{X}_{11,11}^{(S)} \right|^2 - \left| \Gamma_{s_{11}} \mathbf{X}_{11,11}^{(T)} \right|^2 \right)^2} \quad \frac{G'_r (1 - \Gamma_{s_{11}} \mathbf{X}_{11,11}^{(S)})^* \Gamma_{s_{11}} \mathbf{X}_{11,11}^{(T)*} \mathbf{P}^{-2}}{\left(\left| 1 - \Gamma_{s_{11}} \mathbf{X}_{11,11}^{(S)} \right|^2 - \left| \Gamma_{s_{11}} \mathbf{X}_{11,11}^{(T)} \right|^2 \right)^2} \quad \frac{G'_r (1 - \Gamma_{s_{11}} \mathbf{X}_{11,11}^{(S)}) \Gamma_{s_{11}}^* \mathbf{X}_{11,11}^{(T)} \mathbf{P}^2}{\left(\left| 1 - \Gamma_{s_{11}} \mathbf{X}_{11,11}^{(S)} \right|^2 - \left| \Gamma_{s_{11}} \mathbf{X}_{11,11}^{(T)} \right|^2 \right)^2} \quad \frac{G'_r \left| \Gamma_{s_{11}} \mathbf{X}_{11,11}^{(T)} \right|^2}{\left(\left| 1 - \Gamma_{s_{11}} \mathbf{X}_{11,11}^{(S)} \right|^2 - \left| \Gamma_{s_{11}} \mathbf{X}_{11,11}^{(T)} \right|^2 \right)^2} \right] \cdot \begin{bmatrix} \hat{b}'_{gd_{11}} \hat{b}'_{gd_{11}}* \\ \hat{b}'_{gd_{11}} \hat{b}'_{gd_{11}} \\ \hat{b}'_{gd_{11}}* \hat{b}'_{gd_{11}} \\ \hat{b}'_{gd_{11}} \hat{b}'_{gd_{11}} \end{bmatrix} \quad (5.59)$$

With the receiver tuned to the lower offset frequency, an expression for the measured noise power $\hat{p}''_{rx_{11}}$ may be constructed using an approach like that just described.

It's proposed that the receiver's gain-bandwidth product G'_r and output noise power $\overline{\hat{b}'_{r_{21}} \hat{b}'_{r_{21}*}} \mathbf{B}$ in (5.59) will be determined in calibration. Assuming the X-parameters of the NL one-port have been previously extracted by use of the PNA-X/NVNA, the remaining unknowns are the elements of the NL one-port's noise properties $\overline{\hat{b}'_{gd_{11}} \hat{b}'_{gd_{11}*}}$, $\overline{\hat{b}'_{gd_{11}} \hat{b}''_{d_{11}}}$, $\overline{\hat{b}''_{gd_{11}} \hat{b}'_{gd_{11}*}}$, and $\overline{\hat{b}''_{gd_{11}} \hat{b}''_{gd_{11}*}}$. These noise properties may be solved by performing four noise power measurements, each conducted at a distinct source reflection coefficient. The matrices in (5.59) can be expanded to four columns to accommodate for each of the four measurements resulting in

$$\begin{bmatrix} \hat{p}'_{rx_{11(1)}} \\ \hat{p}'_{rx_{11(2)}} \\ \hat{p}'_{rx_{11(3)}} \\ \hat{p}'_{rx_{11(4)}} \end{bmatrix} = \begin{bmatrix} \frac{\left(\left| \mathbf{X}_{11,11}^{(S)} \left(1 - \Gamma_{s_{11(1)}} \mathbf{X}_{11,11}^{(S)} \right)^* + \Gamma_{s_{11(1)}}^* \left| \mathbf{X}_{11,11}^{(T)} \right|^2 + \left| \mathbf{X}_{11,11}^{(T)} \right|^2 \right) kT_s \left(1 - \left| \Gamma_{s_{11(1)}} \right|^2 \right)}{\left(\left| 1 - \Gamma_{s_{11(1)}} \mathbf{X}_{11,11}^{(S)} \right|^2 - \left| \Gamma_{s_{11(1)}} \mathbf{X}_{11,11}^{(T)} \right|^2 \right)^2} & 1 \\ \frac{\left(\left| \mathbf{X}_{11,11}^{(S)} \left(1 - \Gamma_{s_{11(2)}} \mathbf{X}_{11,11}^{(S)} \right)^* + \Gamma_{s_{11(2)}}^* \left| \mathbf{X}_{11,11}^{(T)} \right|^2 + \left| \mathbf{X}_{11,11}^{(T)} \right|^2 \right) kT_s \left(1 - \left| \Gamma_{s_{11(2)}} \right|^2 \right)}{\left(\left| 1 - \Gamma_{s_{11(2)}} \mathbf{X}_{11,11}^{(S)} \right|^2 - \left| \Gamma_{s_{11(2)}} \mathbf{X}_{11,11}^{(T)} \right|^2 \right)^2} & 1 \\ \frac{\left(\left| \mathbf{X}_{11,11}^{(S)} \left(1 - \Gamma_{s_{11(3)}} \mathbf{X}_{11,11}^{(S)} \right)^* + \Gamma_{s_{11(3)}}^* \left| \mathbf{X}_{11,11}^{(T)} \right|^2 + \left| \mathbf{X}_{11,11}^{(T)} \right|^2 \right) kT_s \left(1 - \left| \Gamma_{s_{11(3)}} \right|^2 \right)}{\left(\left| 1 - \Gamma_{s_{11(3)}} \mathbf{X}_{11,11}^{(S)} \right|^2 - \left| \Gamma_{s_{11(3)}} \mathbf{X}_{11,11}^{(T)} \right|^2 \right)^2} & 1 \\ \frac{\left(\left| \mathbf{X}_{11,11}^{(S)} \left(1 - \Gamma_{s_{11(4)}} \mathbf{X}_{11,11}^{(S)} \right)^* + \Gamma_{s_{11(4)}}^* \left| \mathbf{X}_{11,11}^{(T)} \right|^2 + \left| \mathbf{X}_{11,11}^{(T)} \right|^2 \right) kT_s \left(1 - \left| \Gamma_{s_{11(4)}} \right|^2 \right)}{\left(\left| 1 - \Gamma_{s_{11(4)}} \mathbf{X}_{11,11}^{(S)} \right|^2 - \left| \Gamma_{s_{11(4)}} \mathbf{X}_{11,11}^{(T)} \right|^2 \right)^2} & 1 \end{bmatrix} \cdot \begin{bmatrix} G'_r \\ \overline{\hat{b}'_{r_{21}} \hat{b}'_{r_{21}*}} \mathbf{B} \end{bmatrix} +$$

$$\left[\begin{array}{cccc}
 \frac{G'_r \left| 1 - \Gamma_{s_{1(0)}} X_{11,11}^{(S)} \right|^2}{\left(\left| 1 - \Gamma_{s_{1(0)}} X_{11,11}^{(S)} \right|^2 - \left| \Gamma_{s_{1(0)}} X_{11,11}^{(T)} \right|^2 \right)^2} & \frac{G'_r \left(1 - \Gamma_{s_{1(0)}} X_{11,11}^{(S)} \right)^* \Gamma_{s_{1(0)}} X_{11,11}^{(T)*} P^{-2}}{\left(\left| 1 - \Gamma_{s_{1(0)}} X_{11,11}^{(S)} \right|^2 - \left| \Gamma_{s_{1(0)}} X_{11,11}^{(T)} \right|^2 \right)^2} & \frac{G'_r \left(1 - \Gamma_{s_{1(0)}} X_{11,11}^{(S)} \right) \Gamma_{s_{1(0)}}^* X_{11,11}^{(T)} P^2}{\left(\left| 1 - \Gamma_{s_{1(0)}} X_{11,11}^{(S)} \right|^2 - \left| \Gamma_{s_{1(0)}} X_{11,11}^{(T)} \right|^2 \right)^2} & \frac{G'_r \left| \Gamma_{s_{1(0)}} X_{11,11}^{(T)} \right|^2}{\left(\left| 1 - \Gamma_{s_{1(0)}} X_{11,11}^{(S)} \right|^2 - \left| \Gamma_{s_{1(0)}} X_{11,11}^{(T)} \right|^2 \right)^2} \\
 \frac{G'_r \left| 1 - \Gamma_{s_{1(2)}} X_{11,11}^{(S)} \right|^2}{\left(\left| 1 - \Gamma_{s_{1(2)}} X_{11,11}^{(S)} \right|^2 - \left| \Gamma_{s_{1(2)}} X_{11,11}^{(T)} \right|^2 \right)^2} & \frac{G'_r \left(1 - \Gamma_{s_{1(2)}} X_{11,11}^{(S)} \right)^* \Gamma_{s_{1(2)}} X_{11,11}^{(T)*} P^{-2}}{\left(\left| 1 - \Gamma_{s_{1(2)}} X_{11,11}^{(S)} \right|^2 - \left| \Gamma_{s_{1(2)}} X_{11,11}^{(T)} \right|^2 \right)^2} & \frac{G'_r \left(1 - \Gamma_{s_{1(2)}} X_{11,11}^{(S)} \right) \Gamma_{s_{1(2)}}^* X_{11,11}^{(T)} P^2}{\left(\left| 1 - \Gamma_{s_{1(2)}} X_{11,11}^{(S)} \right|^2 - \left| \Gamma_{s_{1(2)}} X_{11,11}^{(T)} \right|^2 \right)^2} & \frac{G'_r \left| \Gamma_{s_{1(2)}} X_{11,11}^{(T)} \right|^2}{\left(\left| 1 - \Gamma_{s_{1(2)}} X_{11,11}^{(S)} \right|^2 - \left| \Gamma_{s_{1(2)}} X_{11,11}^{(T)} \right|^2 \right)^2} \\
 \frac{G'_r \left| 1 - \Gamma_{s_{1(3)}} X_{11,11}^{(S)} \right|^2}{\left(\left| 1 - \Gamma_{s_{1(3)}} X_{11,11}^{(S)} \right|^2 - \left| \Gamma_{s_{1(3)}} X_{11,11}^{(T)} \right|^2 \right)^2} & \frac{G'_r \left(1 - \Gamma_{s_{1(3)}} X_{11,11}^{(S)} \right)^* \Gamma_{s_{1(3)}} X_{11,11}^{(T)*} P^{-2}}{\left(\left| 1 - \Gamma_{s_{1(3)}} X_{11,11}^{(S)} \right|^2 - \left| \Gamma_{s_{1(3)}} X_{11,11}^{(T)} \right|^2 \right)^2} & \frac{G'_r \left(1 - \Gamma_{s_{1(3)}} X_{11,11}^{(S)} \right) \Gamma_{s_{1(3)}}^* X_{11,11}^{(T)} P^2}{\left(\left| 1 - \Gamma_{s_{1(3)}} X_{11,11}^{(S)} \right|^2 - \left| \Gamma_{s_{1(3)}} X_{11,11}^{(T)} \right|^2 \right)^2} & \frac{G'_r \left| \Gamma_{s_{1(3)}} X_{11,11}^{(T)} \right|^2}{\left(\left| 1 - \Gamma_{s_{1(3)}} X_{11,11}^{(S)} \right|^2 - \left| \Gamma_{s_{1(3)}} X_{11,11}^{(T)} \right|^2 \right)^2} \\
 \frac{G'_r \left| 1 - \Gamma_{s_{1(4)}} X_{11,11}^{(S)} \right|^2}{\left(\left| 1 - \Gamma_{s_{1(4)}} X_{11,11}^{(S)} \right|^2 - \left| \Gamma_{s_{1(4)}} X_{11,11}^{(T)} \right|^2 \right)^2} & \frac{G'_r \left(1 - \Gamma_{s_{1(4)}} X_{11,11}^{(S)} \right)^* \Gamma_{s_{1(4)}} X_{11,11}^{(T)*} P^{-2}}{\left(\left| 1 - \Gamma_{s_{1(4)}} X_{11,11}^{(S)} \right|^2 - \left| \Gamma_{s_{1(4)}} X_{11,11}^{(T)} \right|^2 \right)^2} & \frac{G'_r \left(1 - \Gamma_{s_{1(4)}} X_{11,11}^{(S)} \right) \Gamma_{s_{1(4)}}^* X_{11,11}^{(T)} P^2}{\left(\left| 1 - \Gamma_{s_{1(4)}} X_{11,11}^{(S)} \right|^2 - \left| \Gamma_{s_{1(4)}} X_{11,11}^{(T)} \right|^2 \right)^2} & \frac{G'_r \left| \Gamma_{s_{1(4)}} X_{11,11}^{(T)} \right|^2}{\left(\left| 1 - \Gamma_{s_{1(4)}} X_{11,11}^{(S)} \right|^2 - \left| \Gamma_{s_{1(4)}} X_{11,11}^{(T)} \right|^2 \right)^2}
 \end{array} \right] \cdot \begin{bmatrix} \hat{b}_{gd_{11}}' & \hat{b}_{gd_{11}}^* \\ \hat{b}_{gd_{11}}' & \hat{b}_{gd_{11}}'' \\ \hat{b}_{gd_{11}}^* & \hat{b}_{gd_{11}}'' \\ \hat{b}_{gd_{11}}^* & \hat{b}_{gd_{11}}'' \end{bmatrix}$$

(5.60)

The noise properties of the NL-one port may be solved for by matrix manipulation of (5.60).

Should the procedure outlined above be applied with the measurement receiver tuned to the lower offset frequency, the expressions which follow will yield, as expected, a different set of noise properties related to the receiver, i.e. its gain-bandwidth product and output noise density, while the noise properties of the NL one-port remain unchanged.

5.2.4.1.1 Calibration Algorithm

It is envisioned that calibration of the measurement system will involve two primary steps, first will be characterization of the noise measurement receiver and second the setting of prescribed source reflection coefficients which will be sequentially presented to the NL one-port during the measurement process. Figure 5.7 shows a calibrated noise source connected to

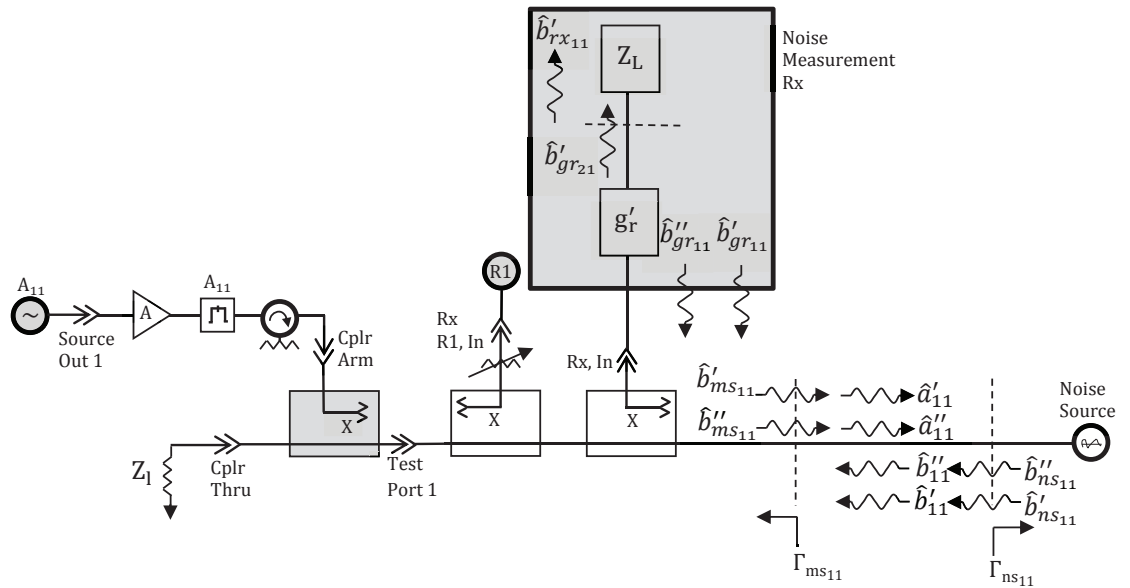


Figure 5.7: Noise Measurement Receiver Calibration for the NL One-Port Network

the measurement system at its reference plane. The dashed vertical lines are actually separated by zero length but are shown in this fashion to highlight the existence of the noise source's incident and scattered waves \hat{a}'_{11} and \hat{b}'_{11} respectively in presence with the characteristic noise out \hat{b}'_{ns11} of the noise source and that of the measurement system distinguished by \hat{b}'_{ms11} . The signal path leading to the test port will be match terminated by impedance Z_1 . The noise source will possess two states of operation, an on-state producing a noise level defined by its excess noise ratio (ENR) and an off-state which acts as a passive termination. The source reflection coefficient of the noise source is expected to change between operating states and will be accounted for in the upcoming formulism. The noise receiver will measure the scattered noise \hat{b}'_{11} incident at its input for both on- and off-states of the noise source. During the calibration process, the A_{11} drive-tone signal and its booster amplifier will be off.

By inspection of Fig. 5.7, the scattered and incident noise waves of the noise source may be written as

$$\hat{b}'_{11} = \Gamma_{ns_{11}} \hat{a}'_{11} + \hat{b}'_{ms_{11}} \quad (5.61)$$

and

$$\hat{a}'_{11} = \hat{b}'_{ms_{11}} \quad (5.62)$$

where the noise source's reflection coefficient $\Gamma_{ns_{11}}$ will take on one of two values depending on its state of operation. Substitution of (5.62) into (5.61) leads to the scattered noise wave expression

$$\hat{b}'_{11} = \Gamma_{ns_{11}} \hat{b}'_{ms_{11}} + \hat{b}'_{ms_{11}} \quad (5.63)$$

The measurement receiver's output noise wave $\hat{b}'_{rx_{11}}$ incident to its match terminated load is a modified version of the scattered noise wave \hat{b}'_{11} summed with its internally generated output noise wave $\hat{b}'_{gr_{21}}$. This may be quantified in (5.64) as

$$\hat{b}'_{rx_{11}} = \tilde{g}'_r \hat{b}'_{11} + \hat{b}'_{gr_{21}} \quad (5.64)$$

where $\tilde{g}'_r \equiv g'_r L$. Recall that g'_r is the linear transmission coefficient of the noise measurement receiver. With respect to Fig. 5.7, L is the transmission coefficient of the signal path from the noise source to the receiver's input.

The contribution of energy delivered to the receiver's load by noise wave $\hat{b}'_{gr_{11}}$ emanating from the receiver's input will be considered negligible. Per Fig. 5.7, with the noise source connected to the measurement plane, the combined effects of the two-way loss of the coupling factor and its reflection from the noise source reduces (5.64) to its present form. If this were not the case, (5.64) would need to include the effects of $\hat{b}'_{gr_{11}}$ at the receiver's load. This will be elaborated in the upcoming NL two-port thought experiment.

Substituting (5.63) into (5.64), the noise wave incident on the receiver's matched load is

$$\hat{b}'_{rx_{11}} = \tilde{g}'_r \hat{b}'_{ms_{11}} + \tilde{g}'_r \Gamma_{ns_{11}} \hat{b}'_{ms_{11}} + \hat{b}'_{g'_{21}} . \quad (5.65)$$

Multiplying (5.65) by its complex conjugate and evaluating its time-average, the power density of noise wave $\hat{b}'_{rx_{11}}$ is acquired. Within the noise bandwidth B of the receiver, the total noise power delivered to the receiver's load is

$$\hat{p}'_{rx_{11}(\text{Cal})} = \overline{\hat{b}'_{rx_{11}} \hat{b}'_{rx_{11}}*} B = |\tilde{g}'_r|^2 B \overline{\hat{b}'_{ms_{11}} \hat{b}'_{ms_{11}}*} + |\tilde{g}'_r|^2 B |\Gamma_{ns_{11}}|^2 \overline{\hat{b}'_{ms_{11}} \hat{b}'_{ms_{11}}*} + \overline{\hat{b}'_{g'_{21}} \hat{b}'_{g'_{21}}*} B . \quad (5.66)$$

Expressing the receiver quantities as $\tilde{G}'_r = |\tilde{g}'_r|^2 B$ and $r'_{22} = \overline{\hat{b}'_{g'_{21}} \hat{b}'_{g'_{21}}*} B$, substituting them into (5.66), and structuring the result in matrix form yields

$$\hat{p}'_{rx_{11}(\text{Cal})} = \begin{bmatrix} \overline{\hat{b}'_{ms_{11}} \hat{b}'_{ms_{11}}*} + |\Gamma_{ns_{11}}|^2 \overline{\hat{b}'_{ms_{11}} \hat{b}'_{ms_{11}}*} & 1 \end{bmatrix} \cdot \begin{bmatrix} \tilde{G}'_r \\ r'_{22} \end{bmatrix} . \quad (5.67)$$

In (5.67), there are two unknown coefficients related to the measurement receiver. Performing two measurements in calibration, one with the noise source in its on-state, and the second in its off-, two independent equations may be formed from which the unknown quantities can be solved.

The noise source in its on-state generates a characteristic noise density $k\hat{T}_{ne}$ such that

$$\overline{\hat{b}'_{ms_{11}} \hat{b}'_{ms_{11}}*} = \overline{\hat{b}'_{hms_{11}} \hat{b}'_{hms_{11}}*} = k\hat{T}_{ne} \quad (5.68)$$

where $\hat{b}'_{hms_{11}}$ is the characteristic noise wave of the noise source in its so called on(hot)-state and \hat{T}_{ne} is its effective noise temperature [1]. The effective noise temperature can readily be determined from the noise source's reported ENR [1]. The source match of the noise source when biased in its hot-state will be given as $\Gamma_{ns_{11}} = \Gamma_{hms_{11}}$. As such, the relationship of the noise source's characteristic and available noise power quantities is [1]

$$k\hat{T}_{ne} B = \hat{P}_{av} \left(1 - |\Gamma_{hms_{11}}|^2 \right) . \quad (5.69)$$

In summary, the total noise power delivered to the measurement receiver's load with the noise source biased to its hot-state is

$$\hat{p}'_{\text{rx}11(\text{Hot,Cal})} = \begin{bmatrix} k\hat{T}_{\text{ne}} + |\Gamma_{\text{hns}11}|^2 k\hat{T}_{\text{ms}} & 1 \\ \tilde{G}'_r & r'_{22} \end{bmatrix} \quad (5.70)$$

where the measurement system's passive test signal path is set at noise temperature \hat{T}_{ms} .

With the noise source bias turned off, the noise source operates as a passive termination in its so called off(cold)-state [1]. In the cold-state, the source generates noise density

$$\overline{\hat{b}'_{\text{ns}11} \hat{b}'_{\text{ns}11*}} = \overline{\hat{b}'_{\text{cns}11} \hat{b}'_{\text{cns}11*}} = k\hat{T}_{\text{cns}} (1 - |\Gamma_{\text{cns}11}|^2) \quad (5.71)$$

where \hat{T}_{cns} and Γ_{cns} are regarded as its physical temperature and reflection coefficient respectively. The total noise power delivered to the receiver's load with the noise source operating in its cold-state is obtained by substituting (5.71) into (5.67) and recognizing the measurement system's noise incident on the noise source will be reflected by $\Gamma_{\text{cns}11}$. Taking this into account, we conclude that

$$\hat{p}'_{\text{rx}11(\text{Cold,Cal})} = \begin{bmatrix} k\hat{T}_{\text{cns}} (1 - |\Gamma_{\text{cns}11}|^2) + |\Gamma_{\text{cns}11}|^2 k\hat{T}_{\text{ms}} & 1 \\ \tilde{G}'_r & r'_{22} \end{bmatrix}. \quad (5.72)$$

Equations (5.70) and (5.72) are two independent linear equations which may be used to solve for the unknown calibration coefficients \tilde{G}'_r and r'_{22} . Combining them in a matrix form returns

$$\begin{bmatrix} \hat{p}'_{\text{rx}11(\text{Hot,Cal})} \\ \hat{p}'_{\text{rx}11(\text{Cold,Cal})} \end{bmatrix} = \begin{bmatrix} k\hat{T}_{\text{ne}} + |\Gamma_{\text{hns}11}|^2 k\hat{T}_{\text{ms}} & 1 \\ k\hat{T}_{\text{cns}} (1 - |\Gamma_{\text{cns}11}|^2) + |\Gamma_{\text{cns}11}|^2 k\hat{T}_{\text{ms}} & 1 \end{bmatrix} \cdot \begin{bmatrix} \tilde{G}'_r \\ r'_{22} \end{bmatrix} \quad (5.73)$$

where $\hat{p}'_{\text{rx}11(\text{Hot,Cal})}$ and $\hat{p}'_{\text{rx}11(\text{Cold,Cal})}$ are the noise power measured by the receiver with the noise source in its on- and off-state respectively.

Solving for \tilde{G}'_r and r'_{22} by matrix manipulation of (5.73) produces

$$\begin{bmatrix} \tilde{G}'_r \\ r'_{22} \end{bmatrix} = \begin{bmatrix} k\hat{T}_{ne} + |\Gamma_{hns}|^2 k\hat{T}_{ms} & 1 \\ k\hat{T}_{cns} (1 - |\Gamma_{cns}|^2) + |\Gamma_{cns}|^2 k\hat{T}_{ms} & 1 \end{bmatrix}^{-1} \begin{bmatrix} \hat{p}'_{rx11(Hot,Cal)} \\ \hat{p}'_{rx11(Cold,Cal)} \end{bmatrix}. \quad (5.74a)$$

Using an analogous approach to that outlined, an expression may be formed with the receiver tuned to the negative offset fundamental frequency. This leads to

$$\begin{bmatrix} \tilde{G}''_r \\ r''_{22} \end{bmatrix} = \begin{bmatrix} k\hat{T}_{ne} + |\Gamma_{hns}|^2 k\hat{T}_{ms} & 1 \\ k\hat{T}_{cns} (1 - |\Gamma_{cns}|^2) + |\Gamma_{cns}|^2 k\hat{T}_{ms} & 1 \end{bmatrix}^{-1} \begin{bmatrix} \hat{p}''_{rx11(Hot,Cal)} \\ \hat{p}''_{rx11(Cold,Cal)} \end{bmatrix}. \quad (5.74b)$$

The second primary step in the calibration process is to establish appropriate measurement system settings which will present a diverse range of source impedance states from the NL one-port DUT's frame of reference. Pertaining to (5.60), there are four noise properties comprising the NL one-port's NCM. Therefore, a minimum set of four distinct impedance states introduced by Z_s will be necessary. Fig. 5.8 illustrates a proposed PNA-X

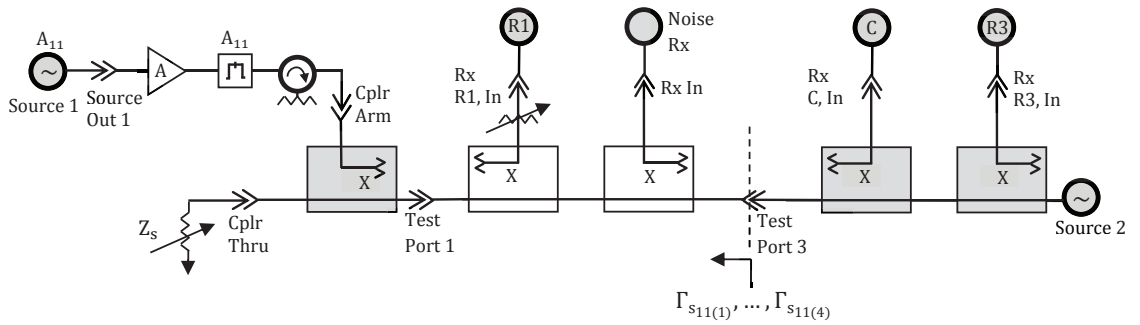


Figure 5.8: Source Match Calibration for the NL One-Port Network

centric measurement system configuration. Source 2 of the PNA-X will be the stimulus directed to test port 3 of the network analyzer. Terminating the main-line of the signal path is a tunable

passive source impedance Z_s . Z_s may be an electronic calibration module or fixed devices such as short, offset short, open, matched load, or arbitrary impedance calibration standards. The calibration plane at test port 3 is distinguished by the vertical dashed line shown in Fig. 5.8. The four distinct reflection coefficients $\Gamma_{S11(1)}, \dots, \Gamma_{S11(4)}$ used in (5.60) will be measured at this plane. The reflection coefficients will be determined by measuring the ratio of the incident and scattered waves using the PNA-X's "R3" and "C" receiver's respectively such that $\Gamma_{S11} = \text{"C" Rx} / \text{"R3" Rx}$. Two points should be noted, first, though the noise receiver is not being used in this calibration step, the incident signal presented at test port 3 will need to be set low enough in amplitude to ensure the measurement receiver is not over-driven leading to possible damage. Second, source 1 of the PNA-X will be turned off during this process. It's expected that the match viewed "looking-into" test port 1 will be unchanged between source 1 on/off states due to the combined isolation of the in-line booster amplifier and isolator. The calibration procedure for the NL one-port measurement is delineated in Appendix C.

5.2.4.1.2 Measurement Algorithm

Assigning a variable to each matrix in the order (5.60) is presented from left-to-right, a more compact form of (5.60) is depicted as

$$\mathbf{P}'_{\text{Meas}} = \mathbf{A} \cdot \mathbf{R}'_{\text{RX}} + \mathbf{B}' \cdot \mathbf{D}'_{\text{DUT}} . \quad (5.75)$$

Matrix manipulation of (5.75) is performed to solve for the noise properties of the NL one-port DUT resulting in

$$\mathbf{D}'_{\text{DUT}} = \mathbf{B}'^{-1} (\mathbf{P}'_{\text{Meas}} - \mathbf{A} \cdot \mathbf{R}'_{\text{RX}}) . \quad (5.76a)$$

With the NL one-port DUT connected to a calibrated measurement system, a minimum of four noise power measurements are made on the DUT; each test is conducted with a predetermined source impedance state presented at its RF input. The calibration and

measurement data sets are then substituted into the elements comprising matrices \mathbf{A} , \mathbf{B}' , $\mathbf{P}'_{\text{Meas}}$, and \mathbf{R}'_{RX} , whereupon (5.76a) is used to solve for the noise properties of the NL one-port.

Applying an approach like the one just described, but with the receiver tuned to the negative offset fundamental frequency, the noise properties of the DUT are expressed by

$$\mathbf{D}''_{\text{DUT}} = \mathbf{B}''^{-1} (\mathbf{P}''_{\text{Meas}} - \mathbf{A} \cdot \mathbf{R}''_{\text{RX}}) . \quad (5.76b)$$

As the frequency offset widens, the variation between \mathbf{D}'_{DUT} and $\mathbf{D}''_{\text{DUT}}$ will depend on the DUT type. Generally, it's expected that as the frequency offset narrows, \mathbf{D}'_{DUT} will approximate $\mathbf{D}''_{\text{DUT}}$.

The test procedure for the NL one-port device is presented in Appendix D.

5.2.4.2 Nonlinear Two-Port Network

By the full in-situ scattered noise matrix [26] expression of (5.41), the noise performance of a nonlinear multiport is described in relation to its connecting networks. Through a hardware measurement and analysis thought experiment, this generalized formalism will now be applied to a match-terminated nonlinear two-port network with purpose to extract its NCM. Evaluation will be restricted to the fundamental frequency and its bounded offsets.

A proposed hardware measurement setup shown in Fig. 5.9 uses the Keysight PNA-X Network Analyzer equipped with a noise measurement receiver. Analogous to the approach

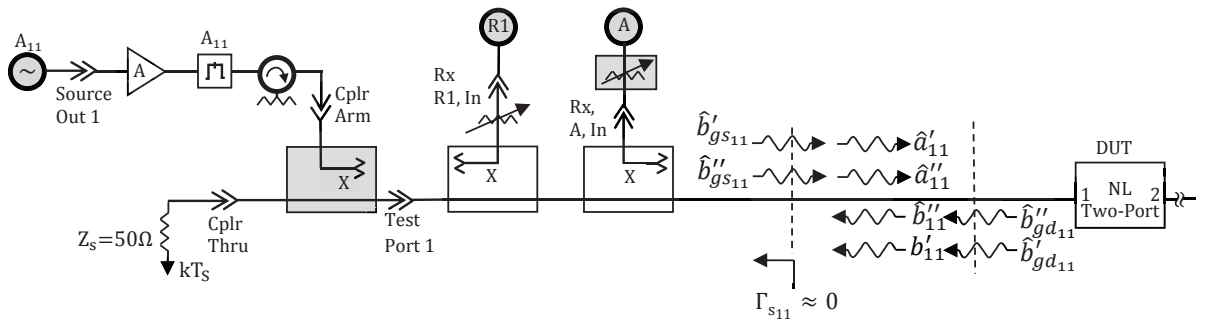


Figure 5.9a: Proposed Measurement Setup for the NL Two-Port Network

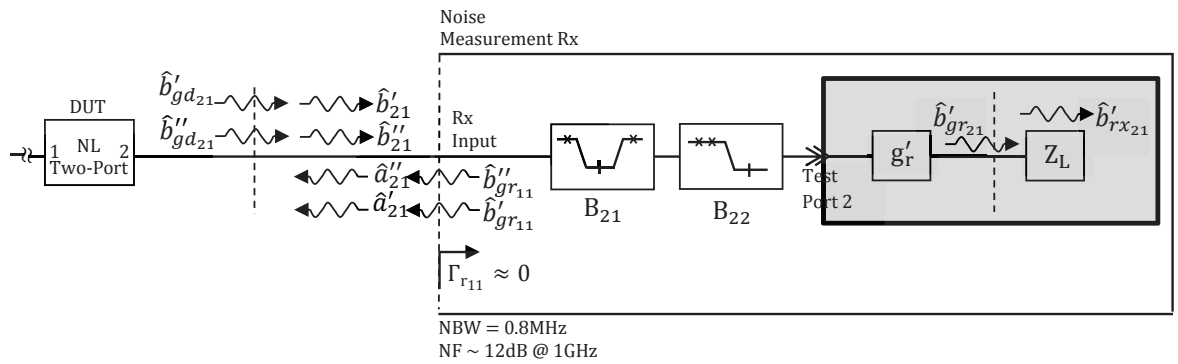


Figure 5.9b: Proposed Measurement Setup for the NL Two-Port Network

in chapter four, the instrument will be used to perform a series of calibrated noise power readings of the nonlinear two-port network while it undergoes a source-pull. The gray and white components within the diagram distinguish those which are internal and external to the PNA-X respectively. In the figure, the A_{11} stimulus is generated by the PNA-X, summed with the thermal noise produced by matched source impedance Z_s via an in-line coupler, and then collectively introduced as the incident signal (plus noise) to the DUT. The NL network's incident drive-tone A_{11} is monitored by a reference receiver "R1" coupled to the network analyzer's test port-one

signal path. Accompanying A_{11} are incident noise waves \hat{a}'_{11} and \hat{a}''_{11} . The noise power ascribed to scattered waves \hat{b}'_{21} and \hat{b}''_{21} will be evaluated by the noise measurement receiver at test port-two. The noise receiver, being active, produces its own noise waves $\hat{b}'_{g'_{r1}}$, and $\hat{b}''_{g''_{r1}}$ emanating from its input while $\hat{b}'_{g'_{s1}}$ and $\hat{b}''_{g''_{s1}}$ are dissipated in the receiver's matched load Z_L . The noise waves emerging from the receiver's input port are expected to contribute to the overall measured noise power due to their reflection at the DUTs output port combined with a low two-way signal path loss influence between them. The two vertical dashed lines present at both the DUTs input and output ports are separated by zero length in the physical setup. They are introduced in the diagram to distinguish the presence of the DUT's incident and scattered noise waves from those internally generated by its noise waves $\hat{b}'_{gd_{11}}$, $\hat{b}''_{gd_{11}}$, $\hat{b}'_{gd_{21}}$, $\hat{b}''_{gd_{21}}$ and the source and load impedance noise waves $\hat{b}'_{gs_{11}}$, $\hat{b}''_{gs_{11}}$, $\hat{b}'_{gr_{11}}$, and $\hat{b}''_{gr_{11}}$ originating from the source impedance and receiver of the measurement system. The dashed lines define the measurement plane.

Illustrated between the NL two-port's output and the receiver input is a notch filter used to remove the scattered fundamental component B_{21} while the low-pass filter rejects harmonics. Together, the filters prevent receiver compression thus ensuring proper performance. The noise at the fundamental offsets, shown by the x-marks, is intended to pass with minimal attenuation.

For fundamental only analysis to be valid, the source and receiver reflection coefficients at $\Gamma_{s_{12}}$, $\Gamma_{s_{13}}$, ... $\Gamma_{s_{1m}}$, and $\Gamma_{r_{12}}$, $\Gamma_{r_{13}}$, ... $\Gamma_{r_{1m}}$, respectively will be quasi-matched and noise-free at these higher-order frequencies. With quality hardware, a matched condition may be approximated. But, noise-free terminations at room temperature are not possible. However, this may be overcome if the X-parameters of the NL two-port corresponding to the translation of incident noise at the higher-order harmonics to the fundamental are at least an order of magnitude less than those restricted to fundamental frequency only. For example, $X_{21,11}^{(S)} \gg X_{21,12}^{(S)}$, $X_{21,11}^{(T)} \gg X_{21,12}^{(T)}$, $X_{21,21}^{(S)} \gg X_{21,22}^{(S)}$, and $X_{21,21}^{(T)} \gg X_{21,22}^{(T)}$ need be satisfied at the second harmonic. The same condition is applicable at the higher-order harmonics. Selection of a DUT

satisfying such X-parameter conditions will be necessary. Otherwise, the expressions for $\overline{\hat{b}'_{rx21} \hat{b}'_{rx21}^*}$ and $\overline{\hat{b}''_{rx21} \hat{b}''_{rx21}^*}$ will need be modified to include higher order X-parameter terms.

Within context of the defined experimental conditions of the measurement setup and the connected NL two-port DUT, (5.41) can be used to model the power spectral densities of the DUTs scattered noise waves \hat{b}'_{21} and \hat{b}''_{21} as well as their correlation to one another yielding

$$\overline{\begin{bmatrix} \hat{b}'_{11} \\ \hat{b}'_{21} \\ \hat{b}''_{11} \\ \hat{b}''_{21} \end{bmatrix} \begin{bmatrix} \hat{b}'_{11} \\ \hat{b}'_{21} \\ \hat{b}''_{11} \\ \hat{b}''_{21} \end{bmatrix}^\dagger} = \mathbf{I}^{-1} \left\{ \begin{bmatrix} X_{11,11}^{(S)} P^0 & X_{11,21}^{(S)} P^0 & X_{11,11}^{(T)} P^2 & X_{11,21}^{(T)} P^2 \\ X_{21,11}^{(S)} P^0 & X_{21,21}^{(S)} P^0 & X_{21,11}^{(T)} P^2 & X_{21,21}^{(T)} P^2 \\ X_{11,11}^{(T)*} P^{-2} & X_{11,21}^{(T)*} P^{-2} & X_{11,11}^{(S)*} P^0 & X_{11,21}^{(S)*} P^0 \\ X_{21,11}^{(T)*} P^{-2} & X_{21,21}^{(T)*} P^{-2} & X_{21,11}^{(S)*} P^0 & X_{21,21}^{(S)*} P^0 \end{bmatrix} \overline{\begin{bmatrix} \hat{b}'_{g'_{21}} \\ \hat{b}'_{g'_{21}} \\ \hat{b}''_{g'_{21}} \\ \hat{b}''_{g'_{21}} \end{bmatrix} \begin{bmatrix} \hat{b}'_{g'_{21}} \\ \hat{b}'_{g'_{21}} \\ \hat{b}''_{g'_{21}} \\ \hat{b}''_{g'_{21}} \end{bmatrix}^\dagger} \begin{bmatrix} X_{11,11}^{(S)} P^0 & X_{11,21}^{(S)} P^0 & X_{11,11}^{(T)} P^2 & X_{11,21}^{(T)} P^2 \\ X_{21,11}^{(S)} P^0 & X_{21,21}^{(S)} P^0 & X_{21,11}^{(T)} P^2 & X_{21,21}^{(T)} P^2 \\ X_{11,11}^{(T)*} P^{-2} & X_{11,21}^{(T)*} P^{-2} & X_{11,11}^{(S)*} P^0 & X_{11,21}^{(S)*} P^0 \\ X_{21,11}^{(T)*} P^{-2} & X_{21,21}^{(T)*} P^{-2} & X_{21,11}^{(S)*} P^0 & X_{21,21}^{(S)*} P^0 \end{bmatrix} + \begin{bmatrix} \hat{b}'_{g'd_{11}} \\ \hat{b}'_{g'd_{21}} \\ \hat{b}''_{g'd_{11}} \\ \hat{b}''_{g'd_{21}} \end{bmatrix} \begin{bmatrix} \hat{b}'_{g'd_{11}} \\ \hat{b}'_{g'd_{21}} \\ \hat{b}''_{g'd_{11}} \\ \hat{b}''_{g'd_{21}} \end{bmatrix}^\dagger \right\} \mathbf{I}^{-1\dagger} \quad (5.77)$$

where the noise waves $\hat{b}'_{g'_{11}}$ and $\hat{b}''_{g'_{11}}$ emerging from the input port of the noise receiver are in corresponding order to the incident noise waves $\hat{b}'_{g'_{21}}$ and $\hat{b}''_{g'_{21}}$ presented to the DUTs output port-two. The presence of the identity matrices \mathbf{I} in (5.77) are a consequence of the NL two-port's connected terminations, i.e. from its connected source and receiver, being matched and isolated from one another.

Having tuned the measurement receiver to the upper fundamental frequency offset, it's evident per Fig. 5.9 that the receiver's incident noise wave \hat{b}'_{21} is influenced by its transmission coefficient g'_r . Calculating the incident noise waves power spectral density $\overline{\hat{b}'_{21} \hat{b}'_{21}^*}$ from (5.57), scaling each of its incident terms by the transmission properties of the receiver, and taking into account the receiver's output noise contribution $\hat{b}'_{g'_{21}}$, the total noise power density $\overline{\hat{b}'_{rx21} \hat{b}'_{rx21}^*}$ incident to the receiver's matched load is

$$\begin{aligned} \overline{\hat{b}'_{rx21} \hat{b}'_{rx21} *} &= |g'_r|^2 X_{21,11}^{(S)} \overline{\hat{b}'_{gs11} \hat{b}'_{gs11} *} X_{21,11}^{(S)*} + |g'_r|^2 X_{21,11}^{(T)} P^2 \overline{\hat{b}''_{gs11} \hat{b}''_{gs11} *} X_{21,11}^{(T)*} P^{-2} + |g'_r|^2 X_{21,21}^{(S)} \overline{\hat{b}'_{gl21} \hat{b}'_{gl21} *} X_{21,21}^{(S)*} + \\ &|g'_r|^2 X_{21,21}^{(T)} P^2 \overline{\hat{b}''_{gl21} \hat{b}''_{gl21} *} X_{21,21}^{(T)*} P^{-2} + X_{21,21}^{(S)} g'_r \overline{\hat{b}'_{gl21} \hat{b}'_{gr21} *} + X_{21,21}^{(S)*} g'_r \overline{\hat{b}'_{gr21} \hat{b}'_{gl21} *} + \overline{\hat{b}'_{gr21} \hat{b}'_{gr21} *} + |g'_r|^2 \overline{\hat{b}'_{gd21} \hat{b}'_{gd21} *} . \end{aligned} \quad (5.78)$$

Examination of the terms in (5.78) suggests that each component in the measurement setup, including those from the source, DUT, and receiver contribute to the noise power measured by the receiver. Noise generators \hat{b}'_{gs11} and \hat{b}''_{gs11} originating from the source Z_S contribute an S- and T-type response respectively at the NL DUTs output. Because the NL two-port is match terminated, the noise power ascribed to \hat{b}'_{gd11} emanating from its input port is fully dissipated in Z_S . Thus, the DUT offers only one contribution to the measured result, that being due to the noise \hat{b}'_{gd21} emerging from its output port. Interestingly, there are five noise contributors due to the receiver. First, there is the noise wave \hat{b}'_{gr11} emanating from the receiver's input port which is presented unchanged to the DUTs output port-two as \hat{b}'_{gl21} . Note, from the DUTs frame of reference, this wave originates from its connected load, i.e. in this setup, the receiver. The incident wave is reflected from the NL DUTs output port as an S-type response, re-introduced to the receiver and processed accordingly as a noise power related to $\overline{\hat{b}'_{gl21} \hat{b}'_{gl21} *} .$ The second receiver related term is due to noise wave \hat{b}''_{gr11} also emanating from the receiver's input port. It's presented unchanged to the DUTs output port-two and denoted by \hat{b}''_{gl21} . This incident wave is reflected as an T-type response from the DUTs output port. Having been transformed by the NL DUT to the upper fundamental frequency offset, the response is processed by the receiver as a noise power related to $\overline{\hat{b}''_{gl21} \hat{b}''_{gl21} *} .$ The third and fourth receiver terms in (5.57) assess the correlation of the previously mentioned S-type reflection response to the receiver's "output" noise wave \hat{b}'_{gr21} . The noise power reading will be dependent in-part on the degree of correlation between the two complex noise quantities. Lastly, the receiver's "output" generated noise power related to $\overline{\hat{b}'_{gr21} \hat{b}'_{gr21} *} is delivered to the receiver's load independent of the source and DUT to which it's connected.$

To extract the noise properties of the DUT, it's convenient to group the terms in (5.78) into two categories, the noise generators of the measurement system and those of the NL two-port. Re-writing (5.78) in matrix form yields,

$$\overline{\hat{b}'_{rx21} \hat{b}'_{rx21} *} = \left[\begin{array}{cccc} |X_{21,11}^{(S)}|^2 & \overline{\hat{b}'_{gs11} \hat{b}'_{gs11} *} & |X_{21,11}^{(T)}|^2 & \overline{\hat{b}''_{gs11} \hat{b}''_{gs11} *} \\ |X_{21,21}^{(S)}|^2 & & |X_{21,21}^{(T)}|^2 & \\ X_{21,21}^{(S)} & & X_{21,21}^{(T)} & \\ & & & 1 \end{array} \right] \cdot \left[\begin{array}{c} |g'_r|^2 \\ |g'_r|^2 \\ |g'_r|^2 \overline{\hat{b}'_{g'_{r11}} \hat{b}'_{g'_{r11} *} *} \\ |g'_r|^2 \overline{\hat{b}''_{g'_{r11}} \hat{b}''_{g'_{r11} *} *} \\ g'_r \overline{\hat{b}'_{g'_{r11}} \hat{b}'_{g'_{r21} *} *} \\ g_r^* \overline{\hat{b}'_{g'_{r21}} \hat{b}'_{g'_{r11} *} *} \\ \overline{\hat{b}'_{g'_{r21}} \hat{b}'_{g'_{r21} *} *} \end{array} \right] + \left[|g'_r|^2 \right] \cdot \left[\overline{\hat{b}'_{gd21} \hat{b}'_{gd21} *} \right] \quad (5.79)$$

where the terms related to the first and second matrix operations in (5.79) are specific to the measurement system and DUT respectively.

Concerning the measurement system, two observations are worth highlighting. First, the passive source impedance Z_s is known to generate a constant broadband thermal noise related to its physical temperature T_s . Given the source is match terminated, its available noise density is $\overline{\hat{b}'_{gs11} \hat{b}'_{gs11} *} = \overline{\hat{b}''_{gs11} \hat{b}''_{gs11} *} = k\hat{T}_s$. Second, the noise measured by the PNA-X receiver is typically confined to a user selected noise bandwidth, typically 4MHz [58]. Whatever the setting, as the receiver is tuned across the lower to upper offset interval bounding a frequency on the harmonic grid, in this case the fundamental frequency, the variation to the receiver's bandwidth is considered negligible, at least for the chosen interval. Therefore, with the receiver tuned to either the lower or upper offset frequency, the receiver's noise bandwidth will be reported by the variable B in units of Hertz. Applying these conditions to (5.79), the noise power measured by the receiver when tuned to the upper offset frequency is

$$\hat{p}_{rx21}'' = \overline{\hat{b}_{rx21}' \hat{b}_{rx21}''} \mathbf{B} = \left[\left(\left| \mathbf{X}_{21,11}^{(S)} \right|^2 + \left| \mathbf{X}_{21,11}^{(T)} \right|^2 \right) k \hat{\Gamma}_s \quad \left| \mathbf{X}_{21,21}^{(S)} \right|^2 \quad \left| \mathbf{X}_{21,21}^{(T)} \right|^2 \quad \mathbf{X}_{21,21}^{(S)} \quad \mathbf{X}_{21,21}^{(S)*} \quad 1 \right] \cdot \begin{bmatrix} \mathbf{G}_r' \\ \frac{\mathbf{G}_r' \hat{b}_{g'11}' \hat{b}_{g'11}''}{g_{g'11}' \hat{b}_{g'11}''} \\ \frac{\mathbf{G}_r' \hat{b}_{g'11}'' \hat{b}_{g'11}''}{g_{g'11}'' \hat{b}_{g'11}''} \\ \frac{g_{g'11}' \hat{b}_{g'11}' \hat{b}_{g'21}''}{g_{g'11}' \hat{b}_{g'21}''} \mathbf{B} \\ \frac{g_{g'11}'' \hat{b}_{g'11}'' \hat{b}_{g'11}''}{g_{g'11}'' \hat{b}_{g'11}''} \mathbf{B} \\ \frac{\hat{b}_{g'21}'' \hat{b}_{g'21}''}{g_{g'21}'' \hat{b}_{g'21}''} \mathbf{B} \end{bmatrix} + \left[\mathbf{G}_r' \right] \cdot \left[\overline{\hat{b}_{gd21}' \hat{b}_{gd21}''} \right] \quad (5.80a)$$

where by use of (5.58), the receiver's gain-bandwidth product \mathbf{G}_r' has been substituted.

With the receiver tuned to the lower fundamental frequency offset, and following a procedure analogous to that described above, leads to the expression

$$\hat{p}_{rx21}'' = \overline{\hat{b}_{rx21}'' \hat{b}_{rx21}''} \mathbf{B} = \left[\left(\left| \mathbf{X}_{21,11}^{(S)} \right|^2 + \left| \mathbf{X}_{21,11}^{(T)} \right|^2 \right) k \hat{\Gamma}_s \quad \left| \mathbf{X}_{21,21}^{(S)} \right|^2 \quad \left| \mathbf{X}_{21,21}^{(T)} \right|^2 \quad \mathbf{X}_{21,21}^{(S)} \quad \mathbf{X}_{21,21}^{(S)*} \quad 1 \right] \cdot \begin{bmatrix} \mathbf{G}_r'' \\ \frac{\mathbf{G}_r'' \hat{b}_{g''11}'' \hat{b}_{g''11}''}{g_{g''11}'' \hat{b}_{g''11}''} \\ \frac{\mathbf{G}_r'' \hat{b}_{g''11}'' \hat{b}_{g''11}''}{g_{g''11}'' \hat{b}_{g''11}''} \\ \frac{g_{g''11}'' \hat{b}_{g''11}'' \hat{b}_{g''21}''}{g_{g''11}'' \hat{b}_{g''21}''} \mathbf{B} \\ \frac{g_{g''11}'' \hat{b}_{g''11}'' \hat{b}_{g''11}''}{g_{g''11}'' \hat{b}_{g''11}''} \mathbf{B} \\ \frac{\hat{b}_{g''21}'' \hat{b}_{g''21}''}{g_{g''21}'' \hat{b}_{g''21}''} \mathbf{B} \end{bmatrix} + \left[\mathbf{G}_r'' \right] \cdot \left[\overline{\hat{b}_{gd21}'' \hat{b}_{gd21}''} \right] \quad (5.80b)$$

It's proposed that the column matrices of (5.80a, b) comprising the receiver's gain-bandwidth and noise properties will be determined in calibration. Assuming the X-parameters of the NL two-port have been previously extracted by use of the PNA-X/NVNA, the remaining unknown are the elements of the NL two-port's noise properties $\overline{\hat{b}_{gd21}' \hat{b}_{gd21}''}$, and $\overline{\hat{b}_{gd12}'' \hat{b}_{gd12}''}$. These noise properties may be solved by performing two noise power measurements, one with the noise receiver tuned to the lower fundamental frequency offset and second at its upper.

5.2.4.2.1 Calibration Algorithm

It is envisioned that calibration of the measurement system will involve characterization of the noise measurement receiver. The calibration coefficients to be determined are delineated by the elements comprising the 6x1 column vectors in (5.80a) and (5.80b). Figure 5.10 illustrates a passive impedance tuner connected to the measurement system's test-port 1 signal path. The dashed vertical lines marking the measurement reference plane at test-ports 1 and 2 are separated by zero length. It's shown this way to highlight the noise receiver's incident and scattered waves \hat{a}'_{11} and \hat{b}'_{11} respectively in presence of the characteristic noise out $\hat{b}'_{gs_{11}}$ of Z_s and that of the measurement system's receiver noise out represented by $\hat{b}'_{gr_{11}}$.

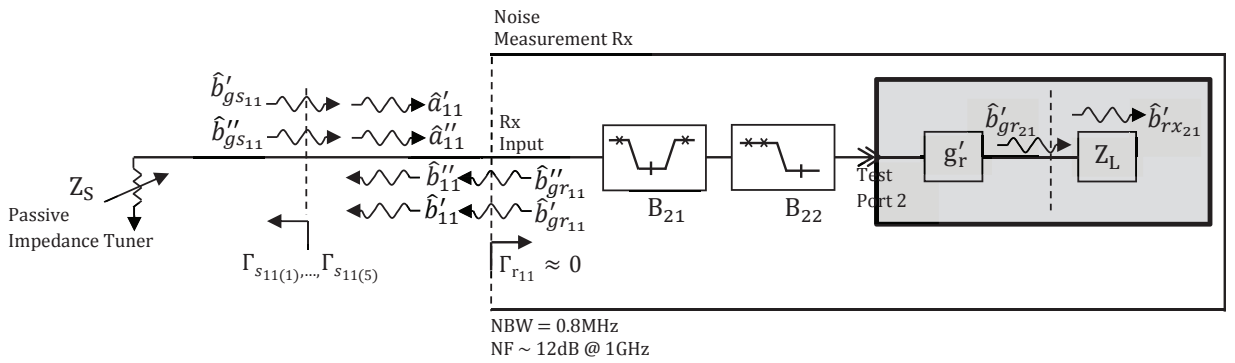


Figure 5.10: Noise Measurement Receiver Calibration for the NL Two-Port Network

By inspection of Fig. 5.10, the scattered and incident noise waves of the measurement system's matched receiver may be written as

$$\hat{a}'_{11} = \Gamma_{s_{11}} \hat{b}'_{11} + \hat{b}'_{gs_{11}} \quad (5.81)$$

and

$$\hat{b}'_{11} = \hat{b}'_{gr_{11}} \quad (5.82)$$

where the source reflection coefficient $\Gamma_{s_{11}}$ will be tunable across a diverse range of impedance states. Substitution of (5.82) into (5.81) produces the receiver's incident wave expression in terms of the measurement system's source and receiver noise contributions such that

$$\hat{a}'_{11} = \Gamma_{s_{11}} \hat{b}'_{g'_{r_{11}}} + \hat{b}'_{g'_{s_{11}}} \quad (5.83)$$

As demonstrated in Fig. 5.10, the receiver is tuned to the upper fundamental frequency offset. Therefore, the receiver's incident noise wave \hat{a}'_{11} will be scaled by the receiver's transmission coefficient g'_r and summed with its "output" noise $\hat{b}'_{g'_{r_{21}}}$ to form

$$\hat{b}'_{rx_{21}} = g'_r \hat{a}'_{11} + \hat{b}'_{g'_{r_{21}}} \quad (5.84)$$

where $\hat{b}'_{rx_{21}}$ is the total noise incident to the receiver's matched load. Substitution of (5.83) into (5.84) yields $\hat{b}'_{rx_{21}}$ in terms of the noise generators associated with the measurement system's source and receiver.

$$\hat{b}'_{rx_{21}} = g'_r \hat{b}'_{g'_{s_{11}}} + g'_r \Gamma_{s_{11}} \hat{b}'_{g'_{r_{11}}} + \hat{b}'_{g'_{r_{21}}} \quad (5.85)$$

where each noise generator undergoes interaction with the measurement system thus influencing the total noise assessed at the receiver's load. This transformation is captured by the coefficients ascribed to each noise source in (5.85).

The noise power density of $\hat{b}'_{rx_{21}}$ can be determined by multiplying both sides of (5.85) by its complex conjugate and evaluating the time-average of their product. The result is

$$\overline{\hat{b}'_{rx_{21}} \hat{b}'_{rx_{21}}*} = |g'_r|^2 \overline{\hat{b}'_{g'_{s_{11}}} \hat{b}'_{g'_{s_{11}}*}} + |g'_r|^2 |\Gamma_{s_{11}}|^2 \overline{\hat{b}'_{g'_{r_{11}}} \hat{b}'_{g'_{r_{11}}*}} + g'_r \Gamma_{s_{11}} \overline{\hat{b}'_{g'_{r_{11}}} \hat{b}'_{g'_{r_{21}}*}} + g'_r* \Gamma_{s_{11}}* \overline{\hat{b}'_{g'_{r_{21}}} \hat{b}'_{g'_{r_{11}}*}} + \overline{\hat{b}'_{g'_{r_{21}}} \hat{b}'_{g'_{r_{21}}*}} \quad (5.86)$$

where the noise from the source and receiver are uncorrelated to one another.

With the receiver set to an effective noise bandwidth B , the measured noise power $\hat{p}'_{rx_{21}}$ of $\hat{b}'_{rx_{21}}$ is

$$\hat{p}'_{rx21} = \overline{\hat{b}'_{rx21} \hat{b}'_{rx21} *} B = |g'_r|^2 \overline{\hat{b}'_{gs11} \hat{b}'_{gs11} *} B + |g'_r|^2 |\Gamma_{s11}|^2 \overline{\hat{b}'_{gr11} \hat{b}'_{gr11} *} B + g'_r \Gamma_{s11} \overline{\hat{b}'_{gr11} \hat{b}'_{gr21} *} B + g_r^* \Gamma_{s11}^* \overline{\hat{b}'_{gr11} \hat{b}'_{gr21} *} B + \overline{\hat{b}'_{gr21} \hat{b}'_{gr21} *} B \quad (5.87)$$

To organize the measurement receiver's calibration coefficients in a column vector, (5.87) is structured in matrix form leading to the expression

$$\hat{p}'_{rx21} = \begin{bmatrix} \overline{\hat{b}'_{gs11} \hat{b}'_{gs11} *} & |\Gamma_{s11}|^2 & \Gamma_{s11} & \Gamma_{s11}^* & 1 \end{bmatrix} \cdot \begin{bmatrix} |g'_r|^2 B \\ |g'_r|^2 \overline{\hat{b}'_{gr11} \hat{b}'_{gr11} *} B \\ g'_r \overline{\hat{b}'_{gr11} \hat{b}'_{gr21} *} B \\ g_r^* \overline{\hat{b}'_{gr11} \hat{b}'_{gr21} *} B \\ \overline{\hat{b}'_{gr21} \hat{b}'_{gr21} *} B \end{bmatrix}. \quad (5.88)$$

Given their ease of measure, it is convenient to express the characteristic noise density $\overline{\hat{b}'_{gs11} \hat{b}'_{gs11} *}$ of the passive source impedance Z_s in terms of its physical temperature T_s and reflection coefficient Γ_{s11} . Further, to simplify notation in (5.88), we assign a single variable to each element in the column vector. Collectively, this generates

$$\hat{p}'_{rx21} = \begin{bmatrix} k\hat{T}_s(1-|\Gamma_{s11}|^2) & |\Gamma_{s11}|^2 & \Gamma_{s11} & \Gamma_{s11}^* & 1 \end{bmatrix} \cdot \begin{bmatrix} G'_r \\ r'_{11} \\ r'_{12} \\ r'_{21} \\ r'_{22} \end{bmatrix}. \quad (5.89)$$

where $\overline{\hat{b}'_{gs11} \hat{b}'_{gs11} *} = k\hat{T}_s(1-|\Gamma_{s11}|^2)$, $G'_r = |g'_r|^2 B$, $r'_{11} = |g'_r|^2 \overline{\hat{b}'_{gr11} \hat{b}'_{gr11} *} B$, $r'_{12} = g'_r \overline{\hat{b}'_{gr11} \hat{b}'_{gr21} *} B$, $r'_{21} = g_r^* \overline{\hat{b}'_{gr11} \hat{b}'_{gr21} *} B$, and $r'_{22} = \overline{\hat{b}'_{gr21} \hat{b}'_{gr21} *} B$. G'_r is the gain-bandwidth product of the measurement receiver at a positive frequency offset from the fundamental frequency. r'_{11} , r'_{12} , r'_{21} , and r'_{22} for our purpose will be referred as the elements comprising the measurement receiver's noise properties. Note, unlike the noise quantities describing the DUT, those of the receiver include the presence of g'_r such that its complex value need not be known. There are five unknowns in the

column vector of (5.89). By sequentially adjusting the source reflection coefficient $\Gamma_{s_{11}}$ and measuring the corresponding noise power $\hat{p}'_{rx_{21}}$, the five unknown properties of the receiver may be determined. To accomplish this, a minimum of five independent equations are created, each by a separate source impedance state. The five linear equations may be organized in a matrix row-expansion of (5.89) forming

$$\begin{bmatrix} \hat{p}'_{rx_{21(1)}} \\ \hat{p}'_{rx_{21(2)}} \\ \hat{p}'_{rx_{21(3)}} \\ \hat{p}'_{rx_{21(4)}} \\ \hat{p}'_{rx_{21(5)}} \end{bmatrix} = \begin{bmatrix} k\hat{T}_s \left(1 - |\Gamma_{s_{11(1)}}|^2\right) & |\Gamma_{s_{11(1)}}|^2 & \Gamma_{s_{11(1)}} & \Gamma_{s_{11(1)}}^* & 1 \\ k\hat{T}_s \left(1 - |\Gamma_{s_{11(2)}}|^2\right) & |\Gamma_{s_{11(2)}}|^2 & \Gamma_{s_{11(2)}} & \Gamma_{s_{11(2)}}^* & 1 \\ k\hat{T}_s \left(1 - |\Gamma_{s_{11(3)}}|^2\right) & |\Gamma_{s_{11(3)}}|^2 & \Gamma_{s_{11(3)}} & \Gamma_{s_{11(3)}}^* & 1 \\ k\hat{T}_s \left(1 - |\Gamma_{s_{11(4)}}|^2\right) & |\Gamma_{s_{11(4)}}|^2 & \Gamma_{s_{11(4)}} & \Gamma_{s_{11(4)}}^* & 1 \\ k\hat{T}_s \left(1 - |\Gamma_{s_{11(5)}}|^2\right) & |\Gamma_{s_{11(5)}}|^2 & \Gamma_{s_{11(5)}} & \Gamma_{s_{11(5)}}^* & 1 \end{bmatrix} \cdot \begin{bmatrix} G'_r \\ I'_{11} \\ I'_{12} \\ I'_{21} \\ I'_{22} \end{bmatrix} \quad (5.90)$$

where $\Gamma_{s_{11(q)}}$ is a set of q-th source reflection coefficients, each corresponding to a distinct noise power measurement $\hat{p}'_{rx_{21(q)}}$. In this case, q takes on integer values from 1 to 5. A sufficient separation of the reflection states is needed to ensure the unknown quantities are accurately assessed; there are many choices, one such example being 0, 1, -1, $1\angle 90^\circ$, and $1\angle -90^\circ$.

The measurement receiver's coefficients may be solved by applying a pre-multiplication matrix inversion to both sides of (5.90) resulting in

$$\begin{bmatrix} G'_r \\ r'_{11} \\ r'_{12} \\ r'_{21} \\ r'_{22} \end{bmatrix} = \begin{bmatrix} k\hat{T}_s \left(1 - |\Gamma_{s_{11(1)}}|^2\right) & |\Gamma_{s_{11(1)}}|^2 & \Gamma_{s_{11(1)}} & \Gamma_{s_{11(1)}}^* & 1 \\ k\hat{T}_s \left(1 - |\Gamma_{s_{11(2)}}|^2\right) & |\Gamma_{s_{11(2)}}|^2 & \Gamma_{s_{11(2)}} & \Gamma_{s_{11(2)}}^* & 1 \\ k\hat{T}_s \left(1 - |\Gamma_{s_{11(3)}}|^2\right) & |\Gamma_{s_{11(3)}}|^2 & \Gamma_{s_{11(3)}} & \Gamma_{s_{11(3)}}^* & 1 \\ k\hat{T}_s \left(1 - |\Gamma_{s_{11(4)}}|^2\right) & |\Gamma_{s_{11(4)}}|^2 & \Gamma_{s_{11(4)}} & \Gamma_{s_{11(4)}}^* & 1 \\ k\hat{T}_s \left(1 - |\Gamma_{s_{11(5)}}|^2\right) & |\Gamma_{s_{11(5)}}|^2 & \Gamma_{s_{11(5)}} & \Gamma_{s_{11(5)}}^* & 1 \end{bmatrix}^{-1} \cdot \begin{bmatrix} \hat{p}'_{rx_{21(1)}} \\ \hat{p}'_{rx_{21(2)}} \\ \hat{p}'_{rx_{21(3)}} \\ \hat{p}'_{rx_{21(4)}} \\ \hat{p}'_{rx_{21(5)}} \end{bmatrix}. \quad (5.91a)$$

Tuning the measurement receiver to the negative offset fundamental frequency and employing a procedure analogous to the one outlined above, the receiver's gain-bandwidth product G''_r and noise properties r''_{11} , r''_{12} , r''_{21} , and r''_{22} are acquired by the solution

$$\begin{bmatrix} G''_r \\ r''_{11} \\ r''_{12} \\ r''_{21} \\ r''_{22} \end{bmatrix} = \begin{bmatrix} k\hat{T}_s \left(1 - |\Gamma_{s_{11(1)}}|^2\right) & |\Gamma_{s_{11(1)}}|^2 & \Gamma_{s_{11(1)}} & \Gamma_{s_{11(1)}}^* & 1 \\ k\hat{T}_s \left(1 - |\Gamma_{s_{11(2)}}|^2\right) & |\Gamma_{s_{11(2)}}|^2 & \Gamma_{s_{11(2)}} & \Gamma_{s_{11(2)}}^* & 1 \\ k\hat{T}_s \left(1 - |\Gamma_{s_{11(3)}}|^2\right) & |\Gamma_{s_{11(3)}}|^2 & \Gamma_{s_{11(3)}} & \Gamma_{s_{11(3)}}^* & 1 \\ k\hat{T}_s \left(1 - |\Gamma_{s_{11(4)}}|^2\right) & |\Gamma_{s_{11(4)}}|^2 & \Gamma_{s_{11(4)}} & \Gamma_{s_{11(4)}}^* & 1 \\ k\hat{T}_s \left(1 - |\Gamma_{s_{11(5)}}|^2\right) & |\Gamma_{s_{11(5)}}|^2 & \Gamma_{s_{11(5)}} & \Gamma_{s_{11(5)}}^* & 1 \end{bmatrix}^{-1} \cdot \begin{bmatrix} \hat{p}''_{rx_{21(1)}} \\ \hat{p}''_{rx_{21(2)}} \\ \hat{p}''_{rx_{21(3)}} \\ \hat{p}''_{rx_{21(4)}} \\ \hat{p}''_{rx_{21(5)}} \end{bmatrix}. \quad (5.91b)$$

Post-processing leads to solving for the remaining noise properties $G'_r \overline{\hat{b}''_{g_{r1}} \hat{b}''_{g_{r1}}}$ and $G''_r \overline{\hat{b}'_{g_{r1}} \hat{b}'_{g_{r1}}}$ in (5.80a) and (5.80b) respectively. Note, regardless whether the DUT is to be measured at the positive or negative fundamental frequency offset, a calibration of the receiver at both positive and negative frequency offsets are required to determine these properties. In

other words, we require the solution set provided by (5.91a) and (5.91b) to compute these remaining noise properties.

To solve for the calibration coefficients of the measurement receiver, an intermediary step is introduced to establish the appropriate source impedance state for each noise power measurement to follow. Per (5.91a), there are five unknown receiver properties. Therefore, a minimum set of five impedance states introduced by Z_s to the receiver are necessary. In Figure

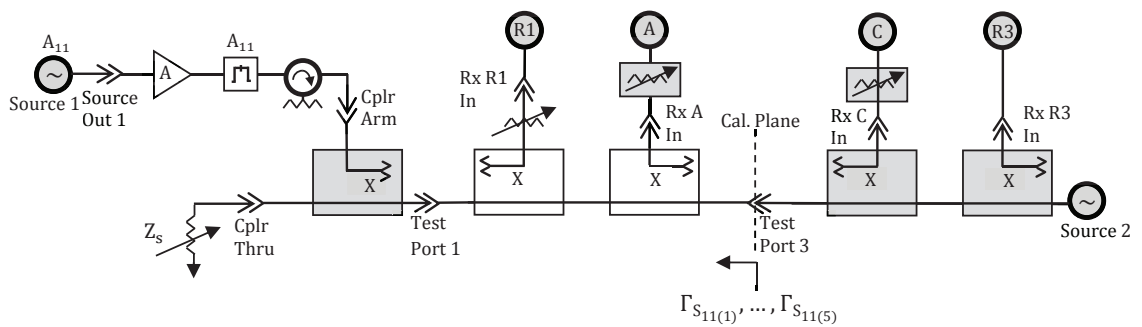


Figure 5.11: Source Match Calibration for the NL Two-Port Network

5.11 illustrates a proposed PNA-X centric measurement system configuration. Source 2 of the PNA-X will be the stimulus directed out test port 3 of the network analyzer. Terminating the main-line of the signal path via connected test port 1 is a tunable passive source impedance Z_s . Z_s may be an electronic calibration module or fixed devices such as short, offset short, open, matched load, or arbitrary impedance calibration standards. The calibration plane at test port 3 is distinguished by the vertical dashed line shown in Fig. 5.11. The five reflection coefficients $\Gamma_{s_{11(1)}}, \dots, \Gamma_{s_{11(5)}}$ used in (5.91a) will be measured at this plane. The reflection coefficients will be determined by measuring the ratio of the incident and scattered waves using the PNA-X's "R3" and "C" receiver's respectively such that $\Gamma_{s_{11}} = "C" Rx / "R3" Rx$. One point to note, unlike the NL two-port measurement configuration, source 1 out 1 of the PNA-X will be terminated during this process. It's expected that the match viewed from the test port 1 frame of reference will be

unchanged between states due to the combined isolation of the in-line booster amplifier and isolator. The discussion above applies as well to (5.91b). Described at upper and lower fundamental frequency offsets, the calibration procedure for the match-embedded NL two-port measurement is delineated in Appendix E.

5.2.4.2.2 Measurement Algorithm

Assigning a variable to each matrix in the order (5.80a) is presented from left-to-right, a more compact form of (5.80a) is depicted as

$$\mathbf{P}'_{\text{Meas}} = \mathbf{A} \cdot \mathbf{R}'_{\text{RX}} + \mathbf{B}' \cdot \mathbf{D}'_{\text{DUT}} . \quad (5.92)$$

Matrix manipulation of (5.92) is performed to solve for the noise properties of the NL two-port DUT resulting in

$$\mathbf{D}'_{\text{DUT}} = \mathbf{B}'^{-1} (\mathbf{P}'_{\text{Meas}} - \mathbf{A} \cdot \mathbf{R}'_{\text{RX}}) . \quad (5.93)$$

With the NL two-port DUT connected to a calibrated match-embedded measurement system, a minimum of one noise power measurement is made on the DUT. The calibration and measurement data sets are then substituted into the elements comprising matrices \mathbf{A} , \mathbf{B}' , $\mathbf{P}'_{\text{Meas}}$, and \mathbf{R}'_{RX} , whereupon (5.93) is used to solve for the noise properties of NL two-port assessed at its output port.

Tuning the receiver to the negative offset fundamental frequency and applying a similar method to the one just described for (5.80b), the noise properties of the DUT are expressed by

$$\mathbf{D}''_{\text{DUT}} = \mathbf{B}''^{-1} (\mathbf{P}''_{\text{Meas}} - \mathbf{A} \cdot \mathbf{R}''_{\text{RX}}) . \quad (5.94)$$

As the frequency offset widens, the variation between \mathbf{D}'_{DUT} and $\mathbf{D}''_{\text{DUT}}$ will depend on the DUT type. Generally, it's expected that as the frequency offset narrows, \mathbf{D}'_{DUT} will approximate $\mathbf{D}''_{\text{DUT}}$. The test procedure for the NL two-port device is presented in Appendix F.

To summarize, a generalized scattered noise behavioral model for time-invariant nonlinear microwave circuits has been presented. The formalism utilizes noise waves and large-signal scattering functions known as X-parameters to extract a multi-port network's noise correlation matrix. From this, expressions representing the network's effective input noise temperature and noise factor have been established. Within the small-signal space, it was demonstrated that the behavioral model reduces to a familiar form describing noise wave influence governed by the network's S-parameter functions. Using the generalized form, two examples using ADS software simulation were given in context of mismatch- and match-embedded nonlinear one-port and two-port configurations respectively. In simulation, the NL-network's source and load terminations were passive. Numerical versus simulated results were compared. The results in the two-port case yielded its noise factor (effective input noise temperature). Lastly, hardware noise measurement thought experiments for the one- and two-port nonlinear network scenarios were designed to determine their noise properties. The generalized scattered noise behavioral model was extended to accommodate for an active loading of the NL network; the active load was used as a noise measurement receiver to offer a practical means by which the noise properties of the NL network DUT may be extracted. The proposed hardware thought experiments were designed using the Keysight PNA-X Vector Network Analyzer and its integrated low noise measurement receiver. Detailed calibration and measurement procedures have been created and are included in Appendices C - F.

Chapter 6

Conclusions and Recommendations

6.1 Conclusions

A generalized noise behavioral model for embedded nonlinear time-invariant microwave networks has been presented. Illustrated in the frequency-domain, the driven nonlinear network's scattering noise matrix was expressed as a linear transformation of the composing (embedded and embedding) networks noise correlation matrices suitably modified by interaction between respective X- and S-type parameters. From this set of equations written in wave vector form, the nonlinear network's (intrinsic) noise correlation matrix across all n-port, m-harmonic indices were extracted. Expressions for noise factor and effective input noise temperature of the nonlinear network were developed by use of the generalized noise behavioral model in context to defined, well established figures-of-merit. Furthermore, it was shown that removal of the nonlinear network's drive-tone reduced the models to the familiar small-signal form, and faithfully described the noise behavior of the network in its linear operation-space. Two examples were considered to validate the generalized noise model in simulation. In the first case, the generalized full-insitu scattered noise matrix expression was applied to a driven nonlinear one-port example circuit connected to a noisy matched termination. A filter was applied to the nonlinear network's incident and scattered noise waves to reject high-order harmonic content and thereby establish a somewhat simplified instance for a bounded fundamental frequency restriction. Evaluated over a range of specific large-signal operating points, computer simulations of the network's scattered noise power density bounding the fundamental frequency compared

very closely with independent numerical calculations. The second case applied the generalized noise model to a driven nonlinear two-port example circuit embedded in a passive, source/load match-terminated network exhibiting isolated noisy ports. Filtering was employed at the nonlinear network's input-output ports to enforce a bounded fundamental frequency condition. Evaluated at specific large (and small) signal operating points, computer simulations faithfully predicted the nonlinear network's scattered noise power density to that of independent results obtained through numerical calculation. From the data results, noise factor and effective input noise temperature of the nonlinear two-port were established.

6.2 Recommendations for Further Work

The generalized noise behavioral model introduced in this discourse is a basis for simulation, modeling, and measurement of driven nonlinear devices, components, and systems. Suggestions for future research endeavors encompass software simulation and measurement activities. In simulation, the match-embedded experiments for the nonlinear one- and two-port cases should be repeated with the filters removed to assess the influence of higher-order harmonic content on the scattered noise power density. Comparison with numerical calculations can be made by including in the formulism dominant X-parameter terms corresponding to the m -th harmonic. Pertaining to measurement, it's proposed that a cold-source measurement technique [58] be devised to extract the noise correlation matrix of a nonlinear network. Attention to practical considerations distinguishing noise of measurement system from the network of interest (extraction) through calibration and signal processing techniques will be required. To facilitate this suggestion, noise models and test procedures supporting calibration and NL device measurement processes have been developed. Finally, perhaps most important, is to extend simulation and measurement activities to the mismatch-embedded nonlinear two-port scenario. Its execution will build on the foundation laid by the match-embedded exercises and the introductory development of mismatch-embedded NL one- and two-port noise models, each founded by the generalized noise behavioral model devised in this work.

Appendices

Appendix A

Mismatch-Embedded Nonlinear One-Port Network

Using the generalized full insitu-noise matrix expression from (5.42), the constituent noise power spectral density expressions for the mismatch-embedded nonlinear one-port network are solved. Analysis is restricted to the fundamental frequency. The following are personal notes presented in hand-written form that can be referred to on the attached CD.

Appendix B

Mismatch-Embedded Nonlinear Two-Port Network

Using the generalized full insitu-noise matrix expression from (5.42), the constituent noise power spectral density expressions for the mismatch-embedded nonlinear two-port network are solved with the aid of MatLab. Analysis is restricted to the fundamental frequency. The following are early stage personal notes that can be referred to on the attached CD.

Appendix C

Mismatch-Embedded NL One-Port Calibration Procedure

1. Determine the measurement receiver's gain-bandwidth product \tilde{G}'_r and output noise power r'_{22} .
 - A. Connect a calibrated noise source to the measurement system.
 - B. Tune the noise measurement receiver to a positive offset frequency from the fundamental as denoted by the “/” symbol.
 - C. Turn the noise source on and measure the noise power $\hat{P}'_{rx1(Hot,Cal)}$.
 - D. Measure noise source match Γ_{hns11} in the on-state.
 - E. Turn the noise source off and measure the noise power $\hat{P}'_{rx1(Cold,Cal)}$.
 - F. Measure noise source match Γ_{cns11} in the off-state.
 - G. Record the physical temperature T_{cns} of the noise source housing.
 - H. Record the physical temperature T_{ms} of measurement system.
2. Determine the measurement receiver's gain-bandwidth product \tilde{G}''_r and output noise power r''_{22} .
 - A. Repeat steps 1A through 1H with the noise measurement receiver tuned to a negative offset frequency from the fundamental as denoted by the “//” symbol.
3. Determine the source match states $\Gamma_{s11,(1)}$, ..., and $\Gamma_{s11,(4)}$.

- A. Perform an S_{11} one-port calibration at test port 3.
 - B. Connect test port 3 to test port 1 via the back-to-back coupler arrangement.
 - C. Set $Z_{s(1)}$.
 - D. Measure $\Gamma_{s_{11(1)}}$.
 - E. Repeat steps 3C and 3D for pairings $Z_{s(2)}, \Gamma_{s_{11(2)}}, \dots$, and $Z_{s(4)}, \Gamma_{s_{11(4)}}$.
4. Connect the nonlinear one-port network to the measurement system.
- A. Measure X-parameters $X_{11,11}^{(S)}(|A_{11}|)$ and $X_{11,11}^{(T)}(|A_{11}|)$ as a function of large-signal drive A_{11} . Note, the procedure for ascertaining measurement derived X-parameters is documented per Keysight Technologies App. Note 1408-20.

Appendix D

Mismatch-Embedded NL One-Port Network Measurement Procedure

1. Connect the nonlinear one-port network to the measurement system.
 - A. Tune the noise measurement receiver to the positive offset frequency from the fundamental as denoted by the “/” symbol.
 - B. Set $Z_{s(1)}$.
 - C. Establish an appropriated large-signal operating point (LSOP), ie., $|A_{11}|$, for the nonlinear one-port network.
 - D. Measure $\hat{p}'_{rx11(1)}$.
 - E. Repeat steps B through D for pairings $Z_{s(2)}, \hat{p}'_{rx11(2)}, \dots$, and $Z_{s(4)}, \hat{p}'_{rx11(4)}$.
 - F. Calculate the noise properties of the nonlinear one-port network per the expression $\mathbf{D}'_{DUT} = \mathbf{B}'^{-1}(\mathbf{P}'_{meas} - \mathbf{A} \cdot \mathbf{R}'_{rx})$.
 - G. Repeat steps 1A-1F with the noise measurement receiver tuned to a negative offset frequency from the fundamental as denoted by the “//” symbol. The expression $\mathbf{D}''_{DUT} = \mathbf{B}''^{-1}(\mathbf{P}''_{meas} - \mathbf{A} \cdot \mathbf{R}''_{rx})$ will be used.

Appendix E

Match-Embedded NL Two-Port Calibration Procedure

1. Determine the measurement receiver's gain-bandwidth product G'_r and its noise properties including r'_{11} , r'_{12} , r'_{21} , and r'_{22} .
 - A. Determine the source match states $\Gamma_{s_{11(1)}}$, $\Gamma_{s_{11(2)}}$, ..., and $\Gamma_{s_{11(5)}}$.
 - A1. Perform an S_{11} one-port calibration at test port 3.
 - A2. Connect test port 3 to test port 1 via the back-to-back coupler arrangement.
 - A3. Set source impedance $Z_{s(1)}$.
 - A4. Measure $\Gamma_{s_{11(1)}}$.
 - A5. Repeat steps A3 and A4 four additional times at unique settings of Z_s . Readings $\Gamma_{s_{11(2)}}$, ..., and $\Gamma_{s_{11(5)}}$ will be recorded.
 - B. Tune the measurement receiver to a positive offset frequency from the fundamental as denoted by the "/" symbol.
 - C. Record the physical temperature T_s of the source impedance Z_s .
 - D. Set the source impedance to $Z_{s(1)}$.
 - E. Measure noise power $p'_{rx_{21(1)}}$.
 - F. Repeat steps 1D and 1E corresponding to each of the unique Z_s settings established in steps 1 through A5. Readings $p'_{rx_{21(2)}}$, $p'_{rx_{21(3)}}$, ..., and $p'_{rx_{21(5)}}$ will be recorded.

- G. Calculate G'_r , r'_{11} , r'_{12} , r'_{21} , and r'_{22} .
2. Determine the measurement receiver's gain-bandwidth product G''_r , and its noise properties including r''_{11} , r''_{12} , r''_{21} , and r''_{22} .
- A. With the noise measurement receiver tuned to the negative offset frequency from the fundamental as denoted by the “//” symbol, repeat steps 1B through 1F. Readings $p''_{rx21(1)}$, $p''_{rx21(2)}$, ..., and $p''_{rx21(5)}$ will be recorded.
- B. Calculate G''_r , r''_{11} , r''_{12} , r''_{21} , and r''_{22} .
- C. Calculate the noise measurement receiver's gain $|g'_r|^2$ and $|g''_r|^2$ from G'_r and G''_r respectively.
- D. Calculate $\widehat{b}'_{r11} \widehat{b}'_{r11*}$ from $|g'_r|^2$ and r'_{11} as well as $\widehat{b}''_{r11} \widehat{b}''_{r11*}$ from $|g''_r|^2$ and r''_{11} .
- E. Using the results from 2C and 2D, calculate calibration coefficients $|g'_r|^2 \widehat{b}'_{r11} \widehat{b}'_{r11*}$ and $|g''_r|^2 \widehat{b}''_{r11} \widehat{b}''_{r11*}$.
3. Connect the NL two-port network to the measurement system.
- A. Determine the network's X-parameters including $X_{21,11}^{(S)}$, $X_{21,11}^{(T)}$, $X_{21,21}^{(S)}$, and $X_{21,21}^{(T)}$ as a function of large-signal drive A_{11} . Note, the procedure for ascertaining measurement derived X-parameters is documented per Keysight Technologies App. Note 1408-20.

Appendix F

Match-Embedded NL Two-Port Measurement Procedure

1. Connect the NL two-port network to the measurement system.
 - A. Tune the noise measurement receiver to a positive offset frequency from the fundamental as denoted by the “/” symbol.
 - B. Establish an appropriate large-signal operating point (LSOP), ie. $|A_{11}|$, for the NL two-port network.
 - C. Measure $\hat{\mathbf{P}}'_{\text{Meas}}$.
 - D. Calculate the noise property of the NL two-port network per the expression $\mathbf{D}'_{\text{DUT}} = \mathbf{B}'^{-1}(\mathbf{P}'_{\text{Meas}} - \mathbf{A} \cdot \mathbf{R}'_{\text{RX}})$ where in this scenario matrix $\mathbf{P}'_{\text{Meas}}$ is equal to $\hat{\mathbf{P}}'_{\text{Meas}}$.
 - E. Repeat steps 1A through 1D with the noise measurement receiver tuned to a negative offset frequency from the fundamental as denoted by the “//” symbol. Apply expression $\mathbf{D}''_{\text{DUT}} = \mathbf{B}''^{-1}(\mathbf{P}''_{\text{Meas}} - \mathbf{A} \cdot \mathbf{R}''_{\text{RX}})$ where $\mathbf{P}''_{\text{Meas}}$ is equal to $\hat{\mathbf{P}}''_{\text{Meas}}$.
 - F. As previously described, the NL two-port’s effective noise temperature T'_e , and noise factor F' , may be determined by use of \mathbf{D}'_{DUT} and its X-parameters. Similarly, T''_e and F'' may be acquired by the NL two-port’s noise matrix $\mathbf{D}''_{\text{DUT}}$ and X-parameters.

Publications

“Noise Characterization and Behavioral Modeling of Nonlinear RF/Microwave Components”

This paper is in process of submission to *The IEEE Transactions on Instrumentation and Measurement*.

References

- [1] "Fundamentals of RF and Microwave Noise Figure Measurements", Keysight Technologies, Inc., Palo Alto, CA, USA, Lit. #: 5952-8255E, Sept. 2017, p. 4.
- [2] H. Hillbrand and P. Russer, "An Efficient Method for Computer Aided Noise Analysis of Linear Amplifier Networks", IEEE Trans. on Circuits and Syst., Vol. 23, No.4, pp. 235-238, Apr. 1976.
- [3] S. Okwit, "An Historical View of the Evolution of Low-Noise Concepts and Techniques", IEEE Trans. on Microwave Theory and Techniques, Vol. MTT-32, No.9, pp. 1068-1082, Sept. 1984.
- [4] J. Johnson, "Thermal Agitation of Electricity in Conductors", Physical Review, Vol. 32, pp. 97-109, July 1928.
- [5] A. Einstein, "Zur Theorie der Brownchen-Bewegung", Ann. Physik (in German), Vol. 19, p. 371, 1906.
- [6] J. Perrin, "Laws of the Brownian Movement", Atoms, pp. 115-133, 1914.
- [7] W. Schottky, "Uber Spontane Stromschwankungen in Verschiedenen Elektrizitatsleitern", Ann. Physik (in German), Vol. 57, pp. 541-567, 1918.
- [8] H. Nyquist, "Thermal Agitation of Electric Charge in Conductors", Physical Review, Vol. 32, pp. 110-113, July 1928.
- [9] F.B. Llewellyn, "A Rapid Method of Estimating the Signal-To-Noise Ratio of a High Gain Receiver", Proc. IRE, Vol. 19, pp. 416-420, Mar. 1931.
- [10] F.C. Williams, "Thermal Fluctuations in Complex Networks", Journal I.E.E., Vol. 81, pp. 751-760, Dec. 1937.

-
- [11] K. Franz, "The Limiting Sensitivity in the Reception of Electric Waves and its Attainability", *Elik. Nachrichtentech*, Vol. 16, p. 92, 1939.
- [12] E.W. Herold, "An Analysis of the Signal-To-Noise Ratio of Ultra High Frequency Receivers", *RCA Rev.*, Vol. 6, No. 3, pp. 302-331, Jan. 1942.
- [13] D. O. North, "The Absolute Sensitivity of Radio Receivers", *RCA Rev.*, Vol. 6, No. 3, pp. 332-344, Jan. 1942.
- [14] H. T. Friis, "Noise Figures of Radio Receivers", *Proc. of the IRE*, Vol. 32, No.7, pp. 419-422, Jul. 1944.
- [15] D. K. MacDonald, "A Note on Two Definitions of Noise Figures in Radio Receivers", *Philo. Mag. And J. Science, Series 7*, Vol. 35, No. 245, pp. 386-395, Jun. 1944.
- [16] P. D. Strum, "A Note on Noise Temperature", *IRE Trans. Microwave Theory Tech.*, Vol. MTT-4, No.3, pp. 145-151, Jul. 1956.
- [17] H. A. Haus et al, "IRE Standards on Methods of Measuring Noise in Linear Two Ports", *Proc. of the IRE*, 59 IRE 20.S1, pp. 60-68, Jan. 1960.
- [18] H. Rothe and W. Dahlke, "Theory on Noisy Fourpoles", *Proc. of the IRE*, pp. 811-818, Jun. 1956.
- [19] P. Penfield Jr., "Wave Representation of Amplifier Noise", *IRE Trans. on Circuit Theory*, pp. 84-86, Mar. 1962.
- [20] Hendrik Bosma, "On The Theory of Linear Noisy Systems", Eindhoven: Technische Hogeschool Eindhoven, Jan. 1967.
- [21] R. P. Meyes, "A Wave Approach to the Noise Properties of Linear Microwave Devices", *IEEE Trans. on Microwave Theory and Techniques*, Vol. MTT-26, No. 1, pp. 34-37, Jan. 1978.
- [22] R. P. Meyes and Michael Milecan, "Noise Waves, A Concept Leading to Deep Insight and Very Accurate Noise Characterization", *IEEE MTT-S Digest*, pp. 351-353, 1982.
- [23] J. A. Dobrowolski, "Introduction to Computer Methods for Microwave Circuit Analysis and Design", Artech House, 1991.
- [24] S. W. Wedge and D. B. Rutledge, "Noise Waves and Passive Linear Multiports", *IEEE Microwave and Guided Wave Letters*, Vol. 1, No. 5, pp. 117-119, May 1991.

-
- [25] S. W. Wedge and D. B. Rutledge, "Wave Techniques for Noise Modeling and Measurement", *IEEE Transactions on Microwave Theory and Techniques*, Vol. 40, No. 11, pp. 2004-2012, Nov. 1992.
- [26] J. Randa, "Noise Characterization of Multiport Amplifiers", *IEEE Transactions on Microwave Theory and Techniques*, Vol. 49, No. 10, pp. 1757-1763, Oct. 2001.
- [27] V. Markovic et al, "Extraction of Noise Wave Sources in MESFET Wave Representations", *Proceedings of International Conference on Microwave and Millimeter Wave Technology – ICMMT'98*, pp. 108-111, Beijing, China, Aug. 1998.
- [28] E. C. Valk et al, "De-embedding Two-Port Noise Parameters Using a Noise Wave Model", *IEEE Transactions on Instrumentation and Measurement*, Vol. 37, No. 2, pp. 195-200, Jun. 1988.
- [29] Hewlett-Packard Co., "S-Parameters Theory and Application", *Hewlett-Packard Journal*, February 1967.
- [30] W. W. Mumford, "A Broadband Microwave Noise Source", *Bell System Tech. J.*, Vol. 28, No.4, pp. 608-618, Oct. 1949.
- [31] E. W. Sard et al, "Final Engineering Report on Measurement of Low Noise Figures", AIL Report No. 5208-1, Jan. 1958.
- [32] Hewlett-Packard Co., "Fundamentals of RF and Microwave Noise Figure Measurements", *Application Note 57-1*, Jul. 1983.
- [33] Agilent Technologies Inc., "High-Accuracy Noise Figure Measurements Using the PNA-X Series Network Analyzer", *Application Note 1408-20*, Sept. 2010.
- [34] P. A. Rizzi, "Microwave Engineering Passive Circuits", Prentice-Hall, 1988.
- [35] G. Gonzalez, "Microwave Transistor Amplifiers Analysis and Design", Second Edition, Prentice-Hall, 1997.
- [36] R. E. Collin, "Foundations for Microwave Engineering", McGraw-Hill, 1966.
- [37] S. W. Wedge, "Computer-Aided Design of Low Noise Microwave Circuits", PhD Thesis, CIT, Pasadena, CA, May 1991.
- [38] W. H. Hayt Jr. and J. E. Kemmerly, "Engineering Circuit Analysis", Third Edition, McGraw-Hill, 1978.

-
- [39] S. Withington, "Scattered Noise Waves in Microwave and mm-Wave Networks", *Microwave Journal*, Jun. 1989.
- [40] W. Marshall Leach, Jr., "Fundamentals of Low-Noise Analog Circuit Design", *Proceedings of the IEEE*, Vol. 82, No. 10, pp. 1515-1538, Oct. 1994.
- [41] B. P. Lathi, "Signals, Systems and Communications", John Wiley & Sons, 1965.
- [42] W. B. Danvenport Jr. and W. L. Root, "An Introduction to the Theory of Random Signals and Noise", McGraw-Hill, 1958.
- [43] R. P. Hecken, "Analysis of Linear Noisy Two-Ports Using Scattering Waves", *IEEE Transactions on Microwave Theory and Techniques*, Vol. MTT-29, No. 10, pp. 997-1004, Oct. 1981.
- [44] G. Strang, "Introduction to Linear Algebra", Fourth Edition, Wellesley-Cambridge Press, 2009.
- [45] M. Planck, "On the Law of Distribution of Energy in the Normal Spectrum", *Annalen der Physik*, Vol. 4, p. 553ff, 1901.
- [46] N. G. Kanaglekar et al, "Wave Analysis of Noise in Interconnected Multiport Networks", *IEEE Transactions on Microwave Theory and Techniques*, Vol. MTT-35, No.2, pp. 112-116, Feb. 1987.
- [47] H. A. Haus et al, "Description of the Noise Performance of Amplifiers and Receiving Systems", *Proceedings of the IEEE*, Sponsored by IRE Committee 7.9 on Noise, pp.436-442, Mar. 1963.
- [48] G. Simpson et al, "A New Noise Parameter Measurement Method Results in more than 100x Speed Improvement and Enhanced Measurement Accuracy", *Maury Microwave Application Note 5A-042*, Mar. 2009.
- [49] K. Wong, R. Pollard, B. Shoulders, L. Rhymes, "Using a Mismatch Transmission Line to Verify Accuracy of a High-Performance Noise Figure Measurement System", *69th ARFTG Conference Digest*, pp. 170-174, Honolulu, HI, Jun. 2007.
- [50] M. Schetzen, "Linear Time-Invariant Systems", John Wiley & Sons, 2003.
- [51] D.E. Root et al, "X-Parameters", Cambridge University Press, 2013.

-
- [52] L. Betts, "A New Theoretical and Experimental Approach to Nonlinear Vector Network and Complex Signal Analysis", PhD Thesis, The University of Leeds, Leeds, UK, Dec. 2009.
- [53] "High Power Amplifier Measurements Using Nonlinear Vector Network Analyzer", Keysight Technologies, Inc., Santa Rosa, CA, Lit. #: 5990-5039EN, p. 3, Jul. 2014.
- [54] A. Cappy, F. Danneville, and G. Dambrine, "Noise Analysis in Devices under Nonlinear Operation," Institut d' Electronique et de Microelectronique du Nord, UMR CNRS 9929. Cite Scientifique, Avenue Poincare – BP69, 59652 Villeneuve d' Ascq Cedex – France.
- [55] J. Verspect, D. E. Root, "Polyharmonic Distortion Modeling", IEEE Microwave Magazine, pp. 44-57, Jun. 2006.
- [56] J. Verspect, D. F. Williams, D. Schreurs, K. A. Remley, M. D. McKinley, "Linearization of Large-Signal Scattering Functions," IEEE Trans. on Microwave Theory and Tech., Vol. 53, No. 4, pp. 1369-1376, Apr. 2005.
- [57] J. A. Dobrowolski, "Noise of Multiport Networks," First Edition, Artech House, 2010.
- [58] "High Accuracy Noise Figure Measurements Using the PNA-X Series Network Analyzer", Keysight Technologies, Inc., Santa Rosa, CA, Lit. #: 5990-5800EN, pp. 8, 19-22, Aug. 2014.
- [59] Sergio Colangeli et al, "Polynomial Noise Modeling of Silicon-Based GaN HEMTs", International Journal of Numerical Modeling – Electronic Networks, Devices and Fields, Vol. 27, Issue 5-6, pp. 812-821, Sep. – Dec. 2014.
- [60] L. Boglione, "A Novel Extraction Procedure to Determine the Noise Parameters of On-Wafer Devices", IEEE MTT-S International Microwave Symposium Digest, Jun. 2-7, 2013.
- [61] Sergio Colangeli et al, "Black-Box Noise Modeling of GaAs HEMTs Under Illumination", International Journal of Numerical Modeling – Electronic Networks, Devices and Fields, Vol. 28, Issue 6, pp. 698-706, Nov./Dec. 2015.
- [62] Vladica Dordevic et al, "Wave Approach for Noise Modeling of Gallium Nitride High Electron-Mobility Transistors", International Journal of Numerical Modeling – Electronic Networks, Devices and Fields, Vol. 30, Issue 1, Jan./Feb. 2017.
- [63] Vittorio Rizzoli et al, "General Noise Analysis of Nonlinear Microwave Circuits by Piece-Wise Harmonic-Balance Technique", IEEE Transactions on Microwave Theory and Techniques, Vol. 42, No. 5, pp. 807-819, May 1994.

- [64] F. Bonani et al, "A General Framework for the Noise Analysis of Semiconductor Devices Operating in Nonlinear (Large-Signal Quasi-Periodic) Conditions", Proc. 14th Int. Conf. on Noise in Phy. Syst. and 1/f Fluctuations, World Scientific Publishing Co., pp. 144-147, 14-18 Jul. 1997.
- [65] Jose Carlos Pedro et al, "Evaluation of Signal-to-Noise Ratio and Distortion Ratio Degradation in Nonlinear Systems", IEEE Transactions on Microwave Theory and Techniques, Vol. 52, No. 3, Mar. 2004.
- [66] Larry Dunleavy et al, "Advanced Nonlinear and Noise Modeling of High-Frequency GaN Devices", Microwaves & RF, Oct. 2017.